INSIGHTS FROM MATHEMATICAL MODELS INTO COVID-19: ANALYZING PUBLIC HEALTH INTERVENTIONS AND IMMUNITY DYNAMICS

Iris Ganser

THÈSE EN COTUTELLE PRÉSENTÉE

POUR OBTENIR LE GRADE DE

DOCTEURE DE L'UNIVERSITÉ DE BORDEAUX ET DE L'UNIVERSITÉ MCGILL

ÉCOLE DOCTORALE : SOCIÉTES, POLITIQUE, SANTÉ PUBLIQUE

SPÉCIALITÉ SANTÉ PUBLIQUE, OPTION ÉPIDÉMIOLOGIE

Par **Iris GANSER**

UTILISATION DES MODÈLES MATHÉMATIQUES FACE À LA COVID-19 : ANALYSE DES EFFETS DES INTERVENTIONS EN SANTÉ PUBLIQUE ET DE LA DYNAMIQUE IMMUNITAIRE

INSIGHTS FROM MATHEMATICAL MODELS INTO COVID-19: ANALYZING PUBLIC HEALTH INTERVENTIONS AND IMMUNITY DYNAMICS

Sous la direction de **Rodolphe THIÉBAUT** et **David L BUCKERIDGE**

Soutenue le 11 décembre 2024 à Bordeaux

Membres du jury

M. THIÉBAUT, Rodolphe, PU-PH, Inserm U1219 ..... Directeur de thèse
M. BUCKERIDGE, David L, Professor, McGill University ..... Co-directeur de thèse
Mme. HILL, Alison, Assistant Professor, Johns Hopkins University ..... Rapporteure
M. PLATT, Robert, Professor, McGill University ..... Rapporteur
M. WHITE, Michael, Directeur de Recherche, Institut Pasteur ..... Rapporteur
Mme. NUNES, Marta, Professeur à l'université, CIRI ..... Examinatrice
Mme. TEMIME, Laura, Professeure, Conservatoire national des Arts et Métiers ..... Présidente du jury
Mme. PRAGUE, Mélanie, Chargée de recherche, Inria ..... Invitée

Abstract

The COVID-19 pandemic, caused by the SARS-CoV-2 virus, has led to significant morbidity and mortality, straining healthcare systems worldwide. Fundamental approaches for controlling viral spread and mitigating its impact are vaccinations and non-pharmaceutical interventions (NPIs). Before vaccines became available, governments relied on NPIs with largely unknown epidemiological and societal impacts. Despite numerous studies, the effectiveness of NPIs on COVID-19 dynamics remained uncertain, especially over multiple pandemic waves. With a gradual roll-out of vaccines, population immunity increased, but this increase in was counteracted by the emergence of immune-escaping variants of concern (VoCs) and waning of both infection- and vaccine-induced immunity. The long-term dynamics of this decline are currently not well characterized, particularly in the context of multiple infections and infections with different VoCs.

Given the only partially observed nature of epidemics and their non-linear dynamics, mathematical models are uniquely suited for their analysis. In my thesis, I applied mathematical models to various COVID-19 data, from aggregated population-level data of infections and hospitalizations to antibody (Ab) titers in individuals, with the goal of quantifying the effectiveness of NPIs and vaccines, identifying protective Ab thresholds, and characterizing immunity waning dynamics.

Specifically, my first objective was to estimate the effectiveness of NPIs and vaccines in France and explore counterfactual NPI and vaccine implementation scenarios. We developed a population-based mechanistic model, which we fit to epidemiological data in France from March 2020 to October 2021. The model showed a significant reduction in viral transmission by lockdowns, school closures, and curfews, though their effectiveness decreased over time. Simulations demonstrated that vaccines had saved nearly 160k lives over the study period, but an earlier implementation or a faster rollout could have prevented even more deaths.

To understand why NPI effectiveness estimates vary across studies, we evaluated two methodologies in my second objective: mechanistic models and a com-

monly used two-step regression approach. The latter first estimates the reproductive number ($\mathcal{R}_t$) and then regresses it against NPI parameters. Using simulated data of varying complexity, mechanistic models consistently showed minimal bias (0-5%) and high confidence interval (CI) coverage, whereas the two-step regressions had biases up to 20% and much lower CI coverage. The bias stemmed from the depletion of susceptibles and challenges in estimating $\mathcal{R}_t$, indicating that caution is warranted with this method despite its simplicity and speed.

Accurate epidemiological models require up-to-date parameters. My third objective was therefore two-fold: 1) to relate SARS-CoV-2 specific Ab levels to the risk of infection and 2) to characterize antibody waning. Using Ab data from over 220k Canadian blood donors between April 2020 and December 2023, we found that both anti-S and anti-N Abs reduced infection risk, with anti-N showing a stronger effect at lower titers. We used biphasic decay models to characterize waning dynamics and estimated that that 51.3% (95% CI 40.6-66.1%) of individuals would drop below detectable anti-N Ab levels within three years after a single infection. The duration of Ab detection increased after subsequent infections. However, antibodies waned within months below thresholds needed to attain substantial protection, even after multiple infections and vaccinations, indicating that continuous vaccine booster doses might be needed to sustain protection.

The analyses I conducted in my PhD research highlight the importance of timely interventions and continuous monitoring of immunity to better prepare for future outbreaks. Moreover, I illustrated that mathematical models are a powerful tool to inform public health decision making and strategies.

Keywords: COVID-19, vaccines, non-pharmaceutical interventions, infectious diseases, mathematical modeling

Résumé

La pandémie de COVID-19, causée par le SRAS-CoV-2, a entraîné une morbidité et une mortalité importantes, mettant à rude épreuve les systèmes de santé mondiaux. Les vaccinations et les interventions non pharmaceutiques (INP) sont essentielles pour contrôler la propagation du virus. Avant les vaccins, les gouvernements s'appuyaient sur des INP dont l'impact épidémiologique et sociétal restait incertain, notamment sur plusieurs vagues pandémiques. Le déploiement des vaccins a augmenté l'immunité collective, mais l'émergence de variants préoccupants (VoCs) échappant à l'immunité et l'affaiblissement de l'immunité induite ont reduit l'immunité effective. La dynamique à long terme de ce déclin est mal comprise, surtout dans le contexte d'infections multiples et par divers VoCs.

Les épidémies étant partiellement observées et leur dynamique non linéaire, les modèles mathématiques sont bien adaptés pour leur analyse. Dans ma thèse, j'ai appliqué ces modèles à diverses données COVID-19, depuis les données agrégées sur les infections et les hospitalisations jusqu'aux titres d'anticorps (Ac) chez les individus, pour quantifier l'efficacité des INP et vaccins, identifier les seuils de protection des Ac et caractériser la décroissance de l'immunité.

Mon premier objectif était d'estimer l'efficacité des INP et des vaccins en France et d'explorer des scénarios contrefactuels des INP et des vaccins. Nous avons développé un modèle mécaniste ajusté aux données épidémiologiques françaises de mars 2020 à octobre 2021. Le modèle a montré une réduction significative de la transmission virale grâce aux INP, bien que leur efficacité ait diminué avec le temps. Les simulations ont montré que les vaccins avaient sauvé près de 160000 vies au cours de la période étudiée, mais qu'une mise en œuvre plus précoce ou un déploiement plus rapide aurait évité encore plus de décès.

Pour comprendre la variabilité des estimations de l'efficacité des INP, nous avons évalué deux méthodologies pour mon deuxième objectif: les modèles mécanistes et une régression en deux étapes couramment utilisée, qui d'abord estime le nombre de reproduction ($\mathcal{R}_t$), puis le regresse sur les paramètres des INP. En utilisant des données simulées, les modèles mécanistes ont montré un biais minimal (0-5%)

et une couverture d'intervalle de confiance (IC) élevée, tandis que les régressions en deux étapes ont montré des biais jusqu'à 20% et une couverture d'IC inférieure. Ce biais était dû à la déplétion des susceptibles et aux difficultés d'estimation de $\mathcal{R}_t$, montrant que cette méthode nécessite prudence malgré sa rapidité.

Les modèles épidémiologiques précis nécessitent des paramètres actualisés. Mon troisième objectif était donc 1) relier les niveaux d'Ac SARS-CoV-2 au risque de (ré)infection et 2) caractériser la décroissance des Ac. Grâce aux données d'Ac de plus de 220000 donneurs de sang canadiens entre avril 2020 et décembre 2023, nous avons constaté que les Ac anti-S et anti-N réduisaient le risque d'infection, avec un effet plus prononcé des anti-N à de faibles titres. J'ai estimé avec des modèles de décroissance biphasique que 51.3% (95% IC 40.6-66.1%) des individus tomberaient en dessous des niveaux détectables d'Ac anti-N dans les trois ans suivant une infection. La durée de détection des Ac augmentait après chaque infection. Cependant, les Ac chutaient en quelques mois en dessous des seuils requis pour une protection substantielle, même après plusieurs infections et vaccinations, indiquant la nécessité d'administrer des rappels régulièrs pour maintenir la protection.

Les analyses dans ma thèse soulignent l'importance des interventions rapides et du suivi continu de l'immunité pour mieux se préparer aux futures épidémies. De plus, j'ai démontré que les modèles mathématiques sont un outil puissant pour orienter la prise de décision en santé publique et les stratégies de prévention.

mots-clés: COVID-19, vaccins, interventions non pharmaceutiques, maladies infectieuses, modélisation mathematique

Contents

List of Figures

List of Tables

Acknowledgements

First and foremost, I would like to thank my supervisors Dr. Rodolphe Thiébaut and Dr. David Buckeridge for their guidance and their trust in me during the last five years. Your constant encouragement and insightful comments helped me to keep going when I felt stuck. Your feedback and mentorship was always appreciated. You made my PhD journey into a great learning experience, challenging and rewarding at the same time. Thank you both also for building the connection between the two universities and your willingness to battle the administrative challenges of a PhD in cotutelle. Rodolphe, thank you also for your great humor. It has been a pleasure to work with you two!

I would like to express my deep gratitude to Dr. Mélanie Prague for supporting my thesis far beyond what is expected from a committee member. You not only helped me with technical questions during countless hours of meetings, but also provided large-picture guidance on projects, while also checking in on my mental health.

I would also like to thank to my other committee member, Dr. Jane Heffernan, for her thoughtful advice and input on my modeling works and the time spent in meetings with me.

My thesis in cotutelle would not have been possible without the people who enabled this program. Thank you, Dr. Rebecca Fuhrer for being a driving force of this collaboration between the two universities. Thank you also for your mentoring and your interest in my progress. I would not be here without your efforts and support. I owe my thanks both to Rebecca Fuhrer and Chloe Garcia from GPS for their support with the never-ending paperwork.

I would also like to thank the administrative staff of the department at McGill and of the SISTM team, in particular André Yves, Katherine, and Sandrine. Thank you for your dedication, patience, super rapid response times and support in all administrative matters.

My thanks goes also to the lab members of the SISTM and MCHI teams (especially Yannan!) for passing time with me at work, your helpful advice, the snacks and coffee, lunches and chats.

I am incredibly grateful towards my PhD cohort members and friends at McGill – Emma, Leah, Chelsea (honorary cohort member), Marshall, Mariam, and Salome. My PhD experience would not have been the same without you. I'm so grateful to have met you and to have made lasting friendships. Emma and Leah, thank you for reading over my thesis (and other documents), providing feedback on figures, and letting me rant about everything that annoyed me without a filter. Chelsea - thank you for being the best roommate during a pandemic that I could have imagined. Leah – thanks for being so generous and hosting me for a few months, also you're the best assignment and TA buddy. Emma – thanks for literally everything: hosting me, working together, your workout motivation (more or less successful), stupid jokes, deep conversations and heartfelt laughs.
I would also like to thank all my other friends whose names I did not mention for their support and understanding during the times I was gone, for all the laughs, good talks, bike trips, and morning yoga sessions, whether we are physically close to each other or not.

A huge thanks to Baptiste for discussing my projects with me, challenging me and letting me not get away with bullshit, for writing emails in French for me, proofreading the French part of this thesis, and providing comments on the discussion. Also—way more importantly—thank you for sharing your life with me, whether we're close to each other or whether an Ocean is separating us. You're making my life bright with your stupid jokes, your ceaseless complaints about the big and small injustices in life, your curiosity and intelligence, your gentleness, and your love.

Lastly, I would like to thank my parents for their unconditional support and love, even though this PhD meant me being away for long times. I would not have achieved all of this without you.

Statement of Financial Support

I would like to thank the *Initiative d'Excellence de l'université de Bordeaux* for the doctoral contract I received during three years (2020-2023) and the *Fonds de Recherche du Québec - Santé* for the stipend I received from 2023-2024. I am grateful to Dr. David Buckeridge for the stipend top-up and the international tuition fees he paid during my time at McGill. I would also like to thank Dr. Rodolphe Thiébaut for supporting me with a doctoral contract for the last few months of my thesis in Bordeaux.

Contributions

Statement of Originality

The work presented in this thesis constitutes original scholarship and contributes to the knowledge base of public health interventions against COVID-19 and potential future pandemics. Manuscript 1 provided robust estimates about the effectiveness of non-pharmaceutical interventions (NPIs) and vaccines in France to policymakers and the general public. Manuscript 2 evaluated two frequent methodologies used in NPI effectiveness studies and highlighted challenges which these methodologies encounter. I was able to outline scenarios where a simple two-step approach might yield accurate results, as well as scenarios where it may introduce bias and should be avoided. Lastly, manuscript 3, the largest study of natural immunity to date, provided estimations of the effectiveness and duration of protection conferred by both infection- and vaccination-derived anti-SARS-CoV-2 antibodies.

Contributions of Authors

Manuscript 1: Ganser I, Buckeridge DL, Heffernan JM, Prague M, Thiébaut R (2024). **Estimating the Population Effectiveness of Interventions Against COVID-19 in France: A Modelling Study**. *Epidemics*, Volume 46, Pages 100744.

My supervisor Dr. Rodolphe Thiébaut and my committee member Dr. Mélanie Prague conceptualized the study. Under their supervision and methodological guidance and the supervision of Dr. David L Buckeridge, we developed the refined research question and developed the mathematical model to analyze the data. Dr. Jane Heffernan (my committee member) provided methodological input and critical feedback. Dr. Mélanie Prague and I curated the dataset for analysis. I analyzed the data and interpreted it with the help of all authors, visualized the results and wrote the original draft of the manuscript, which was revised with the input of all authors for submission and during peer review.

Manuscript 2: Ganser I, Paireau J, Buckeridge DL, Cauchemez S, Thiébaut R, Prague M (2024). **Comparative evaluation of methodologies for estimating the effectiveness of non-pharmaceutical interventions in the context of COVID-19: a simulation study**. *[Under review at American Journal of Epidemiology]*

This study was conceptualized by Dr. Mélanie Prague and Dr. Rodolphe Thiébaut, with my contributions. With the input of Dr. Mélanie Prague, Dr. Rodolphe Thiébaut, and Dr. Simon Cauchemez, and under the supervision of Dr. Mélanie Prague, Dr. Rodolphe Thiébaut, and Dr. David L Buckeridge, I simulated all the datasets and conducted the analyses. All authors provided feedback on the study methodology and interpretation of the analyses. I drafted the original version of the manuscript, which was reviewed for submission by all authors.

Manuscript 3: Ganser I, Murphy T, Prague M, O'Brien S, Thiébaut R, Buckeridge DL (2024). **Investigating waning of natural immunity against SARS-CoV-2: implications for infection risk**. *[In preparation]*

The study was conceptualized by Dr. David L Buckeridge, and me. The blood donor data were provided by Canadian Blood Services (contact person Dr. Sheila F O'Brien) and curated specifically for this analysis by Dr. Tanya Murphy and me. Together, Dr. Tanya Murphy and I developed the algorithm to detect infections and vaccination in the data. I developed the waning and risk of infection models with methodological help from Dr. Mélanie Prague, Dr. David Buckeridge, and Dr. Rodolphe Thiébaut. With their guidance, I analyzed the data, interpreted the results, and drafted the manuscript. All authors reviewed the manuscript for submission.

Acronyms

ABM	Agent-based model
ACE2	Human angiotensin-converting enzyme 2
ASC	Antibody-secreting plasma cell
CCCSL	Complexity Science Hub COVID-19 Control Strategies List
CI	Confidence interval
COI	Cutoff index
CoP	Correlate of protection
COVID-19	Coronavirus disease 2019
ECDC	European center of disease control
EM	Expectation maximization
HR	Hazard ratio
ICU	Intensive care unit
IFN	Interferon
Ig	Immunoglobulin
IQR	Interquartile range
LMIC	Low- and middle-income countries
LOQ	Limit of quantification
MLE	Maximum likelihood estimation
N	Nucleocapsid
nAb	Neutralizing antibody
NLME	Nonlinear mixed effects model
NPI	Non-pharmaceutial intervention
ODE	Ordinary differential equation
OxCGRT	Oxford COVID-19 Government Response Tracker
PDE	Partial differential equation
PHSM	Public health and social measure
PSO	post-symptom onset
S	Spike
SAEM	Stochastic approximation expectation maximization
SARS-CoV-2	Severe acute respiratory syndrome coronavirus 2
SD	Standard deviation
SHM	Somatic hypermutation
VoC	Variant of concern
WHO	World Health Organization

Résumé substantiel en français

Introduction

La pandémie de COVID-19, causée par l'émergence du SRAS-CoV-2, représente une crise sanitaire mondiale sans précédent au XXI^{e} siècle. À travers plusieurs vagues pandémiques, elle a entraîné une morbidité et une mortalité importantes, exerçant une pression immense sur les systèmes de santé et les sociétés du monde entier. En l'absence de vaccins ou de traitements médicaux aux premiers stades, les gouvernements ont dû mettre en place des interventions non pharmaceutiques (INP) pour éviter la saturation des hôpitaux et réduire les décès prématurés. Les INP sont toutes les interventions de santé publique qui ne nécessitent pas de produits médicaux et comprennent des mesures telles que le confinement, le couvre-feu, la fermeture des écoles et le port du masque. Ces mesures ont souvent été imposées de manière urgente, avec des preuves limitées pour orienter les décisions. De nombreuses études ont utilisé diverses méthodologies pour estimer l'efficacité des INP, surtout durant la première vague de la pandémie. Cependant, les résultats varient considérablement, allant d'inefficaces à très efficaces pour presque toutes les INP évaluées. Ainsi, malgré une grande quantité de recherches, l'efficacité à long terme des INP reste incertaine, en particulier après l'apparition de variants préoccupants et l'introduction des vaccins. Un deuxième niveau d'incertitude concerne la méthodologie elle-même: comment les différentes approches analytiques et sources de données influencent les conclusions sur l'efficacité des INP? Après le développement et la distribution des vaccins, les INP ont pu être progressivement assouplies. Bien que les vaccins aient été essentiels pour réduire la transmission virale, la quantification des vies sauvées reste un débat ouvert. De plus, l'efficacité vaccinale contre l'infection a diminué au fil du temps en raison de deux facteurs : (1) la diminution naturelle de l'immunité, et (2) l'apparition de nouveaux variants plus transmissibles et porteurs de mutations échappant à l'immunité. Par conséquent, des doses de rappel fréquentes peuvent être nécessaires pour maintenir une immunité suffisante. Néanmoins, la protection conférée par les vaccins contre les formes graves reste élevée dans le temps. Deux protéines sont les cibles principales des anticorps anti-SRAS-CoV-2: la protéine de surface (spike) et la protéine de nucléocapside. Des nombreuses études ont examiné la dynamique des anticorps

anti-spike générés par la vaccination, les anticorps neutralisants anti-spike ayant été identifiés comme un corrélat de protection. Cependant, les niveaux spécifiques d'anticorps totaux conférant une protection contre l'infection—en particulier contre des variants échappant à l'immunité comme Omicron—restent flous. De plus, peu d'informations sont disponibles sur d'autres composantes de l'immunité, telles que les anticorps anti-nucléocapside ou l'immunité mucosale, qui ne sont générés que par une infection naturelle. En outre, les études sur la dynamique à long terme et les effets protecteurs des anticorps anti-SRAS-CoV-2 dans des cohortes de grande taille ont été rares, laissant une autre lacune dans la compréhension globale du paysage immunologique du COVID-19.

Les objectifs de cette thèse sont donc triples:

1. Estimer l'efficacité des interventions à l'échelle de la population contre la COVID-19 en France, en se concentrant à la fois sur les INP et les vaccins, et en utilisant des données granulaires de haute qualité. Les paramètres d'INP et de vaccin seront estimés à l'aide d'un modèle mécaniste, qui est particulièrement adapté, car il permet d'incorporer des informations biologiques sur l'évolution de la maladie et la protection par la vaccination. Des simulations de scénarios contrefactuels avec le même modèle seront menées pour illustrer l'effet de l'implémentation opportune des INP et des vaccins ou, au contraire, les conséquences de l'absence de vaccins.

2. Évaluer de manière comparative la performance de différentes méthodologies utilisées dans les études sur l'efficacité des INP. À cette fin, le modèle mécaniste développé dans l'objectif 1, qui estime tous les paramètres en une seule étape, sera comparé à un modèle de régression en deux étapes, qui estime d'abord les indicateurs épidémiques, puis les régressent sur les variables INP. Les sources potentielles de biais pour les deux modèles seront explorées.

3. Estimer le risque d'infection basé sur les titres d'anticorps dans une large cohorte de donneurs de sang et de plasma canadiens et identifier des seuils potentiellement protecteurs des anticorps anti-spike et anti-nucléocapside. En outre, les dynamiques de décroissance de ces anticorps seront caractérisées, notamment le temps nécessaire pour que les niveaux d'anticorps tombent en dessous de ces seuils protecteurs.

Les modèles mathématiques ont été des outils essentiels pour fournir aux décideurs des métriques clés de la dynamique épidémiologique, telles que le nombre de reproduction du virus, les prévisions des besoins en ressources de santé et les résultats potentiels de différentes stratégies de santé publique. En particulier, les modèles mathématiques de type SIR, également appelés modèles compartimentaux, ont

été fréquemment utilisés par les chercheurs pendant la pandémie de COVID-19. Dans ces types de modèles, la population étudiée est divisée en états d'infection mutuellement exclusifs, les compartiments, tels que Susceptibles (S), Infectieux (I) et Rétablis (R). Le modèle représentent les flux d'individus entre les compartiments au cours du temps en reproduisant la dynamique temporelle des épidémies de maladies infectieuses avec des équations différentielles ordinaires (EDO). Les EDO peuvent également être utilisées pour décrire les dynamiques intra-hôte, par exemple le mécanisme biologique de production et de décroissance des anticorps.

Dans ma thèse, j'ai utilisé des modèles compartimentaux, parfois seuls, parfois couplés à d'autres types de modèles, tels que des modèles de régression, pour atteindre les objectifs mentionnés ci-dessus.

Manuscrit 1 : Efficacité des interventions contre la COVID-19 en France

Dans ce chapitre, je présente une étude sur l'efficacité des interventions de santé publique contre la pandémie de COVID-19 en France. Nous avons développé un modèle mécaniste à l'échelle de la population qui inclut l'effet des vaccins sur la transmission du SARS-CoV-2 et le risque d'hospitalisation. La partie mécaniste du modèle est illustrée dans la Figure F1. Nous avons ensuite couplé le modèle mécaniste à un modèle linéaire mixte des taux de transmission virale b qui inclut l'impact des interventions non pharmaceutiques (INP). Ce modèle représente le taux de transmission temporel b_t en fonction du taux de transmission de base b_0, des INP, des conditions météorologiques et des variants d'intérêt (VoC), avec des effets aléatoires pour capturer la variabilité résiduelle entre départements:

$$log(b_{i,t}) = b_{0i} + \sum_j \beta_i^j NPI_{i,t}^j + \sum_k \beta_V^k \text{VoC}_{i,t}^k + \beta_w \text{météo}_{i,t}$$

$b_{0i} \sim N(b_{0_{pop}}, \omega)$ pour le département i à temps t, avec le INP j et le VoC k.

Nous avons intégré les effets de la vaccination, en tant qu'effet vaccinal populationnel contre la transmission (e_{vI}) et contre l'hospitalisation (e_{vH}), directement dans le modèle compartimental. Cette approche a permis d'estimer tous les paramètres en une seule étape, en propageant l'incertitude de manière précise. Nous avons ajusté le modèle aux données épidémiologiques fournies par Santé Publique France de mars 2020 à octobre 2021. Les paramètres ont été estimés par maximum de vraisemblance à l'aide d'un algorithme d'approximation stochastique de l'espérance-maximisation (SAEM) implémenté dans le logiciel Monolix. Avec le même modèle, nous avons simulé des scénarios de déploiement vaccinal, en utilisant le logiciel Simulx.

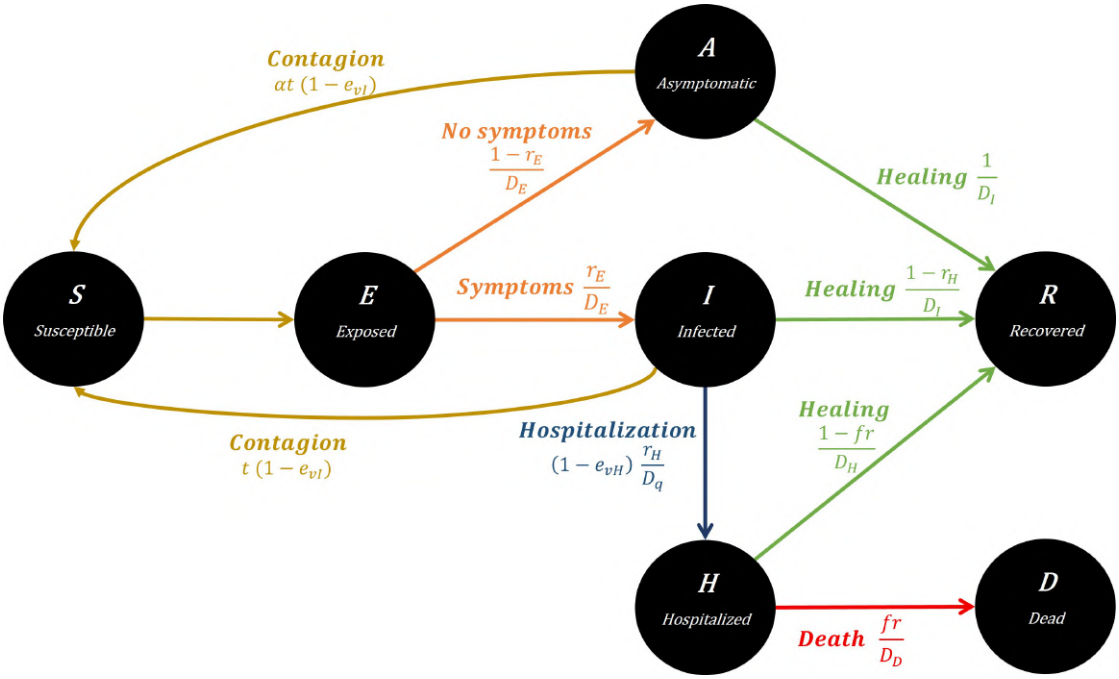

Figure F1: Modèle SEIRAHD

Le modèle a montré que le premier confinement était le plus efficace, réduisant la transmission de 84% (intervalle de confiance (IC) à 95%: 83-85). Les confinements suivants ont montré une efficacité diminuée (réduction de 74% (69-77) et de 11% (9-18), respectivement). Un couvre-feu à 18h a été plus efficace qu'à 20h (68% (66-69) contre 48% (45-49) de réduction), tandis que la fermeture des écoles a réduit la transmission de 15% (12-18). Nous avons également observé une influence significative de la météo sur la transmission du SARS-CoV-2, avec une augmentation moyenne de 10% en conditions hivernales et une diminution moyenne de 20% en conditions estivales par rapport aux conditions météorologiques moyennes en France durant toute la période d'étude. L'effet vaccinal populationnel contre la transmission et l'hospitalisation a augmenté au fil du temps avec la hausse de la couverture vaccinale. Cependant, l'effet du vaccin sur la transmission a plafonné à environ 25% (IC 95%: 22-27) avec la propagation du variant Delta. L'effet populationnel du vaccin contre l'hospitalisation a continué de croître avec l'augmentation de la couverture vaccinale, atteignant 84% (82-85) à la fin de la période d'étude.

Avec ces paramètres d'efficacité vaccinale estimés, nous avons simulé des scénarios contrefactuels de déploiement vaccinal. Dans un scénario sans vaccins avant novembre 2021, le modèle a prédit 159 000 décès supplémentaires, soit une augmentation de 168% (intervalle de prédiction (IP) à 95% : 70-315), ainsi que 1 488 000 hospital-

isations supplémentaires, soit une augmentation de 300% (133-492). Si un vaccin avait été disponible dès 100 jours après le début de l'épidémie, plus de 71 000 décès supplémentaires (16 507-204 249) et 384 000 hospitalisations supplémentaires (88 579-1 020 386) auraient pu être évités. De même, nous avons simulé des scénarios contrefactuels de mise en œuvre des confinements. Si le premier confinement avait été mis en place une semaine plus tôt, 92 000 hospitalisations (IC 95% : 61-118 000) et 20 000 décès (13-26 000) auraient pu être évités.

Les résultats de cette étude mettent en évidence l'impact substantiel des interventions non pharmaceutiques, y compris les confinements et les couvre-feux, dans le contrôle de la pandémie de COVID-19. Nous avons également démontré l'effet des vaccins pour réduire les hospitalisations, les décès et les infections liés à la COVID-19.

Manuscrit 2 : Évaluation comparative des méthodologies d'estimation de l'efficacité des interventions non pharmaceutiques

En comparant les estimations du Manuscrit 1 avec une autre étude sur l'efficacité des INP en France [1], nous avons noté plusieurs divergences dans l'estimation des effets des INP. Nous avons émis l'hypothèse que ces différences provenaient des différentes méthodologies utilisées, à savoir un modèle mécaniste estimant tous les paramètres en une seule étape, et un modèle de régression en deux étapes : 1) estimation du nombre de reproduction effectif $\mathcal{R}_t$ à partir des observations épidémiologiques, et 2) utilisation de $\mathcal{R}_t$ estimé comme variable dépendante dans un modèle de régression, avec les variables indicatrices des INP comme prédicteurs. $\mathcal{R}_t$ est défini comme le nombre moyen de cas secondaires produits par un seul individu infectieux. En raison de sa facilité d'application et de la rapidité des estimations, cette méthodologie a fréquemment été utilisée pour estimer l'efficacité des INP. Dans le Manuscrit 2, nous avons cherché à clarifier les divergences observées en comparant les deux approches méthodologiques en termes de biais des paramètres et de couverture des intervalles de confiance des paramètres d'efficacité des INP.

Nous avons simulé des jeux de données de complexité croissante, allant de modèles mécanistes SIR et SEIRAHD à des modèles multi-agents. Nous avons créé des scénarios comparables aux premiers mois d'une épidémie, avec une première INP, comparable en intensité à un confinement, suivie d'une deuxième INP, comparable à une intervention post-confinement. Dans la procédure de régression en deux étapes, nous avons d'abord estimé $\mathcal{R}_t$ à partir des infections ou des hospital-

isations, séparément pour chaque région simulée, avec une fenêtre de lissage de 7 jours à l'aide du package R EpiEstim. Ensuite, nous avons effectué une régression à effets mixtes avec l'estimation ponctuelle du $\log(\mathcal{R}_t)$ comme variable dépendante et les deux INP comme prédicteurs.

Dans les scénarios SIR simples, le biais des estimations des effets des INP par le modèle de régression en deux étapes augmentait avec la déplétion des individus susceptibles, tandis que le modèle mécaniste estimait constamment la valeur correcte (Tableau F1). Ce biais est expliqué par la variation temporelle du nombre de personnes susceptibles. Dans la procédure de régression en deux étapes, les effets des INP ont été estimés en utilisant le $mathcalR_t$ estimé dans la première étape selon l'équation 1. Avec $\mathcal{R}(t) = \frac{b(t)S(t)}{\gamma N}$ et en remplaçant $b(t)$ par l'équation de transmission $\log(b(t)) = \log(b_0) + \beta_1 NPI_1(t) + \beta_2 NPI_2(t)$, nous obtenons:

$$\log(\mathcal{R}_i(t_{ij})) = \log(b_0) - \log(\gamma N) + \log(S(t)) + \beta_1 NPI_1(t_{ij}) + \beta_2 NPI_2(t_{ij}) + u_i + \epsilon_{ij} \quad (1)$$

Dans cette équation, $\log(b_0)$ et $\log(\gamma N)$ sont des constantes et sont donc inclus dans le terme d'ordonnée à l'origine. En revanche, $\log(S(t))$ varie dans le temps et peut donc fausser les effets estimés de l'INP, un déplétion plus important des susceptibilités au cours de la période d'estimation entraînant un biais plus important.

Bien que les scénarios SIR soient utiles pour comprendre les défis sous-jacents de la procédure de régression en deux étapes, la simplicité du modèle SIR ne permet pas de saisir la complexité des scénarios du monde réel. Dans les scénarios plus réalistes, nous avons maintenu la déplétion des susceptibles à un faible niveau ($\leq 3\%$). Dans les données créées avec le modèle SEIRAHD (Figure F1), les estimations ponctuelles des modèles de régression en deux étapes présentaient un biais important, particulièrement prononcé pour la première INP (biais relatif allant de 18 à 25%) par rapport à la deuxième INP (environ 14 à 18%). De plus, les IC dérivés de ces modèles n'incluaient pas systématiquement les véritables valeurs de l'INP. Comme l'enchaînement de deux étapes d'analyse sous-estime l'incertitude de l'estimation finale, nous avons mis en œuvre une procédure de bootstrap en échantillonnant de manière répétée la distribution $\mathcal{R}_t$. Cette procédure bootstrap a élargi les IC résultants, mais ceux-ci n'incluaient la valeur réelle que pour l'INP 2 et non pour l'INP 1. En revanche, les IC à 95% pour les deux INP dérivés des modèles mécanistes couvraient la valeur réelle dans l'ensemble des 100 jeux de données, tandis que les estimations ponctuelles ne présentaient qu'un biais absolu et relatif minime (¡ 1% pour les deux INP).
En examinant les sources du biais élevé du modèle de régression en deux étapes, nous avons identifié des divergences au début de l'épidémie et un décalage dans l'estimation de $\mathcal{R}_t$ par EpiEstim lorsque le véritable $\mathcal{R}_t$ a subi des changements soudains résultant de la mise en œuvre ou de la levée des INP. Ces décalages

Déplétion de *S*	**2%**		**10%**		**20%**		**40%**		**60%**	
	Reg.	Mech.	Reg.	Mech.	Reg.	Mech.	Reg.	Mech.	Reg.	Mech.
INP 1										
Biais absolu	-0.02	0.00	0.10	0	0.21	0	0.40	0	0.65	0
Biais relatif (%)	1.2	0.2	7.0	0	14.8	0	27.4	0	45.0	0
IC 95% (%)	0	-	0	-	0	-	0	-	0	-
IC 95% bootstrap (%)	100	100	0	100	0	100	0	100	0	100
INP 2										
Biais absolu	0.05	0	0.20	0	0.33	0	0.42	0	0.48	0
Biais relatif (%)	6.6	0.1	24.5	0	40.9	0	51.9	0	59.5	0
IC 95% (%)	0	-	0	-	0	-	0	-	0	-
IC 95% bootstrap (%)	100	100	0	100	0	100	100	100	100	100

Table F1: Paramètres d'évaluation de la simulation SIR. Pour chaque scénario de déplétion des susceptibles, le biais absolu et relatif moyen et le pourcentage d'IC à 95% couvrant la valeur réelle sur 100 jeux de données simulés sont indiqués. Les colonnes indiquent le modèle d'analyse. Les lignes de l'IC indiquent le pourcentage d'ensembles de données pour lesquels l'IC à 95% couvre la valeur réelle. L'IC à 95% du modèle mécaniste a toujours été déterminé par bootstrap.
Reg. modèle de régression en deux étapes, Mech. modèle mécaniste, IC intervalle de confiance, INP intervention non pharmaceutique

ont conduit à une sous-estimation de la force de l'INP 1 et à une surestimation de l'INP 2, car le modèle de régression a estimé une moyenne sur la période d'implémentation des INP.

Outre la sous-estimation de l'incertitude, la déplétion des susceptibles au cours de la période d'étude et les problèmes d'estimation de $mathcal R_t$ peuvent donc fausser les paramètres d'efficacité des INP lors de l'utilisation de la méthode de régression en deux étapes. Nos résultats ont donc des implications significatives pour affiner la méthodologie utilisée pour estimer l'efficacité des INP.

Manuscrit 3: Diminution de l'immunité contre le SARS-CoV-2 au fil du temps

Une étape essentielle pour améliorer les études sur l'efficacité des INP et les autres modèles mathématiques utilisés pendant la pandémie de COVID-19 est le raffinement continu des paramètres d'entrée fixes, tels que la durée de l'immunité. Avec l'émergence du variant Omicron, une grande partie de la population a acquis une immunité hybride, c'est-à-dire une immunité issue à la fois de la vaccination et de l'infection naturelle. Pour adapter et améliorer les modèles aux nouveaux vari-

ants et sous-variants émergents, il est nécessaire de disposer de nouvelles données. L'un des principaux manques de connaissances concernait le niveau de protection immunitaire conféré par la vaccination antérieure et l'infection, ainsi que la durée de cette protection.

La Société canadienne du sang a fourni l'accès à des mesures d'anticorps de plus de 448,270 donneurs de sang au Canada entre avril 2020 et décembre 2023. Étant donné que les vaccins ciblent exclusivement la protéine spike, alors que les anticorps ciblant les protéines spike et nucléocapside sont produits en réponse à une infection, nous avons pu estimer les dates d'infection et de vaccination à partir des profils longitudinaux d'anticorps anti-spike (anti-S) et anti-nucléocapside (anti-N). Une augmentation substantielle des anticorps anti-N indiquait une infection, tandis qu'une augmentation des anticorps anti-S sans augmentation des anti-N indiquait une vaccination (Figure F2).

Nous avons utilisé les dates d'infection déduites pour évaluer l'association entre les niveaux d'anticorps anti-SRAS-CoV-2 et le risque d'infection dans les modèles de risques proportionnels de Cox. Nous avons modélisé l'effet des anticorps anti-S et anti-N sur le risque d'infection sous forme de splines flexibles, en tenant compte du risque d'infection de fond, de la circulation des variantes et de l'âge, du sexe et de l'origine ethnique des donneurs. À l'aide de modèles mécanistes, nous avons caractérisé plus précisément la dynamique de décroissance des anticorps anti-S et anti-N. Avec les paramètres estimés, nous avons simulé les titres d'anticorps sur une période de trois ans afin d'évaluer le temps nécessaire pour atteindre les seuils de protection définis avec les modèles de Cox.

Des titres plus élevés d'anticorps anti-S et anti-N étaient associés à un risque d'infection plus faible. Les titres d'anticorps anti-S présentaient une relation non linéaire avec le risque d'infection, avec un plateau de protection à des niveaux intermédiaires (10 à 1 000 U/mL) et une forte baisse des rapports de risques instantanés (*hazard ratio*, HR) en-deçà de ce niveau (figure F3). Les anticorps anti-N présentaient une relation plus linéaire, avec une augmentation de leur titre diminuant continuellement le risque instantané d'infection et offrant des hautes niveaux de protection. Les modèles mécanistes ont révélé que les niveaux des deux types d'anticorps diminuaient de manière biphasique, avec un déclin initial rapide suivi d'une décroissance plus lente. Les simulations ont montré qu'après trois ans, 48% des personnes ayant contracté une seule infection et plus de 80% de celles ayant contracté plusieurs infections avaient des taux d'anticorps anti-N détectables. Cependant, moins de 5% des personnes ayant contracté une seule infection et seulement 20% environ de celles ayant contracté plusieurs infections ont conservé des niveaux d'anti-N assurant une protection de 50% après deux

H!

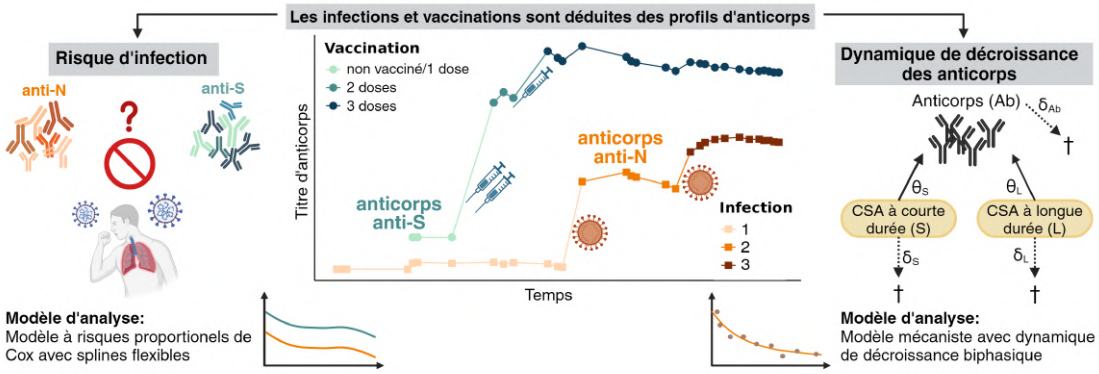

Figure F2: Aperçu des procédures et des objectifs du Manuscrit 3. Image créée avec BioRender (biorender.com)
CSA: cellule sécrétrice d'anticorps.

ans. Les taux d'anticorps anti-S ont chuté encore plus rapidement sous le seuil de protection de 50%, avec seulement environ 5% des individus ayant des taux d'anticorps supérieurs à ce seuil un an après l'immunisation.

Nous avons constaté que les anticorps anti-S et anti-N réduisent de manière significative le risque d'infection, même après l'émergence du variant Omicron. Si les anticorps sériques anti-N ne préviennent pas directement l'infection, ils servent de marqueurs indirects de la protection conférée par l'immunité naturelle. Nos résultats confirment que de multiples épisodes de vaccination sont nécessaires pour atteindre et maintenir des titres d'anticorps élevés afin d'assurer une protection durable. Ces résultats fournissent des indications précieuses pour orienter les stratégies de vaccination et les interventions de santé publique.

Conclusion

Cette thèse a porté sur l'application de modèles mathématiques aux données collectées pendant la pandémie de COVID-19 afin d'améliorer notre compréhension de la manière dont la propagation virale peut être contrôlée. Elle a abouti à plusieurs résultats importants : premièrement, elle a contribué à l'identification d'INP efficaces et a souligné l'importance d'une mise en œuvre rapide des INP. Pour les futures pandémies ou vagues de COVID-19, j'ai montré que les mesures de confinement pourraient être un bon instrument de santé publique pour freiner rapidement et radicalement la propagation. Toutefois, leurs coûts sociaux et économiques pourraient limiter leur faisabilité à long terme. D'une manière générale, plus les INP sont mises en œuvre rapidement, plus elles parviennent à contrôler la propagation virale. Deuxièmement, j'ai montré qu'un déploiement rapide et précoce des

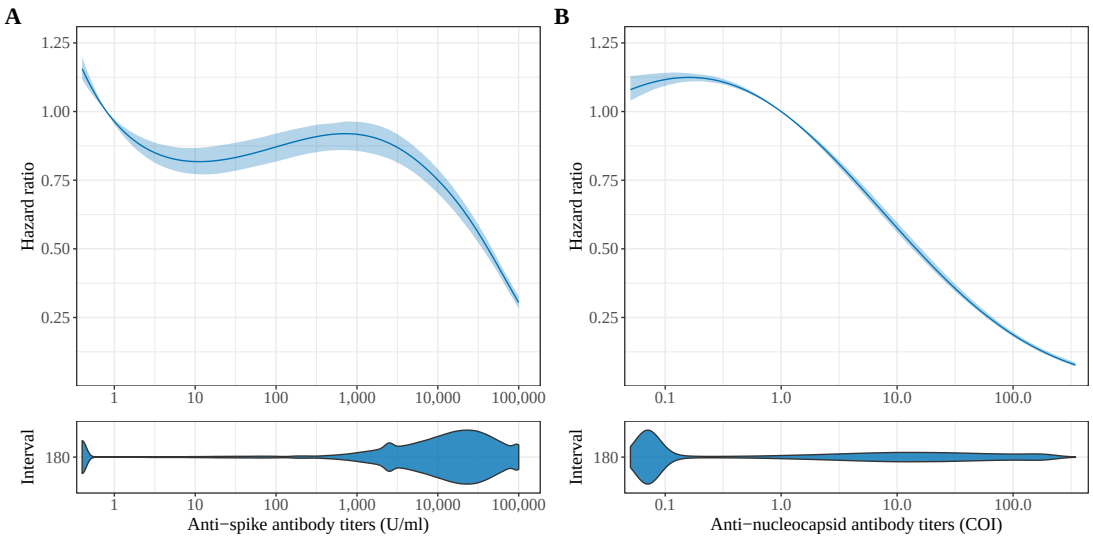

Figure F3: Rapports de risques instantanés ajustés de l'association entre les titres d'anticorps et le risque d'infection. Les rapports de risque et les IC à 95% correspondants sont indiqués pour la gamme des anticorps anti-S (panneau A) et des anticorps anti-N (panneau B). Les rapports de risque pour les anticorps anti-S ont été calculés par rapport au seuil de positivité du test fixé à 0,8, tandis que ceux pour les anticorps anti-N ont été évalués par rapport à un seuil de 1. Les rapports de risque ont été ajustés en fonction de l'âge, du sexe et de l'origine ethnique du donneur, de la différence hebdomadaire de séroprévalence et de la circulation des VoC. Les diagrammes en violon au-dessous indiquent la distribution des titres d'anticorps respectifs.

vaccins est essentiel pour freiner à la fois la transmission virale et les conséquences graves de la maladie. En outre, j'ai démontré que des titres élevés d'anticorps offraient une protection efficace contre l'infection. Ces titres élevés d'anticorps peuvent être atteints à la fois par l'infection et par la vaccination, mais ils diminuent rapidement en dessous des seuils nécessaires pour maintenir une protection élevée. La troisième contribution de ma thèse concerne la méthodologie utilisée dans les études d'efficacité des INP. J'ai montré qu'il fallait faire preuve de prudence lors de l'application de modèles de régression en deux étapes pour estimer l'efficacité des interventions, même s'ils permettent d'obtenir des résultats beaucoup plus rapidement qu'avec des modèles en une étape intégrant la dynamique épidémiologique.

1

Introduction

1.1 Background

The COVID-19 pandemic, caused by the emerging SARS-CoV-2 virus, represents an unprecedented global health crisis in the 21st century. Throughout multiple pandemic waves, it led to extensive morbidity and mortality and put immense pressure on healthcare systems and whole societies worldwide. In the absence of vaccines or other medical treatments during the early stages, governments were compelled to implement non-pharmaceutical interventions (NPIs) to prevent healthcare systems from becoming overwhelmed and to reduce premature deaths. These interventions were often mandated urgently and with a limited evidence base to guide decisions.

Mathematical models have been essential tools to provide decision-makers with critical knowledge, such as the speed of viral reproduction, forecasts of healthcare resource needs, and potential outcomes of various public health strategies. Numerous studies used various types of methodologies to estimate the effectiveness of NPIs, especially during the first wave of the pandemic. However, there is large variation in the results, ranging from non-effective to highly effective for almost all assessed NPIs. Therefore, despite the vast amount of research, the long-term effectiveness of NPIs remains uncertain, particularly after the emergence of viral variants of concern and the introduction of vaccines. A second research gap

emerges in the methodology itself: how do different methodological approaches affect the conclusions about NPI effectiveness?

After the exceptionally fast development and distribution of vaccines, NPIs could be relaxed gradually. While vaccines were essential to curbing the spread, the quantification of lives saved by vaccines is an open debate. Moreover, the effectiveness of vaccines against infection decreased over time due to two factors: (1) the natural waning of immunity, and (2) the emergence of new viral variants with increased transmissibility and immune-escaping mutations. Consequently, frequent booster doses may be necessary to maintain sufficient immunity. Nevertheless, the protection conferred by vaccines against severe disease remained high over time.

Many studies have examined the dynamics of anti-spike antibodies elicited by vaccination as neutralizing anti-spike antibodies have been identified as a correlate of protection. However, the specific overall antibody levels that confer protection against infection—especially against immune-evasive variants like Omicron—are still unclear. Moreover, much less is known about other components of immunity, such as anti-nucleocapsid antibodies or mucosal immunity, which are only elicited by natural infection. Furthermore, studies about the long-term dynamics and protective effects of anti-SARS-CoV-2 antibodies in large cohorts are lacking, leaving another gap in understanding the broader immunological landscape of COVID-19.

1.2 Objectives

The objectives of this thesis are threefold:

1. To estimate the population-wide effectiveness of interventions against COVID-19 in France, focusing on both NPIs and vaccines, and using high-quality data. NPI and vaccine parameters will be estimated with a mechanistic model, which is uniquely suited to the research area, as it allows incorporation of biological information on the course of disease and protection through vaccination. Simulations of counterfactual scenarios with the same model will be conducted to illustrate the effects of timely implementation of NPIs and vaccines or, in contrast, the effects of the absence of vaccines.

2. To evaluate comparatively the performance of different methodologies used in NPI effectiveness studies. To this end, the mechanistic model developed in objective 1, which estimates all parameters in one step, will be compared to a two-step regression model, which first estimates epidemic indicators and then regresses them on NPI variables. The potential sources of bias for both models will be explored.

3. To estimate the risk of infection based on antibody levels in a large cohort of Canadian blood and plasma donors and identify potential protective thresholds of anti-spike and anti-nucleocapsid antibodies. Furthermore, the waning dynamics of these antibodies will be characterized, particularly the time required for antibody levels to fall below these protective thresholds.

1.3 Format

The thesis is comprised of three manuscripts, each addressing the research objectives stated above. Prior to presenting the manuscripts, supporting chapters are included to provide essential context. Chapter 2 reviews the relevant scientific literature, identifying the gaps that the thesis aims to address. Chapter 3 introduces the models I used in my thesis research. Chapters 4 to 6 correspond to the three main objectives. Specifically, Chapter 4 assesses the effectiveness of NPIs and vaccines against COVID-19 in France using a mechanistic model. Chapter 5 evaluates the performance of this model against a more commonly used, but simpler, methodology for estimating NPI effectiveness. Chapter 6 estimates the effect of antibody levels on infection risk, with the aim of establishing protective thresholds. This chapter also models the waning of immunity and predicts when individuals are likely to fall below these thresholds. Finally, Chapter 7 synthesizes the findings from the three manuscripts, discusses the broader implications of the results, addresses common methodological challenges, and Chapter 8 provides an outlook for future research.

2

Review of the Literature

2.1 Brief overview of the COVID-19 pandemic

The coronavirus disease (COVID-19) pandemic was first detected as an outbreak of pneumonia in Wuhan, China, in December 2019 [2, 3]. The disease was caused by a newly emerging virus, which was subsequently named severe acute respiratory syndrome coronavirus 2 (SARS-CoV-2) [4] and spread rapidly around the globe. The World Health Organization (WHO) declared the SARS-CoV-2 outbreak a pandemic on March 11, 2020 [5]. Since then, the COVID-19 pandemic has caused substantial morbidity and mortality and has taken a heavy toll on healthcare systems globally. The severity of COVID-19 disease varies widely, from mild or asymptomatic to severe respiratory distress and death. While asymptomatic disease is not harmful for infected individuals, asymptomatic transmission complicates disease control from a public health perspective [6, 7]. If symptoms are developed, they are usually mild; however, the risk of severe symptoms and death increases with age, up to an estimated infection fatality ratio (IFR) of 8.3% in patients 80 years and older [8]. Other risk factors for severe disease include underlying comorbidities such as cardiovascular disease, chronic kidney disease, chronic pulmonary disease, diabetes, cancer, immunodeficiencies, and obesity [9–11]. These associations persist even after vaccination, although vaccines are highly effective at preventing severe disease [12].

Multiple sources have produced estimates regarding the total number of confirmed cases as well as COVID-19 related deaths. From the start of the pandemic until March 2024, the WHO reported 775 million cases and just over 7 million COVID-19 deaths [13]. Similarly, the widely used Johns Hopkins University coronavirus dashboard reported 676 million confirmed COVID-19 cases and close to 7 million COVID-19 deaths by October 2023 [14]. However, substantial underreporting is likely, particularly for cases, due to a high proportion of asymptomatic infections and a lack of testing infrastructure, especially at the outset of the pandemic. Furthermore, the WHO estimated 14.83 million excess deaths globally from the beginning of the pandemic until December 2021 [15], 2.74 times more than the reported COVID-19 deaths. Another study by Wang et al. suggests that 18.2 million global deaths (95% uncertainty interval 17.1–19.6 million) were caused by the COVID-19 pandemic between Jan 1, 2020, and Dec 31, 2021 [16], though their methodology has been heavily debated [17–20]. Excess mortality includes deaths from the virus itself as well as deaths due to indirect impacts of the COVID-19 pandemic, such as healthcare disruptions.

Indeed, the overall impact of the COVID-19 pandemic was not limited to COVID-19 patient surges in hospitals, but also included the effects of government interventions. Many countries implemented highly restrictive non-pharmaceutical interventions (NPIs) avoid overwhelming the healthcare systems until vaccines were available. These NPIs deeply interfered with daily life, economic activities, and personal freedoms. Healthcare systems were restructured to manage surges of COVID-19 patients, leading to a neglect of routine care. For example, the initial pandemic waves saw a marked reduction in healthcare services such as cancer screening [21], management of chronic diseases [22–25], and the administration of childhood vaccines [26]. Moreover, the COVID-19 pandemic (as most, if not all infectious diseases) proved to be not only an infectious disease problem but also exacerbated existing social and health inequalities, disproportionately affecting disadvantaged populations [27]. Significant geographical inequalities in COVID-19 mortality have been observed, with higher case and mortality rates in areas of greater socioeconomic disadvantage [28, 29]. The disproportionate outcomes among those with chronic diseases were seen particularly in under-resourced or rural areas [22]. Striking inequalities were also evident in the global vaccine distribution and through differential vaccination rates, with lower vaccination rates in economically disadvantaged populations [30]. The WHO officially declared the pandemic over on May 5th, 2023 [31], but SARS-CoV-2 continues to spread endemically worldwide.

2.2 SARS-CoV-2 biology

Coronaviruses are enveloped, positive-sense, single-stranded RNA viruses, and SARS-CoV-2 belongs to the betacoronaviruses of group 2B. The SARS-CoV-2 genome encodes four structural proteins—spike (S), envelope (E), membrane (M), and nucleocapsid (N)—as well as sixteen non-structural proteins (nsp1-16). Genomic analyses of SARS-CoV-2 reveal a high similarity to coronaviruses of bat origin, and a 79% similarity to SARS-CoV [32]. However, the exact origin of SARS-CoV-2 remains a subject of scientific debate, with most studies supporting the hypothesis of a zoonotic event [33–36].

2.2.1 SARS-CoV-2 life cycle

Understanding the SARS-CoV-2 life cycle is crucial for grasping the basics of its transmission. Its life cycle starts with contagion: The virus is primarily spread through respiratory droplets when an infected person coughs or sneezes, and via aerosols (Figure 2.1) [37–39]. Transmission through contact with contaminated surfaces is also possible, though less common [37]. Droplet and aerosol transmission enable SARS-CoV-2 to have a relatively high basic reproduction number ($\mathcal{R}_0$), estimated at 2.87 (95% confidence interval, CI, 2.39–3.44) for the original strain, meaning that each infected person is likely to infect 2-3 others [40]. The virus is particularly contagious in indoor settings with poor ventilation, which can lead to superspreading events [41].

The infectious cycle of SARS-CoV-2 begins when virions enter the upper airways. The spike protein binds to the human angiotensin-converting enzyme 2 (ACE2) receptor on the surface of target cells in the respiratory tract[1]. The S1 subunit of the spike protein facilitates receptor binding, while the S2 subunit mediates membrane fusion between the virion and the host cell [44]. Following fusion, the viral genome is released into the host cell cytoplasm, where it is translated by the host cell machinery (Figure 2.2). Viral RNA is replicated, new viral proteins are synthesized, and both proteins and RNA are packed into new viral particles. Mature virions are transported to the cell surface in vesicles and secreted from infected cells by exocytosis [45]. Once released, the virus can infect other cells.

After an incubation period of approximately 4-5 days (for the ancestral strain [46]), viral replication and release in the lung cells can cause respiratory symptoms (e.g. coughing and sneezing) and non-specific disease symptoms such as fever, myalgia, and headache. Loss of smell and taste are also possible. With the ancestral

[1]The ACE2 receptor is expressed ubiquitously in the human body. Therefore, SARS-Co-V-2 can spread and replicate in other organs, which can lead to local damage outside of the lungs [43].

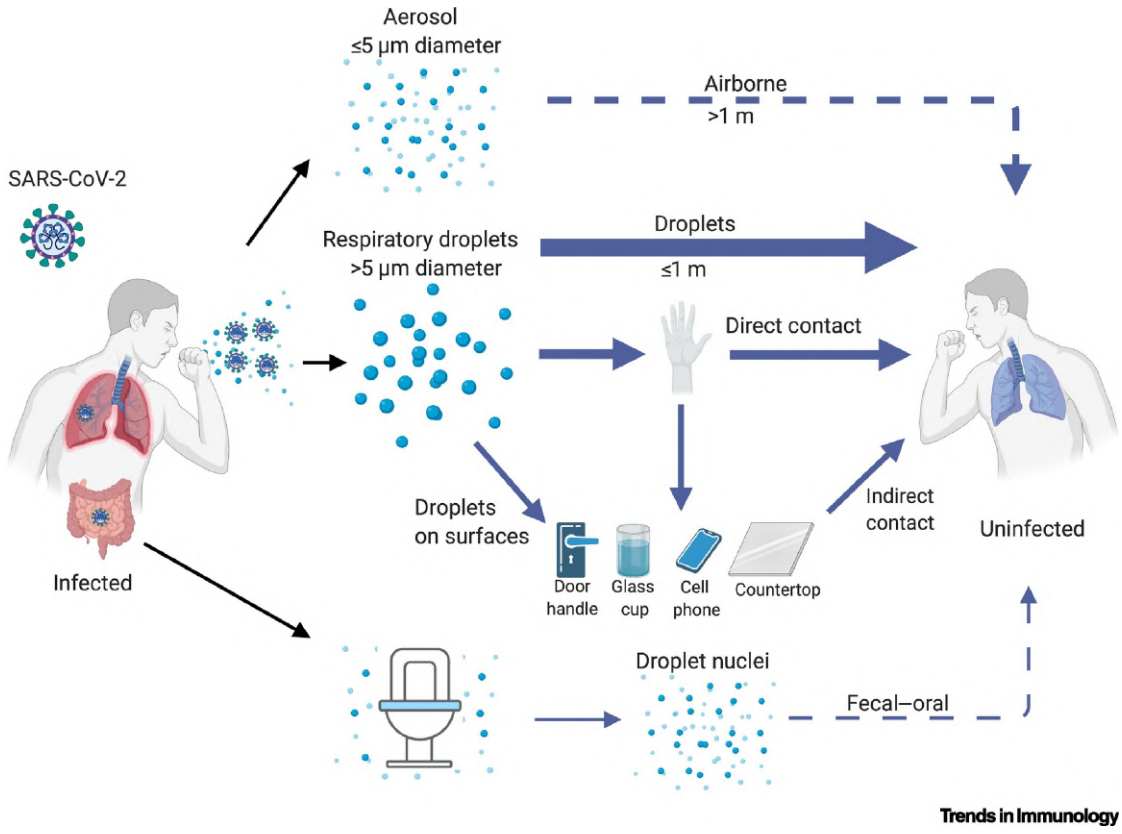

Figure 2.1: SARS-CoV-2 transmission routes. From reference [42]

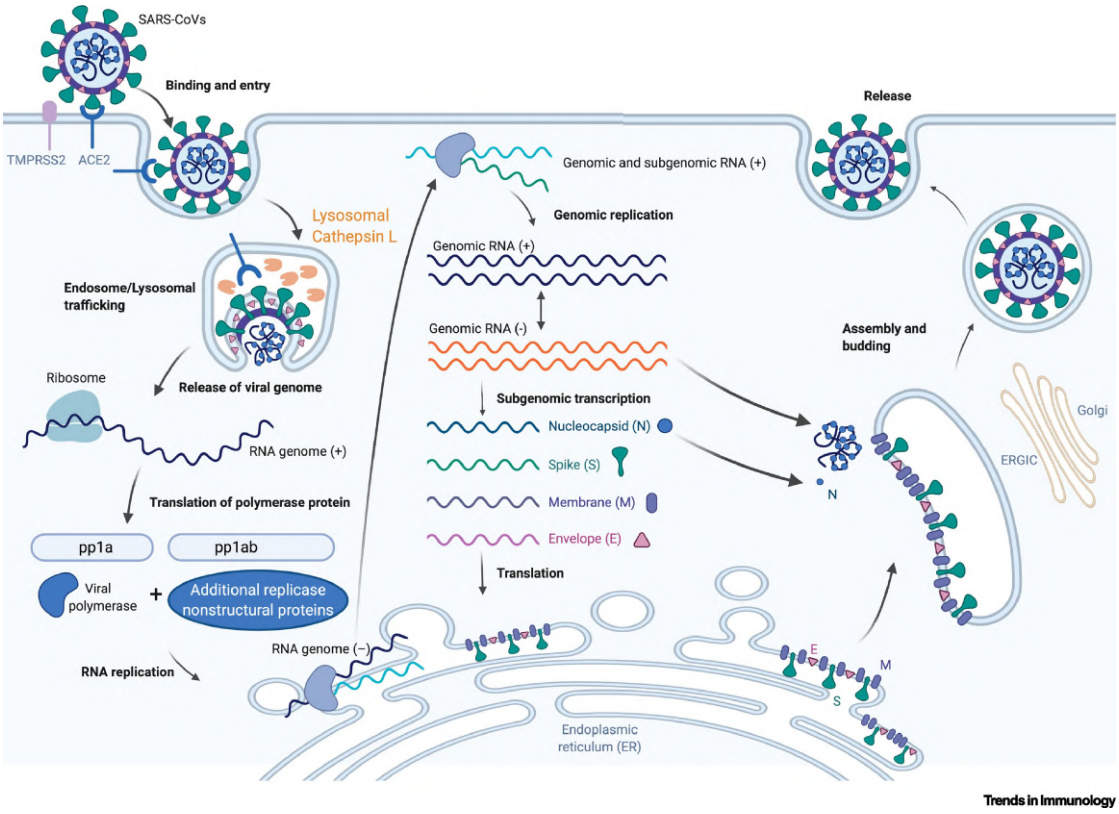

Figure 2.2: SARS-CoV-2 lifecycle. The SARS-CoV-2 lifecycle begins with the spike protein binding to the ACE2 receptor, followed by host cell entry via TMPRSS2 or cathepsin L-mediated fusion. The RNA genome is then released, translated, and replicated within virus-induced double-membrane vesicles. Structural and accessory proteins are assembled in the ER–Golgi intermediate compartment, leading to the formation and secretion of new virions. From reference [42]

strain, a high proportion of infections were asymptomatic, with estimates ranging from 15.6% [47] to 40% [48]. However, it is clear that asymptomatic individuals can still transmit the virus [49].

Within-host modeling of viral load measurements in sputum and pharyngeal swabs confirms high initial viral loads in the upper airways at symptom onset, which decline over the course of 1-2 weeks, once an effective immune response is mounted by the host [50–53]. There is uncertainty about the viral load in asymptomatically infected individuals: Some studies describe little to no difference in viral load between pre-symptomatic, asymptomatic and symptomatic patients [52], while other studies found that infectiousness correlated well with the logarithm of viral load [54, 55]. Individuals are highly infectious in the early symptom phase, but also before symptom onset. Further, viral RNA has been detectable in sputum even after symptoms resolved, suggesting prolonged shedding and potential infectivity [56].

2.2.2 Viral evolution and SARS-CoV-2 variants

SARS-CoV-2 relies on its RNA-dependent RNA polymerase for replication. The error rate of this polymerase is estimated to be around 1-2 mutations per million nucleotides [57], which results in a high number of mutations and therefore fast viral evolution. Additionally, host-mediated genome editing by innate immune mechanisms may introduce mutations into the SARS-CoV-2 genome, and recombination of genomes is possible when a host is co-infected with two genetically distinct viruses [57] (Figure 2.3). While most mutations are neutral or detrimental to the virus, some can lead to increased transmission or immune-escaping capabilities.

The first divergent SARS-CoV-2 lineages appeared about eight months into the pandemic (for a timeline of viral variants in France and Canada, see Figure 2.4). Each variant has several designations based on the nomenclature used by distinct phylogenetic classification systems, among which the Pango nomenclature is most commonly referenced [59, 60]. The WHO later classified the most notable variants as *variants of concern* (VoCs) and named them using Greek letters [61, 62]. VoCs are characterized by higher transmissibility, immune evasion, and increased pathogenicity [63–66]. For example, the D614G mutation and H69/V70 deletion increased viral fitness without significant immune escape in the Alpha variant (Pango B.1.1.7 lineage) [67, 68], while mutations like E484K and N501Y significantly reduced vaccine-induced neutralization of Alpha [69, 70]. The Delta variant (Pango B.1.617.2 lineage), which emerged in India during the spring of 2021, had a combination of mutations that conferred advantages in transmissibility, infectivity, and immune evasion [71–73]. These properties of increased viral fitness allowed the VoCs to rapidly outcompete the ancestral strain and other, less transmissible, previously circulating VoCs.

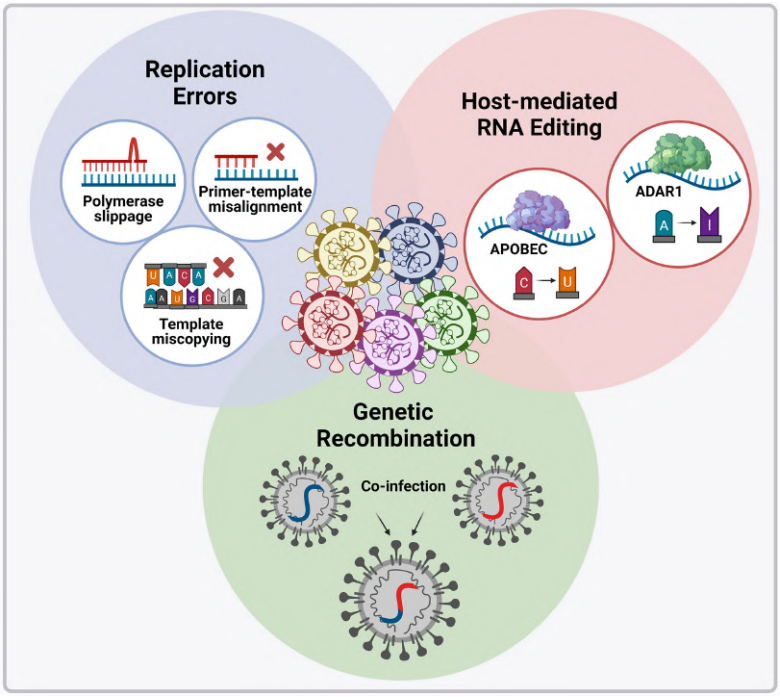

Figure 2.3: Mechanisms of SARS-CoV-2 viral evolution. Nucleotide changes may arise naturally through replication errors or through host-derived RNA editing enzymes (APOBEC, ADAR1), which introduce specific point mutations (C to U and A to I) into the viral genome. Recombination may occur if two viral variants co-infect the same cell, leading to the packaging of genetic material from both into a single virion. From reference [58].

The emergence of the Omicron variant (B.1.1.529) in October 2021 marked the start of a new phase of the pandemic with subsequent sweeps of Omicron sub-lineages [57, 74]. Omicron's extremely high transmissibility and immune evasion from previous infection- and vaccination-acquired immunity drove its rapid spread [75–79], although it generally caused less severe disease than previous VoCs [80, 81]. The impact of VoCs on immunity will be discussed in section 2.5.6, after having introduced relevant aspects of the immmunity towards SARS-CoV-2.

2.3 Immunity to SARS-CoV-2

Mounting an effective immune response is crucial for clearing a SARS-CoV-2 infection and involves a complex, multi-step process. The innate immune system acts as the first line of defense, limiting viral replication and spread, and activating the adaptive immune system. Next, the coordinated response of the adaptive immune system leads to clearance of the virus from the body. After the infec-

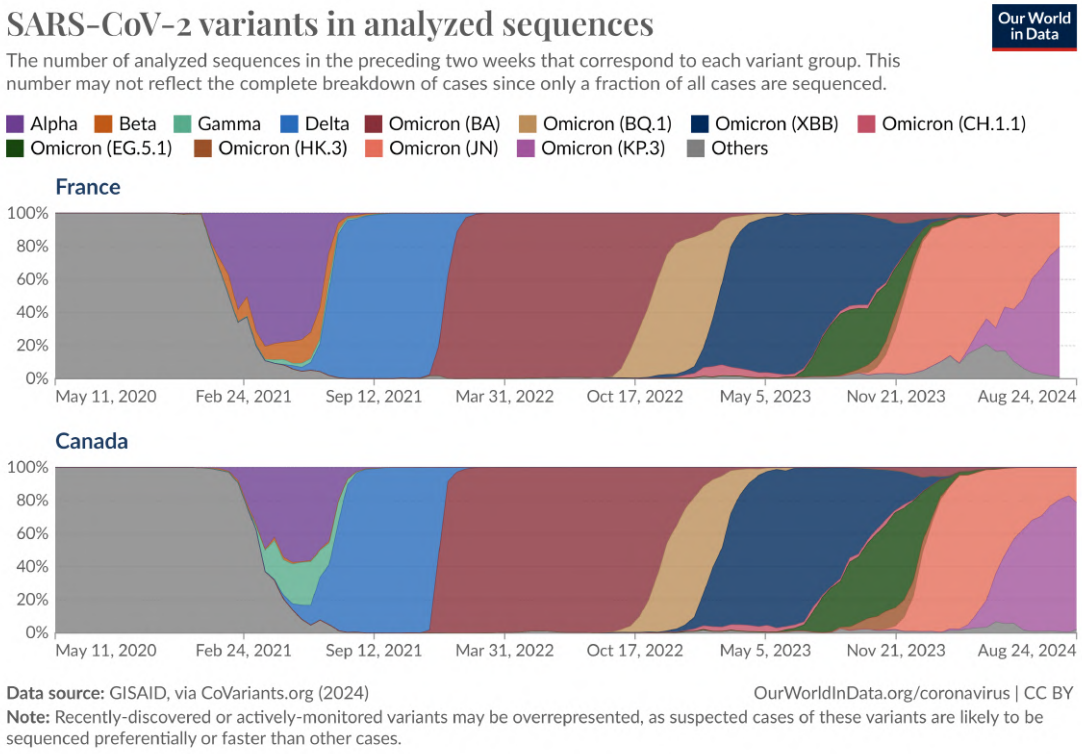

Figure 2.4: Timeline of SARS-CoV-2 variants of concern in France and Canada. Figure generated on OurWorldInData [82].

tion is resolved, the adaptive immune system's memory cells—memory B cells and memory T cells—persist long-term. These memory cells provide lasting immunity by rapidly reacting to future exposures to the virus, thereby reducing the probability of (symptomatic) reinfection. If reinfection occurs, the disease severity is usually lower, as the immune system is able to mount a faster and more efficient response. Thus, immunological memory is a key factor in preventing transmission and severe disease in subsequent SARS-CoV-2 infections. In the following section, I review the functions of the immune system in general and the immune reaction to SARS-CoV-2 in particular.

2.3.1 Innate immunity

The detection of a foreign entity triggers the human immune system. As a first line of defense, the innate immune response is activated by cellular pattern-recognition receptors, which react to general pathogen-associated molecular patterns. The innate immune system has three primary functions: 1) limiting viral replication within infected cells, 2) creating an antiviral environment in the surrounding tissue, which includes recruiting effector cells of the innate immune system (such as macrophages, neutrophils, and dendritic cells), and 3) initiating the adaptive immune response [83]. The activation of receptors on innate immune cells initiates signaling pathways that result in the release of pro-inflammatory cytokines, type I and III interferons (IFNs), and the elimination of infected cells (Figure 2.5). In order to establish a sustained infection, viruses must interfere with the innate immune system. Otherwise, the infection would be cleared efficiently without symptoms, precluding the potential for spread. SARS-CoV-2 effectively evades early innate immune responses, such as IFNs [84–86] and pro-inflammatory cytokines [83]. Moreover, SARS-CoV-2 infection causes suppression of host cell protein synthesis, which enables more efficient translation of viral mRNA and attenuates immune responses [86]. While the innate immune response is indispensable for controlling viral infections, excessive pro-inflammatory cytokine production can cause significant tissue damage and is often observed in severe disease [45, 83].

2.3.2 Adaptive immunity

The adaptive immune response consists of cellular components—$CD4^+$ and $CD8^+$ T-cells—and humoral components—pathogen-specific antibodies produced by B-cells. Both types of cells recognize specific antigens of pathogens, and, in contrast to the innate immune system, can mount a pathogen-targeted response. In simple terms, antibodies prevent viruses from infecting cells, while T-cells eliminate viruses that have already entered cells. Antibodies can also induce the killing of virally infected cells, an important mechanism in vivo [87, 88].

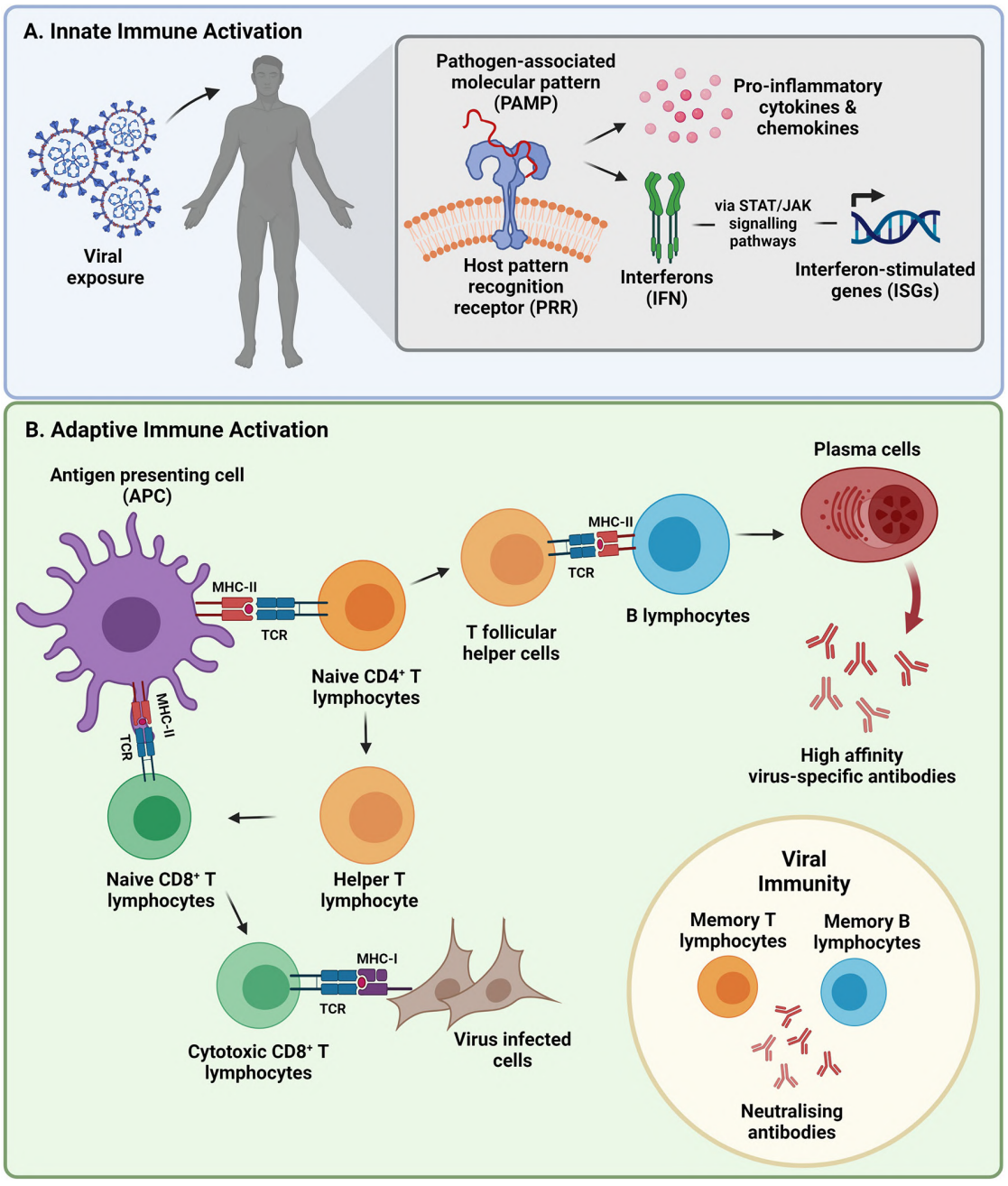

Figure 2.5: Overview of the immune response to viral infection and the development of immunity. A: The innate immune response is activated within hours of viral exposure, serving as the first line of defense by releasing antiviral molecules at the infection site. **B:** The adaptive immune response is triggered days later, following priming by the innate system, and initiates pathogen-specific cellular and humoral responses. Immune memory cells persist after viral clearance, providing long-term immunity. From reference [58]

STAT, signal transducer and activator of transcription; JAK, Janus kinase; CD, cluster of differentiation; MHC, major histocompatibility complex; TCR, T-cell receptor.

2.3.2.1 Humoral adaptive immunity

The humoral immune response produces highly specific antibodies, or immunoglobulins (Ig), to foreign antigens. The recognition of an antigen with membrane-bound antibodies (also called B-cell receptors) activates B-cells to proliferate and differentiate into antibody-secreting plasma cells (ASCs) and memory B-cells. ASCs secrete large amounts of antibodies to neutralize antigens, while memory B-cells provide long-term immunity by responding quickly to future encounters with the same antigen. B-cell activation also triggers a process called "somatic hypermutation" (SHM), where the B-cells undergo rapid mutations to produce higher-affinity antibodies. The affinity maturation also involves switching from less specific IgM to higher-affinity IgA and IgG.

The vast majority of SARS-CoV-2 infected individuals seroconvert (i.e. produce detectable levels of antibodies in serum) within 5-15 post-symptom onset (PSO), with about 90% of individuals having seroconverted by day 10 PSO [89, 90] (Figure 2.6). The antigenic targets which are most frequently monitored are the spike and nucleocapsid proteins. IgM, IgA, and IgG are detectable approximately at the same time [91]. IgM follows a rise and fall pattern, with a peak two to five weeks PSO and a quick decline afterwards [90, 92, 93]. IgG levels peak around 25 days PSO and are much more durable than IgM antibodies [92–95]. IgA antibodies, which play a crucial role in mucosal immunity, are thought to have approximately the same dynamics as IgM [91, 93, 96], but are less studied overall [90, 97]. A strong positive correlation between disease severity and the height of antibody peak levels as well as response duration has been documented [91, 98–100]. Independent correlations with age, sex, and other factors are debated, but not consistent across studies [101].

Antibodies provide protective immunity mainly by preventing the spike protein from binding to the ACE2 receptor on host cells. Thus, the spike protein is the sole target of SARS-CoV-2 neutralizing antibodies (nAbs), and therefore the most relevant antigen for vaccine development [91]. However, the nucleocapsid protein is still an important antigenic target, as antibodies targeting it can trigger the removal of already infected cells [102].

The majority of antibody measurements in humans are conducted on blood samples, as this method is the most convenient for evaluating immune responses. However, serum antibodies might not accurately represent antibody levels in mucosal tissues, which are more relevant for protection from subsequent infection [89]. Both IgG and IgA are produced in mucosal tissues but are frequently measured in serum. However, the close connection between the lungs and the circulatory system suggests that IgG and IgA levels in serum are likely mirrored in the mucosal

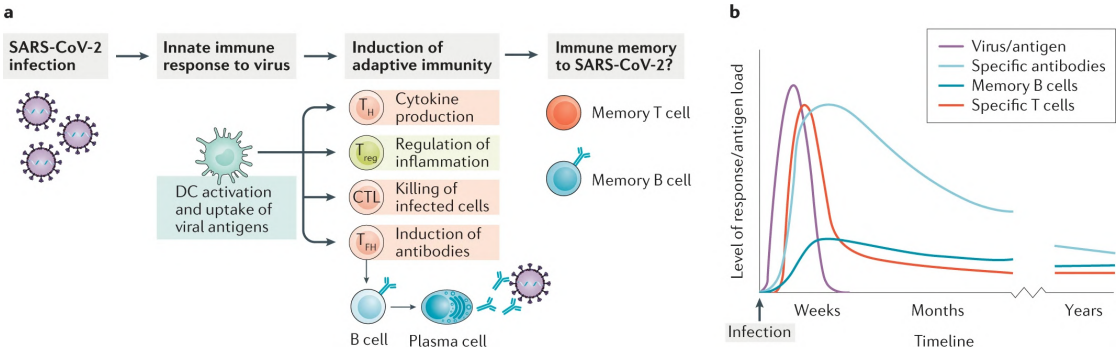

Figure 2.6: Timeline of immune reactions to SARS-CoV-2. From [103]

tissues of the airways. Indeed, a strong correlation between levels of spike-specific serum and mucosal IgG has been observed [104].

2.3.2.2 Cellular adaptive immunity

SARS-CoV-2 specific T-cells can be detected as early as 2 to 4 days PSO [105] (Figure 2.6). $CD4^+$ T-cells have been detected after almost all SARS-CoV-2 infections, and are associated with control of primary infection. In contrast, poor disease outcomes correlate with scarcity of naive T-cells, which decrease with age [106]. $CD4^+$ T cells differentiate into various helper and effector cell types and have the capacity to 1) help $CD8^+$ T-cells or B-cells, 2) recruit innate immunity cells, 3) have direct antiviral activities, and 4) facilitate tissue repair. $CD8^+$ T cells are associated with better COVID-19 outcomes, as they can kill infected cells, but are less consistently observed than $CD4^+$ T-cells [106].

2.4 Non-pharmaceutical interventions

In the battle against infectious diseases like COVID-19, two main strategies are employed to curb viral spread and thus reduce the burden on healthcare systems: non-pharmaceutical interventions (NPIs) and vaccines. NPIs encompass a range of actions, policies, or strategies designed to curb disease transmission without the use of medications. These interventions, also known as public health and social measures (PHSM), are critical at the onset of outbreaks when vaccines or treatments are not yet available or equitably distributed [107]. NPIs can reduce pathogen transmission by either reducing the number of transmission-relevant exposures and/or making them safer. It is important to note that NPIs not only serve as the first line of defense in public health emergencies but also continue to play an important role alongside medical countermeasures throughout the whole duration of an outbreak.

There are many ways to group and classify NPIs (see Section 2.4.2). For the purpose of this literature review, they were grouped into these broad categories:

- **Containment and closure measures:** these include lockdowns, stay-at-home orders, social distancing, restrictions on gathering sizes, and closures of public spaces such as schools, workplaces, and businesses.
- **Health system interventions:** strategies like contact tracing, testing policies, quarantine measures, and public information campaigns fall into this category.
- **International or domestic travel restrictions:** Measures to limit or control cross-border or across-region movement to prevent the spread of the virus.
- **Individual hygiene measures:** these include practices like mask-wearing and hand washing, which are critical in reducing transmission on a personal level.
- **Economic measures:** although not strictly NPIs, economic interventions like income support or governmental stimulus spending often accompany NPIs to mitigate their socioeconomic impacts.

During the early stages of the COVID-19 pandemic, it became clear that strong NPIs were necessary to stop the exponential spread of SARS-CoV-2. Governments around the world rapidly implemented a broad spectrum of NPIs in response to the evolving situation. NPI implementation strategies were highly heterogeneous and based on a multitude of country-specific factors, such as the severity of local outbreaks, political and social factors, and economic conditions [108]. These interventions were instrumental in "flattening the curve" of the epidemic, thereby preventing the overwhelming of healthcare systems until vaccines could be developed and distributed.

Before the COVID-19 pandemic, the effectiveness of most NPIs was not well understood, and much of the existing literature focused on seasonal or pandemic influenza [109]. Recommendations were limited to a few NPIs like hand hygiene and respiratory etiquette, surveillance and case reporting, and rapid viral diagnosis [110]. Interventions like widespread mask use were often discouraged due to practical constraints [109]. Therefore, in the beginning of the COVID-19 pandemic, NPIs were implemented without a clear knowledge base of their effectiveness, and many scientific recommendations were given based on infectious disease models [111, 112].

Evidence of the effectiveness of individual NPIs is, however, of great importance, as it helps policymakers implement the most effective and cost-efficient measures to control the spread of an epidemic. Moreover, it is important to develop evidence so that the benefits of NPIs can be weighed against their detrimental societal and economic impacts [113]. During the COVID-19 pandemic, the evidence base grew due to a plethora of effectiveness studies being conducted, but the lack of a robust pre-existing knowledge base led to researchers from diverse fields approaching NPI assessment with a wide range of methodologies [114]. Disentangling the effectiveness of individual NPIs is inherently challenging, in part due to the simultaneous implementation of multiple interventions, the dependence of implemented NPIs on the epidemiological situation, and the infeasibility of controlled trials. In what follows, I will review the literature on NPI effectiveness and the methodologies used for estimation.

2.4.1 Effectiveness studies of non-pharmaceutical interventions

Studies assessing the effectiveness of NPIs during the COVID-19 pandemic have yielded a wide range of results, from findings of ineffectiveness to evidence of significant impact for each NPI. This variation in outcomes can be attributed to several factors, including differing methodological approaches, data sources, definitions of NPIs and combinations of NPIs implemented together, timing of NPI implementation, geographical scope, and populations studied. Heterogeneity in approaches is not inherently negative, as it allows for the assessment of the robustness of results across different approaches and assumptions. However, variation presents challenges for study comparability in systematic reviews and meta-analyses, which are crucial for drawing conclusive knowledge. Moreover, it can also introduce bias when a significant portion of the methods lack validity.

Systematic reviews Several systematic reviews have been conducted to summarize NPI effectiveness studies, but each review only includes a subset of the available studies [115–123]. This can be justified by the timing and specific scope of each review, such as focusing solely on mask-wearing [124] or school closures [122, 123], as well as inclusion and exclusion criteria regarding study design, which were sometimes highly restrictive. For example, some reviews only included studies that used COVID-19 deaths as outcomes [117], others excluded certain study types (e.g. those that involved mathematical modeling [117, 119]), or had very vague inclusion criteria [118]. However, each review captures only a portion of the available evidence, which complicates NPI comparison and the generation of comprehensive evidence.
Systematic reviews have highlighted the low quality of many NPI effectiveness studies and high heterogeneity in findings [115, 116, 123]. However, there is a

general consensus that earlier NPI implementation leads to higher effectiveness in controlling viral spread [115, 116]. Most studies conducted on NPIs were based on data from the first wave of the pandemic, and therefore most systematic reviews only generated evidence on this period [114–116, 119].

All NPIs and summary indices A meta-analysis concluded that implementing any NPI led to an approximate 5% reduction in the daily growth rate of COVID-19 cases or deaths [115]. However, since the heterogeneity was high across studies and effectiveness of individual NPIs, the utility of a meta-analysis is somewhat questionable. Similarly, a pooled analysis of 149 countries found that implementing any physical distancing intervention was associated with a 13% reduction in COVID-19 incidence [125]. There are conflicting findings regarding the strength of NPIs parameterized in a stringency index [116, 126]. Some studies found strong associations between higher stringency and reduced transmission [127, 128], while others found no significant effect [129].

Lockdowns The impact of lockdowns on COVID-19 transmission has been extensively studied, with most research indicating significant reductions in COVID-19 indicators during and immediately after lockdowns [115, 116]. For example, one study in the U.S. found that lockdowns reduced the reproduction number $\mathcal{R}_t$ by 51% [130], and another study on European countries estimated an 81% transmission reduction during lockdowns [131]. Another U.S.-based study concluded that lockdowns were the only intervention that consistently lowered $\mathcal{R}_t$ below 1 [132], which means that the disease will eventually stop spreading. However, some studies reported more modest effects, with national lockdowns in European countries reducing $\mathcal{R}_t$ by only 25% [133], 13% [134] or even only 4% [135].
The variability in these findings is likely due to differences in how lockdowns are defined and the combination of other NPIs studied alongside them (for an in-depth discussion, see Section 2.4.2). For example, when additional measures such as business closures, cancellation of public events, and gathering bans are estimated on top of lockdowns, the incremental effectiveness of the lockdown or stay-at-home order may be diminished [134, 135]. However, if one assumes that all these NPIs are considered part of a lockdown, the effectiveness of the lockdown will be the combined effectiveness of the single NPIs and will thus be much higher.

Gathering bans The effect of added effectiveness can clearly be seen in studies that assessed gathering bans alongside lockdowns: for example, a ban on gatherings of more than 10 people was associated with a 19% reduction in transmission in a study by Liu et al. [130] and around 40% in two other studies that did not attribute high effectiveness to lockdowns [134, 135]. Another study found that cancelling small gatherings led to an 83% reduction in $\mathcal{R}_t$ [133]. In general, gathering bans

were found to be effective in reducing transmission, with their impact increasing as the permitted group size decreased [116, 134].

Business closures The effectiveness of business closures also varied depending on how they were assessed—whether as part of a broader lockdown or as an individual NPI. When evaluated independently, business closures were associated with significant reductions in COVID-19 growth rates, ranging from around a 5 percentage point reduction in daily COVID-19 growth rate in the U.S. [136] to a 27% reduction in Rt when non-essential businesses were closed in a European study [134].

School closures Closure of educational institutions was the most frequently assessed NPI together with lockdowns [114]. A systematic review by Mendez-Brito et al. found that school closures were among the most effective measures, as they based their assessment on how many studies found the closures effective [116]. Another review was more cautious, concluding that the effectiveness of school closures remains uncertain [123]. However, the majority of studies reported significant reductions in SARS-CoV-2 transmission rates, with some studies finding reductions as high as 73% [133] and 60% [134, 137]. A few studies found more modest reductions ($\mathcal{R}_t$ reduced by 10% [130]) or no significant impacts [136, 138]; this limited effect might be due to confounding from other NPIs which were implemented simultaneously or variations in the type of educational institutions that were closed.

Testing and contact tracing The effectiveness of testing and contact tracing strategies is difficult to assess because these NPIs will initially lead to more detected cases and therefore seem ineffective. An early study suggested that contact tracing and quarantine in Portugal did not reduce secondary cases of COVID-19, as the contact patterns of infected individuals simply shifted from the community to household members [139]. Regarding a more pertinent outcome, a systematic review did not find any evidence that testing and contact tracing strategies were associated with a reduction in COVID-19 deaths [116].

Border closures Studies conducted at the onset of the COVID-19 epidemic in China found that there was a high correlation between the movement out of Wuhan and the magnitude of the early epidemic [140]. Thus, it is not surprising that travel restrictions enforced by the Chinese government were estimated to decrease the daily rate of exportation by 81.3% [141]. Later studies in Europe also found that international border closures reduced transmission, with one study estimating a 10% reduction in $\mathcal{R}_t$ [135] and another one estimating a 56% decrease [133]. While border restrictions were thus effective in slowing down the early spread of the pandemic, they might have become less important once local transmission was established [142, 143].

Face masks and other hygiene measures Face masks were widely recommended both to protect individuals from SARS-CoV-2 infection and to control the spread of the virus from infected people. An early meta-analysis, which also included evidence from SARS-CoV-1 and MERS-CoV, suggested that mask-wearing reduced infections by 66%, with N95 masks being particularly effective [144]. In general, there is a consensus that masking is a very effective NPI [129, 130, 145]. For example, one modeling study concluded that mandating face masks early in the pandemic could have reduced national U.S. deaths by 19 to 47% [146]. Mask effectiveness was sometimes assessed in combination with other hygiene measures, such as handwashing or surface disinfection. One meta-analysis concluded that mask-wearing reduced transmission by 53%, that hand washing reduced transmission by the same amount, and that surface disinfection reduced transmission by 77% [119]. These measures seem unrealistically high and are likely confounded by other health-protective behaviors. Conversely, Haug et al. ranked environmental measures such as surface disinfection as the least effective NPIs [133].

Second and third-wave studies The majority of NPI effectiveness studies are focused on the first wave of the pandemic. Only a few studies have assessed NPIs implemented during the second and third waves, which were more complex to analyze due to more overlapping NPIs, increased diversity in NPI strategies, the introduction of vaccines, the appearance of VoCs, and changing population behavior due to pandemic fatigue. All conducted studies agree that while NPIs continued to reduce transmission during these later waves, their effectiveness was diminished compared to the first wave [147–149]. Specifically, the effectiveness of lockdowns was found to decrease over time [1, 149, 150]. Curfews—which had rarely been implemented during the first wave, or only in combination with stay-at-home orders—became more common in later waves and were estimated to reduce transmission by 13% [147] or approximately 30% [1].

2.4.2 Summary of NPI effectiveness assessment methodologies

In this section, I review the differences in methodologies across NPI effectiveness studies in detail, as they are an important factor contributing to study heterogeneity.

Outcomes Studies on NPI effectiveness used a wide range of health-related outcomes or proxy outcomes to measure their impact. Commonly used outcomes include confirmed SARS-CoV-2 cases or incidence rates [119, 125, 133, 151], though case numbers were not reliable due to heavy underreporting of cases, especially in the first wave of the pandemic [152]. Moreover, reporting guidelines and the availability of tests changed frequently. Therefore, many studies opted for epidemi-

ological indicators that were hypothesized to be have a more consistent relationship with the true infection incidence, such as hospital or intensive care unit (ICU) admissions and COVID-19 deaths [119, 131, 153]. An alternative approach was to use metrics believed to be independent of the reporting process or where the same bias would uniformly apply across all reported numbers, effectively cancelling it out. Such metrics are the case growth rate [149], the death growth rate [146, 154], and the reproduction number $\mathcal{R}_t$, which are calculated in intermediate steps, and then used in further analyses. Especially $\mathcal{R}_t$ has been widely used in studies as an indicator of transmission dynamics [1, 130, 131, 133, 147, 155]. However, even the calculated metrics can be biased if reporting of the indicators used to derive $\mathcal{R}_t$ is not consistent across populations and over time.
Mobility tracking using mobile phone data has also been used as an endpoint of NPI studies to represent either a surrogate outcome for more relevant epidemiological data or an indicator for population compliance with the imposed measures. During the COVID-19 pandemic, mobility data could be obtained from internet and technology companies like Google [156], Apple (no longer available online), and Baidu [157].
Epidemiological data was usually obtained from national or sub-national health authorities or other governmental bodies [114]. Additionally, large international databases were created to provide and consolidate data across countries. Notable examples include the database by the European center of disease control (ECDC[158], e.g. used by reference [131]), the Johns Hopkins University dashboard [14] (e.g. used by reference [133]), Worldometer [159] (e.g. used by reference [130]), and Our World in Data [82] (e.g. used by reference [153]).

Exposures Several databases were created to track NPI implementation types and dates across different regions during the COVID-19 pandemic:

- Oxford COVID-19 Government Response Tracker (OxCGRT): this database gathered global NPI information from 2020-2022 [126]. It also features a stringency index, an index which summarizes the number and severity degree of policies in place in a given area.
- Complexity Science Hub COVID-19 Control Strategies List (CCCSL): this global dataset structures NPI into four hierarchal levels with eigh overarching themes NPIs [108].
- COVID-19 Government Measures Dataset from ACAPS [160]
- WHO PHSM initiative: this initiative harmonizes data from various sources, including OxCGRT, CCCSL, and ACAPS, to provide a comprehensive view of global NPI implementation. [107]

Many studies relied on NPI data supplied by these curated trackers, while only a few studies used self-collected data [1, 147]. The most frequently used tracker was OxCGRT [114, 149, 153]. A more comprehensive list with more details on individual trackers can be found in reference [161].

Methodological approach Conducting controlled trials to assess NPI effectiveness was largely infeasible due to ethical concerns and the urgency of implementing interventions. It would have been ethically unacceptable to withhold potentially life-saving measures from any segment of the population in the face of a fast-spreading and deadly virus. Exceptions are individualized interventions like mask-wearing, where some trials were conducted [162–164]. Thus, the large majority of study designs were observational. Studies either exploited variations in NPI implementation over time (i.e. comparing one population before and after NPI implementation), variation in NPI implementation between multiple populations, or both.

A systematic review summarized the methodology of NPI effectiveness studies during the COVID-19 pandemic [114]. Many studies used methods like interrupted time series analyses to compare raw epidemiological or computed outcomes before and after the implementation of NPIs [151]. Expanding on that methodology, the difference-in-difference design [165], sometimes with synthetic controls [153], combines changes over time with differences between populations.

Non-mechanistic models, such as (generalized) linear regression models, were often used to establish an association between NPIs and outcomes [125, 138]. Many of these employed a two-step approach, where intermediate outcomes—such as $\mathcal{R}_t$—were estimated in the first step and then regressed on NPI dummy variables that indicated whether a particular NPI was in effect [1, 133, 148, 155]. Approx. 50% of the computed outcomes were used in a chained second analysis [114].

Semi-mechanistic or mechanistic models were also frequently fit to epidemiological observations to compute intermediate outcomes such as transmission rates or reproduction numbers, which were then related to NPI implementation [131, 132, 134, 150]. Most mechanistic models were compartmental transmission models. Another approach was to add extra compartments into the model to directly estimate the effectiveness of certain interventions, for example quarantine [166].

Counterfactual approaches were used with both mechanistic and non-mechanistic models, where models were calibrated to pre-NPI implementation data and then used to project epidemiological outcomes under different NPI implementation scenarios [140, 167, 168]. Similar procedures were applied to model the effects of lifting NPIs [169].

Geographical scope The geographical scope of studies is crucial, as NPI effectiveness can vary significantly between populations due to differences in age structure, compliance, mask-wearing behavior, and other factors. Additionally, whether studies accounted for sub-national variations is important, particularly in later pandemic waves, where heterogeneity increased [147]. Most studies examined NPIs implemented in the USA, China, and Europe [114]. Notably, some studies compared NPIs globally [127, 149, 155], with or without forming subgroups across which NPI effects were allowed to vary.

2.4.3 Challenges in NPI effectiveness studies

Data challenges Using epidemiological surveillance data gathered during the COVID-19 pandemic can come with several challenges: Firstly, data reporting delays and case underreporting are common and can be both systematic and random, such as the notable reductions in reported cases during weekends and holidays. Reported data may also change based on retrospective updates, and these corrections can lead to the appearance of spikes in observations or negative values [13]. In general, reporting quality depends heavily on the strength of a country's health system. Moreover, testing policies evolved throughout the pandemic, impacting the comparability of data over time. Initially, many countries had limited testing capacity and prioritized severely ill patients or high-risk groups, such as contacts of confirmed cases and healthcare workers [131]. Secondly, data sharing by governmental or other official bodies posed problems, including the unwillingness to share data openly [170]. Thirdly, there exists substantial ambiguity in parameter definitions across countries. For example, some countries reported only PCR-confirmed cases, while others included suspected or symptomatic cases. In hospitals, distinctions were not always made between admissions or deaths with COVID-19 versus those due to COVID-19, a distinction which became more pronounced particularly during the Omicron period [171, 172]. Data quality also varied in regards to geographical and time resolution—some sources only reported weekly aggregated data or only on the national level, where sub-national data would have been more informative.

Data from NPI trackers, while invaluable for analyzing NPIs, also present challenges. One issue is the absence of a standardized terminology for NPIs, with each tracker separately defining their NPI terms. Timing discrepancies—such as differences between the announcement and implementation of measures—further complicate data compilation and analysis [161].

The absence of a standard terminology for NPIs is also a common problem for aggregating information from individual studies in reviews. For example, the term "lockdown" has been used to refer to a wide range of measures, from curfews over business closures to stay-at-home orders, leading to inconsistencies in data collection and analysis. "Shelter-in-place order," "stay-at-home order," or "internal

movement restrictions" can also refer to the concept of a "lockdown" [155]. Alternatively, analyses examined a combination of interventions and referred to this combination as "lockdown" [114]. The scope and design of the studies differed in terms of how NPIs were assessed. Often, the effects of individual NPIs could not be disentangled because many were implemented simultaneously, so studies evaluated combinations of interventions together.

Methodological challenges Many studies estimating NPI effectiveness used a two-step approach. While this can simplify models and increase comparability across populations, it often fails to account for the uncertainty of the first step. This uncertainty can stem from the estimation process as well as from the use of uncertain epidemiological characteristics of SARS-CoV-2, like the distribution of the serial interval. Consequently, the overall uncertainty in the estimates is often underestimated.
One of the key challenges in estimating NPIs is that their implementation is not independent of epidemiological situations, thus complicating causal inference in an observational study design. This issue is referred to as "selection into treatment" in an econometric study [153], while epidemiologists describe this issue as "unmeasured confounding" [116]. Across-time or across-population comparisons can be heavily confounded by population differences as well. For example, one study compared countries which implemented "more restrictive NPIs"-like England, France, and Germany-with countries implementing "less restrictive NPIs" (South Korea and Sweden) [173]. However, they failed to account for voluntary anti-contagion measures, such as voluntary confinement or mask-wearing, population density, national surveillance strategies, and infrastructural and demographic factors [174]. Co-implemented NPIs can also lead to a bias in NPI effectiveness estimates, as already mentioned with the example of school closures (Section 2.4.1).

Moreover, there is a time lag between the implementation of NPIs and their effect on the epidemiological outcome of interest, which needs to be taken into account. For example, using mortality data as outcomes, Hale et al. lagged the stringency index by 28 days [127], and Haug et al. explored NPI lags ranging from 1 to 28 days [133]. Other approaches include to back-calculating from observations to the infection dynamics at the time of NPI implementation [131].

2.4.4 Summary of NPI studies

In summary, the estimation of NPI effectiveness during the COVID-19 pandemic has revealed substantial variation across studies. There is mainly a qualitative consensus about the effect of different types of NPIs, but the effects are not consistently quantified, especially since interest waned after the first pandemic wave.

However, subsequent waves led to the implementation of more NPIs in different combinations. Additionally, the low quality of many NPI studies is a significant limitation. Many studies did not report the uncertainty surrounding their estimates of NPI effectiveness [114], used data of uncertain quality, inconsistent NPI definitions, inadequate measures of effectiveness [114, 175], or made highly confounded cross-country comparisons [173]. All of these points complicate the interpretation of findings and diminish their utility. Consequently, there is a need for confirmatory studies with more rigorous methodologies.
The quality of available data has since improved with the establishment of more robust and comprehensive surveillance systems. For example, datasets provided by Santé Publique France offer high-quality data with a high geographic resolution across multiple waves. These datasets provide a unique opportunity for more robust analyses. Furthermore, as the urgency of the pandemic has subsided, we have time for the development of more sophisticated models, which may require longer development and estimation times, but are potentially more accurate.
In Manuscript 1, I used these high-quality data to estimate the effectiveness of NPIs and vaccines in France using a mechanistic model of disease transmission spanning multiple waves. I also simulated counterfactual scenarios of NPI and vaccine implementations. Mechanistic models offer a structured way to model the dynamics of disease spread, the impact of interventions, and the interplay between immunity and infection rates. In Manuscript 2, I conducted a simulation study, where I compared the performance of mechanistic models to that of chained two-step regression models and illustrated in depth the challenges encountered by the latter model type.

2.5 SARS-CoV-2 vaccines

Besides NPIs, vaccines are a crucial public health strategy to limit the spread of pathogens. During a natural infection, the immune system generates pathogen-specific B-cells and T-cells, which can offer protection against future infections. However, the initial infection itself can be severe or even life-threatening. This is where vaccines play a crucial role. Vaccines mimic an infection by stimulating the immune response through exposure to weakened or inactivated pathogens, or components of a pathogen. This process allows the body to build immunological memory, enabling a more effective defense when faced with the actual infection. Vaccination remains the most successful method for preventing infections [176, 177].

Vaccine platform	Manufacturer (Vaccine name)	Clinical trial regime	Endpoint	Efficacy
mRNA	Pfizer–BioNTech (**BNT162b2**)	2 doses (21 days apart)	Symptomatic COVID-19 and positive RT–PCR test result	95%
	Moderna (**mRNA-1273**)	2 doses (28 days apart)	Symptomatic COVID-19 and positive RT–PCR test result	94%
Viral vector	AstraZeneca–University of Oxford (**AZD1222** (Vaxzevria, Covishield))	2 doses (<6 weeks apart)	Symptomatic COVID-19 and positive nucleic acid amplification test result	55%
		2 doses (>12 weeks apart)		81% (Pooled efficacy 67%)
	Johnson & Johnson (**Ad26.COV2-S**)	1 dose	Symptomatic COVID-19 and positive RT–PCR test result	66%
	Gamaleya (**Sputnik V**)	2 doses (21 days apart)	Symptomatic COVID-19 and positive RT–PCR test result	92%
Inactivated whole virus	Sinovac Biotech (**CoronaVac**)	2 doses (14 days apart)	Symptomatic, virologically confirmed COVID-19	50.7% Brazil, 56.5% Chile, 65% Indonesia, 78% Brazil, 91% Turkey
Protein subunit	Novavax (**NVX-CoV2373**)	2 doses (21 days apart)	Symptomatic COVID-19 and positive RT–PCR test result at least 7 days after 2nd dose	89%

Figure 2.7: Overview over most frequently used SARS-CoV-2 vaccines. Values are taken from reference [179].

2.5.1 Overview of SARS-CoV-2 vaccines

SARS-CoV-2 vaccines were developed exceptionally fast [178] and were crucial in controlling the pandemic [179]. Several vaccine types, including mRNA vaccines (Pfizer-BioNTech BNT162b2, Moderna mRNA-1273), recombinant adenoviral vector vaccines (AstraZeneca ChadOx AZD1222, Johnson & Johnson Ad26.COV2.S, Gamaleya Sputnik V), and whole inactivated virus vaccines (Sinovac Biotech CoronaVac) were rapidly developed, clinically tested, and approved for emergency use [179, 180]. An overview of vaccines is given in Figure 2.7.

mRNA vaccines contain modified nucleosides encoding the receptor binding domain of the SARS-CoV-2 spike protein [181]. After delivery into the cells in lipid nanoparticles, the cells transiently express spike proteins from the mRNA and display them on their surface, which allows for immune system recognition and antibody generation. Unlike live attenuated or killed virus vaccines, mRNA vaccines do not carry any risk of infection or integration into the genome, as mRNA is naturally broken down by the body. Additionally, they allow for rapid, scalable, and cost-effective production, making them highly adaptable for responding to

emerging pathogens [182].
In contrast, viral vectors vaccines against SARS-CoV-2 rely on recombinant adenoviruses to deliver DNA encoding the spike protein into the recipient's cells. The adenovirus used as a backbone is modified to be replication-deficient, i.e. it cannot cause disease, and the DNA encoding the spike protein is inserted. Once inside the cells, the cells produce spike protein, triggering an immune response. A key advantage of viral vector vaccines is that they can stimulate a strong immune response without the need for an adjuvant, as the viral vector itself activates the innate immune system. Additionally, because the virus replicates within cells, spike protein is continuallly produced, which enhances immunogenicity. However, this also raises concerns about potential adverse effects, particularly in immunocompromised individuals. Moreover, pre-existing immunity to the backbone adenovirus may reduce the vaccine's effectiveness [183].
Viral subunit vaccines consist of recombinant SARS-CoV-2 spike protein, often bound to nanoparticles, along with an adjuvant to enhance the immune response [184]. Once the immune system recognizes these spike proteins, it generates antibodies that target the virus. By including only the necessary antigens, subunit vaccines minimize side effects, and they are safe for immunocompromised individuals. However, they may require booster shots to maintain long-term protection. Inactivated coronavirus vaccines, which use the entire killed virus, work similarly by inducing an immune response without causing infection [185]. However, like subunit vaccines, they may also need boosters for sustained immunity.
Vaccine efficacy was demonstrated in accelerated phase three clinical trials, where mRNA vaccines demonstrated around 95% efficacy against symptomatic infection and close to 100% efficacy against severe disease [186, 187] (Figure 2.7). All approved vaccines have been found to be safe, with minor side effects like pain at the injection site, and very rare cases of severe reactions such as anaphylaxis and myocarditis [179]. The efficacy estimates were important for the regulatory approval of vaccines. However, vaccine effectiveness in real-world settings can be lower due to various factors, such as differences in vaccinated populations, vaccination schedules, and VoCs [188].

Clinical trials for SARS-CoV-2 vaccines generally followed a two-dose regimen, with doses administered three or four weeks apart [186, 187]. However, due to vaccine shortages during roll-out, variations from this schedule were frequent, such as extending the interval between doses or mixing different vaccines (see Section 2.5.7). To sustain immunity and maintain high antibody levels in individuals, booster doses were introduced soon after the initial series, as it was assumed that vaccine-derived antibodies wane faster than natural infection-derived antibodies [189] and emerging SARS-CoV-2 variants increasingly escaped vaccine-induced

immunity [190, 191] (see Section 2.5.6). The mRNA vaccines by Pfizer-BioNTech and Moderna were widely rolled out in Europe and North America. In the same regions, as there were rare reports of thrombocytopenia induced by AstraZeneca's ChAdOx-1 vaccine, this vaccine was restricted in certain age groups [192, 193]. Consequently, mRNA vaccines became the primary choice in vaccination campaigns in North America and Europe. As my research covers populations in France and Canada, the majority of the studies discussed here focus on immunity induced by mRNA vaccines.

2.5.2 Population effects of vaccines

In the first year of vaccine availability, from December 2020 to December 2021, 8.33 billion doses were administered to 4.36 billion people globally. As of August 2024, the total number of administered vaccine doses has increased to 13.58, with 5.36 billion people having received at least one dose [82, 194]. It was estimated that globally, vaccines prevented 19.8 million deaths in the first year of vaccinations alone [195].
However, the distribution of vaccines has been markedly uneven. High-income countries quickly achieved high vaccine coverages and even extended vaccine protocols to booster doses, while low-income countries had limited access to vaccines [30]. As successful immunization programs require high vaccination rates, vaccine hesitancy also poses a major challenge [196, 197]. This disparity has resulted in high infection rates in under-vaccinated populations [198], despite research showing that equitable vaccine distribution would result in positive outcomes for both vaccine-giving and vaccine-receiving countries [199]. For example, modeling studies estimated that with a more equitable vaccine rollout, attaining a vaccine coverage of only 20% in low-income countries, an estimated 156,900 additional deaths could have been averted, while attaining the WHO goal of 40% vaccine coverage in all countries by the end of 2021 would have prevented an additional 599,300 deaths [195, 200].

However, it is challenging to estimate the number of deaths averted by vaccines, as the comparator of no vaccine distribution is necessarily counterfactual. Therefore, these studies rely on unbiased models, and a misspecification of the model will result in bias in the estimates. Moreover, determining the counterfactual transmission (i.e. transmission in the absence of vaccines) is challenging, as alternative interventions to curb viral spread would likely have been implemented. Thus, the impact of the vaccine was most pronounced in countries with high vaccination rates, which allowed them to relax NPIs. The study by Watson et al. relies also on the estimation of excess deaths [195], which are difficult to estimate. Also, it is of course more challenging to fit a model to global data than to national

or regional data, because the model needs to be flexible enough to take different reporting structures and other data biases into account, for example uncertainties in the true number of deaths, the circulating variants of concern and their immune escape capabilities, and the true number of vaccines administered [195]. **In Manuscript 1, I address these challenges by fitting an detailed model to SARS-CoV-2 transmission in France and estimate the number of lives saved under different vaccination scenarios**.

2.5.3 Vaccine-induced immunity

All the above-mentioned vaccines target the spike protein to induce an immune response, specifically the interaction between the receptor-binding domain and the ACE2 receptor as the most vulnerable site of SARS-CoV-2. Thus, vaccinated individuals develop anti-spike antibodies from vaccination, but no anti-nucleocapsid antibodies. These can only be developed after natural infection (along with anti-spike antibodies of course). Measuring anti-spike and anti-nucleocapsid antibodies thus allows distinguishing naturally infected from vaccinated individuals.
mRNA vaccines were found to elicit high anti-spike antibody titers [186, 187], while individuals vaccinated with adenoviral vaccines do not develop very high, but potentially more durable antibody titers, and may elicit stronger cellular responses [201]. Moreover, it was shown that vaccination alone does not elicit high enough mucosal antibody titers (i.e. antibodies in the tissues of the respiratory tract), which are important for granting sterilizing immunity [202, 203]. Far less is known about T-cell responses than antibody responses following vaccination, although T-cells form an important part of immunity against SARS-CoV-2. For instance, longitudinal studies have shown that T-cell responses induced by the original vaccines remain >80% cross-reactive against multiple viral variants [204, 205].

2.5.4 Correlates of protection

At the time of initial vaccine release, no single antibody level or threshold beyond which SARS-CoV-2 infection risk is eliminated could be determined. Rather, it was found that the infection risk decreases progressively as antibody levels rise. In Moderna's phase III trial, both binding and neutralizing anti-spike antibody titers were strongly correlated with vaccine efficacy [206, 207]. The spike receptor-binding site on S1 subunit is the target of SARS-CoV-2 most neutralizing antibodies (nAbs) [208, 209]. However, other spike areas, such as the S2 subunit or the N-terminal domain of S1, are also recognized by nAbs [180, 209]. nAbs develop rapidly in most SARS-CoV-2-infected individuals, even with minimal somatic hypermutation, indicating that nAb generation is relatively straightforward and can be achieved by many B-cells [89]. As nAbs can prevent the virus from infecting cells by blocking its attachment to the ACE2 receptor on host cells, they have been

explored as correlates of protection (CoPs) in vaccine efficacy trials and studies of sera from naturally infected individuals [91, 180, 210, 211].
Plotkin and Gilbert defined a CoP as an immune marker that is statistically linked to vaccine efficacy, distinguishing between markers that directly cause protection (mechanistic CoPs) and those that correlate with another protective immune response (non-mechanistic CoPs) [212]. Serum nAbs have thus been discussed as mechanistic CoPs. However, these studies were conducted before the emergence of the Omicron variant, which showed significant immune escape (see Section 2.5.6). Another potential CoP are CD8+ T-cells, whose responses are critical for preventing severe disease and who remain cross-reactive against the Omicron variant [213].

2.5.5 Persistence of immunity

Immunological memory is the source of protective immunity against subsequent infections. There are four major components of immunological memory towards viruses: antibodies, memory B cells, memory $CD4^+$ T cells, and memory $CD8^+$ T cells, which can be found in local tissues, the bloodstream, and the bone marrow [89]. It is evident that immunity, both from vaccination and infection, wanes over time [101]. The process of waning immunity has been studied with two interrelated approaches: by assessing the effectiveness of previous immune-conferring events in preventing subsequent infections over time or by measuring the decline of biological markers, such as antibody or T-cell levels over time.

Initially, protection against re-infection conferred by a first infection was reported to be very high, with estimates ranging from 80-98% [101]. However, these studies typically spanned no more than eight months and were conducted before vaccines became available. A systematic review found that previous SARS-CoV-2 infection was associated with a significantly reduced risk of re-infection, with protection lasting for at least one year and showing only a moderate decrease over that interval [214]. In contrast, the waning of vaccine effectiveness has been observed both in mRNA vaccines and adenoviral vector vaccines [77, 215–217]. While vaccine effectiveness against symptomatic infection decreased significantly over the course of several months, it remained high against severe disease [218, 219]. There is evidence which suggests that immunity from natural infection offers better protection against re-infection than vaccination alone [215, 220, 221]. However, these studies may be subject to additional confounding and selection biases, as they conduct comparisons not only of infected versus uninfected individuals, but additional comparisons between vaccinated and non-vaccinated individuals [101]. An influence of age on the rate of waning has been discussed, but the evidence remains inconclusive [101].

Early studies on SARS-CoV-2 specific antibodies with limited follow-up duration indicated that after natural infection, anti-spike antibodies could generally be detected for up to 5-7 months PSO [102, 222, 223]. However, these studies often only had small and highly selected cohorts with limited follow-up periods and were conducted before vaccines were widely available. A few studies with longer follow-up periods determined that the waning kinetics of anti-spike antibodies, derived both from natural infection and vaccination, displayed two- or three-phase decay dynamics, with an initial sharp decrease that stabilizes later, suggesting longer-lasting immunity [224, 225]. Few studies have examined anti-nucleocapsid antibody kinetics. Those that did found rapidly decaying anti-nucleocapsid antibody levels, but showed the same limitations as previously mentioned—short follow-up periods and low participant numbers [95, 223].
While the presence of circulating and neutralizing antibodies correlates with protection against infection, other immune mechanisms, such as cellular immunity and memory cells, can be quickly reactivated upon re-exposure. Research on the waning of cellular immunity is sparse and conducted in small cohorts. One systematic review included four studies and found that $CD4^+$ cells only waned slightly over 6-8 months, but $CD8^+$ cells showed a more steady decline, with only 50% of participants remaining positive 6-8 months post-infection [226]. Similar findings of decreasing cellular immunity were reported after vaccination [227, 228]. It was also shown that the magnitude of memory T cells was not significantly correlated with antibody titers [102].

2.5.6 Immunity towards SARS-CoV-2 variants

Since the vaccination efficacy trials, genetic mutants of SARS-CoV-2 with immune-escaping capabilities have started to emerge (Section 2.2.2). This emergence of variants added another variable to the discussion on the duration of immunity, as VoCs significantly reduced the protective effects of vaccines and previous infections [229]. This reduction coincided with the natural waning of immunity from the initial waves of vaccination [217].
While mRNA vaccine boosters were shown to increase levels of neutralizing antibodies against the Omicron variant, their effectiveness diminishes quickly [91, 230, 231]. The pronounced immune evasion by Omicron is illustrated by estimates showing only 20-25% protection after the primary vaccination series and immunity from combined vaccination and infection waning to 42% at 6 months after the first booster dose and further declining to 30% nine months post-booster [229, 232]. Omicron also evades neutralization from most available therapeutic antibodies [233]. Nevertheless, although Omicron has greatly reduced the neutralizing capacity of antibodies generated by current SARS-CoV-2 vaccines, T-cell responses have remained relatively unaffected [101]. Furthermore, vaccines have continued to offer substantial defense against severe illness caused by these vari-

ants, including Omicron [234].
In response, both Moderna and Pfizer/BioNTech developed bivalent mRNA vaccines targeting both the original and Omicron BA.1 or BA.4/5 spike proteins [235, 236], which provided better protection against severe disease compared to monovalent boosters [237, 238]. However, the rapid emergence of new Omicron subvariants with the capability to evade immunity acquired from previous Omicron subvariants makes further vaccine development challenging [239].

2.5.7 SARS-CoV-2 immunologic landscape

The global immunologic landscape against SARS-CoV-2 is highly diverse, shaped by a combination of different vaccination schedules, vaccine types, and exposure to multiple viral variants. Due to limited vaccine availability, many individuals delayed their second vaccine dose by several weeks to months. This has been shown to increase vaccine effectiveness compared to the standard three- or four-week regimen tested in randomized trials [240–242]. Additionally, heterologous vaccination regimens have been demonstrated to elicit at least as high or higher immune responses compared to homologous vaccine schedules [243, 244].

As vaccination campaigns progressed, some individuals had already been infected with SARS-CoV-2, while others experienced breakthrough infections after vaccination. Initially, there was hope that vaccines would provide long-lasting immunity against infection and significantly reduce transmission. However, while vaccines are very effective and durable in preventing severe disease, their effectiveness has been more short-lived and lower than anticipated, particularly against the Omicron variant [245].
The exposure to both vaccines and natural infection leads to an immunity profile known as "hybrid immunity." There is evidence that individuals with hybrid immunity possess higher antibody levels and greater protection against disease compared to either vaccination or infection alone and that hybrid immunity declines at slower rates [214, 225, 232, 246, 247]. This enhanced immunity can be attributed to several factors: the breadth of neutralizing and non-neutralizing antibody responses has been shown to improve substantially with hybrid immunity, also showing cross-variant neutralizing activity [248–250]. Moreover, hybrid immunity can lead to distinct T-cell responses due to the recognition of a wider array of antigens, as vaccinations only target the spike protein [250]. Hybrid immunity has been shown to be effective even against Omicron [234], but immunity needs to be sustained with booster doses [229, 232].

2.5.8 Summary SARS-CoV-2 immunity

Estimating the magnitude and durability of protection at the population level has become challenging due to the highly diverse immunological landscape, character-

ized by varying rates and timings of past infection and vaccinations, different vaccine types, and viral variants that can escape pre-existing immunity [232]. Much of the research has focused on anti-spike antibodies, as the spike protein is the only antigen targeted by most vaccines. Other aspects of immunity, such as cellular immunity and anti-nucleocapsid antibodies, have been less studied. To date, there have been no long-term studies conducted on anti-nucleocapsid antibody dynamics, and various factors, such as multiple VoCs and recurrent infections and vaccinations further complicate the understanding of immunity.
There are also significant gaps in the literature regarding how antibody levels correlate with protection, especially in populations with hybrid immunity [232]. While some studies have tried to establish protective antibody thresholds, they only focused on anti-spike antibodies [251–253]. This gap in knowledge is significant as natural and hybrid immunity are critical factors for public health. Understanding the duration of natural and hybrid immunity and their effectiveness in preventing reinfection, particularly with variant viral strains, is essential for guiding public health policies and vaccination strategies.

In Manuscript 3, I address these challenges by analyzing antibody levels from a large cohort of Canadian blood donors and relating levels of both anti-nucleocapsid and anti-spike antibodies to the risk of infection. Additionally, I characterize the antibody-waning dynamics of these antibodies with non-linear mixed effects models and evaluate the time to falling under protective thresholds.

3

Mathematical models

3.1 Introduction to mathematical models

3.1.1 What are mathematical models?

Models are found everywhere in science. For the purpose of this thesis, I define a model as a simplified and interpreted representation of a system, phenomenon, or process, designed to understand, quantify, or predict its behaviors or outcomes. At their core, models provide simplified representations of reality intended to facilitate understanding of complex relationships. As famously noted by statistician George R. Box, "all models are wrong, but some are useful" [254], when he discussed the inherent trade-off between model complexity and usefulness. Despite their simplifications, models enable researchers to generate and explore hypotheses, make predictions, and guide decision-making processes across a wide range of disciplines.

In epidemiology, models are critical for understanding disease dynamics and informing public health interventions. Epidemiological models can broadly be categorized into two categories:

1. **Phenomenological models** extract information about statistical relationships from data without considering the temporal evolution of the underlying process, especially if this process is non-linear. These include regression models, which specify a relationship between an outcome and predictor variables, or machine learning approaches, which can scan big datasets for relationships between variables.

2. **Mechanistic models** incorporate explicit hypotheses about these underlying processes [255–257]. They are also called dynamical models, systems models, or mathematical models[1] [256]. These models directly specify the underlying biological processes—with ordinary differential equations or partial differential equations—making them ideal to study infectious diseases, both infection dynamics within an infected individual (so-called "within-host" models) and transmission in populations ("between-host" models).

I will discuss the trade-offs between these model types further in section 3.1.3. In general, one needs to further distinguish between i) models for statistical inference, ii) models for prediction, and iii) exploratory models for hypothesis generation.

Mechanistic models can be further divided into compartmental and agent-based models [258]. To mimic the mechanism of disease progression and disease transmission, **compartmental (SIR-type) models** partition the population under study into mutually exclusive sets of disease states, so-called compartments, such as susceptible, infectious, or recovered [259]. For within-host models, compartments can represent different cell or pathogen populations [51]. The temporal dynamics of the system are typically described with a set of ordinary differential equations (ODEs), parameterized in terms of the fluxes between compartments. Compartmental models can be imagined as breaking the population into different states and modeling the rates of flow between these states. Compartmental models provide insights into disease transmission and the impact of interventions on a population level but may overlook individual-level dynamics, as all entities within a compartment or state are assumed to be identical.

In contrast, **agent-based models (ABMs)** offer a more detailed representation of individual behavior, allowing for the exploration of complex interactions within populations. Instead of tracking groups of populations, agent-based models simulate the trajectories of each individual (i.e. agent) within a population and their interactions with other agents. Through these interactions, pathogens can be transmitted in the population. The diverse behavior of individual agents is determined by parameters sampled from probability distributions, which allows for stochasticity in the simulations. Thus, ABMs allow for more detail in the model and an analysis on the individual scale, which is useful when individual behavior matters or when more complex interactivity is needed. However, these models come with computational challenges, need a lot of data for accurate parameterization, and require extensive validation [260]. As I used compartmental models in my thesis as models for analysis, I will focus on these models in the next sections.

[1] Without clear definitions for each of these terms

3.1.2 From SIR models to more complicated models

The development of compartmental models dates back over a century. One of the earliest and most influential models of infectious disease transmission was the mathematical model developed by Ronald Ross in a series of articles between 1908 and 1917 [261–264], where he modeled the dynamics of human and mosquito populations to understand malaria transmission and assessed intervention strategies. His models highlighted the role of vectors in malaria dynamics and showed that vector control is crucial for controlling the disease [261].

The most renowned and still widely used model for infectious diseases in human populations was published by Kermack and McKendrick in 1927 [265]. What has become known as the "Kermack–McKendrick model" or simply "SIR model" is a special case of the model described in reference [265].[2] The model includes three compartments: Susceptible (S), Infectious (I), and Removed (R). The model tracks changes in the proportion of the population in each compartment over time by reproducing the progression of infectious disease epidemics. Susceptible individuals can contract the pathogen of interest, infectious individuals have contracted the pathogen and can spread it to others, and removed individuals have overcome the disease and developed immunity or are deceased and therefore no longer participate in transmission. In a simple SIR model, transition rates between the compartments are defined by a constant infection rate (β) and a constant recovery rate (γ) (Figure 3.1 left side). An example of a dynamic governed by a SIR model is illustrated in Figure 3.1, right side.

While a simplified version of reality, SIR models can capture well the non-linear effects of epidemic spread. A fundamental property of this model is that when an epidemic ends, some members of the population remain uninfected, as evident in Figure 3.1, right side. In this figure, the epidemic starts with 1% of the population in the Infectious compartment (blue curve). The infection spreads exponentially at first, but as more individuals become infected and then recover (orange curve), the number of susceptibles (red curve) decreases significantly.
Once a substantial fraction of the population is immune, not enough people are within reach of the infectious individuals to sustain the infection rate, which slows disease transmission. This indirect protection of individuals who are still susceptible to disease (i.e. who have no immune protection on their own) is called herd immunity [266]. Herd immunity implies that the susceptible population at the end

[2]The famous Kermack–McKendrick paper from 1927 originally presented a more complex structure than the simplified version commonly cited today. They build their model under the assumption that the time spent in the infectious compartment changes infectivity and the probability of removal from that compartment. Then, they present the now commonly cited SIR model as a special case with constant rates. They also extend the model to diseases which require an intermediate host (malaria).

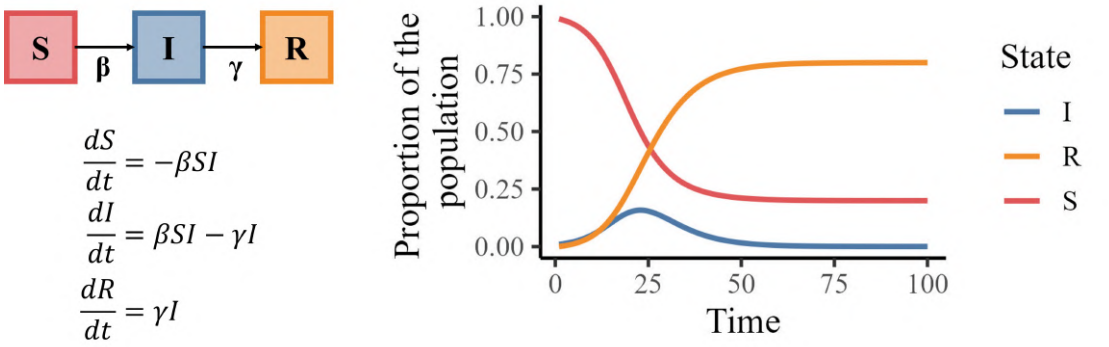

Figure 3.1: SIR dynamics. The left side shows the dynamics in a schema and as differential equations. The right side illustrates the temporal evolution of compartments.

of an epidemic is always larger than zero, and this fraction depends on the basic reproduction number $\mathcal{R}_0$. $\mathcal{R}_0$ is the average number of secondary cases produced by a single infectious individual in a completely susceptible population and serves a measure of how fast a disease spreads [267]. In a SIR model, $\mathcal{R}_0$ is calculated straightforwardly as the rate of infection divided by the rate of recovery (β/γ). The herd immunity threshold can be derived from $\mathcal{R}_0$ using the formula $1 - \frac{1}{\mathcal{R}_0}$. For example, in the epidemic in Figure 3.1, which was simulated with an $\mathcal{R}_0$ of 2, the epidemic begins to decline once the proportion of susceptibles drops below 0.5. The concept of herd immunity also applies to immunity gained by vaccination, where the threshold is then termed "critical vaccination threshold" [268].

Mechanistic models based on ODEs make several important simplifying assumptions: First, they assume **homogeneous mixing** of the population, meaning every individual has an equal probability of coming into contact with every other individual in the population. This assumption overlooks real-world complexities, where social networks and interaction patterns create more uneven interaction patterns. Second, these models assume **uniform transitioning parameters** across all individuals, i.e. all individuals have the same level of infectiousness, susceptibility to infection, and rate of recovery, disregarding variations due to factors such as health status, age, or viral load, unless explicitly modelled. This also implies that SIR models are inherently memory-less, meaning that every individual has the same probability of transitioning to the next compartment, regardless of the time spent in the current compartment (**Markovian property**). This results in exponentially distributed waiting times in each compartment. Third, an important corollary from ODEs is that **transition rates are applied according to the law of mass action**: the number of people transitioning to the next state is proportional to the number of individuals in each compartment.

To overcome the memorylessness of compartmental models, alternative modeling approaches, such as partial differential equations (PDEs) or expanded compartments (e.g. *I1*, *I2*, *I3*), can be considered [269–272]. For models running over longer periods, population dynamics, including births and deaths, should be accounted for [268]. Since compartmental models are deterministic and apply the law of mass action, they will always produce the same output, given a set of starting conditions and transmission parameters. This makes them less suitable for the early or late stages of epidemics, where random events like super-spreading incidents can significantly influence the trajectory of an epidemic. Stochastic models provide a more accurate representation of these phases, capturing the inherent randomness in the early and late epidemic dynamics [273, 274].

Moreover, the basic SIR model with only three compartments assumes no incubation period (i.e. individuals become infectious immediately after their infection) and no waning of immunity (i.e. recovered individuals do not become susceptible again). More complex models can incorporate additional compartments to more accurately reflect the clinical and epidemiological characteristics, to align with specific research questions, and to use available data for inference. For example, the frequently used SEIR model adds an "exposed" (E) compartment between the susceptible and the infectious compartment, accounting for the incubation period where individuals are already infected but not yet infectious. Moreover, individuals infected with SARS-CoV-2 can be asymptomatic but still transmit the virus; thus, an asymptomatic compartment should be added. Other common extensions include models allowing for waning of immunity (e.g. SIRS, SEIRS), and adding compartments for severity of symptoms (mild, severe, hospitalized, ICU). For example, one of the pertinent questions at the start of the SARS-CoV-2 pandemic was how many people would have to be hospitalized simultaneously. In this case, introducing a hospitalized compartment can provide a straightforward answer. If the number of deceased patients is of interest for the model outputs or if it is used as an observation, a death compartment can be included. Other common expansions include compartments reflecting NPIs, such as diagnosed and quarantined [275, 276], or compartments for the vaccinated [277, 278]. Another way of incorporating NPIs is to model the effects of interventions on a time-varying transmission rate. This requires extending the model to accommodate time-varying transmission or piecewise model fitting [279, 280].

Another important extension for infectious disease models is metapopulation models, which contain several subpopulations, each of them representing a class of more homogeneous individuals. These subpopulations often correspond to age classes or spatial areas. This allows for some heterogeneity in the population, mak-

ing the model more realistic, as it is known that age strongly influences important model parameters, such as the risk of severe COVID-19. However, it also requires additional data for model parameterization and assumptions about contact rates between age groups, typically formulated using contact matrices [6, 169, 281]. With spatial structures, interactions and movements between different subpopulations can be investigated, and high-risk areas can be identified. However, the number of compartments increases exponentially with each stratification variable, limiting the model's scalability. For more detailed population variability, ABMs might thus be more suitable [255].

3.1.3 Discussion of dynamical models compared to phenomenological models

As previously stated, mathematical models integrate knowledge about the underlying processes governing a system, whereas phenomenological models abstract relationships between the variables under study without explicitly regarding the underlying mechanisms. For studying infectious diseases, which are inherently dynamic systems, mathematical models offer some key advantages:

1. **Integration of biological knowledge**: humans exist in mutually exclusive states of susceptibility, exposure, infection or immunity. Mechanistic models allow the integration of this knowledge about the natural history of disease and additional factors which are important for disease transmission—such as human behaviors and interventions—into the model.

2. **Integration of data from different scales**: these models link observations across different scales, for example within-host dynamics (like antibody levels), with population-level epidemiological trends (like transmission). Likewise, for vector-transmitted diseases, vector dynamics and disease states in humans can be integrated into one model.

3. **Forecasting and counterfactual scenario simulation**: insights about the disease dynamics over time can be used to make both short-term and long-term forecasts. In practice, this means that similar models can be used to study both immediate effects, for example, the impact of NPIs on the number of SARS-CoV-2 hospitalizations, and explore long-term outcomes of the pandemic, such as the annual dynamics. Moreover, mathematical models can easily project scenarios under a range of "what if" scenarios. This allows for studying the influence of internal factors or external disruptors while incorporating uncertainty about the projections [167, 170, 282]. Through a deeper understanding of the system under study, mechanistic models can easily simulate the system even under assumed changes to the system dynamics, such as lockdowns or increases in vaccination coverage.

4. **Dependent Dynamics**: unlike regression models, mechanistic models account for the interdependence of disease transmission among individuals, making them more suitable for studying effects like herd immunity or determining critical vaccine thresholds.

Phenomenological models, such as regression models or machine learning models, can extract or predict statistical relationships from observed data patterns if sufficient data are available. The advantage of phenomenological models is that they do not require explicit knowledge about the system under study or about the relationships between variables in the system [257].[3] These models can be highly effective for short-term forecasts, particularly when data is abundant, but they may not capture the deeper dynamics needed for long-term predictions or complex scenarios [283]. While phenomenological models are powerful in their flexibility, mechanistic models provide more accurate predictions when data is sparse or of low quality and the underlying biological mechanisms are necessary to construct meaningful models [257]. However, mechanistic models are constrained by the uncertainties in biological knowledge and thus more prone to model misspecification.

In selecting between these approaches, it is essential to consider factors like data quality, model complexity, and computational demands. For example, during the COVID-19 pandemic, phenomenological models were found to be better suited for short-term forecasts, where actual infection dynamics matter less and the autocorrelated nature of the data mattered more, but mechanistic models performed better over longer-term horizons [283]. Mechanistic models can also be coupled with phenomenological models to enhance model flexibility and reduce complexity. For example, in Manuscript 1, we integrated a linear mixed effects model into a mechanistic model of SARS-CoV-2 transmission to include the effects of NPIs in the model dynamics. We chose a mechanistic way to model SARS-CoV-2 transmission to be able to integrate biological knowledge about the spread of SARS-CoV-2. In contrast, modeling the direct mechanistic effects of NPIs would have required making numerous assumptions, fixing many parameters, and adding compartments, making the model overly complex. Therefore, we included NPI terms as predictors in a regression model with the transmission as the outcome. One major advantage of our model was that all parameters could be estimated in a single step. Additionally, by regressing the transmission rate directly on the NPIs—rather than regressing epidemiological observations on NPIs—we did not

[3]However, if a model is used in a causal inference problem, careful parameter selection based on background knowledge is required in order to avoid confounding and selection bias. This applies less for prediction models, but even then careful parameter selection is required in order to avoid overfitting.

have to account for uncertain time lags between the implementation of NPIs and their observable effects on epidemiological observations.

3.1.4 Application of mathematical models to the COVID-19 pandemic

Mathematical models serve as essential tools in the scientific analysis of complex systems. Thus, the application of mathematical modeling to inform public health policy is not new, but mathematical modeling has gained public attention during the COVID-19 pandemic, as models have played an unprecedented role in public health decision-making. Historical models used during previous public health emergencies include responses to pandemic and seasonal influenza, among many others. For instance, an age-stratified transmission model of influenza suggested that expanding vaccination to school-aged children could enhance the overall effectiveness of flu vaccination programs [284]. Similarly, early mathematical models of the 2009 influenza A/H1N1 pandemic provided crucial estimates of the reproductive number and serial interval [285]. Additionally, Ferguson et al. explored various mitigation strategies for influenza, showing that interventions like school closures and antiviral treatments could significantly impact the course of a pandemic [286]. Likewise, models were instrumental in guiding critical interventions during Ebola outbreaks. Alarming forecasts from mathematical models [287] prompted rapid international aid and supported the implementation of public health measures such as patient isolation and safe burial practices. Other studies [288, 289] focused on transmission dynamics and the impact of interventions like increasing hospital capacity and distributing protective kits.

Early in the COVID-19 pandemic, as immediate and effective action was required, both the public and policymakers turned their attention to infectious disease modelers to understand and predict the trajectory of the virus. From the early days of the pandemic, researchers utilized a range of mathematical modeling techniques to infer epidemiological parameters, predict epidemic trajectories and inform public health responses. Mathematical models have been used in several key areas: inferring epidemiological characteristics of the new virus, improving situational awareness, and informing mitigation strategies.

3.1.4.1 Key epidemiological characteristics

In the early stages of the pandemic, key epidemiological parameters, transmission pathways, and clinical features of SARS-CoV-2 were unknown. Mathematical models were widely used for estimating and inferring these parameters. To assess the transmissibility of SARS-CoV-2, a range of studies estimated the basic transmission number of SARS-CoV-2, $\mathcal{R}_0$. They all placed it between 2-3 [290–292]. The rapid spread of the virus was also confirmed through fitting growth rate mod-

els after its emergence [293]. The potential for asymptomatic transmission was quickly identified as a critical factor in SARS-CoV-2 spread [49, 290]. Early estimates suggested a low case ascertainment rate of approx. 5% [291], indicating that many infections went undetected alongside many asymptomatic infections. Other studies provided estimates of the symptomatic case fatality ratio in Wuhan as 1.4% (0.9–2.1%) with an age-structured SIR model [294] and forecasted its potential for domestic and international spread of SARS-CoV-2 with a metapopulation SEIR model [295]. This emphasized the urgent need for public health interventions at both population and personal levels to prevent a global pandemic. As VoCs emerged, new studies were required to re-estimate transmission parameters [66, 73, 296].

Mathematical models have also been used on the host level to estimate viral kinetics of acute infections in cohorts of healthy individuals [53] and hospitalized patients [51, 297]. Moreover, intra-host models have been used to distinguish viral kinetics of VoCs in vaccinated and unvaccinated individuals [298] and to predict the effectiveness of antiviral medications [51, 299, 300].

3.1.4.2 Situational awareness and mitigation strategies

As SARS-CoV-2 spread globally, forecasting models became essential for situational awareness and decision-making regarding interventions. In response to early warnings from modeling studies about the potential for healthcare systems to be overwhelmed, countries implemented lockdowns and other stringent measures [257, 301]. A model from the Institute for Health Metrics and Evaluation (IHME), which was published in April 2020, greatly influenced the strategy in the U.S. for the first wave but severely underestimated the number of deaths from COVID-19 [112], and was soon criticized as methodologically flawed [302, 303].

Forecasting hospital demand became a crucial application of mathematical models during the COVID-19 pandemic [304–307]. Soon, forecasting teams and hubs, such as the CDC's COVID-19 Forecast Hub (www.covid19forecasthub.org), were established to use the power and robustness of ensemble forecast models to predict hospitalizations [308–310]. Ensemble forecasts proved more accurate and precise than individual models, though accuracy varied during critical moments of the pandemic [310, 311]. The COVID-19 Scenario Modeling Hub, which had been created from the COVID-19 Forecast Hub, further extended these efforts, providing long-term projections for federal and local health authorities in the U.S. (www.covid19scenariomodelinghub.org).

3.1.4.3 Effectiveness of mitigation strategies

Early models demonstrated the effectiveness of NPIs in "flattening the curve" and reducing infection rates. The models emphasized the importance of early and in-

tense NPIs to reduce the effective reproduction rate below one, thus controlling the epidemic [312, 313]. Premature lifting of NPIs without adequate compensatory measures was shown to risk a resurgence of infections [169, 314]. Studies on the effectiveness of quarantine measures in Wuhan provided early evidence supporting strict containment strategies [315], and other researchers modeled the effectiveness of combinations of public health interventions [316, 317]. After the first pandemic wave, influential papers were published confirming the effectiveness of NPIs [131, 133, 134]. As the pandemic progressed, Ferretti et al. demonstrated the potential of digital contact tracing in augmenting traditional public health measures to control the spread of COVID-19 [318]. Vaccination strategies were later incorporated into models to assess efficient roll-out strategies [319–321] and re-vaccination strategies [322], and modeling vaccine and NPI strategies simultaneously [282, 323–326]. Moreover, compartmental models were also used to identify areas of uncertainty where more research was needed, such as the duration of protection conferred by vaccines and the rate of serious adverse events following vaccination [327]. Indeed, models have been fitted to antibody dynamics to gain insights about the duration of detectable antibodies in serum [225].

The previous examples underscore the importance of mathematical modeling in informing and optimizing public health policies infectious disease outbreaks. I also demonstrated that they can be powerful and effective tools during a public health emergency. While I focused on how mathematical models aid public health policy in understanding key epidemiological parameters, guiding intervention strategies, and predicting possible future scenarios, it is worth noting that they also serve other purposes, such as generating hypotheses about complex system dynamics.

3.2 Mathematical model development and model fitting

3.2.1 Identifiability

One aspect of models that is not explained in detail in the manuscripts, but that warrants attention and poses problems during model development, is the issue of identifiability. A model is identifiable if the values of its parameters can be determined uniquely from knowledge of its inputs and outputs [328]. On the contrary, if a model is non-identifiable, different values of parameters can produce the same predictions or fit to data. Non-identifiability leads to wrong parameter estimates and bad uncertainty quantification [329, 330], that is, misleading models. Models can for instance be unidentifiable if they include too many compartments for which observations are not available, models with complex interactions, or models with a high number of parameters relative to the amount of data [328].

Identifiability can be further divided into structural and practical identifiability [331]. Structural identifiability refers to whether unique parameter estimation is theoretically possible for an ideal, error-free system based on the model structure and output relations. It assesses the intrinsic capability of the model structure to provide unique parameter solutions. There are techniques to formally verify structural identifiability, such as the software DAISY [332], which uses a differential algebra algorithm to perform parameter identifiability analysis.
However, even when a model is structurally identifiable, in practice, parameters may still be non-identifiable due to real-life limitations, such as the amount and quality of the data available and/or the number of parameters that are jointly estimated from the available data. This is commonly referred to as practical non-identifiability, and is more aligned with the practical challenges faced during modeling [331]. Practical non-identifiability can for example be assessed by running several parameter estimations on the same dataset with random starting values. If the different estimates do not converge, this can be caused by a problem of practical identifiability.

3.2.2 Parameter estimation methods

Many models are fitted using *maximum likelihood estimation* (MLE), a statistical method which aims to find the parameter values that make the observed data most probable under the assumed model. The term "likelihood" in this context was first used by Fisher in 1922 [333]. The likelihood of a model quantifies how well a model, given its parameters, explains the observed data. Mathematically, it is expressed as: $\mathcal{L}(\boldsymbol{\theta} \mid \boldsymbol{y})$, where $\boldsymbol{\theta} = [\theta_1, \theta_2, \ldots, \theta_k]$ is the vector of k model parameters to be estimated in the parameter space Ω and $\boldsymbol{y} = (y_1, y_2, \ldots, y_3)$ denotes the n observed data points.

In a maximum likelihood approach, the objective is to find the parameter set for which the observed data have the highest joint probability, i.e. that maximize the likelihood function under the assumed statistical model:

$$\hat{\boldsymbol{\theta}} = \text{argmax}_{\theta \in \Omega} \mathcal{L}(\boldsymbol{\theta} \mid \boldsymbol{y})$$

In practice, since the likelihood values tend to be extremely small, it is more common to work with the natural logarithm of the likelihood, known as the log-likelihood and defined as $l(\boldsymbol{\theta}, \boldsymbol{y}) = \log(\mathcal{L}(\boldsymbol{\theta} \mid \boldsymbol{y}))$. Since the logarithm is a monotonic function, the maximum of the log-likelihood occurs at the same point as the maximum of the likelihood function. Thus, the parameter space can be searched for values of the parameters which result in the maximum of the log-likelihood to find the most plausible model parameter values, given the observed data. In most cases,

an analytic solution to this function does not exist, and numerical optimization algorithms are required to estimate $\hat{\boldsymbol{\theta}}$, such as the well-known Newton-Raphson algorithm [334].

In nonlinear models, such as those governed by a set of ODEs and using random effects, a different approach is needed for parameter estimation. One common method, used when the model depends on unobserved latent variables, is the expectation-maximization (EM) algorithm—an iterative method to find the maximum of the log-likelihood function with unobserved variables [335]. The EM algorithm operates by iteratively applying two steps: the expectation (E) step and the maximization (M) step. In the E step, the algorithm calculates the value of the log-likelihood, based on the current estimates of the parameters. In the M step, it updates the parameter estimates by maximizing this expected log-likelihood. These newly estimated parameters are then used in the next E step to refine the distribution of the latent (unobserved) variables, and the process repeats until convergence.
For nonlinear mixed effects models (NLME), a more efficient version of the EM algorithm has been developed: the stochastic approximation expectation-maximization (SAEM) algorithm [336]. SAEM improves efficiency by simulating random effects from the conditional parameter distribution at each iteration, thereby updating the unknown parameters of the model. This method has been shown to converge quickly towards the maximum likelihood estimator [336, 337]. The SAEM algorithm is implemented in the Monolix software [338], and was used for parameter estimation with the mechanistic models presented in Manuscripts 1 and 2.

4

Manuscript 1

4.1 Preface to Manuscript 1

As outlined in the literature review, considerable uncertainty about the effectiveness of NPIs remained, even after a considerable number of NPI studies. Moreover, the number of studies after the first pandemic wave decreased significantly, despite the fact that in subsequent waves, more NPIs were implemented in varying combinations and at smaller geographical scale. For instance, in France, new strategies such as curfews, gathering size restrictions (e.g. bans on gatherings of fewer than 10 people), and lockdown measures less stringent than the first lockdown were enforced. These measures coincided with the rollout of vaccines and the emergence of VoCs.

Given this complexity of public health intervention decisions, compounded by the lack of high-quality, consistent evidence about many facets of these interventions, it is crucial for decision-makers to have updated and accurate estimates of NPI effectiveness, for future SARS-CoV-2 waves as well as future pandemics. As NPIs were shown to vary greatly across countries, we decided to focus on NPIs in France. Several studies have previously evaluated NPI effectiveness in France [1, 150, 169, 270], but there remain significant opportunities for refinement. The studies by Roux. et al. [270] and DiDomenico et al. [169] covered only the first wave in France, while Collin et al. [150] used a coarse geographical scale (12 regions instead of 94 departments) and limited their analysis to data up until April

2021. Paireau et al. [1] extended their analysis until May 2021 but used a two-step regression model for analysis, which might not have accurately quantified the uncertainty in estimates or been suitable for assessing the combined effects of NPIs and vaccination (see chapter 5).

To address these limitations, we developed a population-based mechanistic model to estimate NPI and vaccine effectiveness throughout three pandemic waves in France. The mechanistic model presented in this manuscript is structured into three layers: 1) The mechanistic layer includes biological information and models the transmission process and vaccine effects mechanistically, similar to Collin et al. [150]; 2) In the statistical layer, a mixed effects regression model is used to include the effects of the NPIs on the transmission rate; and, 3) The observation layer models four types of epidemiological data to explicitly account for errors in reported data. To illustrate the impact of NPIs and vaccines beyond relative effectiveness measures, we conducted simulations under counterfactual scenarios, such as earlier vaccine rollouts and alternative NPI implementation timelines. These simulations explicitly quantify the number of saved lives by timely interventions, providing valuable insights for future pandemic preparedness and policy planning.

The following manuscript was published in Epidemics in March 2024.

4.2 Manuscript 1: Estimating the population effectiveness of interventions against COVID-19 in France: A modelling study

Iris Ganser[a,b], David L Buckeridge[b], Jane Heffernan[c], Mélanie Prague[a,d,e], Rodolphe Thiébaut[a,d,e,f,*]

[a]Univ. Bordeaux, Inserm, BPH Research Center, SISTM Team, UMR 1219, Bordeaux, France
[b] McGill Health Informatics, School of Population and Global Health, McGill University, Montreal, Quebec, Canada
[c] Mathematics & Statistics, Centre for Disease Modelling, York University, Toronto, Ontario, Canada
[d] Inria, Inria Bordeaux - Sud-Ouest, Talence, France
[e] Vaccine Research Institute, Creteil, France
[f] Bordeaux University Hospital, Medical Information Department, Bordeaux, France
[*] Corresponding author at: Univ. Bordeaux, Inserm, BPH Research Center, SISTM Team, UMR 1219 Bordeaux, France.
E-mail address: rodolphe.thiebaut@u-bordeaux.fr (R. Thiébaut).

Abstract

Background Non-pharmaceutical interventions (NPIs) and vaccines have been widely used to manage the COVID-19 pandemic. However, uncertainty persists regarding the effectiveness of these interventions due to data quality issues, methodological challenges, and differing contextual factors. Accurate estimation of their effects is crucial for future epidemic preparedness.
Methods To address this, we developed a population-based mechanistic model that includes the impact of NPIs and vaccines on SARS-CoV-2 transmission and hospitalization rates. Our statistical approach estimated all parameters in one step, accurately propagating uncertainty. We fitted the model to comprehensive epidemiological data in France from March 2020 to October 2021. With the same model, we simulated scenarios of vaccine rollout.
Results The first lockdown was the most effective, reducing transmission by 84% (95% confidence interval (CI) 83-85). Subsequent lockdowns had diminished effectiveness (reduction of 74% (69-77) and 11% (9-18), respectively). A 6 pm curfew was more effective than one at 8 pm (68% (66-69) vs. 48% (45-49) reduction), while school closures reduced transmission by 15% (12-18). In a scenario without vaccines before November 2021, we predicted 159,000 or 168% (95% prediction interval (PI) 70-315) more deaths and 1,488,000 or 300% (133-492) more hospitalizations. If a vaccine had been available after 100 days, over 71,000 deaths

(16,507-204,249) and 384,000 (88,579-1,020,386) hospitalizations could have been averted.
Conclusion Our results highlight the substantial impact of NPIs, including lockdowns and curfews, in controlling the COVID-19 pandemic. We also demonstrate the value of the 100 days objective of the Coalition for Epidemic Preparedness Innovations (CEPI) initiative for vaccine availability.

Keywords: COVID-19, SARS-CoV2, epidemics, dynamics, mathematical model, non-pharmaceutical interventions, vaccines

Introduction

The COVID-19 pandemic has caused substantial morbidity and mortality and taken a heavy toll on healthcare systems globally. As no vaccine or other treatment for COVID-19 was available at the beginning of the pandemic, governments around the world implemented non-pharmaceutical interventions (NPIs) with mostly unknown epidemiological and societal impacts to contain viral spread. Such NPIs consisted for example of border closures, cancellation of public events and gatherings, school and workplace closures, stay-at-home restrictions, testing and contact tracing, and mandated wearing of face masks [126]. Due to the high transmissibility of SARS-CoV-2, rapid vaccine development and distribution programs were implemented, and in late 2020, several became available. By the Spring of 2021, vaccination efforts were ramped up, and booster doses were made available in the Fall of 2021 in high-income countries because of waning vaccination immunity [219]. Due to good protection against severe disease, NPIs were relaxed in the Summer of 2021 in countries with high vaccination coverage, despite the emergence of viral variants of concern (VoCs) with increased transmission and virulence.

Despite numerous studies [116, 119, 339], the effectiveness of NPIs on decreasing SARS-CoV-2 transmission remains uncertain, especially over longer periods of time and at a high geographical resolution. However, given the economic, psychological, and social costs associated with these interventions, estimating their effectiveness, particularly in combination with vaccination, is crucial. Previous studies on the effectiveness of NPIs, such as lockdowns and school closures, during the COVID-19 pandemic have yielded mixed results [115, 116], and many of the studies have focused solely on the first pandemic wave, either estimating NPI effectiveness [131] or simulating NPI exit scenarios [169]. However, relying solely on first-wave estimates is not sufficient to fully comprehend the effects of NPIs during a pandemic. After the initial wave, social interactions did not return to pre-pandemic levels, population compliance with NPIs decreased [340], viral mutations started to emerge, and population immunity increased through vaccination and previous infections. Several simulation studies investigated optimized vaccine rollout and NPI relaxation scenarios [282], but there is a lack of retrospective analyses of vaccine rollout and studies which include estimates on NPI and vaccine effectiveness from observational studies. Additionally, weather is hypothesized to have an impact on SARS-CoV-2 transmission, with higher temperatures and ambient humidity decreasing transmission [341–343].

Country-specific cultural, demographic, and environmental factors make it relevant to look at NPIs in different contexts. International studies combining data from multiple countries have been conducted, but they often ignore geographical variability, use heterogeneous NPI definitions, and suffer from cross-country confounding. This is why in the present study, we focus on the level of administrative

sub-regions of France, where exceptionally rich data were available on a daily basis thanks to the *Santé Publique France* agency. We aim to build on previous work conducted in France [1, 150] by extending the study period, including a more granular analysis of VoCs and explicit modelling of vaccinations in the epidemic dynamics. To this end, we propose a SARS-CoV-2 compartmental model that incorporates the effect of NPIs, vaccination, viral variants of concern (VoCs), and weather. To ensure accurate propagation of uncertainty, we employ a statistical approach that estimates all model parameters in one step. A further refinement is the quality of the information used to estimate these effects, as we use four types of observations and retrospectively corrected data. To better illustrate the impact of vaccines and the complex interplay between NPIs and vaccination, we perform simulations of various counterfactual scenarios.

Methods

Data

COVID-19 hospitalizations, deaths, and cases We used four types of observational data, aggregated at the departmental level, published by *Santé Publique France*. In France, a department is an administrative area with a median of approx. 500k inhabitants (Figure S4.1). As all data were available in aggregated form in the public domain, no ethical regulations were applicable to this study. For each department, daily COVID-19-related hospital data, including admissions and occupancy from the SI-VIC database [344] (available since March 1st, 2020), deaths in hospitals from SI-VIC [344] (available since March 18th, 2020), and PCR-confirmed COVID-19 cases from the SI-DEP database [345] (available since May 13th, 2020), were collected on a daily basis until October 31st, 2021. In April 2022, we downloaded the final dataset encompassing this entire period. More information on epidemiological data can be found in the Supplementary Methods Sections. We excluded the two Corsican departments entirely from the analysis, and department 5 (Hautes Alpes) from February 17, 2021, onwards, due to missing weather data. We smoothed the hospital admission, death and case time series with a centered 7-day moving average to account for the day-of-week effect. Our study period extended until October 31st, 2021. After this date, very few NPIs were enforced in France, and the Omicron VoC disrupted the epidemiological dynamics.

Non-pharmaceutical interventions During the study period, a wide range of NPIs of varying stringency were implemented in France. We collected the NPI data from official government websites and news articles and focused on the following NPIs: i) The three periods of lockdowns with varying levels of restrictions, including a separate lockdown 2 before Christmas, where stores were allowed to re-open, which we refer to as "lockdown 2 light"; ii) school closures; iii) curfews

either starting at 8 or 9 pm or at 6 or 7 pm; and iv) four periods of barrier gestures, where the first three directly follow the lifting of lockdowns, and the fourth period starts with the implementation of a vaccine passport, which restricted access to public areas for the unvaccinated. Barrier gestures encompass NPIs and behavioral changes, such as mask wearing, remote working, and compliance with hygiene protocols, which we were not able to model separately. The population adherence to these measures was parameterized based on surveys of barrier gesture adoption in France by *Santé Publique France* [346], as a continuous variable ranging between 1 (indicating full population compliance) and 0 (no compliance). A more in-depth description of NPIs can be found in the Supplementary Methods. Due to identifiability issues, we did not succeed in quantifying the effect of bar and restaurant closures, workplace closures, bans on large public events, travel bans, enhanced testing, or contact tracing. Some of these effects may thus be absorbed in lockdowns, curfews, and barrier gestures.

Exogeneous variables: SARS-CoV-2 variants of concern, vaccinations, weather **Variants of concern:** During our study period, the predominant VoCs in France were B.1.1.7 (Alpha), B.1.351 (Beta), P.1 (Gamma), and B.1.617.2 (Delta). The percentage of SARS-CoV-2 VoCs among all sequenced samples at the departmental level was published by SI-DEP starting February 12th, 2021. More information on reporting of VoCs by SI-DEP can be found in the Supplementary Methods. As no VoC data were available before this date, we used a logistic regression model to extrapolate departmental Alpha and Beta/Gamma circulation, assuming no VoC circulation before January 1st, 2021. We fit binomial models separately for each department and VoC. The proportion of circulating VoC was regressed on the calendar day as the only predictor, using data of the first three months of VoC circulation (February 2021-April 2021). The predictions from these models were then used to impute VoC circulation for each department between January 1st, 2021 and February 12th, 2021. Since the reported data were aggregated by week and there was high variance in the VoCs captured by sequencing, the percentages of VoCs among all sequenced samples were smoothed over 14 days to account for random fluctuations in testing.

Vaccination: The proportion of the population vaccinated with one or two doses was obtained from the VAC-SI database [347]. We did not consider additional vaccine doses as the proportion of people who received a booster by the end of our analysis period was low (2.7% of the population). The effects of vaccine doses were lagged by 21 days to account for the time needed to develop immunity after vaccination.

Weather: To account for the potential impact of climate on SARS-CoV-2 transmission [348], we extracted daily weather data from the National Oceanic and Atmospheric Administration database using the R package WORLDMET. The

data was collected from all meteorological stations located in France. We calculated a daily weather variable for each department combining temperature and humidity (see Supplementary Methods).

Modeling approach and estimation

We modeled the SARS-CoV-2 epidemic in France from March 1st, 2020, to Oct 31st, 2021, using an extended SEIR model, adapted from previous studies [150, 349–352]. This model has already undergone strong identifiability analysis [150], but compared to previous models, our model has some novelties. First, we divided the population into seven compartments: Susceptible (S), latently Exposed (E), symptomatically Infected (I), Asymptomatically infected (A), Hospitalized (H), Recovered (R), and Deceased (D). We modeled the flow of individuals in the population through these compartments according to the diagram shown in Figure 4.1a. In short, viral transmission occurs from the individuals in the I and A compartments to the S compartment. After a latent period with an average duration of 5 days in the E compartment, infected individuals progress to the I or A compartments. Individuals in I will become symptomatic during their infection, while individuals in A will stay asymptomatic for the whole duration of their infection. From there, they can either recover and progress to the R compartment, or symptomatically infected individuals can be hospitalized. We assumed that individuals in the H compartment are no longer infectious and can either recover or progress to the D compartment. For a more comprehensive description of the model dynamics, the differential equations, and the parameters governing the system, the reader is referred to the Supplementary Methods Section *Model* and Table S4.1.

Second, we linked the mechanistic model to a linear mixed effects model of the viral transmission rate b. This model represents the time-varying transmission rate b_t as a function of a basic transmission rate b_0, NPIs, weather, and VoCs, as in Collin et al. [150]:

$$log(b_{i,t}) = b_{0i} + \sum_j \beta_i^j NPI_{i,t}^j + \sum_k \beta_V^k VoC_{i,t}^k + \beta_w weather_{i,t}$$

, where $b_{0i} \sim N(b_{0_{pop}}, \omega)$ for department i at time t, NPI j and VoC k. The basic transmission rate b_0 is thus allowed to vary across departments, which accounts for inter-departmental variations in age structure, population density, and contact patterns. The percent transmission reduction of NPIs was calculated with the respective β coefficients as $(1 - e^{\beta}) \times 100$.

Third, we included the effects of vaccination as the population vaccine effect against transmission (e_{vI}) and the population vaccine effect against hospitalization (e_{vH}) directly in the compartmental model. We define the vaccine effect to be the

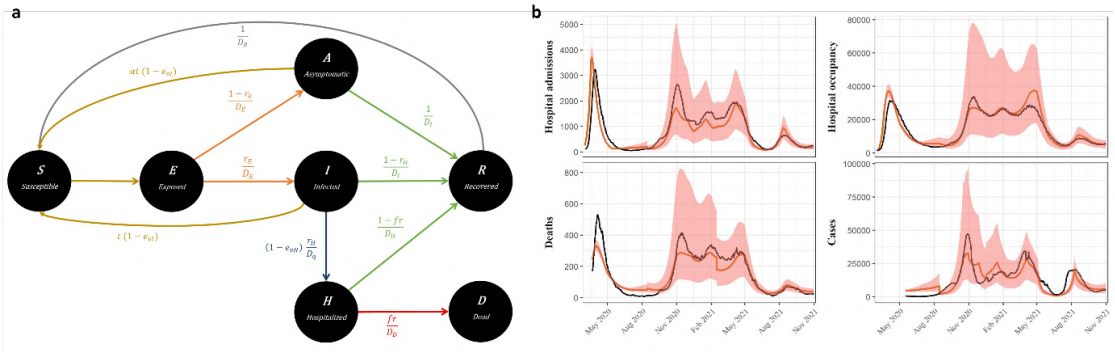

Figure 4.1: SEIRAHD model representation and model fits. (a) The 7 compartments of our model structure with the transition parameters are shown. (b) Model fits for all four types of observed data for the entirety of France are shown. Black lines indicate the observed data, red lines the model fit, and shaded areas the 95% prediction interval.

product of the vaccine efficacy (estimated by the model) and the population vaccine coverage at the departmental level.

Lastly, we explicitly modelled the effect of VoCs on transmission and risk of hospitalization, with VoCs increasing both transmission and risk of hospitalization according to strain-specific, previously published values (Table S1). As observations, we jointly modelled COVID-19 deaths, cases, hospital admissions, and hospital occupancy, assuming Normal distributions and combined error models. Hospital admissions were modeled as the influx of individuals into the H compartment, hospital occupancy as the number of individuals in the H compartment, cases as the influx of individuals into the I compartment, and deaths as the influx of individuals into the D compartment for all departments i and all observation times t. All modelling choices and assumptions are recalled and discussed in the Supplementary Methods Section *Modeling assumptions*.

Parameters were estimated using maximum likelihood estimation using a stochastic approximation expectation maximization (SAEM) algorithm implemented in the software Monolix, version 2019R2 (http://www.lixoft.com). Due to practical identifiability issues, some parameters were fixed or estimated with profile likelihood estimation (see Supplementary Methods Section *Parameter estimation*). Standard errors for the calculation of 95% confidence intervals were obtained by 100 bootstrap replicates. For each bootstrap replicate, we randomly sampled 94 departments (with replacement) from the entire department pool and conducted the estimation procedure (see Supplementary Methods). Furthermore, for each estimation, the initial population parameters were randomly sampled from a uni-

form distribution ranging between half and twice the assumed values. We repeated the bootstrap procedure 100 times and determined the lower and upper limits of the 95% confidence intervals by extracting the 2.5th and 97.5th percentiles from each parameter distribution.

For comparability with other studies, we calculated the basic reproductive number (R_0) and the effective reproductive number over time ($R_{eff}(t)$) with a next-generation matrix from the basic transmission rate b_0 and the time-varying transmission rate, respectively [150, 353] (see Supplementary Methods).

We performed extensive model selection and goodness-of-fit analyses to arrive at our final model. First, we checked for structural identifiability using DAISY (Differential Algebra for Identifiability of Systems) [332] and we ensured that no NPIs in our NPI matrix effect overlapped completely (Figure S4.2 in Supplementary Methods). Next, we checked practical identifiability by performing convergence assessments, in which we confirmed the stabilization of the SAEM algorithm towards the same value from a wide range of starting values (Section *Model selection* in Supplementary Methods). Then, we performed parameter selection, with final models being chosen based on the Akaike Information Criterion (AIC), while paying attention to the problems of non-identifiability of effects.

Simulations

We simulated the following scenarios: No vaccine availability until the end of the study period, faster vaccine rollout (1% of the population vaccinated per day), and the vaccine becoming available after 100 days, as called for by the Coalition for Epidemic Preparedness Innovations (CEPI) initiative (www.cepi.net). t_0 for the 100-day scenario was January 11th, 2020, following the publication of the complete genomic sequence of SARS-CoV-2 [354]. Thus, in this scenario, vaccinations started approximately 8 months earlier than the actual vaccine rollout in France. Compared to the fast rollout scenario, the observed vaccine rollout was very slow in the first months, with no more than 0.3% of the population vaccinated per day, and picked up speed when more vaccine doses were available. However, it never passed 0.8% of the population vaccinated per day. Additionally, we conducted simulations in which the first lockdown was implemented one or two weeks earlier. For each week shift, we simulated two scenarios: in one, the lockdown 1 was lifted as observed (May 5th, 2020) and one where the length of the lockdown was kept constant (54 days).

Simulations were performed with Simulx software version 2020R1 (`www.lixoft.com`). We conducted 1000 simulations per scenario, with parameters drawn from their respective estimated distributions. 95% prediction intervals were derived by taking the 2.5th and 97.5th percentile of the distribution of simulations. We chose to use the model's predictions under the observed scenario as comparisons for the

counterfactual scenarios instead of the actual data. This ensures more accurate comparisons, considering the model's imperfect fit to the observed data. For all simulations, we assumed that immunity through vaccination did not decline or that booster vaccinations were available to maintain protection. Moreover, we assessed all scenarios under waning immunity. We assumed that the protection from vaccines waned according to results from Clairon et al. who modeled waning immunity as the probability of detecting neutralizing antibodies above a protective threshold [355]. We applied these waning curves to the daily number of vaccinations to derive the percentage of the population with active protection against the original SARS-CoV-2 strain and the Delta VoC at each day.

Results

$\mathcal{R}_t$ over time

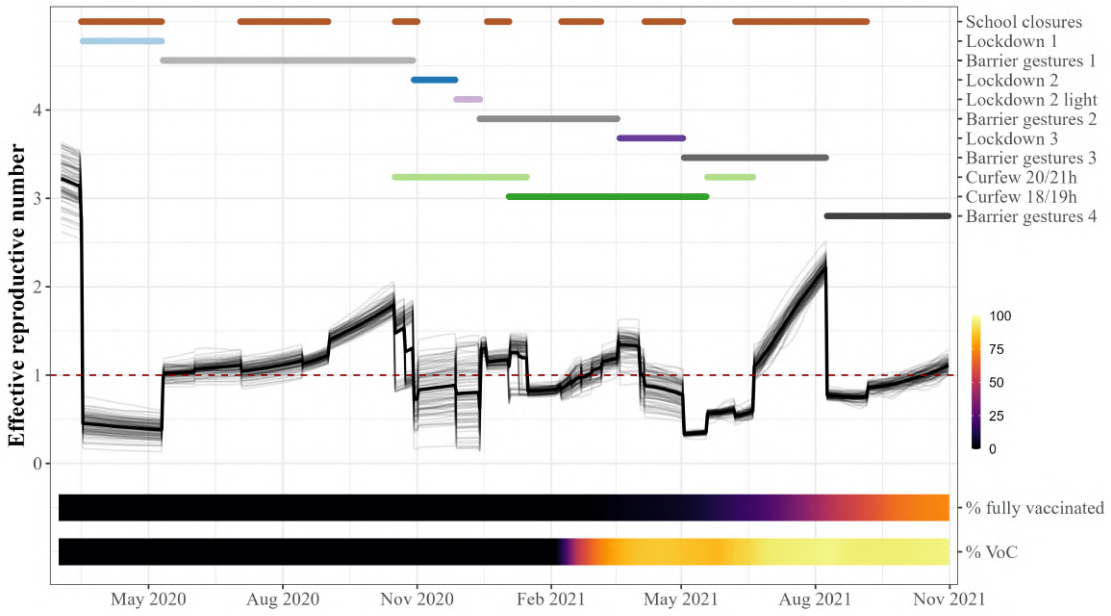

Figure 4.2: Effective reproductive number ($\mathcal{R}_t$) as estimated by the model in relation to implemented NPIs, variants of concern (VoC) and vaccinations. The thin black lines depict $\mathcal{R}_t$ trajectories for each French department, while the thick black line shows the average across France. The NPI lines are plotted if the NPI was active in at least one department. The dashed line indicates the $\mathcal{R}_t$ threshold of 1, below which an epidemic will eventually die out.

The model effectively captured the trajectories of all four types of observations, although it exhibited a slight underestimation during the second wave (around

November/December 2020) and for deaths (Figure 4.1b for the entirety of France and Figure S4.4 in Supplementary Results for selected departments). Before the initial lockdown, our model estimated that $\mathcal{R}_t$ varied around three. However, with the implementation of the lockdown, it decreased to below one, and subsequently fluctuated around one with two notable increases. The first occurred in Fall 2020 at the onset of the second wave, while the second happened in the summer of 2021 due to the increased circulation of the Delta VoC (Figure 4.2).

Effects of NPIs and vaccination

Based on the calibrated model representing the COVID-19 epidemic in France, we demonstrated that all the tested NPIs deployed by the French government significantly reduced SARS-CoV-2 transmission. Specifically, the first lockdown led to an 84% decrease in viral transmission (95% CI 83.1 - 84.7), while the second and third lockdowns resulted in a 73.8% (69.4 - 76.5) and 11.2% (9.4 - 18.3) reduction in transmission, respectively (Figure 4.3). We also found that the 6/7 pm curfew was more effective than the 8/9 pm curfew, reducing transmission by 67.9% (66.2 - 68.5) and 47.5% (45.0 - 49.0), respectively. Although school closures had a smaller effect, they still significantly reduced transmission by 14.5% (11.5 - 17.8). We chose to include intermediate periods of moderate restrictions into our model (termed "barrier gestures"), which substantially reduced transmission (between 16.1% and 60.1% with 70% adherence, which represented the median of population adherence). Finally, during the fourth period of barrier gestures, which included a vaccine passport in addition to hygiene protocols and mask-wearing, we estimated a reduction in transmission of 61.0% (59.6 - 62.9) due to this package of interventions, independently of the vaccine's effect. We found that weather had a significant influence on SARS-CoV-2 transmission, with an average increase of 10% in winter conditions and an average decrease of 20% in summer conditions, compared to the average weather conditions in France over the whole study period. The results were robust to changes in fixed parameters (see Supplementary Results Section *Sensitivity analyses*).

The population vaccine effect against both transmission and hospitalization increased over time as the population coverage increased (Figure 4.4a). However, after the emergence of the Delta variant, the vaccine's effect on transmission (e_{vI}) started to decline and first plateaued around 25% (95% CI 22 - 27) protective effect, indicating that it prevented 25% (22 - 27) of all new infections. With further increase in population vaccine coverage, e_{vI} stabilized at approximately 34% (30 - 38). e_{vH} increased steadily with increasing population vaccine coverage and was estimated to reach 84% (82 - 85) by the end of the study period. Thus, the overall protective effect against hospitalization, taking into account protection against infection and subsequent hospitalization, reached 89% (87-91) by the end of October 2021. If the whole population had been fully vaccinated with 2 doses

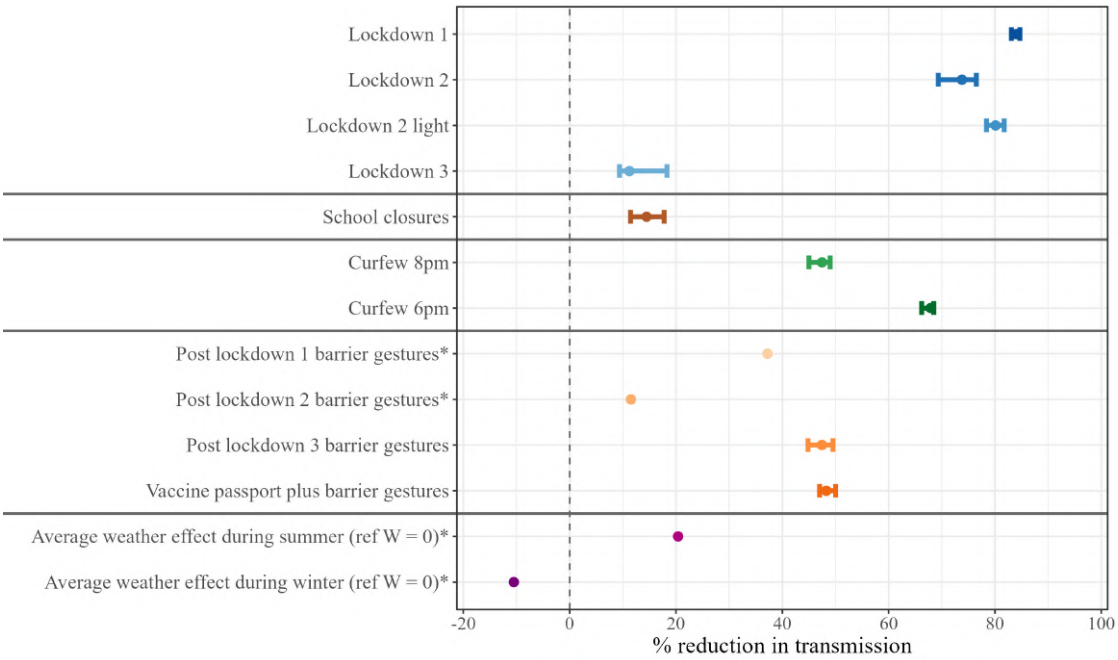

Figure 4.3: Estimation of the effect of NPIs and weather on SARS-CoV-2 transmission. Point estimates with 95% confidence interval. A negative percent transmission reduction indicates an increase in transmission (observed only for weather effect during winter).
Summer conditions during June - August, winter conditions during December - February. The transmission reduction of barrier gestures is shown assuming 70% population compliance, which was the median of the population compliance parameterization.
*Confidence intervals are not available for parameters whose effect was estimated by profile likelihood.

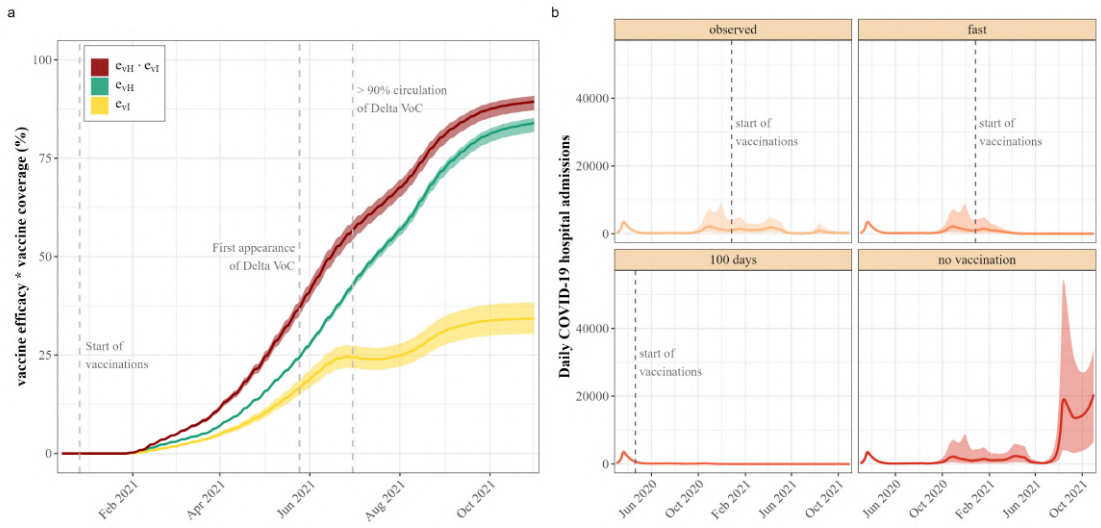

Figure 4.4: Vaccine effects. (a) Estimated protective effect conferred by vaccination. The population vaccine effect against transmission (e_{vI}) is depicted in yellow, the population vaccine effect against hospitalization (e_{vH}) among infected in green, and the total population vaccine effect against hospitalization ($e_{vH} \cdot e_{vI}$) in red. (b) Simulated hospital admissions in France under different vaccination scenarios. The solid lines depict the median of 1000 simulations, while the shaded areas show the 95% prediction interval. In the "Fast" scenario, the start of the vaccinations was held constant, but 1% of the population was vaccinated per day. In the "100 days" scenario, the vaccine was available 100 days after the publication of the full genomic sequence of SARS-CoV-2 (April 20, 2020). In the "No vaccination" scenario, no vaccines were available until the end of the study period.

and only the original strain of SARS-CoV-2 was circulating, our analysis therefore predicts a vaccine efficacy against hospitalization of 98% (85-100) and a vaccine efficacy against transmission of 87.5% (78-98). However, with 100% Delta VoC circulation, the vaccine efficacy against transmission reduced to 44% (39-49).

Compared to a scenario where no vaccines were available until the end of the study period and all NPIs were implemented and lifted as observed, the availability of vaccines saved 158,523 lives (95% prediction interval [PI] 39,518-348,958) and prevented 1,488,142 hospitalizations (95% PI 383,515-3,084,308) (Table 1). In relative terms, this corresponds to 168% more deaths (95% PI 69.5-314.8) and 300.1% (95% PI 132.9-492.0) more hospitalized patients. This would have exceeded the hospital capacity of all existing beds except psychiatry (332,785 beds) [356] on October 23, 2021, assuming that the entirety of hospital beds was available for COVID-19 patients. Under the more realistic assumption that 20% of the pre-pandemic hospital capacity would be available for COVID-19 patients, the

national hospital bed capacity would have been exceeded by August 6, 2021. The importance of NPIs in the absence of vaccines is underscored by the fact that deaths and hospitalizations surged after NPIs were lifted in the summer of 2021 (Figure 4.4b).

Scenario	**Number of observations · 1000 [95% PI]**	**Difference to observed scenario · 1000 [95% PI]**	**Percentage change to observed scenario [95% PI]**
Hospitalizations			
observed	470 [163; 1,348]		
fast	330 [131;950]	-146 [-373; -34]	-29.5% [-45.9; -15.6]
100 days	116 [85; 170]	-384 [-1,020; -89]	-79.9% [-89.1; -52.1]
no vaccination	1,930 [534; 4,597]	1,488 [384; 3,084]	300.1% [132.9; 492.0]
Deaths			
observed	92 [32; 262]		
fast	72 [28; 208]	-20 [-51; -5]	-21.5% [-35.4; -11.1]
100 days	24 [17; 37]	-71 [-204; -17]	-78.9% [-88.4; -51.3]
no vaccination	249 [71; 619]	159 [40; 349]	168.3% [69.5; 314.8]
Cases			
observed	10,306 [4,817; 25,264]		
fast	8,392 [4,388; 19,648]	-2,007 [-5,277; -463]	-19.2% [-34.4; -8.0]
100 days	4,650 [3,560; 6,571]	-6,141 [-16,114; -1,459]	-62.1% [-77.3; -30.7]
no vaccination	20,269 [7,489; 46,198]	10,174 [2,774; 19,654]	93.3% [43.9; 147.2]

Table 4.1: Counterfactual vaccine scenarios. In the "Fast" scenario, the start of the vaccinations was held constant, but 1% of the population was vaccinated per day. In the "100 days" scenario, the vaccine was available 100 days after the publication of the full genomic sequence of SARS-CoV-2 (April 20, 2020). In the "No vaccination" scenario, no vaccines were available until the end of the study period.
NA not applicable, PI prediction interval

If a vaccine had been available after 100 days and had been rolled out at the same speed and coverage as observed, but all NPIs had been implemented as they were in reality, 384,490 (95% PI 88,579-1,020,386) fewer people would have been hospitalized and 71,398 (16,507-204,249) fewer would have died. This corresponds to an 80% (95% CI 52-89) reduction in hospitalizations and 79% (51-88) reduction

in deaths while maintaining NPIs. We also demonstrated a significant reduction of hospitalizations and deaths if the vaccine had been rolled out faster, with 1% of the population vaccinated each day. The simulation outcomes for scenarios involving waning immunity were not substantially changed, even in the 100-day scenario. This finding can be explained by the fact that the vaccines combined with NPIs would have been sufficiently efficient to limit further transmission, so that the epidemics in each department concluded before any notable decline in vaccine-induced immunity (Figure S4.5 and Table S4.2 in Supplementary Results). In our simulations of earlier lockdown 1 implementation, we found that if the lockdown 1 had been implemented one week earlier, but the length of the lockdown would have still been 54 days, 92k (95% CI 61-118k) hospitalizations and 20k (13-26k) deaths could have been prevented, which corresponds to a 20.1 (8.6-39.7) and 21.9 (10.5-40.6) percent reduction of hospitalizations and deaths, respectively. If the lockdown had been advanced by two weeks, 33k (21-44k) lives could have been saved, which corresponds to a reduction in mortality of 35.2% (18.6-58.8) over the whole study period. Additional results with longer lockdown 1 duration are presented in the Supplementary Results Table S4.3 and Figure S4.6.

Discussion

Accurately estimating the effects of past interventions is critical for better preparation against future pandemics. In this study, we used a compartmental model to estimate the joint impact of NPIs and vaccinations in France over a prolonged period, with high geographic resolution. We found that all analyzed NPIs significantly reduced SARS-CoV-2 transmission. Nevertheless, we observed that the effectiveness of lockdowns decreased over time, potentially due to reduced intervention stringency and/or population compliance. During the third lockdown, VoC spread increased transmission while vaccinations were being rapidly administered, which may have weakened the effectiveness of this NPI. We also demonstrated that curfews were effective in reducing viral spread, with the 6/7 pm curfew being more effective than the 8/9 pm curfew. This suggests that earlier curfews were more effective, although one study in Greece concluded that an earlier curfew only led to a very minor increase in residential spaces, and no change in time spent in essential businesses [357].

Similar findings were reported in two studies conducted on French data during a similar study period [1, 150]. However, our estimates for the first lockdown, curfews, and school closures are higher, while the third lockdown estimate is significantly lower. The effects of weather, parameterized as IPTCC by Collin et al. and included as only temperature by Paireau et al. were close to our estimates. The differences in results can be explained by the modeling approach used. Whereas Paireau et al. first estimated $\mathcal{R}_t$ from hospital admissions and then used a linear mixed regression model to derive NPI effectiveness estimates, Collin et al. used a

two-step estimation procedure with a compartmental model and Kalman filtering. In contrast, we used a compartmental model that explicitly modeled the viral dynamics and vaccination and estimated all parameters in one step. By modeling the dynamics of the disease directly, we believe that our approach can give more accurate results than observing correlations in regression models. Additionally, our model is on a more granular geographical scale (departmental vs. regional) compared to Collin et al. [150].

Our study's estimates for the effectiveness of the first lockdown in France align with those found by Flaxman et al. (81% (75–87) reduction in $\mathcal{R}_t$)[131], who conducted pooled analyses of European countries, and Salje et al. (77% (76-78) reduction in $\mathcal{R}_t$)[269], who studied the effectiveness of the French lockdown during the first wave. Similar to our results, curfews were estimated to effectively reduce mobility in Quebec, Canada [358], and reduced viral transmission in French Guiana [359]. However, conflicting results were found in Germany [360], which suggests that curfews highly depend on the context in which they are implemented and on the stringency of implementation or the methods used to assess the effect.

In contrast to the commonly used two-step study approach for estimating NPI effectiveness, which involves estimating an epidemic parameter (e.g., reproductive number) separately and then using it in a regression model [1, 155], we estimated all model parameters simultaneously. This ensures accurate estimation of parameter uncertainty, in contrast to the two-step approach, where the uncertainty from the initial estimation step is not considered in the final result. Furthermore, regressions cannot account for population immunity and are susceptible to confounding, given the non-independent implementation of NPIs in relation to the epidemiological situation. In contrast, compartmental models offer the advantage of a clear causal framework [361], explicitly modelling epidemic dynamics and accounting for the depletion of susceptible individuals.

Our results showed a strong effect of vaccines against hospitalization, which is consistent with previous studies [362], and a smaller but still significant real-life effectiveness of vaccines against transmission [363]. Since we had precise data on the number of vaccine doses administered per day per department, it was not necessary to model vaccinated compartments as unknowns, but we included them as terms reducing transmission and hospitalization. The simulations showed that 158,523 (39,518 - 348,958) lives were saved, which conflicts with estimates from Watson et al. who suggest that vaccination averted 571,100 (535,700 - 608,600) deaths in France over a study period of one month longer than our study [195]. However, the methodology used by Watson et al. to estimate excess deaths, on which their estimates are based, has been criticized for over-estimating deaths [17, 20].

Our study has some limitations that must be acknowledged when interpreting our findings. First, we were unable to incorporate an age structure into our analysis due to the unavailability of age-stratified hospital data at the departmental level. Thus, we assumed uniform susceptibility across the population, which may lead to an underestimation of the vaccine's effectiveness against hospitalization. This is because older individuals, who are more susceptible to severe disease, hospitalization, and death, were vaccinated first and have a higher vaccine coverage than younger age groups. We attempted to mitigate the problem by introducing random effects at the departmental level, which could take into account some of the intrinsic differences between the departments, such as the different age structure and population density. Nevertheless, our estimates should be considered conservative and a lower bound of the vaccine's effectiveness. Due to collinearity, the effects of other NPIs, such as non-essential store closures or bar and restaurant closures, could not be estimated separately. These effects are therefore included in the estimated NPIs and the moderate restriction periods. Several more complex alternatives to our chosen model could have been considered, such as incorporating an additional presymptomatic-and-infectious compartment[269, 270], including vaccinated compartments [278, 364], or chaining progressive stages of compartments [271, 278]. However, opting for such models requires the estimation or fixation of additional parameters. Faced with identifiability issues, we chose to adhere to a simpler model, as many models similar to ours have been used to fit SARS-CoV-2 dynamics [150, 350–352].

In conclusion, our study provides valuable insights into the effectiveness of various NPIs and vaccines in reducing COVID-19 transmission, hospitalizations, and deaths in France. Our analysis shows that the implementation of stringent NPIs, such as lockdowns, curfews, and school closures, contributed significantly to reducing the spread of the virus. Moreover, vaccination was found to be effective in reducing COVID-19 hospitalizations, deaths, and infections. Our dynamical model allowed us to quantify the impact of vaccines in counterfactual scenarios, highlighting the importance of early and fast vaccine rollout in preventing further epidemic resurgences and controlling other emerging respiratory infectious diseases. Our findings can aid in the development of effective mitigation policies for future COVID-19 waves and other respiratory diseases. However, our findings should be generalized to other settings with caution, as the effectiveness of NPIs and vaccines may vary across different countries, depending on the local context, population behavior, and implementation strategies. Further research is needed to better understand the heterogeneity of NPI and vaccine effectiveness across regions and to inform mitigation policies for further COVID-19 waves or other respiratory diseases.

Funding

This work has been pursued in the EMERGEN project framework of the French Agency for Research on AIDS and Emerging Infectious Diseases (ANRS0151) and supported by INSERM and the Investissements d'Avenir program, Vaccine Research Institute (VRI), managed by the ANR under reference ANR-10-LABX-77-01. The funding source was not involved in the design, execution, analysis, interpretation of the research findings, or manuscript writing.

CRediT authorship contribution statement

Jane Heffernan: Methodology, Supervision, Writing – review & editing. **Rodolphe Thiebaut:** Conceptualization, Methodology, Supervision, Writing – review & editing. **Mélanie Prague:** Conceptualization, Data curation, Methodology, Supervision, Writing – review & editing. **David L. Buckeridge:** Methodology, Supervision, Writing – review & editing. **Iris Ganser:** Formal analysis, Methodology, Visualization, Writing – original draft, Data curation.

Declaration of Competing Interest

The authors declare that they have no known competing financial interests or personal relationships that could have appeared to influence the work reported in this paper.

Data availability

All data are available in the public domain at the indicated references.

Acknowledgements

We thank Simulations Plus, Lixoft division for the free academic use of the MonolixSuite. Numerical computations were in part carried out using the PlaFRIM experimental testbed, supported by Inria, CNRS (LABRI and IMB), Université de Bordeaux, Bordeaux INP, and Conseil Régional d'Aquitaine (see `https://www.plafrim.fr`). IG is supported within the framework of the PIA3 (Investment for the Future), project reference: 17-EURE-0019, and by a doctoral award from the Fonds de recherche du Québec-Santé. JH acknowledges funding by NSERC, PHAC-NSERC EIDM, and the York Research Chair Program.

4.3 Manuscript 1: References

1. Paireau J, Charpignon ML, Larrieu S, et al. Impact of non-pharmaceutical interventions, weather, vaccination, and variants on COVID-19 transmission across departments in France. *BMC Infect. Dis.* 2023; 23(1):1–12.

17. Schöley J, Karlinsky A, Kobak D, Tallack C. Conflicting COVID-19 excess mortality estimates. *The Lancet*. 2023; 401():431–432. URL: `https://linkinghub.elsevier.com/retrieve/pii/S0140673623001162`.

20. Bager P, Nielsen J, Bhatt S, Nielsen LB, Krause TG, Vestergaard LS. Conflicting COVID-19 excess mortality estimates. *The Lancet*. 2023; 401():432–433. URL: `https://linkinghub.elsevier.com/retrieve/pii/S0140673623001150`.

115. Iezadi S, Gholipour K, Azami-Aghdash S, et al. Effectiveness of non-pharmaceutical public health interventions against COVID-19: A systematic review and meta-analysis. *PLoS One*. 2021; 16(11):e0260371.

116. Mendez-Brito A, El Bcheraoui C, Pozo-Martin F. Systematic review of empirical studies comparing the effectiveness of non-pharmaceutical interventions against COVID-19. *J. Infect.* 2021; 83(3):281–293.

119. Talic S, Shah S, Wild H, et al. Effectiveness of public health measures in reducing the incidence of covid-19, SARS-CoV-2 transmission, and covid-19 mortality: systematic review and meta-analysis. *BMJ*. 2021; 375():e068302.

126. Hale T, Angrist N, Goldszmidt R, et al. A global panel database of pandemic policies (Oxford COVID-19 Government Response Tracker). *Nat. Hum. Behav.* 2021; 5():529–538.

131. Flaxman S, Mishra S, Gandy A, et al. Estimating the effects of non-pharmaceutical interventions on COVID-19 in Europe. *Nature*. 2020; 584():257–261.

150. Collin A, Hejblum BP, Vignals C, et al. Using a population-based Kalman estimator to model the COVID-19 epidemic in France: estimating associations between disease transmission and non-pharmaceutical interventions. *International Journal of Biostatistics*. 2023; 20(1):13–41.

155. Liu Y, Morgenstern C, Kelly J, Lowe R, Jit M. The impact of non-pharmaceutical interventions on SARS-CoV-2 transmission across 130 countries and territories. *BMC Med.* 2021; 19(1):1–12.

169. Di Domenico L, Pullano G, Sabbatini CE, Boëlle PY, Colizza V. Impact of lockdown on COVID-19 epidemic in Île-de-France and possible exit strategies. *BMC Med.* 2020; 18(1):1–13.

195. Watson OJ, Barnsley G, Toor J, Hogan AB, Winskill P, Ghani AC. Global impact of the first year of COVID-19 vaccination: a mathematical modelling study. *Lancet Infect. Dis.* 2022; 22(9):1293–1302.

219. Feikin DR, Higdon MM, Abu-Raddad LJ, et al. Duration of effectiveness of vaccines against SARS-CoV-2 infection and COVID-19 disease: results of a systematic review and meta-regression. *Lancet*. 2022; 399(10328):924–944.

269. Salje H, Kiem CT, Lefrancq N, et al. Estimating the burden of SARS-CoV-2 in France. *Science*. 2020; 369():208–211. URL: https://dx.doi.org/10.1126/science.abc3517.

270. Roux J, Massonnaud CR, Colizza V, Cauchemez S, Crépey P. Modeling the impact of national and regional lockdowns on the 2020 spring wave of COVID-19 in France. *Sci. Rep.* 2023; 13(1834):1–9.

271. Sofonea MT, Reyné B, Elie B, et al. Memory is key in capturing COVID-19 epidemiological dynamics. *Epidemics*. 2021; 35():100459.

278. Childs L, Dick DW, Feng Z, Heffernan JM, Li J, Röst G. Modeling waning and boosting of COVID-19 in Canada with vaccination. *Epidemics*. 2022; 39():100583.

282. Moore S, Hill EM, Tildesley MJ, Dyson L, Keeling MJ. Vaccination and non-pharmaceutical interventions for COVID-19: a mathematical modelling study. *Lancet Infect. Dis.* 2021; 21(6):793–802.

332. Bellu G, Saccomani MP, Audoly S, D'Angio L. DAISY: A new software tool to test global identifiability of biological and physiological systems. *Computer Methods and Programs in Biomedicine*. 2007; 88(1):52–61. URL: https://dx.doi.org/10.1016/j.cmpb.2007.07.002.

339. Bestetti RB, Furlan-Daniel R, Couto LB. Nonpharmaceutical public health interventions to curb the COVID-19 pandemic: a narrative review. *The Journal of Infection in Developing Countries*. 2022; 16():583–591. URL: https://dx.doi.org/10.3855/jidc.14580.

340. Crane MA, Shermock KM, Omer SB, Romley JA. Change in Reported Adherence to Nonpharmaceutical Interventions During the COVID-19 Pandemic, April-November 2020. *JAMA*. 2021; 325():883. URL: https://dx.doi.org/10.1001/jama.2021.0286.

341. Landier J, Paireau J, Rebaudet S, et al. Cold and dry winter conditions are associated with greater SARS-CoV-2 transmission at regional level in western countries during the first epidemic wave. *Scientific Reports*. 2021; 11(1). URL: https://dx.doi.org/10.1038/s41598-021-91798-9.

342. Wang J, Tang K, Feng K, et al. Impact of temperature and relative humidity on the transmission of COVID-19: a modelling study in China and the United States. *BMJ Open*. 2021; 11(2):e043863. URL: https://dx.doi.org/10.1136/bmjopen-2020-043863.

343. Romero Starke K, Mauer R, Karskens E, et al. The Effect of Ambient Environmental Conditions on COVID-19 Mortality: A Systematic Review. *International Journal of Environmental Research and Public Health*. 2021; 18(12):6665. URL: https://dx.doi.org/10.3390/ijerph18126665.

344. Santé publique France. *Données hospitalières relatives à l'épidémie de COVID-19 (SI-VIC)*. 2021. URL: https://www.data.gouv.fr/fr/datasets/donnees-hospitalieres-relatives-a-lepidemie-de-covid-19/.

345. Santé publique France. *Données relatives aux résultats des tests virologiques COVID-19 (SI-DEP)*. 2020. URL: https://www.data.gouv.fr/fr/datasets/old-donnees-relatives-aux-resultats-des-tests-virologiques-covid-19/.

346. Santé publique France. *CoviPrev : une enquête pour suivre l'évolution des comportements et de la santé mentale pendant l'épidémie de COVID-19*. 2023. URL: https://www.santepubliquefrance.fr/etudes-et-enquetes/coviprev-une-enquete-pour-suivre-l-evolution-des-comportements-et-de-la-sante-mentale-pendant-l-epidemie-de-covid-19.

347. Santé publique France. *Données relatives aux personnes vaccinées contre la Covid-19 (VAC-SI)*. 2021. URL: https://www.data.gouv.fr/fr/datasets/donnees-relatives-aux-personnes-vaccinees-contre-la-covid-19-1/.

348. Majumder P, Ray PP. A systematic review and meta-analysis on correlation of weather with COVID-19. *Scientific Reports*. 2021; 11(). URL: https://dx.doi.org/10.1038/s41598-021-90300-9.

349. Pan A, Liu L, Wang C, et al. Association of Public Health Interventions With the Epidemiology of the COVID-19 Outbreak in Wuhan, China. *JAMA*. 2020; 323():1915. URL: https://dx.doi.org/10.1001/jama.2020.6130.

350. Li Y, Wang LW, Peng ZH, Shen HB. Basic reproduction number and predicted trends of coronavirus disease 2019 epidemic in the mainland of China. *Infectious Diseases of Poverty*. 2020; 9(1). URL: https://dx.doi.org/10.1186/s40249-020-00704-4.

351. McCarthy Z, Xiao Y, Scarabel F, et al. Quantifying the shift in social contact patterns in response to non-pharmaceutical interventions. *Journal of Mathematics in Industry*. 2020; 10(1). URL: https://dx.doi.org/10.1186/s13362-020-00096-y.

352. Tang B, Wang X, Li Q, et al. Estimation of the Transmission Risk of the 2019-nCoV and Its Implication for Public Health Interventions. *Journal of Clinical Medicine*. 2020; 9(2):462. URL: https://dx.doi.org/10.3390/jcm9020462.

353. Heffernan JM, Smith RJ, Wahl LM. Perspectives on the basic reproductive ratio. *Journal of The Royal Society Interface*. 2005; 2():281–293. URL: https://dx.doi.org/10.1098/rsif.2005.0042.

354. Gralinski LE, Menachery VD. Return of the Coronavirus: 2019-nCoV. *Viruses*. 2020; 12():135. URL: https://dx.doi.org/10.3390/v12020135.

355. Clairon Q, Prague M, Planas D, et al. Modeling the kinetics of the neutralizing antibody response against SARS-CoV-2 variants after several administrations of Bnt162b2. *PLoS Comput. Biol.* 2023; 19(8):e1011282.

356. DREES. *Les établissements de santé - édition 2022 — Direction de la recherche, des études, de l'évaluation et des statistiques (DREES)*. 2022. URL: https://drees.solidarites-sante.gouv.fr/publications-documents-de-reference-communique-de-presse/panoramas-de-la-drees/les-etablissements.

357. Velias A, Georganas S, Vandoros S. COVID-19: Early evening curfews and mobility. *Social Science & Medicine*. 2022; 292():114538. URL: https://www.sciencedirect.com/science/article/pii/S0277953621008704.

358. Ghasemi A, Daneman N, Berry I, et al. Impact of a nighttime curfew on overnight mobility. 2021(). URL: https://dx.doi.org/10.1101/2021.04.04.21254906.

359. Andronico A, Kiem CT, Paireau J, et al. Evaluating the impact of curfews and other measures on SARS-CoV-2 transmission in French Guiana. *Nature Communications*. 2021; 12(). URL: https://dx.doi.org/10.1038/s41467-021-21944-4.

360. Apel J, Rohde N, Marcus J. The effect of a nighttime curfew on the spread of COVID-19. *Health Policy*. 2023; 129():104712. URL: https://www.sciencedirect.com/science/article/pii/S0168851023000295.

361. Aalen OO, Røysland K, Gran JM, Ledergerber B. Causality, Mediation and Time: A Dynamic Viewpoint. *J. R. Stat. Soc. Ser. A Stat. Soc.* 2012; 175(4):831–861.

362. Zheng C, Shao W, Chen X, Zhang B, Wang G, Zhang W. Real-world effectiveness of COVID-19 vaccines: a literature review and meta-analysis. *International Journal of Infectious Diseases*. 2022; 114():252–260. URL: http://www.ijidonline.com/article/S1201971221008572/fulltext.

363. Hall VJ, Foulkes S, Saei A, et al. COVID-19 vaccine coverage in health-care workers in England and effectiveness of BNT162b2 mRNA vaccine against infection (SIREN): a prospective, multicentre, cohort study. *The Lancet*. 2021; 397():1725–1735. URL: https://dx.doi.org/10.1016/s0140-6736(21)00790-x.

364. Viana J, Van Dorp CH, Nunes A, et al. Controlling the pandemic during the SARS-CoV-2 vaccination rollout. *Nature Communications*. 2021; 12(1). URL: https://dx.doi.org/10.1038/s41467-021-23938-8.

4.4 Manuscript 1: Supplementary Methods

Data description

Epidemiological data

All epidemiological data were made available by Santé Publique France. COVID-19-related hospital admissions and occupancy were obtained from the SI-VIC (*Système d'Information pour le suivi des VICtimes*) database as of March 1st, 2020 [344]. The SI-VIC database includes all patients treated in private or public hospitals with either a laboratory-confirmed diagnosis of COVID-19 or a chest CT indicative of the diagnosis of COVID-19. Data on deaths of patients with COVID-19 in hospitals could be obtained from the SI-VIC database as of March 18th, 2020. Since this was the only source of death data on the departmental level, we make the assumption in our model that only hospitalized people died. We corrected this assumption in the simulations and the model fits (see "Observation model" in Supplementary Methods). PCR-confirmed COVID-19 cases were available from the SI-DEP database (*Système d'Informations de DEPistage*) as of May 13th, 2020 [345]. All data were aggregated at the departmental level. A French department is a small administrative region with a median of approx. 550k inhabitants (Figure S4.1).

NPI data

We separated the lockdown periods into three distinct measures as they encompassed different interventions with varying levels of stringency, which may have different impacts on transmission. During the first lockdown, the personal time and radius of movement of individuals was restricted to one hour a day and one kilometer around the place of residence. Exceptions were made only for critical workers, while all other individuals were required to work from home. In the second lockdown, on-site work was allowed if remote working was not feasible, and the personal radius around the place of residence was expanded to 20 km. Prior to Christmas 2020, non-essential stores were permitted to reopen. To account for this in our model, we introduced the NPI of "lockdown 2 light," whose effect is estimated separately from the effect of the second lockdown. In contrast to the second lockdown, where schools remained open, schools were closed during the third lockdown and the personal radius was restricted to 10 km. In the coding of the school closure variable, we did not differentiate between regular and pandemic-related school closures. However, we accounted for two reopening phases from the end of the first lockdown (May 11, 2020) until the end of the school year (July 4, 2020) during which student enrollment returned to normal. A summary of NPI implementation and relaxation dates across all departments can be found in Figure S4.2.

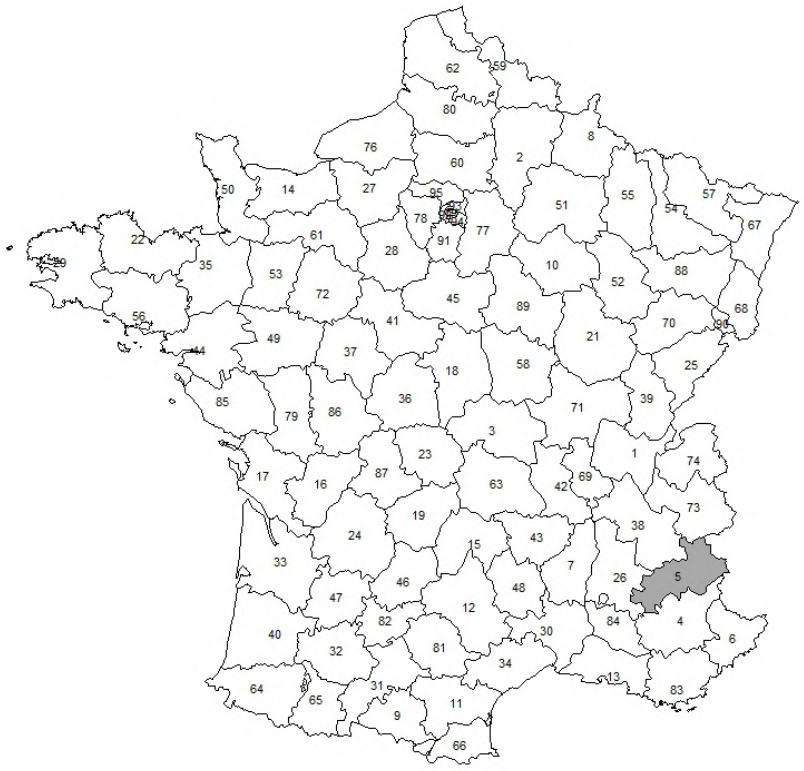

Figure S4.1: Map of French non-insular departments. The department number is indicated at the center of each department. Department 5 (Hautes Alpes) is highlighted because it was excluded from the analysis due to missing weather data after February 17, 2021.

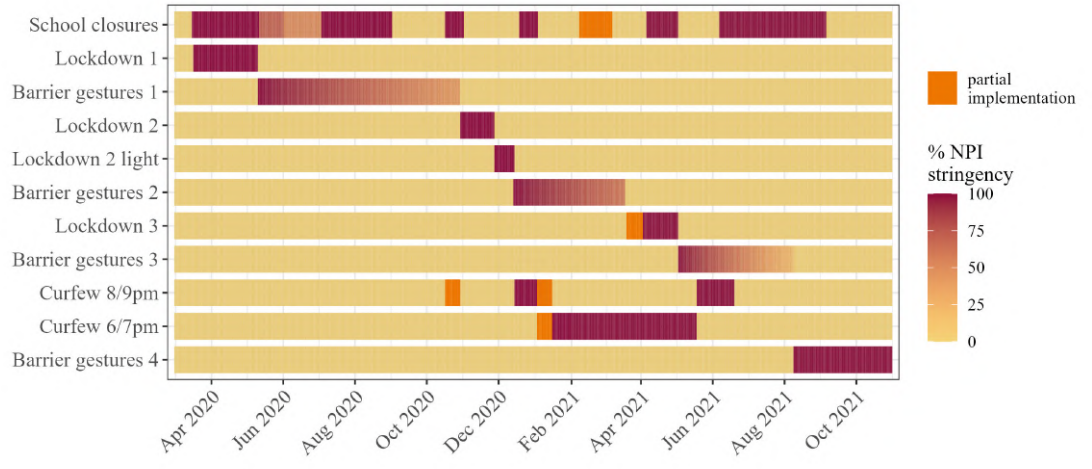

Figure S4.2: NPI implementation and relaxation dates in France. While the lockdown and curfew NPIs were parameterized as either in effect or not (1 vs. 0), the school closure and barrier gesture NPIs could vary in stringency over time. This parameterization is reflected in varying shades of red. Additionally, sometimes NPIs were implemented only in some French departments, which is depicted in bright orange.

SARS-CoV-2 variants

In late 2020, the emergence of SARS-CoV-2 variants with increased transmissibility, virulence, and decreased effectiveness of pharmaceutical interventions prompted health authorities to classify these viral mutants as "variants of concern" (VoCs). The methodology for reporting variants in SI-DEP changed over time: until the end of May 2021, variants were indicated as 20I/501Y.V1 (Alpha), 20H/501Y.V2 (Beta), and 20J/501Y.V3 (Gamma).2 Afterwards, only the percentage of typical mutations were reported, but they were not attributed directly to any VoC, and no Alpha-specific mutations were reported. However, when the reporting switch occurred, the alpha variant was found in close to 100% of all sequenced samples. Therefore, we assumed that the percentage of Alpha mutates stayed around that level and was gradually replaced by Delta. We defined all samples with an E484K mutation as Beta/Gamma VoC, and all samples with a L452R mutation as Delta. Omicron mutations were disregarded since our study ended on October 31st, 2021.

Weather

A daily weighted average temperature in Celsius (T), absolute humidity in g/m3 (AH), and relative humidity in percent (RH) was calculated for each geographical unit, where the weights correspond to the population within a 10 km radius around the weather station in order to account for varying population density. To keep the model sparse, we combined temperature and humidity into the Index PREDICT

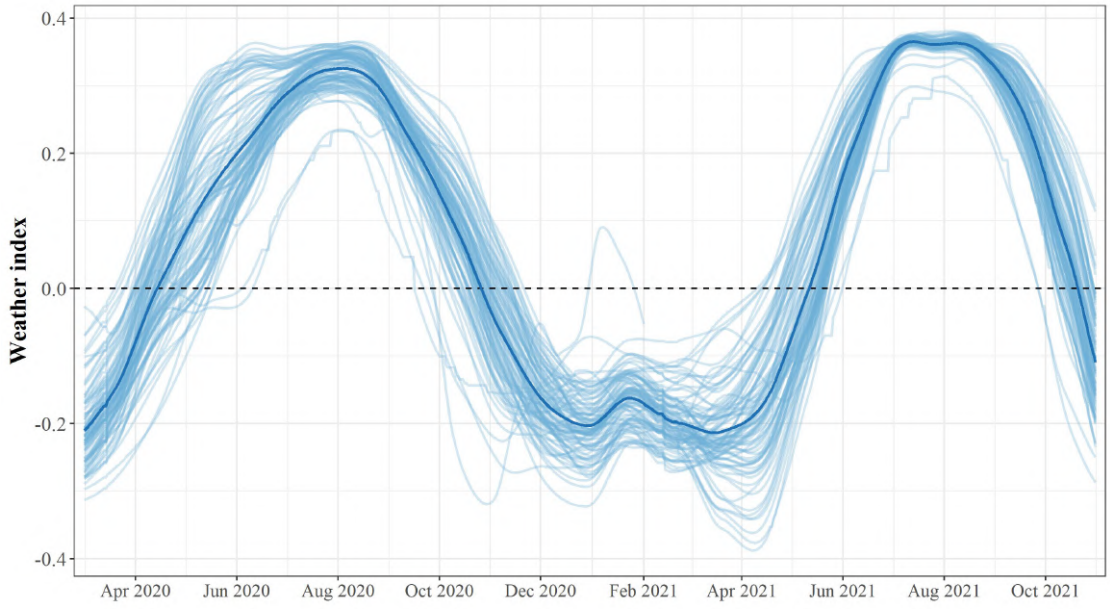

Figure S4.3: Weather index. The thin lines indicate the weather index in each department, while the thicker line indicates the median of all departments.

of Transmissibility of COVID-19 (IPTCC) [365, 366]:

$$IPTCC = 100 \times exp^{-\frac{1}{2}\left[\frac{(T-7.5)^2}{196}+\frac{(RH-75)^2}{625}+\frac{(AH-6)^2}{2.89}\right]} \tag{S4.1}$$

The IPTCC ranges between 0% and 100%, with lower values indicating less favorable conditions for SARS-CoV-2 transmission. To facilitate interpretation, we normalized the index (i.e., forced its range to 1), subtracted the annual mean, and inverted it. Thus, the annual average across all departments is set to 0, with high values in summer and low values in winter. We also applied a *loess* smoothing with a span of 0.2 to account for seasonal differences in SARS-CoV-2 transmissibility, resulting in a smooth weather variable W (Figure S4.3).

Model

Compartmental model

Our model divided the population into seven compartments: susceptible individuals (S), latently exposed individuals (E), symptomatically infectious individuals (I), asymptomatically infectious individuals (A), hospitalized individuals (H), recovered individuals (R), and deceased individuals (D). We assumed that individuals were initially susceptible (S) and could be exposed to the virus but not yet

infectious (E). After 5.1 days, exposed individuals could progress to either the symptomatically infectious (I) or asymptomatically infectious (A) compartment, based on their probability of being symptomatic.5 Individuals in these compartments could then infect susceptible individuals at a time-varying transmission rate. We assumed that asymptomatic individuals were 45% less infectious than symptomatically infected individuals [367]. Individuals spent an average of 5 days in the A compartment before recovering and progressing to the R compartment. Symptomatically infected individuals could either be hospitalized after a certain time (DQ) or recover based on a time-varying risk of hospitalization. We assumed that hospitalized individuals were no longer infectious and remained in the hospital for a department-specific and time-varying period (DH) or died after an average of 15 days. Due to waning immunity, recovered individuals will become susceptible again after an average duration of 180 days. Additionally, we included parameters e_{vI} and e_{vH} in the model to account for vaccine protection against transmission and hospitalization, respectively. The dynamics of this model are given in equation S4.2.

$$
\begin{aligned}
\dot{S} &= -b(1-e_{vI})S\frac{I+\alpha A}{N} + \frac{R}{D_R} \\
\dot{E} &= b(1-e_{vI})S\frac{I+\alpha A}{N} - \frac{E}{D_E} \\
\dot{I} &= \frac{r_E E}{D_E} - (1-e_{vH})\frac{r_H I}{D_Q} - \frac{(1-r_H)I}{D_I} \\
\dot{A} &= \frac{(1-r_E)E}{D_E} - \frac{A}{D_I} \\
\dot{H} &= (1-e_{vH})\frac{r_H I}{D_Q} - \frac{(1-fr)H}{D_H} - \frac{frH}{D_D} \\
\dot{R} &= \frac{(1-fr)H}{D_H} + \frac{(1-r_H)I + A}{D_I} - \frac{R}{D_R} \\
\dot{D} &= \frac{frH}{D_D}
\end{aligned}
\tag{S4.2}
$$

Our model relies on fixed estimates for some epidemiological parameters, such as the duration of infection, the probability of being symptomatic, and transition probabilities from some compartments to others (D_E, D_I, D_R, and D_D). Other parameters such as D_Q, D_H, r_I, and fr were estimated in two time periods to account for changes in case reporting and treatment availability after the first wave. Finally, the transmission rate t is time-varying and was estimated as a function of NPIs and other factors influencing transmission (see 4.4). Table S4.1 contains a

detailed listing of the parameters, their interpretation, values, and sources used in defining the compartmental model.

The dynamics were estimated in a population approach, i.e., they described the epidemics at the departmental level (= 94 units of observation) while also accounting for inter-individual variability and estimating shared parameters. E_0, D_Q, and b_0 were estimated with random effects, i.e., separately for each department but with a shared population value, to account for differences between departments in population density, contact rates, starting conditions at the beginning of the study period (the pandemic started in the East and Paris regions), and hospital conditions in each department.

We assume that VoCs alter risk of hospital admission because of increased disease severity according to values published in a systematic review [369]. Therefore, the time-varying risk of hospitalization is modeled as a function of VoC circulation:

$$r_{H_i} = r_{WT} \cdot \%_{WT_i} + r_{\alpha} \cdot r_{WT} \cdot \%_{\alpha_i} + r_{\beta\gamma} \cdot r_{WT} \cdot \%_{\beta\gamma_i} + r_{\delta} \cdot r_{WT} \cdot \%_{\delta_i} \tag{S4.3}$$

In our model, we separately evaluated the vaccines' effect as the population vaccine effect against transmission (e_{vI}) and the population vaccine effect against hospitalization (e_{vH}). We define the vaccine effect to be the product of the vaccine efficacy (estimated by the model) and the population vaccine coverage at the departmental level. Since hospitalized patients need to be infected first, the total protection is the product of vaccine effect against transmission and vaccine effect against hospitalization. As it has been shown that VoCs reduce vaccine effectiveness against transmission, but not vaccine effectiveness against hospitalization [372, 373], we included VoC circulation in the e_{vI} model only. Since we assume that after vaccination, immunity takes three weeks to fully develop, we lagged the effect of all vaccine doses by three weeks, both for dose one and two.

$$\begin{aligned} e_{vH} &= VE_{H1} \cdot cov_{dose1_i} + \boldsymbol{VE_{H2}} \cdot cov_{dose2_i} \\ e_{vI} &= VE_{I1} \cdot cov_{dose1_i} \cdot (1 - \%_{\delta_i}) + \boldsymbol{VE_{I2}} \cdot cov_{dose2_i} \cdot (1 - \%_{\delta_i}) + VE_{I2\delta} \cdot cov_{dose2_i} \cdot \%_{\delta_i} \end{aligned} \tag{S4.4}$$

where $VE_{H1} = 0.7VE_{H2}$ [374], $VE_{I1} = 0.5VE_{I2}$ [187], and $VE_{I2\delta} = 0.5VE_{I2}$ [375].

Statistical model

In order to account for geographic variability across departments, we used a linear mixed effects model to describe the logarithm of the transmission rate at a given time as a function of time, NPIs, weather, and VoCs. We fixed the effect VoCs to previously published values (transmission is increased by 50% for

Parameter	Interpretation	Value
b_t	time-varying transmission rate of infections cases	Estimated
b_0	Basic transmission rate of infections cases	Estimated - department-specific
r_E	Ratio of symptomatic cases among all infected	0.844 [47]
r_H	Hospitalization rate	Time-varying, dependent on VoC circulation
r_{WT}	Risk of hospitalization when infected with original SARS-CoV-2 strain	Fixed via profile likelihood in 2 periods: 0.15 for first wave, 0.04 after
D_E	Latent (incubation) period (days)	5.1 days [46]
D_I	Infectious period (days)	5 days [368]
α	Ratio of transmission between A and I	0.55 [367]
D_Q	Duration from infection to hospitalization (days)	Estimated in 2 periods (department-specific)
D_H	Length of stay in hospital (days)	Estimated from hospital admissions and hospital occupancy (department-specific)
D_D	Duration from hospital admission to death (days)	15 (fixed with profile likelihood)
D_R	Duration of waning of infection-acquired immunity (days)	365 days [247]
E_0	Initial condition of exposed compartment	Estimated – department-specific
cov	population vaccine coverage	time-varying, from VAC-SI [347]
VE	vaccine efficacy	Estimated
$\%_{VoC}$	proportion of VoC among all sequenced samples. $\%_{WT}$ is calculated as $1 - \sum \%_{VoC}$	time-varying, from SI-DEP [345]
r_α	proportional risk increase of hospitalization when infected with Alpha VoC	1.5 [369]
$r_{\beta\gamma}$	proportional risk increase of hospitalization when infected with Beta or Gamma VoC	2.4 [369, 370]
r_δ	proportional risk increase of hospitalization when infected with Delta VoC	3 [369, 371]
e_{vI}	Population vaccine effect against infection	Calculated as vaccine efficacy parameter (estimated)*population vaccine coverage
e_{vH}	Population vaccine effect against hospitalization	Calculated as vaccine efficacy parameter (estimated)*population vaccine coverage

Table S4.1: Definition of model parameters and associated values.

Alpha/Beta/Gamma VoCs [375] and 100% for Delta [73, 375]) as they were not identifiable due to temporal interactions with vaccinations and NPIs. Since we used a logarithmic transformation, we assumed that NPIs and other covariates have a multiplicative effect on the transmission rate. A multiplicative effect is also more appropriate to ensure that NPIs can be effective even if transmission is low, and a log transformation automatically ensures positive transmission values.

$$log(b_{i,t}) = b_{0i} + \sum_j \beta_i^j NPI_{i,t}^j + \sum_k \beta_V^k VoC_{i,t}^k + \beta_w weather_{i,t} \tag{S4.5}$$

where $b_{0i} \sim N(b_{0_{pop}}, \omega)$ for department i at time t, NPI j and VoC k. We included a random effect only for the lockdown parameters and the basic transmission rate b_0, assuming that the effect of other interventions is consistent across all departments. Extending the random effect estimation to other NPI parameters did not improve model fits but increased identifiability issues.

Observation model

We jointly modeled COVID-19 deaths, cases, hospital admissions, and hospital occupancy as observations with a Normal distribution. We account for the uncertainty of observations by including a combined error model of the form $y = f + (a + bf)\epsilon$, where f is the model's prediction for each observation, respectively, a is a constant error term, and b is a proportional error term, denoting that the errors' amplitude increases with the predicted value's size.

To account for differential reporting, we applied a reporting correction factor on observed cases. This parameter was determined through profile likelihood (see below) as 0.2 during the first wave and 0.85 afterwards. As we assumed in our model that only hospitalized individuals could proceed to the D compartments, we applied an inflation factor of 1.33 (1/0.75) to all modelled deaths. This number was derived from data from *Santé Publique France*, which showed that approximately 75% of all COVID-19 deaths were occurring in hospitals [376]. To facilitate model fitting across compartments, we standardized all observations to the population size of the respective department.

$$\begin{aligned} Hospital\ admissions : Y_{i,t}^{Had} &= (1 - e_{vH})\frac{r_H I}{D_Q} \\ Hospital\ occupancy : Y_{i,t}^{H} &= H_{i,t} \\ Cases : Y_{i,t}^{I} &= \frac{r_E E}{D_E} \\ Deaths : Y_{i,t}^{D} &= \frac{frH}{D_D} \end{aligned} \tag{S4.6}$$

Parameter estimation

Some of the parameters in the compartmental and the statistical model were fixed based on literature or profile likelihood estimation. The profile likelihood estimation process consists of i) defining a range of values for the parameter to be evaluated, ii) sequentially fixing the parameter to the pre-defined value, iii) estimating all other parameters that are not fixed by maximizing the log-likelihood, and iv) selecting the parameter that results in the model with the highest likelihood value (and therefore the lowest AIC) [377]. This approach was applied in a sequential way to all parameters estimated using profile likelihood (influence of weather on transmission, D_D, r_{WT}, and the β parameters for barrier gesture periods one and two). The remaining parameters were estimated using maximum likelihood estimation using a stochastic approximation expectation maximization (SAEM) algorithm implemented in the software Monolix, version 2019R2 (http://www.lixoft.com).

Modeling assumptions

As in all SEIR-type models, we assume homogeneous mixing, uniform susceptibility of the population, no stochasticity in transmission, and mutual independence between units of observation (departments). Moreover, we assume that population dynamics, i.e., births or deaths other than from COVID-19 are negligible, since we applied our model only for 1.5 years. The effects of NPIs are assumed to be immediate and constant over the time they are implemented. However, a lag from implementation to effect on the observations is implicitly incorporated through the modelled period from viral transmission to case detection, from infection to hospitalization, and from hospitalization to death. Furthermore, we assume that a combined error model of the form $y = f+(a+bf)\epsilon$ is adequate for all observations, where f is the structural model, a is constant error term, and b is proportional error term. For the statistical model, we assume a linear relationship between log(transmission) and the continuous covariates (weather and barrier gestures), and independence of observations, given random effects.

While we accounted for waning immunity among naturally infected individuals, we did not consider the waning of vaccine immunity, since our study period after vaccination was relatively short, with most of the population having received their vaccinations in the early summer of 2021. It is reasonable to assume that booster vaccinations would be administered to maintain immunity in simulations of early vaccination scenarios. In addition, we assumed that VoCs emerged as they did in reality, despite the different vaccination schedule. We conducted separate sensitivity analyses where we assumed that early vaccination prevented the emergence of VoCs.

Reproductive number

The next-generation matrix is a method to derive the basic or effective reproduction number for a compartmental model. For its calculation, only the "infected" compartments are used, so E, I, and A. Let $x_i, i = 1, 2, 3, \ldots, m$ be the numbers of infected individuals in the i^th infected compartment at time t. Then, two matrices can be built: 1) $V_i(x)$, which represents the arrivals and departures from one of the infected compartments to another, and 2) $F_i(x)$, which describes the arrivals of new infections in compartment i. The matrices $V_i(x)$ and $F_i(x)$ are therefore constructed as [353]:

$$V_i(x) = \begin{pmatrix} \frac{1}{D_E} & 0 & 0 \\ -\frac{r_E}{D_E} & \frac{r_H(1-e_{vH})}{D_Q} + \frac{(1-r_H)}{D_I} & 0 \\ -\frac{(1-r_E)}{D_E} & 0 & \frac{1}{D_I} \end{pmatrix} \tag{S4.7}$$

$$F_i(x) = \begin{pmatrix} 0 & b\frac{S(1-e_{vI})}{N} & b\frac{\alpha S(1-e_{vI})}{N} \\ 0 & 0 & 0 \\ 0 & 0 & 0 \end{pmatrix} \tag{S4.8}$$

Then, it has been shown that $R_t = \rho FV^{-1}$, where ρFV^{-1} is the spectral radius (or largest eigenvalue) of the Next Generation Matrix FV^{-1}. One can picture the entries of FV^{-1} as the rate at which infected individuals in x_j produce new infections in x_i, times the average length of time an individual spends in compartment j. For a proof, see for example Perasso [378]. Therefore, we obtain:

$$R_t = transmission(1 - e_{vI})S(t)\left(D_I\alpha(1 - r_E) + \frac{D_I D_Q r_E}{D_Q(1 - r_H) + D_I(1 - e_{vH})r_H}\right) \tag{S4.9}$$

Model selection

Our model selection process was guided by the key principle of effect identifiability. To assess practical non-identifiability, we performed convergence assessments, in which we confirmed the stabilization of the SAEM algorithm towards the same value from a wide range of starting values. We conducted five SAEM estimations per converge assessment and observed the SAEM traces and final parameter estimates for signs of non-identifiability. For example, we noticed that the addition of random effects on NPI covariates beyond the lockdown betas greatly decreased identifiability and lead to non-convergence of the SAEM algorithm. We selected the final models from a set of models that included additional NPIs (such as bar

and restaurant closures), alternative formulations of the weather variable (temperature only, temperature and relative humidity), higher temporal resolution of estimation periods for parameters such as case detection rate and death rate, and additional or fewer random effects. We performed extensive model selection based on the Akaike Information Criterion (AIC), with lower AIC values indicating better model fit.

4.5 Manuscript 1: Supplementary Results

Model fits

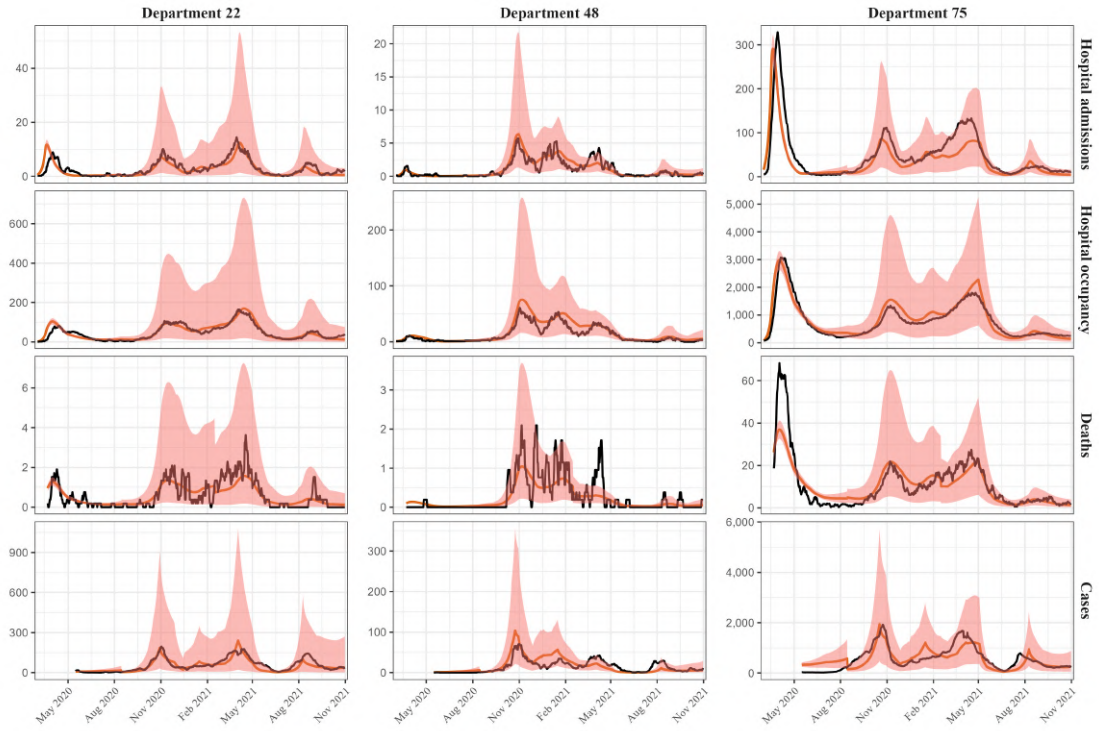

Figure S4.4: Model fits to all four types of observations for three selected departments. The black line indicates the observed data, the red line the model fit, and the shaded area the 95% prediction interval. We selected the departments to capture a maximum of variability in department size and population density. Department 22 (Côtes-d'Armor) has a population size of approx. 600k and is located at the Atlantic Ocean. Department 48 (Lozère) is the least populated department with a population of approx. 80k and is in Southern France. In contrast, department 75 (Paris) is the second most populated department with a very high population density.

Additional simulation results

Vaccine simulations

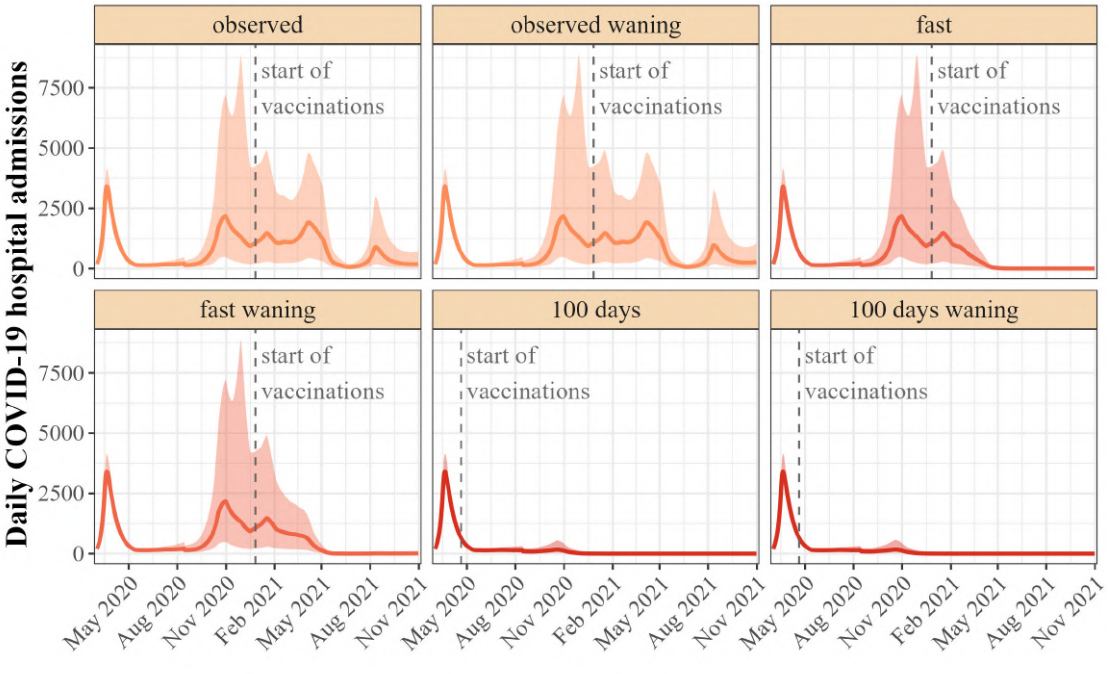

Figure S4.5: Simulated hospital admissions in France under waning and non-waning vaccination scenarios. For comparison with Figure 4.4b in the main text, we included scenarios with waning vaccine immunity for the observed, fast, and 100 days scenarios. The solid lines depict the median of 1000 simulations, while the shaded areas show the 95% prediction interval. In the "Fast" scenario, the start of the vaccinations was held constant, but 1% of the population was vaccinated per day. In the "100 days" scenario, the vaccine was available 100 days after the publication of the full genomic sequence of SARS-CoV-2 (April 20, 2020).

Scenario	Number of observations · 1000 [95% PI]	Difference to observed scenario · 1000 [95% PI]	Percentage change to observed scenario [95% PI]
Hospitalizations			
observed	470 [163; 1,348]		
observed waning	476 [164; 1,369]	6 [1; 21]	1.6% [0.6; 3.8]
fast	330 [131;950]	-146 [-373; -34]	-29.5% [-45.9; -15.6]
fast waning	350 [136; 1,004]	-126 [-323; -29]	-25.0% [-40.4; -13.0]
100 days	116 [85; 170]	-384 [-1,020; -89]	-79.9% [-89.1; -52.1]
100 days waning	116 [86; 171]	-384 [-1,019; -88]	-79.8% [-89.0; -52.1]
Deaths			
observed	92 [32; 262]		
observed waning	92 [33; 264]	1 [0; 2]	0.9% [0.3; 2.3]
fast	72 [28; 208]	-20 [-51; -5]	-21.5% [-35.4; -11.1]
fast waning	75 [29; 216]	-17 [-43; -4]	-18.0% [-30.6; -9.1]
100 days	24 [17; 37]	-71 [-204; -17]	-78.9% [-88.4; -51.3]
100 days waning	24 [17; 37]	-71 [-204; -16]	-78.8% [-88.3; -51.2]
Cases			
observed	10,306 [4,817; 25,264]		
observed waning	10,396 [4,835; 25,558]	90 [18; 290]	1.1% [0.3; 2.6]
fast	8,392 [4,388; 19,648]	-2,007 [-5,277; -463]	-19.2% [-34.4; -8.0]
fast waning	8,684 [4,455; 20,434]	-1,693 [-4,552; -390]	-16.1% [-30.1; -6.6]
100 days	4,650 [3,560; 6,571]	-6,141 [-16,114; -1,459]	-62.1% [-77.3; -30.7]
100 days waning	4,657 [3,562; 6,602]	-6,133 [-16,086; -1,457]	-62.0% [-77.1; -30.7]

Table S4.2: Counterfactual vaccine scenarios including waning vaccine immunity. In the "fast" scenario, the start of the vaccinations was held constant, but 1% of the population was vaccinated per day. In the "100 days" scenario, the vaccine was available 100 days after the publication of the full genomic sequence of SARS-CoV-2 (April 20, 2020).
NA not applicable, PI prediction interval

Lockdown 1 simulations

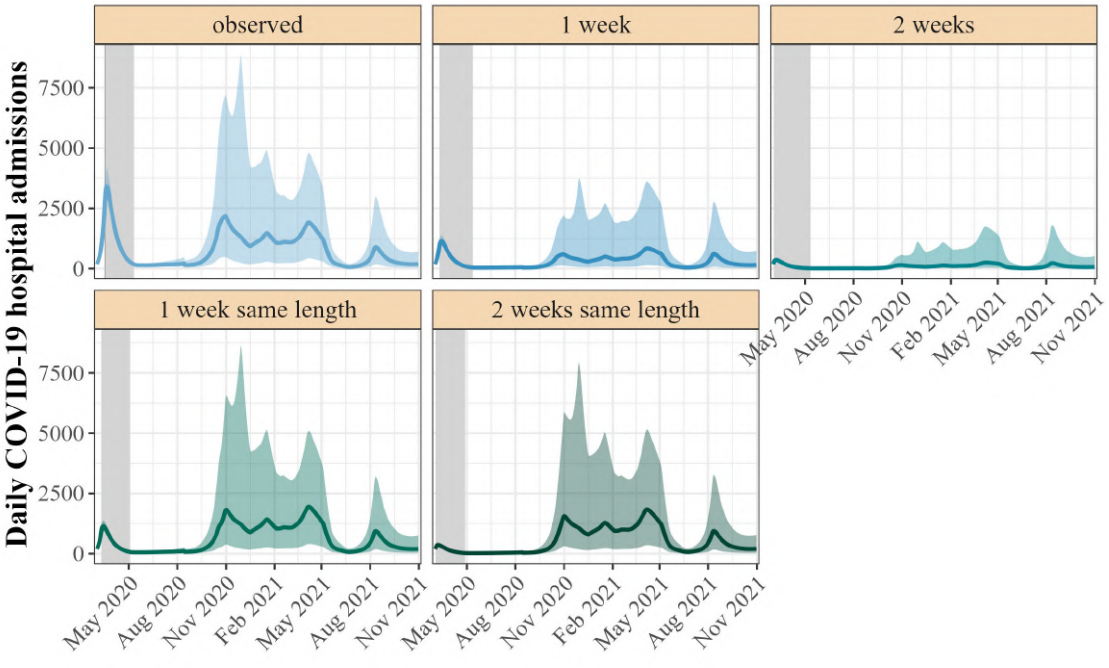

Figure S4.6: Simulated hospital admissions in counterfactual lockdown 1 scenarios. The solid lines depict the median of 1000 simulations, while the shaded areas show the 95% prediction interval. They grey shaded areas indicate the time period in which the lockdown 1 was active.

Scenario	Number of observations · 1000 [95% PI]	Difference to observed scenario · 1000 [95% PI]	Percentage change to observed scenario [95% PI]
Hospitalizations			
observed	470 [163; 1,348]		
1 week	179 [53; 732]	-308 [-523; -126]	-66.8% [-71.4; -50.3]
2 weeks	55 [15; 319]	-442 [-874; -168]	-90.7% [-92.4; -80.5]
1 week same length	377 [98; 1,237]	-92 [-118; -61]	-20.1% [-39.7; -8.6]
2 weeks same length	319 [68; 1,146]	-153 [-199; -97]	-32.5% [-57.7; -15.3]
Deaths			
observed	92 [32; 262]		
1 week	33 [10; 131]	-62 [-116; -24]	-68.2% [-71.8; -55.2]
2 weeks	10 [3; 53]	-86 [-185; -32]	-91.1% [-92.4; -83.8]
1 week same length	72 [19; 236]	-20 [-26; -13]	-21.9% [-40.6; -10.5]
2 weeks same length	59 [13; 215]	-33 [-44; -21]	-35.2% [-58.8; -18.6]
Cases			
observed	10,306 [4,817; 25,264]		
1 week	3,807 [1,569; 12,876]	-6,826 [-10,644; -3,576]	-67.1% [-70.7; -52.7]
2 weeks	1,153 [450; 5,458]	-9,626 [-17,027; -4,800]	-90.8% [-92.3; -81.7]
1 week same length	7,061 [2,363; 21,257]	-3,248 [-3,884; -2,569]	-30.1% [-50.6; -15.8]
2 weeks same length	5,477 [1,356; 18,922]	-4,872 [-5,949; -3,688]	-45.0% [-70.8; -24.7]

Table S4.3: Counterfactual lockdown 1 scenarios. In the "1 week" and "2 weeks" scenarios, the beginning of lockdown 1 was accelerated by one or two weeks, respectively, but the lockdown always ended on May 5th, 2020. In the "1 weeks same length" and "2 weeks same length" scenarios, the lockdown is shifted forwards by one or two weeks, respectively, thus keeping the length of the lockdown 1 constant at 54 days.
NA not applicable, PI prediction interval

Simulation scenarios without VoCs

Scenario	Number of observations * 1000 [95% PI]	Difference to observed scenario * 1000 [95% PI]	Percentage change to observed scenario [95% PI]	Difference to scenario without VoCs * 1000 [95% PI]	Percentage change to scenario without VoCs [95% PI]
Hospitalizations					
observed	470 [163; 1,348]				
observed without VoCs	332 [132; 956]	-144 [-367; -33]	-28.7% [-44.7; -15.1]		
100 days without VoCs	116 [85; 170]	-384 [-1,020; -89]	-79.9% [-89.1; -52.1]	-223 [-742; -49]	-71.0% [-84.9; -40.6]
Deaths					
observed	92 [32; 262]				
observed without VoCs	72 [28; 209]	-20 [-50; -5]	-21.0% [-34.6; -10.8]		
100 days without VoCs	24 [17; 37]	-71 [-204; -17]	-78.9% [-88.4; -51.3]	-49 [-166; -11]	-72.7% [-85.7; -42.9]
Cases					
observed	10,306 [4,817; 25,264]				
observed without VoCs	8,329 [4,373; 19,469]	-2,080 [-5,442; -480]	-19.6% [-35.0; -8.2]		
100 days without VoCs	4,650 [3,560; 6,571]	-6,141 [-16,114; -1,459]	-62.1% [-77.3; -30.7]	-3,781 [-12,163; -857]	-51.8% [-71.4; -22.4]

Table S4.4: Counterfactual vaccine scenarios in absence of SARS-CoV-2 variants of concern (VoCs). In the "100 days" scenario, the vaccine was available 100 days after the publication of the full genomic sequence of SARS-CoV-2 (April 20, 2020). PI prediction interval, VoCs variants of concern

Sensitivity analyses

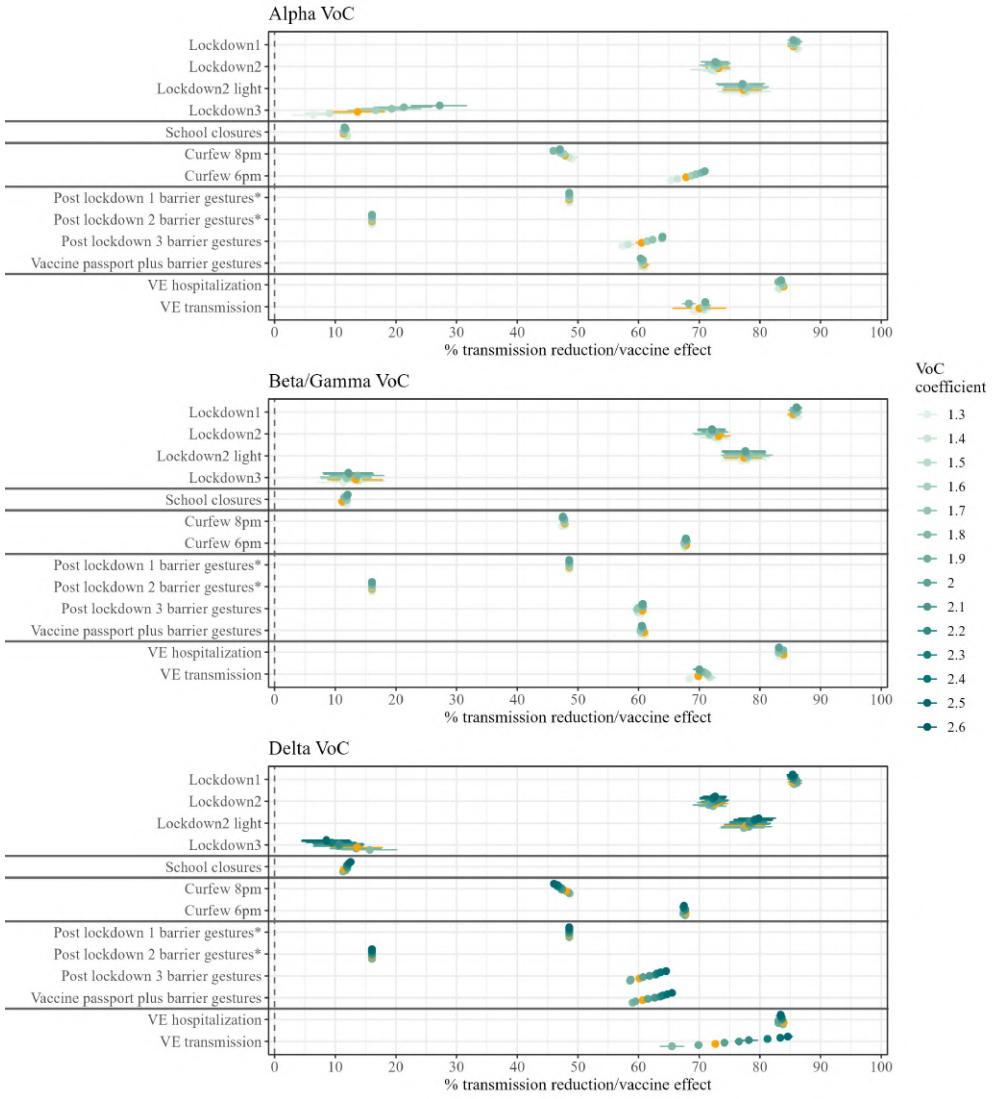

Figure S4.7: Sensitivity analysis: Influence of VoCs on SARS-CoV-2 transmission. The VoC coefficients were varied around their fixed value and their influence on NPI effectiveness and vaccine effect is shown. For the vaccine effect, we depict the effect with a population vaccine coverage of 75%. The value used in the main analysis is depicted in orange.
VE: vaccine effect; VoC: variant of concern

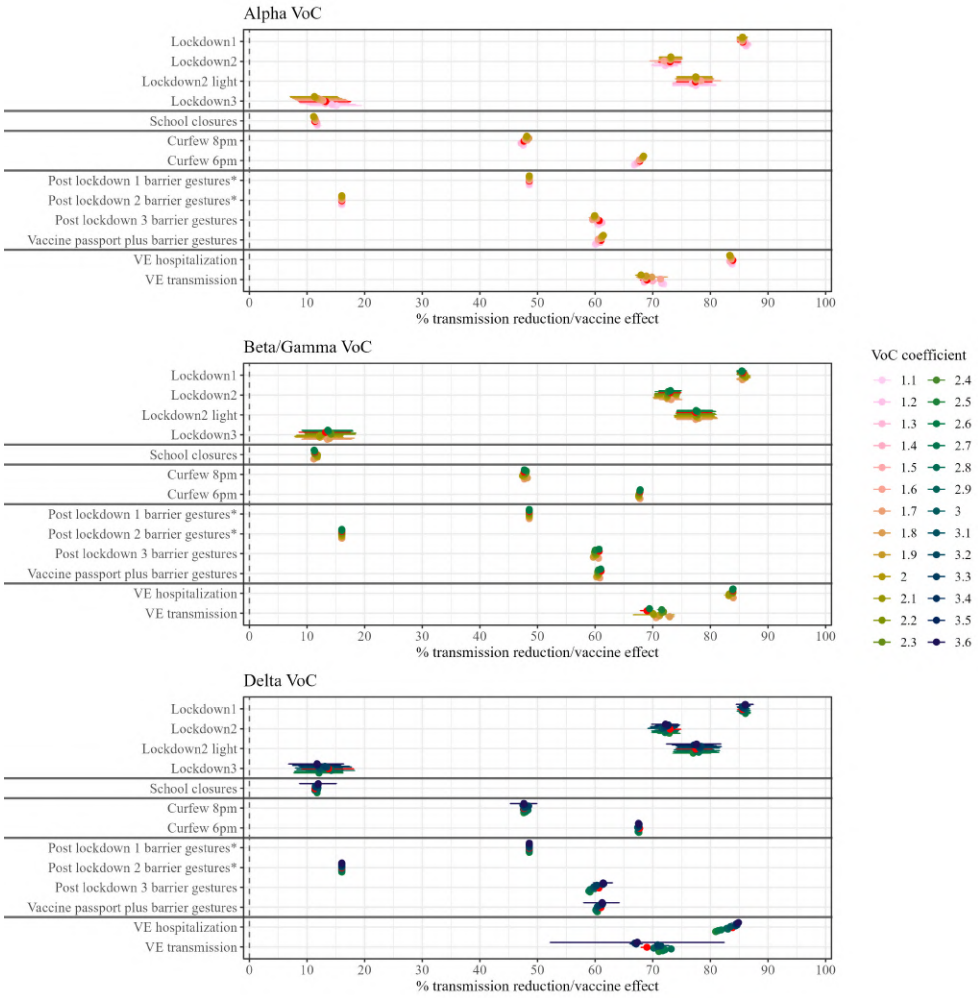

Figure S4.8: Sensitivity analysis: Influence of VoCs on the risk of COVID-19 hospitalization. The VoC coefficients were varied around their fixed value and their influence on NPI effectiveness and vaccine effect is shown. For the vaccine effect, we depict the effect with a population vaccine coverage of 75%. The value used in the main analysis is depicted in red.
VE: vaccine effect; VoC: variant of concern

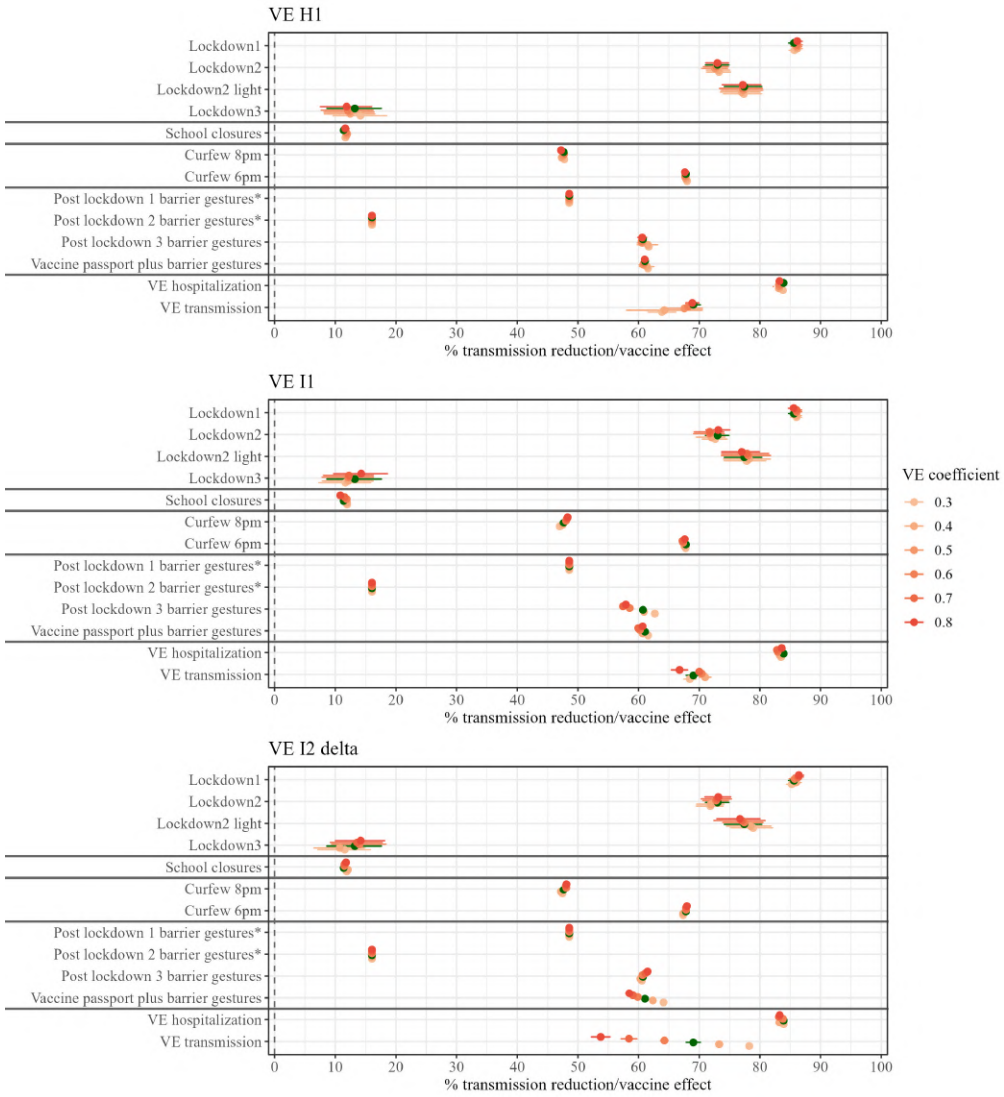

Figure S4.9: Sensitivity analysis: Influence of fixed vaccine effectiveness relations. The VE coefficients were varied around their fixed value and their influence on NPI and vaccine effect is shown. For the vaccine effect, we depict the effect with a population vaccine coverage of 75%. The value used in the main analysis is depicted in green.
VE: vaccine effect; VE H1: vaccine effectiveness of one vaccine dose against hospitalization; VE I1: vaccine effectiveness of one vaccine dose against infection; VE I2 delta: vaccine effectiveness of two vaccine doses against infection with the delta variant.

4.6 Manuscript 1: Supplementary References

46. Lauer SA, Grantz KH, Bi Q, et al. The Incubation Period of Coronavirus Disease 2019 (COVID-19) From Publicly Reported Confirmed Cases: Estimation and Application. *Ann. Intern. Med.* 2020().

47. He J, Guo Y, Mao R, Zhang J. Proportion of asymptomatic coronavirus disease 2019: A systematic review and meta-analysis. *Journal of Medical Virology*. 2021; 93():820–830. URL: https://onlinelibrary.wiley.com/doi/abs/10.1002/jmv.26326.

73. Campbell F, Archer B, Laurenson-Schafer H, et al. Increased transmissibility and global spread of SARS-CoV-2 variants of concern as at June 2021. *Eurosurveillance*. 2021; 26(24):2100509.

187. Polack FP, Thomas SJ, Kitchin N, et al. Safety and Efficacy of the BNT162b2 mRNA Covid-19 Vaccine. *N. Engl. J. Med.* 2020().

247. Hall V, Foulkes S, Insalata F, et al. Protection against SARS-CoV-2 after Covid-19 Vaccination and Previous Infection. *N. Engl. J. Med.* 2022().

344. Santé publique France. *Données hospitalières relatives à l'épidémie de COVID-19 (SI-VIC)*. 2021. URL: https://www.data.gouv.fr/fr/datasets/donnees-hospitalieres-relatives-a-lepidemie-de-covid-19/.

345. Santé publique France. *Données relatives aux résultats des tests virologiques COVID-19 (SI-DEP)*. 2020. URL: https://www.data.gouv.fr/fr/datasets/old-donnees-relatives-aux-resultats-des-tests-virologiques-covid-19/.

347. Santé publique France. *Données relatives aux personnes vaccinées contre la Covid-19 (VAC-SI)*. 2021. URL: https://www.data.gouv.fr/fr/datasets/donnees-relatives-aux-personnes-vaccinees-contre-la-covid-19-1/.

353. Heffernan JM, Smith RJ, Wahl LM. Perspectives on the basic reproductive ratio. *Journal of The Royal Society Interface*. 2005; 2():281–293. URL: https://dx.doi.org/10.1098/rsif.2005.0042.

365. Roumagnac A, Carvalho Filho E de, Bertrand R, Banchereau AK, Lahache G. Étude de l'influence potentielle de l'humidité et de la température dans la propagation de la pandémie COVID-19. *Médecine de Catastrophe - Urgences Collectives*. 2021; 5():87–102. URL: https://www.sciencedirect.com/science/article/pii/S1279847921000021.

366. D'Albis H, Coulibaly D, Roumagnac A, Filho EDC, Bertrand R. Quantification of the effects of climatic conditions on French hospital admissions and deaths induced by SARS-CoV-2. *Scientific Reports*. 2021; 11(). URL: https://dx.doi.org/10.1038/s41598-021-01392-2.

368. Cevik M, Tate M, Lloyd O, Maraolo AE, Schafers J, Ho A. SARS-CoV-2, SARS-CoV, and MERS-CoV viral load dynamics, duration of viral shedding, and infectiousness: a systematic review and meta-analysis. *The Lancet Microbe*. 2021; 2():e13–e22. URL: https://dx.doi.org/10.1016/s2666-5247(20)30172-5.

369. Dol J, Boulos L, Somerville M, et al. Health system impacts of SARS-CoV-2 variants of concern: a rapid review. *BMC Health Services Research*. 2022; 22(). URL: https://dx.doi.org/10.1186/s12913-022-07847-0.

370. Veneti L, Seppälä E, Larsdatter Storm M, et al. Increased risk of hospitalisation and intensive care admission associated with reported cases of SARS-CoV-2 variants B.1.1.7 and B.1.351 in Norway, December 2020 –May 2021. *PLOS ONE*. 2021; 16(10):1–12. URL: https://doi.org/10.1371/journal.pone.0258513.

371. Twohig KA, Nyberg T, Zaidi A, et al. Hospital admission and emergency care attendance risk for SARS-CoV-2 delta (B.1.617.2) compared with alpha (B.1.1.7) variants of concern: a cohort study. *The Lancet Infectious Diseases*. 2022; 22():35–42. URL: https://dx.doi.org/10.1016/s1473-3099(21)00475-8.

372. Zeng B, Gao L, Zhou Q, Yu K, Sun F. Effectiveness of COVID-19 vaccines against SARS-CoV-2 variants of concern: a systematic review and meta-analysis. *BMC Medicine*. 2022; 20(). URL: https://dx.doi.org/10.1186/s12916-022-02397-y.

373. Shao W, Chen X, Zheng C, et al. Effectiveness of COVID-19 vaccines against SARS-CoV-2 variants of concern in real-world: a literature review and meta-analysis. *Emerging Microbes & Infections*. 2022; 11():2383–2392. URL: https://dx.doi.org/10.1080/22221751.2022.2122582.

374. Rahmani K, Shavaleh R, Forouhi M, et al. The effectiveness of COVID-19 vaccines in reducing the incidence, hospitalization, and mortality from COVID-19: A systematic review and meta-analysis. *Frontiers in Public Health*. 2022; 10(). URL: https://www.frontiersin.org/articles/10.3389/fpubh.2022.873596.

375. Yu F, Lau LT, Fok M, Lau JYN, Zhang K. COVID-19 Delta variants—Current status and implications as of August 2021. *Precision Clinical Medicine*. 2021; 4():287–292. URL: https://dx.doi.org/10.1093/pcmedi/pbab024.

376. Santé publique France. *Synthèse des indicateurs de suivi de l'épidémie COVID-19*. 2021. URL: https://www.data.gouv.fr/fr/datasets/synthese-des-indicateurs-de-suivi-de-lepidemie-covid-19/.

377. Murphy SA, Vaart AWVD. On Profile Likelihood. *Journal of the American Statistical Association*. 2000; 95():449–465. URL: https://dx.doi.org/10.1080/01621459.2000.10474219.

378. Perasso A. An Introduction to The Basic Reproduction Number in Mathematical Epidemiology. *ESAIM: Proceedings and Surveys*. 2018; 62():123–138. URL: https://dx.doi.org/10.1051/proc/201862123.

5

Manuscript 2

5.1 Preface to Manuscript 2

In Manuscript 1, we developed a detailed mechanistic model of SARS-CoV-2 transmission to estimate the effectiveness of NPIs and vaccines in France. When comparing our estimates with an article by Paireau et al. that also aimed to assess NPI effects in France [1], we noted several discrepancies in the estimated NPI effectiveness parameters. While Paireau et al. used the same data, analyzed at the same geographical scale, and focused on similar key NPIs (such as lockdowns, school closures, and curfews) over a slightly shorter time frame (March 2020 – May 2021), they used a different estimation method. The comparison of the estimates found in the two studies is illustrated in Figure 5.1.

The method used by Paireau et al. is a two-step estimation process, which was widely applied during the COVID-19 pandemic to estimate NPI effectiveness [1, 133, 148, 155, 379]. This approach involves two sequential steps: 1) estimating the effective reproductive number $\mathcal{R}_t$ from epidemiological observations, such as hospital admissions, and 2) using the estimated $\mathcal{R}_t$ as the outcome in a regression model, with NPI dummy variables as predictors. The NPI parameters from the second step can then be interpreted as the effects of NPIs on viral spread. Although this method reduces the complexity of the estimation process, it comes with potential limitations. For instance, the uncertainty from the estimation in the first step is not propagated into the second step, leading to an underestimation of the overall uncertainty. Furthermore, challenges in estimating $\mathcal{R}_t$ may arise, especially early

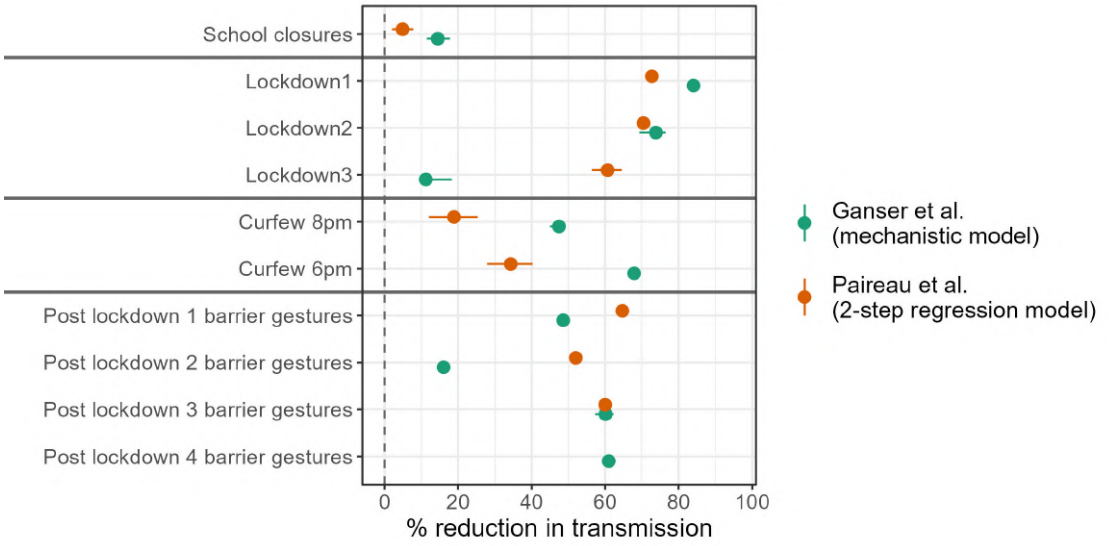

Figure 5.1: Comparison of the NPI effectiveness estimates found in Manuscript 1 (Ganser et al. using a mechanistic model for estimation) and by Paireau et al. (using a two-step regression model [1]).

in the epidemic when case numbers are low. Additionally, linear regression models cannot account for factors like herd immunity, which may complicate the causal interpretation of NPI effects.

Given these concerns, we conducted a simulation study of a simple scenario with two NPIs. We simulated epidemiological data with two complex models and compared the performance of the mechanistic model used in Manuscript 1 with the two-step regression model applied by Paireau et al. Our aim was to investigate in depth potential biases in the two-step approach and the mechanistic model, in order to better understand why our estimates, based on real-world COVID-19 data, differed from each other.

This manuscript is under review for publication to the American Journal of Epidemiology (AJE) and is available on medrxiv [380].

5.2 Manuscript 2: Comparative evaluation of methodologies for estimating the effectiveness of non-pharmaceutical interventions in the context of COVID-19: a simulation study

Iris Ganser[1,2], Juliette Paireau[3,4], David L Buckeridge[2], Simon Cauchemez[3], Rodolphe Thiébaut[1,5,6,7,*], Mélanie Prague[1,5,6]

[1]Univ. Bordeaux, Inserm, BPH Research Center, SISTM Team, UMR 1219, Bordeaux, France
[2] McGill Health Informatics, School of Population and Global Health, McGill University, Montreal, Quebec, Canada
[3] Institut Pasteur, Mathematical Modelling of Infectious Diseases Unit, Paris, France
[4] Infectious Diseases Department, Santé publique France, Saint Maurice, France
[5] Inria, Inria Bordeaux - Sud-Ouest, Talence, France
[6] Vaccine Research Institute, Creteil, France
[7] Bordeaux University Hospital, Medical Information Department, Bordeaux, France
[*] Corresponding author

Abstract

Numerous studies assessing the effectiveness of non-pharmaceutical interventions (NPIs) against COVID-19 have produced conflicting results, partly due to methodological differences. This study aims to clarify these discrepancies by comparing two frequently used approaches in terms of parameter bias and confidence interval coverage of NPI effectiveness parameters. We compared two-step approaches, where NPI effects are regressed on by-products of a first analysis, such as the effective reproduction number $\mathcal{R}_t$, with more integrated models that jointly estimate NPI effects and transmission rates in a single-step approach. We simulated datasets with mechanistic and an agent-based models and analyzed them with both mechanistic models and a two-step regression procedure. In the latter, $\mathcal{R}_t$ was estimated first and then used as the outcome in a linear regression with NPI variables as predictors. Mechanistic models consistently outperformed two-step regressions, exhibiting minimal bias (0-5%) and accurate confidence interval coverage. Conversely, the two-step regression showed bias up to 25%, with significantly lower-than-nominal confidence interval coverage, reflecting challenges in uncertainty propagation. We identified additional challenges in the two-step regression method, such high depletion of susceptibles and time lags in observational data. Our findings suggest caution when using two-step regression methods for estimating NPI effectiveness.

Keywords: dynamical models, non-pharmaceutical interventions, simulations, reproductive number, non-linear mixed effects models

The emergence of novel infectious agents, such as the SARS-CoV-2 virus responsible for the COVID-19 pandemic, has highlighted the importance of non-pharmaceutical interventions (NPIs) in mitigating the impact of infectious diseases. NPIs encompass a wide range of public health measures, including social distancing, quarantine, mask-wearing, and school closures, all implemented with the primary goal of reducing disease transmission. The effectiveness of NPIs as a means to mitigate pandemics has been the subject of extensive research during the COVID-19 pandemic [115, 116, 119]. Insights from these studies are crucial in guiding evidence-based public health responses to future pandemics. Various methods and models have been devised to assess NPI impact on disease transmission, ranging from straightforward descriptive techniques [381, 382] and regression models [131, 134] to advanced dynamic models [269, 383] and machine learning approaches [166, 384]. While this diversity of approaches contributes to the robustness of the estimates, it can introduce bias in systematic reviews and meta-analyses if a significant proportion of the methods are potentially unreliable. For example, different estimates of lockdown effectiveness have been found during the first wave in the United States, ranging from no reduction in case growth rates to a reduction by >50% [130, 132, 149, 384], which can at least partially be attributed to different methodologies being used.

One systematic review reported that the most frequently used methodologies are descriptions of change over time (48% of reviewed studies), non-mechanistic models such as regression models (27%), and mechanistic models (15%).[114] Among the latter two, many approaches involve the estimation of intermediary outcomes, primarily the effective reproductive number $\mathcal{R}_t$, from raw epidemiological data. These intermediary outcomes are then typically used in regression analyses to derive an estimate of NPI effectiveness. This strategy, which we call "two-step regression approach,", has been used across a range of studies.[1, 133, 148, 155, 379] Dividing the estimation process into two steps has the advantage of reducing model complexity. However, in addition to the challenges of estimating $\mathcal{R}_t$, this approach fails to propagate the uncertainty associated with $\mathcal{R}_t$ estimation in the first step to the final estimates. Despite the frequent application of two-step models, the impact of chaining two analysis steps on confidence interval (CI) coverage and parameter bias has not been explored. Moreover, the performance of the one-step approach in estimating NPI effectiveness in mechanistic models remains an open area of investigation, both in terms of parameter bias and correct estimation of uncertainty.[385] Here, we describe an extensive methodological study of the two approaches in the context of COVID-19 pandemic inspired by previous results on French data [1, 383].

Methods

Study design

Our primary objective was to construct a straightforward example for a meaningful comparison of two methodological approaches. We generated epidemic data with a mechanistic Susceptible-Infected-Recovered (SIR) model, a more complex mechanistic SEIRAHD model, and agent-based models (ABM) and then compared the performance of mechanistic models with two-step regression models on the simulated data. We used the SIR-generated data as a proof-of-principle to understand the general challenges of the two-step regression approach, while in the SEIRAHD- and ABM-created data, we explored challenges to both methodological approaches in more realistic scenarios. With each simulation method, we generated a total of 100 datasets, each comprising 94 distinct geographical regions [1, 383]. With both data generation models, we assumed entirely susceptible closed populations. The population sizes for each region were set to the respective population sizes of French departments (range 80k - 2.6 million, median 560k). We created scenarios comparable to the first months of an epidemic, with a first NPI, comparable in strength to a lockdown, followed by a second NPI, comparable to a post-lockdown intervention (Figures S5.3 and S5.6). Both NPIs were assumed to abruptly reduce transmission on a multiplicative scale, with an immediate and constant effect throughout their implementation. See Table 5.1 for an overview of which data were analyzed with which models.

Data generation model	**Data analysis models**	**Observations**
SIR	1. SIR 2. Two-step regression	Cases
SEIRAHD	1. SEIRAHD 2. SEIR 3. Two-step regression	Cases, deaths, hospitalizations Cases Cases / hospitalizations
ABM	1. SEIR 2. Two-step regression	Cases

Table 5.1: Overview of data generation and data estimation plan.

Data generation with a SIR model We generated data with a deterministic SIR model, which consisted of a mathematical model using ordinary differential equations (ODEs) to describe the dynamics of SARS-CoV-2 transmission according to equation 5.1 and a linear mixed model that determined the transmission rate as a function of NPIs according to equation 5.2. To allow the basic transmission rate to vary across regions, we included a random intercept [150]. We generated 100 datasets each under five conditions, with increasing depletion of susceptibles,

i.e. greater spread of infection prior to NPI implementation (2%, 10%, 20%, 40% and 60% depletion of susceptibles before implementation of NPI 1). For parameters used in each scenario, refer to Table S5.1. The true $\mathcal{R}_t$ was calculated as $\frac{b_t S_t}{\gamma N}$, where b represents the transmission rate, γ the recovery rate, S the number of susceptibles, and N the total population. In equation 5.1, D_I represents the duration of the infectious period, i.e. $1/\gamma$.

$$\begin{aligned} \dot{S} &= -\frac{bSI}{N} \\ \dot{I} &= \frac{bSI}{N} - \frac{I}{D_I} \\ \dot{R} &= \frac{I}{D_I} \end{aligned} \tag{5.1}$$

$$\begin{aligned} log(b_i(t)) &= log(b_0) + \beta_1 NPI_1(t) + \beta_2 NPI_2(t) + u_i^b \\ u_i^b &\sim N(0, \omega_b) \end{aligned} \tag{5.2}$$

Data generation with a SEIRAHD model To create more realistic scenarios, we generated data with a mechanistic SEIRAHD model, which has been used previously to estimate NPI and vaccine effectiveness [150, 383]. Equation 5.2 was again used to model the transmission rate as a function of NPIs, and the mathematical model to describe the dynamics of SARS-CoV-2 transmission is presented in equation 5.3. The mathematical model comprised seven compartments (Susceptible, latently Exposed, symptomatically Infected, Asymptomatically infected, Hospitalized, Recovered, and Deceased), encompassing various stages of infection (see Figure S5.1). r_E represents the proportion of symptomatic cases among all infected, r_H the hospitalization rate, D_E the duration of the incubation period, D_I the duration of the infectious period, D_Q the duration from infection to hospitalization, D_H the duration of hospitalization, D_D the duration from hospital admission to death, α the ratio of transmission between A and I, and fr the death rate of hospitalized patients. For a description of the data generation, see Supplementary Methods Section *SEIRAHD model structure and parameters* and for model parameters, see Table S5.2. To more closely represent real-life data, we added measurement error to the simulated observations (see Table S5.5). We kept the initial numbers of infected individuals low in order to have a very low depletion of susceptibles (<2% before implementation of NPI 1).

$$
\begin{aligned}
\dot{S} &= -bS\frac{I+\alpha A}{N} \\
\dot{E} &= bS\frac{I+\alpha A}{N} - \frac{E}{D_E} \\
\dot{I} &= \frac{r_E E}{D_E} - \frac{r_H I}{D_Q} - \frac{(1-r_H)I}{D_I} \\
\dot{A} &= \frac{(1-r_E)E}{D_E} - \frac{A}{D_I} \\
\dot{H} &= \frac{r_H I}{D_Q} - \frac{(1-fr)H}{D_H} - \frac{frH}{D_D} \\
\dot{R} &= \frac{(1-fr)H}{D_H} + \frac{(1-r_H)I + A}{D_I} \\
\dot{D} &= \frac{frH}{D_D}
\end{aligned}
\tag{5.3}
$$

Data generation with agent-based models We generated data with a deterministic ABM under two different scenarios: in the random mixing scenario, every agent had an equal probability of coming into contact with any other agent in the population, with an equal probability of transmission for each contact. Conversely, in the multi-layer scenario, interactions were divided into layers of school, workplace, households, and community encounters, with varying transmission probabilities (Table S5.3). In the multi-layer scenarios, we assumed that NPIs did not affect household transmission, and disease progression was age-specific (Table S5.4). The population size mirrored French departments, and for the multi-layer scenarios, the age distribution and contact structure were set according to the French population. Epidemics were seeded by sampling the number of initially infected agents and the basic transmissibility per contact (vt) from lognormal distributions (Table S5.3). Similar to the SEIRAHD models, we kept the depletion of susceptibles very low (2-3%) before the first NPI implementation. Stochastic measurement error was added similar to the SEIRAHD-generated data.

Parameter estimation with mechanistic models

All mechanistic models consisted of three layers: the differential equations (ODE) layer, a statistical layer modeling NPI effects on transmission, and an observational layer, taking into account measurement errors (described in Supplementary Methods: Observation model for mechanistic model data generation and estimation). The SEIR model used for analyzing SEIRAHD- and ABM-generated data is described in equation 5.4).

$$
\begin{aligned}
\dot{S} &= -\frac{bSI}{N} \\
\dot{E} &= \frac{bSI}{N} - \frac{E}{D_E} \\
\dot{I} &= \frac{E}{D_E} - \frac{I}{D_I} \\
\dot{R} &= \frac{I}{D_I}
\end{aligned}
\tag{5.4}
$$

To increase comparability across geographical regions and therefore facilitate estimation, incidence data were scaled to 10,000 population. We fixed the progression parameters in the ODEs (D_I, D_E, etc.) to their respective true values. Parameters were estimated in a population approach, i.e., we modeled the dynamics at the regional level while also accounting for inter-regional variability and estimating shared parameters. The initial conditions of the I compartment (SIR model) or E compartment (SEIR/SEIRAHD model) and b_0 were estimated with random effects, i.e., separately for each department but with a shared population value, to account for differences between regional units [383]. NPI parameters were estimated with fixed effects only.

Parameter estimation with two-step regression

The approach for the $\mathcal{R}_t$ regression was based on Paireau et al. [1]. First, we estimated $\mathcal{R}_t$ from incident infections or hospital admissions, separately for each simulated region, with a smoothing window of 7 days. In the SIR-generated datasets, we applied no smoothing because the data were generated without measurement error. The approach requires the input of a generation interval. In the SIR model, the generation interval is equal to the D_I parameter, i.e. 5 days. For the data generated with the SEIRAHD model, case and hospitalization data (i.e. entries into the I and H compartments) were used as observations. For both, we calculated a generation interval with a mean of 10.1 days and a standard deviation of 8.75 days according to Wallinga et al. [386] (for details, see Supplementary Methods Section *Generation intervals*). In the ABMs, we only used symptom onset data for the analysis, and the distribution of the generation interval was calculated directly during simulation, with a mean of 8.45 and a standard deviation of 4.45 for random mixing models and 7.8 and 4.4 for multi-layer models. Second, we ran a mixed-effects regression with the point estimate of the derived $\log(\mathcal{R}_t)$ as outcome and the two NPIs as predictors. Using discretization, for region $i = 1...94$ at weekly time points $j = 1...17$, we modeled:

$$
\begin{aligned}
log(\mathcal{R}_i(t_{ij})) &= log(\mathcal{R}_{0_{pop}}) + \beta_1 NPI_1(t_{ij}) + \beta_2 NPI_2(t_{ij}) + u_i^R + \epsilon_{ij} \\
u_i^R &\sim N(0, \omega_R) \\
\epsilon_{ij} &\sim N(0, \sigma)
\end{aligned} \tag{5.5}
$$

When using data generated with an incubation period (SEIRAHD models and ABMs), we lagged NPIs by 5 days for $\mathcal{R}_t$ estimated from cases, and by 10 days for $\mathcal{R}_t$ estimated from hospitalizations, to account for transition periods. We performed sensitivity analyses with different lagging periods. We reported the 95% CI using the Normal Distribution, i.e. the mean plus or minus 1.96 times the standard error.

To take into account the uncertainty from the $\mathcal{R}_t$ estimation in the regression step, we also implemented a bootstrap procedure by repeatedly sampling from the $\mathcal{R}_t$ distribution (details in Supplementary Methods Section *Bootstrapping 2-step regression*).

Performance evaluation

For comparison of methods, we compared the absolute and relative bias, which we calculated as $|\hat{\beta} - \beta|$ and $\frac{|\hat{\beta}-\beta|}{\beta}$, respectively. Additionally, we assessed 95% CI coverage as the percentage of datasets where the 95% CI contained the true value, separately for each estimated NPI parameter.

Implementation

We used the Simulx software version 2021 R2 [338] to simulate the mechanistic model datasets. We used the Python package Covasim version 3.1.4 [387] for ABM simulations, with "new infectious cases" as observations for further analysis. In the mechanistic model approach, parameters were estimated using maximum likelihood estimation using a stochastic approximation expectation maximization (SAEM) algorithm implemented in Monolix. [338] Standard errors for calculating 95% CIs were derived from 100 bootstrap samples (by resampling on the 94 geographical regions and varying the algorithm starting point).

The two-step regression analysis was conducted in R version 4.2.3 [388] with the packages EpiEstim [389, 390] using recommendations from references [391] and [392] to estimate $\mathcal{R}_t$ and lme4 [393] for the mixed effects regression. All code is publicly available on GitHub (`https://github.com/sistm/SEIR_vs_RTreg`).

Bias exploration

To detect possible issues in the regression step, we ran linear mixed models with the true $\mathcal{R}_t$ as the outcome variable. In the SEIRAHD-created datsets, the true $\mathcal{R}_t$ was calculated as a linear transformation of the transmission parameter, using the next generation matrix approach (see Supplementary Methods Section *Next generation*

matrix approach) [353]. In the ABM datasets, $\mathcal{R}_t$ was computed directly during the simulation as the quotient of new infections on day t over the number of infectious agents on the same day, multiplied by the average duration of infectiousness [387].

To investigate the potential impact of NPI strength and implementation time on the two-step model performance, we simulated data with diverse NPI implementation times (ranging from a 20-day to a 60-day NPI-free period) and varied NPI 1 strengths (coefficients ranging from -0.5 to -2, corresponding to a percentage reduction in transmission between 39% and 86%).

Results

Exploring bias in the two-step regression models

Data created with SIR model First, we analyzed data generated with a simple SIR model, and different scenarios of depletion of susceptibles (ranging from 2% to 60%). We found that the bias in NPI effect estimations from the two-step regression model increased with greater depletion of susceptibles, whereas the mechanistic model consistently estimated the correct value (Table 5.2). For example, with a 2% depletion of susceptibles, the bias of the two-step regression model in estimating NPI 1 was 1%, which increased to 15% at 20% depletion of susceptibles and 45% at 60% depletion of susceptibles. Moreover, the 95% CI of the mechanistic model covered the true value in all 100 simulated datasets. In contrast, the CIs from the two-step regression procedure were consistently too narrow, failing to cover the true value even in scenarios with little bias. The CI width was improved by bootstrapping the two-step regression procedure, but adequate coverage was only achieved in the scenario with the least bias. Of note, in the 40% and 60% depletion of susceptible scenarios, the 95% CIs for NPI 2 showed good coverage despite a large bias. This anomaly can be attributed to the absence of viral transmission during the NPI 2 period, due to the high prior depletion of susceptibles (illustrated in Figure S5.4). Consequently, NPI 2 could only be estimated with high uncertainty, with 95% CIs ranging from -2.57 to -0.37, corresponding to a percentage reduction in transmission from 31% to 92%, making the CIs so wide that they are practically meaningless (Figure S5.5).

The influence of the depletion of susceptibles on the bias of estimates can be understood analytically. In the two-step regression procedure, NPI effects were estimated using the $\mathcal{R}_t$ estimated in the first step according to equation 5.5. With $\mathcal{R}(t) = \frac{b(t)S(t)}{\gamma N}$ and replacing b by equation 5.2, we derive:

$$log(\mathcal{R}_i(t_{ij})) = log(b_0) - log(\gamma N) + log(S(t)) + \beta_1 NPI_1(t_{ij}) + \beta_2 NPI_2(t_{ij}) + u_i + \epsilon_{ij} \tag{5.6}$$

In this equation, $log(b_0)$ and $log(\gamma N)$ are constants and thus included in the intercept term. In contrast, $log(S(t))$ is time-varying and thus has the potential to

bias the estimated NPI effects, with a greater depletion of susceptibles over the estimation period leading to an increased bias.

Depletion of S	**2%**		**10%**		**20%**		**40%**		**60%**	
	Reg.	Mech.	Reg.	Mech.	Reg.	Mech.	Reg.	Mech.	Reg.	Mech.
NPI 1										
Absolute bias	-0.02	0.00	0.10	0	0.21	0	0.40	0	0.65	0
Relative bias (%)	1.2	0.2	7.0	0	14.8	0	27.4	0	45.0	0
95% CI (%)	0	-	0	-	0	-	0	-	0	-
95% bootstrap CI (%)	100	100	0	100	0	100	0	100	0	100
NPI 2										
Absolute bias	0.05	0	0.20	0	0.33	0	0.42	0	0.48	0
Relative bias (%)	6.6	0.1	24.5	0	40.9	0	51.9	0	59.5	0
95% CI (%)	0	-	0	-	0	-	0	-	0	-
95% bootstrap CI (%)	100	100	0	100	0	100	100	100	100	100

Table 5.2: Evaluation metrics from SIR simulation. For each scenario of depletion of susceptibles, the mean absolute and relative bias and percentage of CIs covering the true value across 100 simulated datasets are shown. The columns indicate the analysis model. The CI rows show the percentage of datasets where the 95% CI covers the true value. The 95% CI of the mechanistic model was always determined with bootstrap. Reg. two-step regression model, Mech. mechanistic model, CI confidence interval, NPI non-pharmaceutical intervention

Data created with SEIRAHD model While the SIR scenarios are useful to understand the general underlying challenges of the two-step regression procedure, the SIR model's simplicity does not capture the complexity of real-world scenarios. The data generated by the SEIRAHD model address this limitation by offering a more realistic representation of an epidemic. The point estimates from the two-step regression models displayed substantial bias, particularly pronounced for the first NPI (relative bias ranging from 18-25%) compared to the second NPI (approximately 14-18%, see Table 5.3). Throughout all datasets, using hospitalizations for $\mathcal{R}_t$ estimation and subsequent regression consistently resulted in higher bias compared to using case data. Moreover, the CIs derived from these models consistently failed to include the true NPI values. When the two-step regression procedure was bootstrapped, the CIs were wider and included the true value for NPI 2, but not for NPI 1.

In contrast, the 95% CIs for both NPIs derived with the mechanistic models covered the true value in all 100 datasets, while the point estimates exhibited only minimal absolute and relative bias (<1% for both NPIs, detailed in Table 5.3).

The exceptional accuracy of the SEIRAHD model was anticipated, as it was the model used for data generation.

Metric	SEIR model	SEIRAHD model	Regression model cases	Regression model hosp.
NPI 1				
Absolute bias	0.00	0.01	-0.26	-0.37
Relative bias (%)	0.3	0.4	18.3	25.4
95% CI (%)	-	-	0	0
95% bootstrap CI (%)	100	100	0	0
NPI 2				
Absolute bias	0.01	0.00	-0.11	-0.15
Relative bias (%)	0.8	0.7	13.7	18.5
95% CI (%)	-	-	0	0
95% bootstrap CI (%)	100	100	99	100

Table 5.3: Evaluation metrics over 100 datasets created with the mechanistic SEIRAHD model. The columns indicate the analysis model. The CI rows show the percentage of datasets where the 95% CI covers the true value. The 95% CI of the mechanistic model was always determined with bootstrap.
CI confidence interval, hosp. hospitalization, NPI non-pharmaceutical intervention

Origins of bias

In light of the substantial bias observed in the two-step regression model when a more realistic model was used for data generation, we investigated in depth the origins of this issue. Firstly, we examined the regression analysis step by running the linear mixed-effects model with the true $\mathcal{R}_t$ values as the outcome variable. While the regression model fitted the true $\mathcal{R}_t$ almost perfectly and estimated NPI effects with only slight bias for data generated by the SEIRAHD model (Table S5.6 and Figure 5.2A), the CIs failed to cover the true values due to the estimation of extremely small standard errors. However, based on these findings, we ruled out the regression step as the primary contributor to the bias.

Comparing the $\mathcal{R}_t$ curves estimated in the two-step procedure to the true $\mathcal{R}_t$ from the mechanistic SEIRAHD model, we identified discrepancies at the onset of the epidemic and a lag in $\mathcal{R}_t$ estimation by EpiEstim when the true $\mathcal{R}_t$ underwent sudden changes resulting from the implementation or lifting of NPIs (Figure 5.2B). These lags led to an underestimation of the strength of NPI 1 and overestimation of NPI 2, as the regression model estimated an average of the NPI periods. The pronounced decline in the first days contributed to the regression model consistently overestimating $\mathcal{R}_0$, i.e. $\mathcal{R}_t$ at the onset of the epidemic.

We proceeded to investigate whether NPI strength had any discernible impact on the bias in $\mathcal{R}_t$ estimation. For NPI 1, we observed that both absolute and

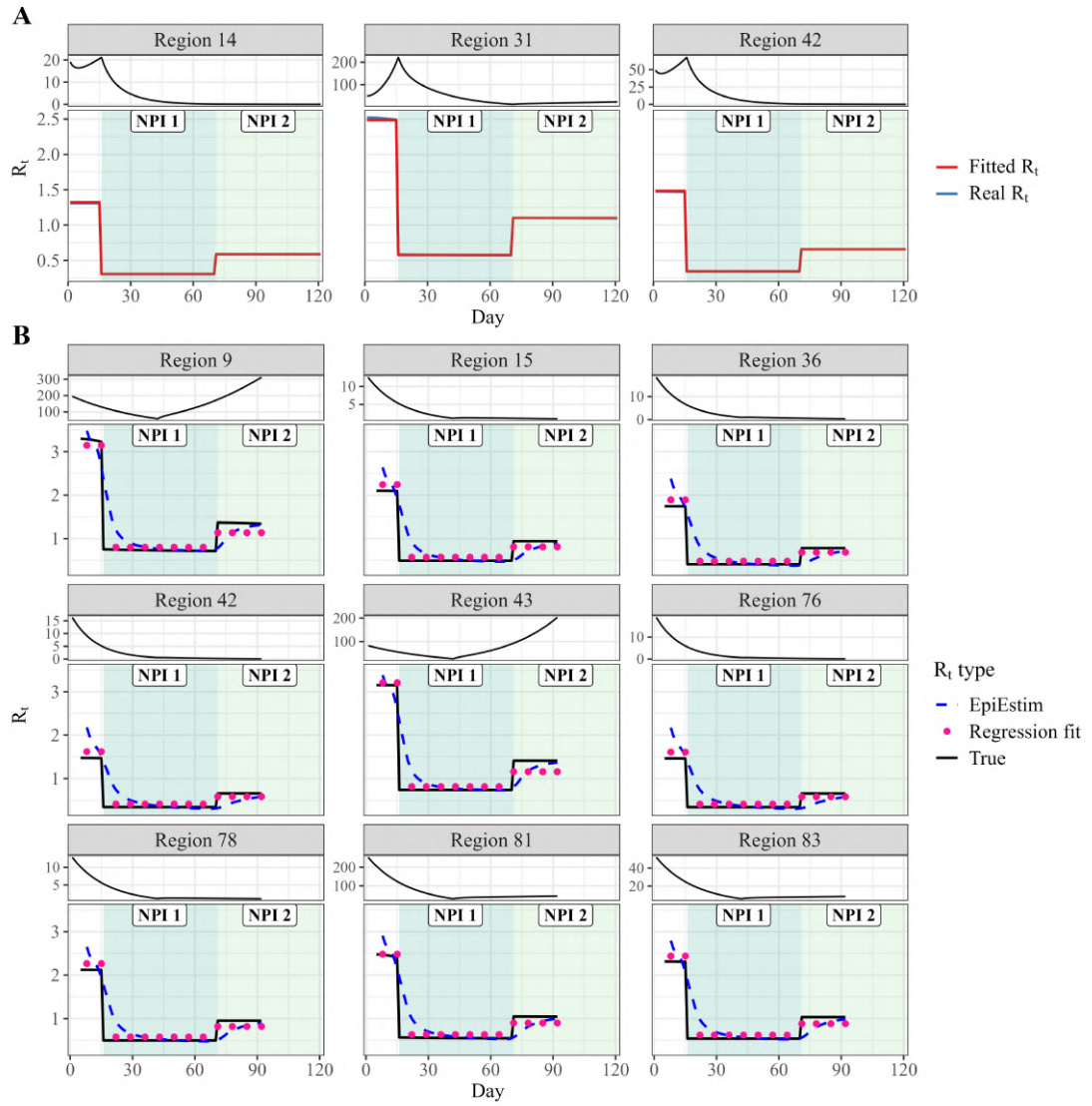

Figure 5.2: 2-step regression bias exploration. A: Regression fits of true $\mathcal{R}_t$ in three randomly selected regions. Each panel represents one geographic region with data generated by the mechanistic SEIRAHD model. The true $\mathcal{R}_t$ is depicted in blue and the corresponding regression fit in red. The panels on top show the respective case time series.
B: $\mathcal{R}_t$ fits by the two-step procedure and subsequent regression for data generated by the mechanistic SEIRAHD model. Each panel represents one geographic region. The highlighted regions indicate which NPI was active at which time. The top panels the respective case time series. Note that we followed EpiEstim guidelines in terms of not estimating $\mathcal{R}_t$ before 2 generation times after the start of the epidemic, but these 2 weeks are cut off from the plot.

relative bias increased with the rise in NPI strength. Regarding NPI 2, the bias followed a U-shaped pattern with increasing NPI 1 strength, with an underestimation of $\mathcal{R}_t$ during the NPI 2 period by all models (Figures S5.8 and S5.9). A more gradual NPI implementation period, involving a linear increase and decrease of NPIs from 0 to 1 over 1 or 2 weeks, did not improve $\mathcal{R}_t$ estimation nor the bias in regression coefficients (Figure S5.10 and Table S5.7).

We hypothesized that errors in more complex scenarios could stem from an incorrect specification of the delay between infection and the observations used to estimate $\mathcal{R}_t$. The most pertinent data for $\mathcal{R}_t$ estimation is the timing of infections, represented as entries into the E compartment in the SEIRAHD model, reflecting real-time transmission. When relying on case data (entry into the I compartment) or hospitalization data (entry into the H compartment) for $\mathcal{R}_t$ estimation, these observations are assumed to have fixed delays relative to the infections. However, in reality, these delays follow distributions, which "dilutes" the original infection timeline. Indeed, estimating $\mathcal{R}_t$ based on newly infected (corresponding to entry into the E compartment) instead of newly symptomatic (entry into I compartment) resulted in a notable reduction in relative bias for NPI 1, diminishing to 4.5%. However, the bias in NPI 2 estimation increased to 22.9% (see Table S5.8).

Limitations of the mechanistic approach in the context of misspecified models

To assess the robustness of the mechanistic model approach in the face of model misspecification, we generated data with ABMs, which include more heterogeneous individual behavior and population interactions, and a different underlying disease progression than assumed in the SEIRAHD model. We observed that even within the ABM framework, the mechanistic SEIR model in general demonstrated superior performance in terms of bias and coverage compared to the two-step regression model. The SEIR model effectively estimated NPI 1 with minimal bias around 2% and 95% CIs covered the true value in more than 95% of datasets, regardless of whether the data were generated using random mixing or the multi-layer ABM (Table 5.4). However, for NPI 2, CI estimated by the SEIR model covered the true value in only 71% of the random mixing datasets but 100% of the multi-layer datasets. For NPI 1, the CIs derived from the regression model (both bootstrapped and non-bootstrapped) systematically failed to cover the values and displayed significant underestimation (relative bias of 12% for random mixing and 19% for multi-layer). However, the bias for NPI 2 was substantially lower (5% for random mixing and 1% for multi-layer).

Discussion

We compared the performance of mechanistic models with two-step $\mathcal{R}_t$ estimation and subsequent regression modelling for estimating the relative reduction in viral

	SEIR random mixing	SEIR multi-layer	Reg model random mixing	Reg model multi-layer
NPI 1				
Absolute bias	0.04	-0.02	-0.18	-0.27
Relative bias (%)	2.6	1.3	12.2	18.7
95% CI (%)	-	-	0	0
95% bootstrap CI (%)	100	100	0	0
NPI 2				
Absolute bias	-0.04	0.02	-0.0.5	-0.01
Relative bias (%)	4.7	3.2	5.7	1.5
95% CI (%)	-	-	0	91
95% bootstrap CI (%)	71	100	0	95

Table 5.4: Evaluation metrics for 100 datasets created with the agent-based model. The CI rows show the percentage of datasets where the 95% CI covers the true value. The 95% CI of the mechanistic model was always determined with bootstrap. ABM agent-based model, CI confidence interval, NPI non-pharmaceutical intervention, reg regression

transmission caused by NPIs. Mechanistic models consistently outperformed the two-step approach both in terms of bias and CI coverage. The two-step procedure underestimated standard errors of parameter estimates across all analyses, failing to propagate the error in $\mathcal{R}_t$ estimation into the final estimate. We showed that this issue could be mitigated by repeatedly sampling from the posterior distribution of the $\mathcal{R}_t$ estimated in the first step.

Similar to Gostic et al. [392], in basic SIR scenarios without weekly smoothing of observations and minimal depletion of susceptibles, $\mathcal{R}_t$ was estimated accurately, leading to nearly unbiased NPI effectiveness parameters. However, in scenarios with higher depletion of susceptibles, the bias increased substantially. As an epidemic progresses and the number of susceptibles diminishes, $\mathcal{R}_t$ naturally decreases. While not problematic for $\mathcal{R}_t$ estimation itself, the regression procedure misattributes the decrease in $\mathcal{R}_t$ to the NPIs, thus overstating their effectiveness, with bias worsening as the depletion of susceptibles increases.

In the more realistic scenarios generated by the SEIRAHD and ABM models, compared those generated by SIR models, the two-step regression procedure showed greater bias in the point estimates, particularly for the first NPI. This bias can be attributed to several factors. First, the representation of the natural history of infection in the SEIRAHD model and ABM differs from that assumed by EpiEstim. If we had generated data with a mechanism consistent with EpiEstim, (i.e. the generation time distribution as an input), mechanistic models might also show bias. This is because misspecification of the generation time distribution can

bias estimates of the reproduction number, regardless of the approach used [386]. Whether it is more realistic to simulate with the generation time as a parameter or an underlying compartmental structure remains debatable.
Second, the inability to capture the sharp decline induced by NPIs stems from the long smoothing time window (7 days) coupled with a lengthy generation interval (10.1 days in SEIRAHD models). This gradual convergence of the estimated to the true $\mathcal{R}_t$ following NPIs led to inaccurate estimations of NPI effectiveness, as regression models fit an average across the entire NPI period. However, we found that gradually implementing NPIs did not reduce the bias in regression estimates. Moreover, smoothing remains necessary to handle measurements errors and other irregularities in observational data.
Third, the lag in observational time series behind real-time transmission might contribute to the bias, as symptomatic infections or hospitalizations capture transmission events that occurred in the past. This delay cannot be rectified by merely lagging the NPIs, and could explain why estimates from hospitalizations were less accurate than estimations from cases, as we only shifted NPI periods without considering the involved delay distributions [392]. Indeed, using transmission-related observations directly (entry into the E compartment) helped reduce this bias. Several R packages for back-calculating transmission events from cases or hospitalizations are now available, such as EpiNow2 and EstimateR. [394, 395]

Using regression analyses without accounting for the depletion of susceptibles also precludes strong causal conclusions about the effect of NPIs. Mechanistic models, which explicitly consider viral transmission mechanisms and therefore depletion of susceptibles, offer an alternative for causal interpretation [385], but require detailed data and time to develop and estimate models. Running 100 bootstrap repetitions on 100 SIR datasets parallelized on 20 high-performance computing nodes took approximately 42 hours. Since the two methodologies were run on different computing platforms, their computing times are hard to compare. Nevertheless, the two-step regression procedure, parallelized on 16 conventional laptop cores, required only four hours of computing time. In an early epidemic or pandemic setting, timely results are of great importance, so this trade-off between speed and accuracy of the results needs to be taken into account when deciding on a model. Therefore, developing user-friendly software for rapid epidemiological modeling in such scenarios is essential.

Our study comes with limitations that need to be acknowledged. First, it is important to note that our simulations do not prove that the mechanistic approach will always be unbiased. Indeed, in estimating parameters in datasets created by ABMs, we observed a reduced CI coverage with mechanistic models. Second, our simulated datasets did not consider various systematic biases, such as reporting delays, significant under-reporting or missing observations. The only measure-

ment error present was random noise on observations, and we did not incorporate weekly trends or seasonal changes in transmission. Moreover, we simulated only two consecutive NPIs with no overlap. Our most realistic scenarios were therefore simpler than real-life scenarios during the COVID-19 pandemic, with spatial structures, multiple overlapping NPIs implemented to varying degrees, behavioural dynamics, and more. It is likely that in a real-life scenario, the problem could be even more exacerbated because of practical identifiability issues. However, our primary objective was to illustrate and compare the performance of two analysis methods under close-to-optimal conditions, and these limitations to not threaten the validity of our results. To address some of these simplifications, we included simulations using ABM. However, we acknowledge that when analyzing real-world data, misspecification of the mechanistic model (for example, assumptions about the natural history of infection) might equally lead to bias. This is particularly true in the context of real-time modelling of emerging pathogens.

Improving the public health response during an epidemic depends on informed decision-making about NPIs. Our findings have significant implications for refining the methodology used to estimate the effectiveness of NPIs. Our findings highlight the potential for a systematic underestimation of uncertainty in the two-step regression procedure, raising concerns about the reliability of its effectiveness estimates across different scenarios. While compartmental models demonstrate superior performance over simpler models, their resource requirements, as they also require more time and expertise to implement, must be weighed against their benefits.

Contributions

Conceptualization: MP, RT, IG. supervision: MP, DLB, and RT. Formal analysis, writing - original draft: IG. Methodology and writing - review & editing: all.

Declaration of interests

The authors declare no competing interests.

Data sharing

All data are simulated. All code is available at the SISTM team's GitHub (`https://github.com/sistm/SEIR_vs_RTreg`).

Acknowledgements

We thank Lixoft SAS for their support. Numerical computations were in part carried out using the PlaFRIM experimental testbed, supported by Inria, CNRS (LABRI and IMB), Université de Bordeaux, Bordeaux INP, and Conseil Régional d'Aquitaine (see https://www.plafrim.fr).

Funding

IG is supported by the Digital Public Health Graduate Program within the framework of the PIA3 (Investment for the Future), project reference: 17-EURE-0019, and by a doctoral award from the Fonds de recherche du Québec-Santé. This work has been pursued in the EMERGEN project framework of the French Agency for Research on AIDS and Emerging Infectious Diseases (ANRS0151) and supported by INSERM and the Investissements d'Avenir program, Vaccine Research Institute (VRI), managed by the ANR under reference ANR-10-LABX-77-01.

5.3 Manuscript 2: References

1. Paireau J, Charpignon ML, Larrieu S, et al. Impact of non-pharmaceutical interventions, weather, vaccination, and variants on COVID-19 transmission across departments in France. *BMC Infect. Dis.* 2023; 23(1):1–12.

114. Banholzer N, Lison A, Özcelik D, Stadler T, Feuerriegel S, Vach W. The methodologies to assess the effectiveness of non-pharmaceutical interventions during COVID-19: a systematic review. *Eur. J. Epidemiol.* 2022; 37(10):1003–1024.

115. Iezadi S, Gholipour K, Azami-Aghdash S, et al. Effectiveness of non-pharmaceutical public health interventions against COVID-19: A systematic review and meta-analysis. *PLoS One.* 2021; 16(11):e0260371.

116. Mendez-Brito A, El Bcheraoui C, Pozo-Martin F. Systematic review of empirical studies comparing the effectiveness of non-pharmaceutical interventions against COVID-19. *J. Infect.* 2021; 83(3):281–293.

119. Talic S, Shah S, Wild H, et al. Effectiveness of public health measures in reducing the incidence of covid-19, SARS-CoV-2 transmission, and covid-19 mortality: systematic review and meta-analysis. *BMJ.* 2021; 375():e068302.

130. Liu X, Xu X, Li G, et al. Differential impact of non-pharmaceutical public health interventions on COVID-19 epidemics in the United States. *BMC Public Health.* 2021; 21(1):1–7.

131. Flaxman S, Mishra S, Gandy A, et al. Estimating the effects of non-pharmaceutical interventions on COVID-19 in Europe. *Nature.* 2020; 584():257–261.

132. Olney AM, Smith J, Sen S, Thomas F, Unwin HJT. Estimating the Effect of Social Distancing Interventions on COVID-19 in the United States. *Am. J. Epidemiol.* 2021; 190(8):1504–1509.

133. Haug N, Geyrhofer L, Londei A, et al. Ranking the effectiveness of worldwide COVID-19 government interventions. *Nat. Hum. Behav.* 2020; 4():1303–1312.

134. Brauner JM, Mindermann S, Sharma M, et al. Inferring the effectiveness of government interventions against COVID-19. *Science.* 2020; 371(6531).

148. Li Y, Campbell H, Kulkarni D, et al. The temporal association of introducing and lifting non-pharmaceutical interventions with the time-varying reproduction number (R) of SARS-CoV-2: a modelling study across 131 countries. *Lancet Infect. Dis.* 2021; 21(2):193–202.

149. Ge Y, Zhang WB, Liu H, et al. Impacts of worldwide individual non-pharmaceutical interventions on COVID-19 transmission across waves and space. *Int. J. Appl. Earth Obs. Geoinf.* 2022; 106():102649.

150. Collin A, Hejblum BP, Vignals C, et al. Using a population-based Kalman estimator to model the COVID-19 epidemic in France: estimating associations between disease transmission and non-pharmaceutical interventions. *International Journal of Biostatistics*. 2023; 20(1):13–41.

155. Liu Y, Morgenstern C, Kelly J, Lowe R, Jit M. The impact of non-pharmaceutical interventions on SARS-CoV-2 transmission across 130 countries and territories. *BMC Med.* 2021; 19(1):1–12.

166. Dandekar R, Rackauckas C, Barbastathis G. A Machine Learning-Aided Global Diagnostic and Comparative Tool to Assess Effect of Quarantine Control in COVID-19 Spread. *Patterns*. 2020; 1(9):100145.

269. Salje H, Kiem CT, Lefrancq N, et al. Estimating the burden of SARS-CoV-2 in France. *Science*. 2020; 369():208–211. URL: https://dx.doi.org/10.1126/science.abc3517.

338. Lixoft. *Simulx 2021R2*. 2021. URL: https://simulx.lixoft.com/.

353. Heffernan JM, Smith RJ, Wahl LM. Perspectives on the basic reproductive ratio. *Journal of The Royal Society Interface*. 2005; 2():281–293. URL: https://dx.doi.org/10.1098/rsif.2005.0042.

379. He Y, Chen Y, Yang L, Zhou Y, Ye R, Wang X. The impact of multi-level interventions on the second-wave SARS-CoV-2 transmission in China. *PLOS ONE*. 2022; 17(9):1–12. URL: https://doi.org/10.1371/journal.pone.0274590.

380. Ganser I, Paireau J, Buckeridge DL, Cauchemez S, Thiebaut R, Prague M. Comparative evaluation of methodologies for estimating the effectiveness of non-pharmaceutical interventions in the context of COVID-19: a simulation study. *medRxiv*. 2024():2024.10.14.24314896. eprint: 2024.10.14.24314896. URL: https://doi.org/10.1101/2024.10.14.24314896.

381. McGrail DJ, Dai J, McAndrews KM, Kalluri R. Enacting national social distancing policies corresponds with dramatic reduction in COVID19 infection rates. *PLOS ONE*. 2020; 15(7):e0236619. URL: https://dx.doi.org/10.1371/journal.pone.0236619.

382. Lurie MN, Silva J, Yorlets RR, Tao J, Chan PA. Coronavirus Disease 2019 Epidemic Doubling Time in the United States Before and During Stay-at-Home Restrictions. *The Journal of Infectious Diseases*. 2020; 222(10):1601–1606. URL: https://dx.doi.org/10.1093/infdis/jiaa491.

383. Ganser I, Buckeridge DL, Heffernan J, Prague M, Thiébaut R. Estimating the population effectiveness of interventions against COVID-19 in France: A modelling study. *Epidemics*. 2024; 46():100744. URL: https://www.sciencedirect.com/science/article/pii/S1755436524000057.

384. Cobb J, Seale M. Examining the effect of social distancing on the compound growth rate of COVID-19 at the county level (United States) using statistical analyses and a random forest machine learning model. *Public Health*. 2020; 185():27–29. URL: https://www.sciencedirect.com/science/article/pii/S0033350620301219.

385. Prague M, Commenges D, Gran JM, et al. Dynamic models for estimating the effect of HAART on CD4 in observational studies: Application to the Aquitaine Cohort and the Swiss HIV Cohort Study. *Biometrics*. 2017; 73():294–304. URL: https://dx.doi.org/10.1111/biom.12564.

386. Wallinga J, Lipsitch M. How generation intervals shape the relationship between growth rates and reproductive numbers. *Proceedings of the Royal Society B: Biological Sciences*. 2007; 274(1609):599–604. URL: https://dx.doi.org/10.1098/rspb.2006.3754.

387. Kerr CC, Stuart RM, Mistry D, et al. Covasim: An agent-based model of COVID-19 dynamics and interventions. *PLOS Computational Biology*. 2021; 17(7):e1009149. URL: https://dx.doi.org/10.1371/journal.pcbi.1009149.

388. R Core Team. *R: A Language and Environment for Statistical Computing*. Vienna, Austria: R Foundation for Statistical Computing, 2023. URL: https://www.R-project.org/.

389. Cori A. *EpiEstim: Estimate Time Varying Reproduction Numbers from Epidemic Curves*. 2.2-4. 2021. URL: https://CRAN.R-project.org/package=EpiEstim.

390. Cori A, Ferguson NM, Fraser C, Cauchemez S. A New Framework and Software to Estimate Time-Varying Reproduction Numbers During Epidemics. *American Journal of Epidemiology*. 2013; 178(9):1505–1512. URL: https://doi.org/10.1093/aje/kwt133.

391. Nash RK, Nouvellet P, Cori A. Real-time estimation of the epidemic reproduction number: Scoping review of the applications and challenges. *PLOS Digital Health*. 2022; 1(6):e0000052. URL: https://dx.doi.org/10.1371/journal.pdig.0000052.

392. Gostic KM, McGough L, Baskerville EB, et al. Practical considerations for measuring the effective reproductive number, Rt. *PLOS Computational Biology*. 2020; 16(12):e1008409. URL: https://dx.doi.org/10.1371/journal.pcbi.1008409.

393. Bates D, Mächler M, Bolker B, Walker S. Fitting Linear Mixed-Effects Models Using lme4. *Journal of Statistical Software*. 2015; 67(1):1–48.

394. Sam Abbott, Joel Hellewell, Katharine Sherratt, et al. *EpiNow2: Estimate Real-Time Case Counts and Time-Varying Epidemiological Parameters*. 2020.

395. Scire J, Huisman JS, Grosu A, et al. estimateR: an R package to estimate and monitor the effective reproductive number. *BMC Bioinformatics*. 2023; 24(1). URL: https://dx.doi.org/10.1186/s12859-023-05428-4.

5.4 Manuscript 2: Supplementary Methods

Parameters used in SIR data generation

Parameter	Interpretation	Scenario	Value
b_0	Basic transmission rate	all	$\sim \mathcal{N}(0.425, 0.01)$
D_I	Infectious period (days)	all	5 days [368]
γ	recovery rate (1/days)	all	0.2 ($= 1/D_I$)
log(initI)	initial number of infected individuals per region	2% S depletion	$\sim \mathcal{N}$(-3, 0.4)
		10% S depletion	$\sim \mathcal{N}$(-1.2, 0.4)
		20% S depletion	$\sim \mathcal{N}$(-0.4, 0.4)
		40% S depletion	$\sim \mathcal{N}$(-0.6, 0.4)
		60% S depletion	$\sim \mathcal{N}$(-1.6, 0.4)
β_1	Effectiveness parameter of NPI 1	all	-1.45 [383]
β_2	Effectiveness parameter of NPI 2	all	-0.8 [383]

Table S5.1: Parameters governing the SIR model.

SEIRAHD model structure and parameters

The values of parameters governing the SEIRAHD model were sampled from prior distributions to achieve different realizations of epidemics: We seeded the epidemic in each region by randomly sampling an initial number of exposed, and set the initial values of the I, A, H, and R compartments as functions of this number. The D compartment was assumed to be empty at the beginning of simulations, and S was set to complete a population size of the geographical region. From the seeded compartment values and basic transmission rate, our model simulated daily compartment values deterministically, under the assumption of random mixing and uniform disease progression. The values of all model parameters can be found in Table S5.2.

ABM model structure and parameters

To simulate observations with random mixing and hybrid models, we used the standard Sim function from the Python Covasim module. Details on Covasim can be found in the original publication [387] or in the Covasim tutorial (`https://docs.idmod.org/projects/covasim/en/latest/tutorials.html`). We simulated 100 datasets containing observations for 94 regions over 120 days each. The chosen transmission and initial parameters are listed in Table S5.3, and the code is available on Github (`https://github.com/sistm/SEIR_vs_RTreg`). In the multi-layer scenarios, agent interactions were simulated to occur in four layers: households, schools, workplaces, and the community. The assumed daily numbers of contacts per agent per layer and the risk of transmission multipliers for each layer are also listed in Table S5.3. In multi-layer simulations, the risk

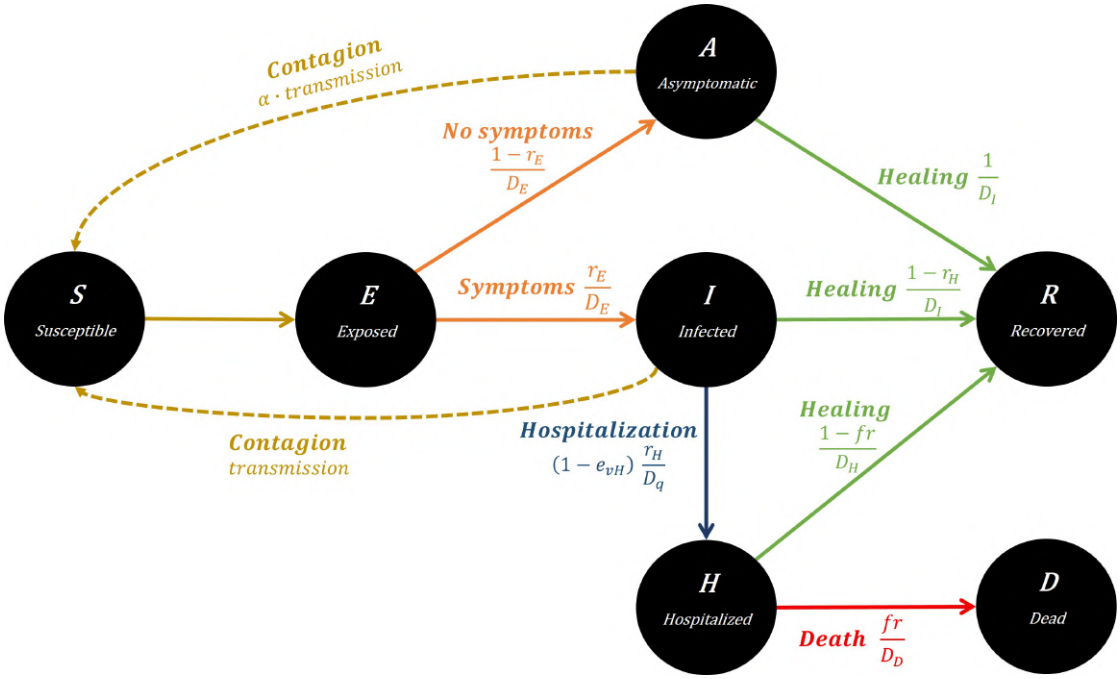

Figure S5.1: Flowchart of SEIRAHD model.

Parameter	Interpretation	Value
r_E	Proportion of symptomatic cases among all infected	0.85 [47]
r_H	Hospitalization rate	0.1
D_E	Latent (incubation) period (days)	5.1 days [46]
D_I	Infectious period (days)	5 days [368]
α	Ratio of transmission between A and I	0.55 [290]
D_Q	Duration from infection to hospitalization (days)	5 [383]
D_H	Length of stay in hospital (days)	18 [150]
D_D	Duration from hospital admission to death (days)	10 [396]
fr	Death rate of hospitalized patients	0.1 [383]
log(initE)	initial number of exposed individuals per region	$\sim \mathcal{N}(2, 0.9)$ [383]
b_0	Basic transmission rate	$\sim \mathcal{N}(0.5, 0.1)$ [383]
β_1	Effectiveness parameter of NPI 1	-1.45 [383]
β_2	Effectiveness parameter of NPI 2	-0.8 [383]

Table S5.2: Parameters governing the SEIRAHD data generation models.

of progression to more severe states was simulated stratified by age, in brackets

of ten years (Table S5.4). NPIs in the multi-layer model were assumed to reduce transmission risk in all layers except households.

Observation model for mechanistic model data generation and estimation

With the SEIRAHD and ABM models, we generated time series of cases, hospital admission and occupancy, and deaths as observations. We assumed full reporting of all observations. With the SEIRAHD model, the observations were taken as:

$$\begin{aligned} \text{Hospital admissions: } Y_{i,t}^{Had} &= \frac{r_H I}{D_Q} \\ \text{Hospital occupancy: } Y_{i,t}^{H} &= H_{i,t} \\ \text{Cases: } Y_{i,t}^{I} &= \frac{r_E E}{D_E} \\ \text{Deaths: } Y_{i,t}^{D} &= \frac{frH}{D_D} \end{aligned} \tag{5.7}$$

For the ABM, we used the following outputs from the Covasim simulations: "new infectious" (cases), "new severe" (hospital admissions), "n severe" (hospital occupancy), and "new deaths", although in the end, we only used cases as observations for further analysis.

To account for measurement errors in epidemiological data, stochastic noise was added to generated observations Y^* with a combined error model containing a constant error term a and a proportional error term b as $Y^{obs} = Y^* + (a + bY^*)\epsilon$, with $\epsilon \sim \mathcal{N}(\begin{pmatrix} 0 \\ 0 \\ 0 \\ 0 \end{pmatrix}, \begin{pmatrix} 1 & 0 & 0 & 0 \\ 0 & 1 & 0 & 0 \\ 0 & 0 & 1 & 0 \\ 0 & 0 & 0 & 1 \end{pmatrix})$ The values we used for a and b are listed in Table S5.5). The same observational model was used in the estimation process.

Exemplary datasets of the resulting simulations are shown in Figure S5.6.

Generation intervals

In the SEIRAHD model, several distributions of waiting times have to be taken in to account to calculate the distribution of the generation interval. The SEIRAHD model used to generate the data has two infectious compartments (A, I) and two compartments which infectious individuals can progress to (R, H). However, very conveniently, the waiting times in all infectious compartments ($A \to R$, $I \to R$, $I \to H$) are all exponentially distributed with a mean of 5 days (and therefore a rate parameter of 0.2). Therefore, the three above processes can be combined

into one, and the SEIRAHD model can be simplified to a SEIR model for the calculation of the generation interval.
Following Wallinga et Lipsitch [386], there is a relationship between the reproductive number $\mathcal{R}_t$, the growth rate r, and the generation interval GI (with its distribution $g(a)$). More specifically, $\mathcal{R}_t$ is related to r according to the moment-generating function (MGF) of the GI $M_{g(a)}$. A MGF, if it exists, uniquely characterizes the shape of the entire probability distribution: $M(z)$ determines $g(a)$ and, conversely, $g(a)$ determines $M(z)$. Thus, in order to find the distribution $g(a)$, we can use the corresponding MGF $M_{g(a)}$.
For an exponentially distributed random variable of mean $1/\lambda$, the moment generating function is $M(z) = \frac{\lambda}{\lambda - z}$. For successive stages of disease (E and I in the SEIR model), the MGFs of individual stages can be chained to calculate the generation interval:

$$M_g(z) = M_E(z) \times M_I(z) = \frac{\lambda_E}{\lambda_E - z} \times \frac{\lambda_I}{\lambda_I - z} \tag{S5.1}$$

where $M_E(z)$ is the MGF of the time spent in compartment E and $M_I(z)$ is the MGF of the time spent in compartment I.

The first derivative of the MGF evaluated at z=0 is the mean of the generation interval. In our case:

$$M_g'(0) = \frac{1}{\lambda_E} + \frac{1}{\lambda_I} \tag{S5.2}$$

With $\lambda_E = \frac{1}{5.1} day^{-1}$ and $\lambda_I = \frac{1}{5} day^{-1}$, we thus obtain $E[GI] = 5.1 + 5 = 10.1$.

The second derivative of the MGF evaluated at z=0 is the variance of the generation interval.

$$M_g''(0) = \frac{1}{\lambda_E^2} + \frac{1}{\lambda_E \lambda_I} + \frac{1}{\lambda_I^2} \tag{S5.3}$$

Thus, $\sigma^2(GI) = 26.01 + 25.5 + 25 = 76.51$ and $\sigma(GI) = 8.75$.

Since individuals in the hospitalized compartment are assumed not to be infectious, the contribution of the hospitalized compartment to the generation interval is 0. Thus, when using hospitalizations as observations, we used the same generation interval as for case observations, but lagged the NPIs by the average time from infection to hospitalization (10 days).

Bootstrapping 2-step regression

To bootstrap, the 2-step regression approach, we first ran the $\mathcal{R}_t$ estimation normally. Next, ran 500 bootstrap iterations as follows: First, we sampled a constant quantile value from a Beta(2,2) distribution. Then, we extracted the quantile value of the $\mathcal{R}_t$ distribution ($\mathcal{R}_t$ is assumed to be gamma-distributed) for each weekly data point (illustrated in Figure S5.2A), and these $\mathcal{R}_t$ values were then used in

the mixed effects model to estimate the NPI parameters. After 500 iterations, we calculated the 2.5th and 97.5th percentiles of the estimated parameters to derive lower and upper bounds of the CIs, respectively (Figure S5.2B).

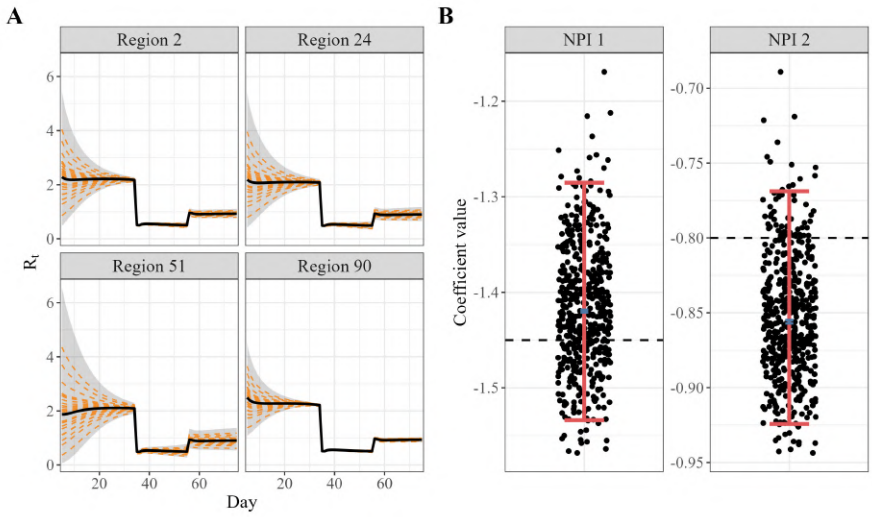

Figure S5.2: Illustration of the quantile bootstrap method. A: The $\mathcal{R}_t$ point estimate is shown as a solid black line, while the estimated 95% CI is depicted with the grey shaded area. Each dashed orange line represents the bootstrap draw of one constant quantile over time (only 50 iterations are shown for clarity). B: The NPI parameter distribution of all 500 bootstrap iterations is shown as black dots. The blue dot illustrates the point estimate and the red bars the 95% CI estimated from the bootstrap.

Next generation matrix approach

The next-generation matrix is a method to derive the basic or effective reproduction number for a compartmental model. For its calculation, only the "infected" compartments are used, so E, I, and A. Let $x_i, i = 1, 2, 3, \ldots, m$ be the numbers of infected individuals in the i^{th} infected compartment at time t. Then, two matrices can be built: 1) $V_i(x)$, which represents the arrivals and departures from one of the infected compartments to another, and 2) $F_i(x)$, which describes the arrivals of new infections in compartment i. The matrices $V_i(x)$ and $F_i(x)$ are therefore constructed as [353]:

$$V_i(x) = \begin{pmatrix} \frac{1}{D_E} & 0 & 0 \\ -\frac{r_E}{D_E} & \frac{r_H(1-e_{vH})}{D_Q} + \frac{(1-r_H)}{D_I} & 0 \\ -\frac{(1-r_E)}{D_E} & 0 & \frac{1}{D_I} \end{pmatrix} \tag{S5.4}$$

$$F_i(x) = \begin{pmatrix} 0 & b\frac{S(1-e_{vI})}{N} & b\frac{\alpha S(1-e_{vI})}{N} \\ 0 & 0 & 0 \\ 0 & 0 & 0 \end{pmatrix} \tag{S5.5}$$

Then, it has been shown that $\mathcal{R}_t = \rho FV^{-1}$, where ρFV^{-1} is the spectral radius (or largest eigenvalue) of the Next Generation Matrix FV^{-1}. One can picture the entries of FV^{-1} as the rate at which infected individuals in x_j produce new infections in x_i, times the average length of time an individual spends in compartment j. For a proof, see for example Perasso [378]. Therefore, we obtain:

$$\mathcal{R}_t = transmission(1 - e_{vI})S(t)\left(D_I\alpha(1 - r_E) + \frac{D_I D_Q r_E}{D_Q(1 - r_H) + D_I(1 - e_{vH})r_H}\right) \tag{S5.6}$$

Parameter	Interpretation	Value
General parameters		
vt (random mixing)	Basic viral transmissibility per contact in random mixing models	$\sim log\mathcal{N}(0.016,\ 0.02)$ [387]
vt (multi-layer)	Basic viral transmissibility per contact in multi-layer models	$\sim log\mathcal{N}(0.017,\ 0.02)$ [387]
Initial exposed	Initial number of exposed individuals per region	$\sim \mathcal{N}(50,\ 5)$
NPI 1	% reduction in transmission by NPI 1	75%
NPI 2	% reduction in transmission by NPI 2	55%
Duration parameters: time for disease progression		
exp2inf	Duration from exposed to infectious	$\sim log\mathcal{N}(4.5,1.5)$
inf2sym	Duration from infectious to symptomatic	$\sim log\mathcal{N}(1.1,0.9)$
sym2sev	Duration from symptomatic to hospitalization	$\sim log\mathcal{N}(6.6,4.9)$
sev2crit	Duration from hospitalization to requiring ICU	$\sim log\mathcal{N}(1.5,2.0)$
Duration parameters: time for disease recovery		
asym2rec	Duration for asymptomatic people to recover	$\sim log\mathcal{N}(8.0,2.0)$
mild2rec	Duration for people with mild symptoms to recover	$\sim log\mathcal{N}(8.0,2.0)$
sev2rec	Duration for hospitalized people to recover	$\sim log\mathcal{N}(18.1,6.3)$
crit2rec	Duration for people with critical symptoms to recover	$\sim log\mathcal{N}(18.1,6.3)$
crit2die	Duration from critical symptoms to death	$\sim log\mathcal{N}(10.7,4.8)$
Additional parameters for multi-layer model		
vt weights	Multiplier for vt in specific transmission layers	Household = 3 School = 0.6 Workplace = 0.6 Community = 0.3
N contacts	Number of contacts per person per day n specific transmission layers	Household = 2 School = 20 Workplace = 16 Community = 20

Table S5.3: Parameters governing the ABM data generation models. The duration and additional parameters are the default parameters provided in Covasim [387].

Age cutoffs	Susceptibility OR	Symptomatic probability	Hospitalization probability	Critical probability	Death probability
0	0.34	0.5	0.0005	0.00003	0.00002
10	0.67	0.55	0.00165	0.00008	0.00002
20	1	0.6	0.0072	0.00036	0.0001
30	1	0.65	0.0208	0.00104	0.00032
40	1	0.7	0.0343	0.00216	0.00098
50	1	0.75	0.0765	0.00933	0.00265
60	1.24	0.8	0.1328	0.03639	0.00766
70	1.47	0.85	0.20655	0.08923	0.02439
80	1.47	0.9	0.2457	0.1742	0.08292
90	1.47	0.9	0.2457	0.1742	0.1619

Table S5.4: Age-specific parameters for disease risk in the ABM data generation models. These parameters are the default parameters provided in Covasim [387].

Parameter	Interpretation	Value
a_c	additive error cases	0.0408
b_c	multiplicative error cases	0.1
a_d	additive error deaths	2×10^{-4}
b_d	multiplicative error deaths	0.0754
a_{Ha}	additive error hospital admissions	3.62×10^{-3}
b_{Ha}	multiplicative hospital admissions	0.05
b_{Ho}	multiplicative hospital occupancy	0.139

Table S5.5: Measurement error parameters for data creation with the SEIRAHD model. Note that hospital occupancy was only modelled with a multiplicative error, no additive error.[383] All error parameters are given on a normalized scale, i.e. they are applied to observations that have been scaled to 10000 population.

5.5 Manuscript 2: Supplementary Results

SIR-generated data

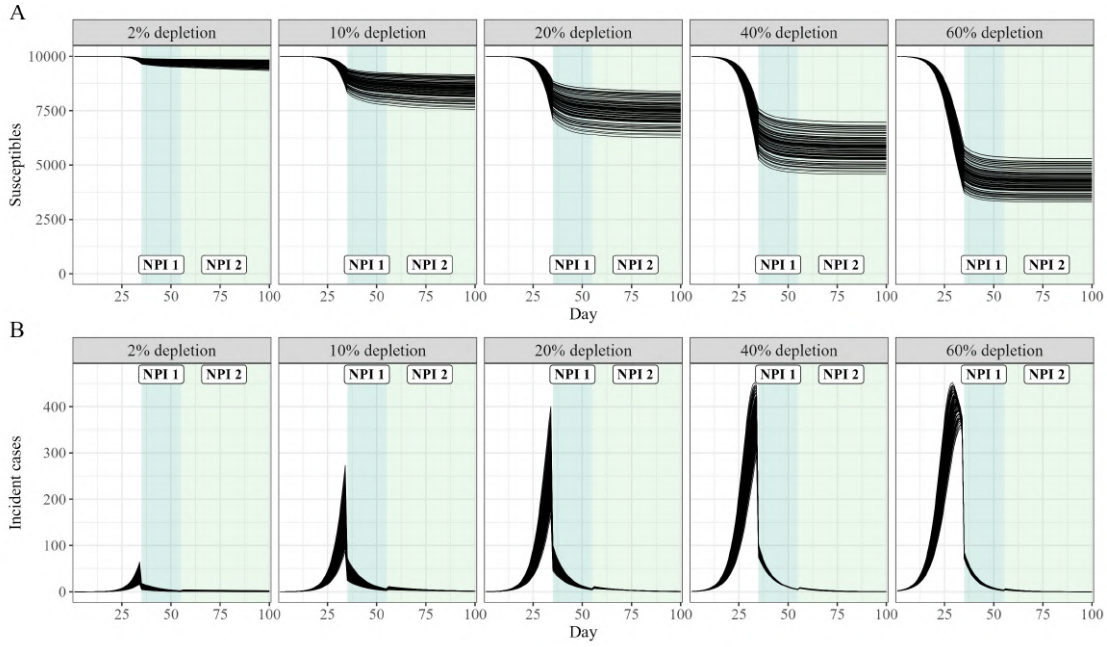

Figure S5.3: Example of created datasets with SIR models.
A: Plots of depletion of susceptibles, separated by depletion scenario, normalized to 10,000 population.
B: Plots of daily incident cases, separated by depletion scenario, with populations equally normalized to 10,000.

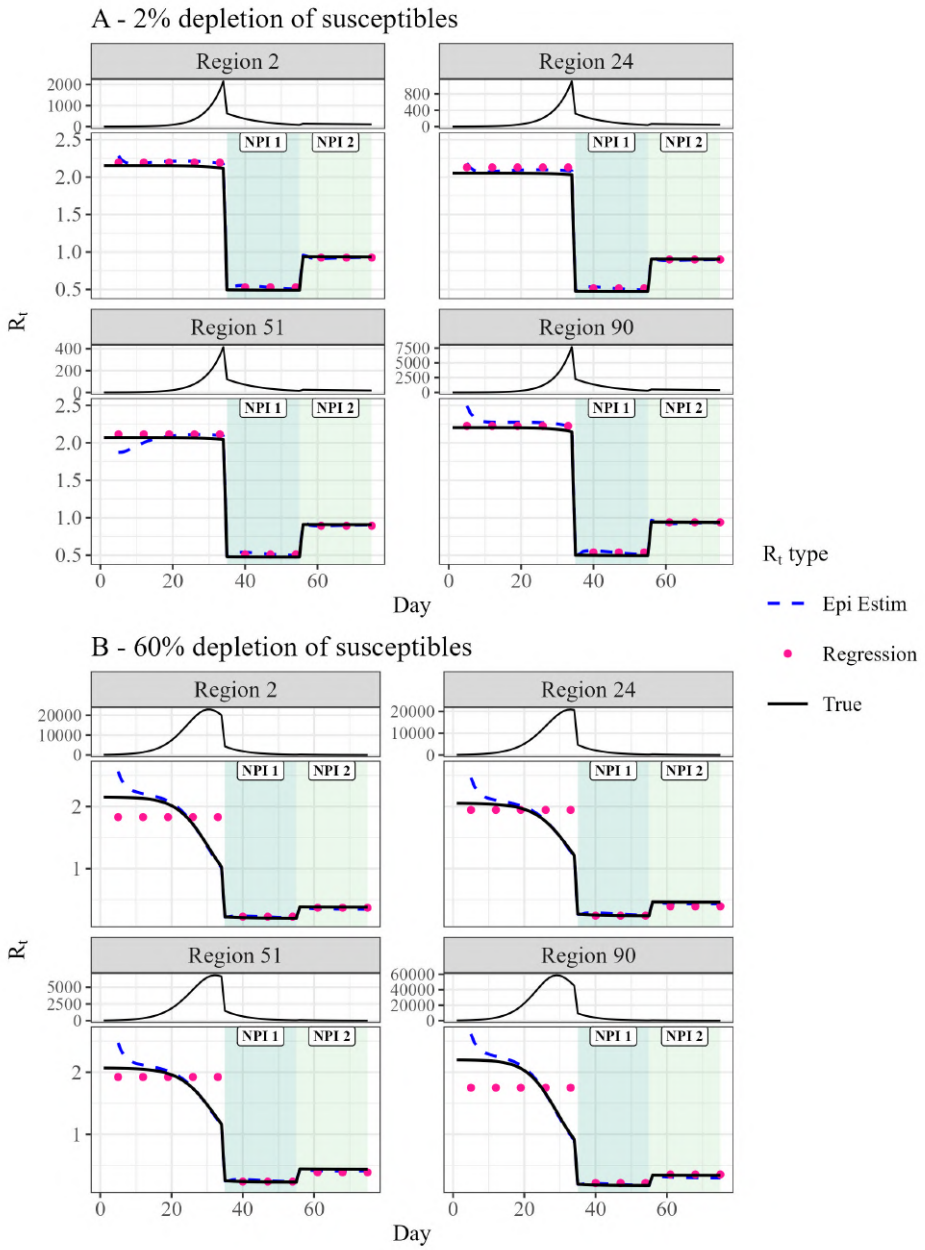

Figure S5.4: Comparison of $\mathcal{R}_t$ and regression fits from the two-step model on SIR-simulated datasets. A: Datasets generated with approx. 2% of susceptibles depleted at the time of NPI 1 implementation. **B:** Datasets generated with approx. 60% of susceptibles depleted at the time of NPI 1 implementation. Each panel represents one geographic region. The highlighted regions indicate which NPI was active at which time. The panels on top show the respective case time series.
NPI: non-pharmaceutical intervention

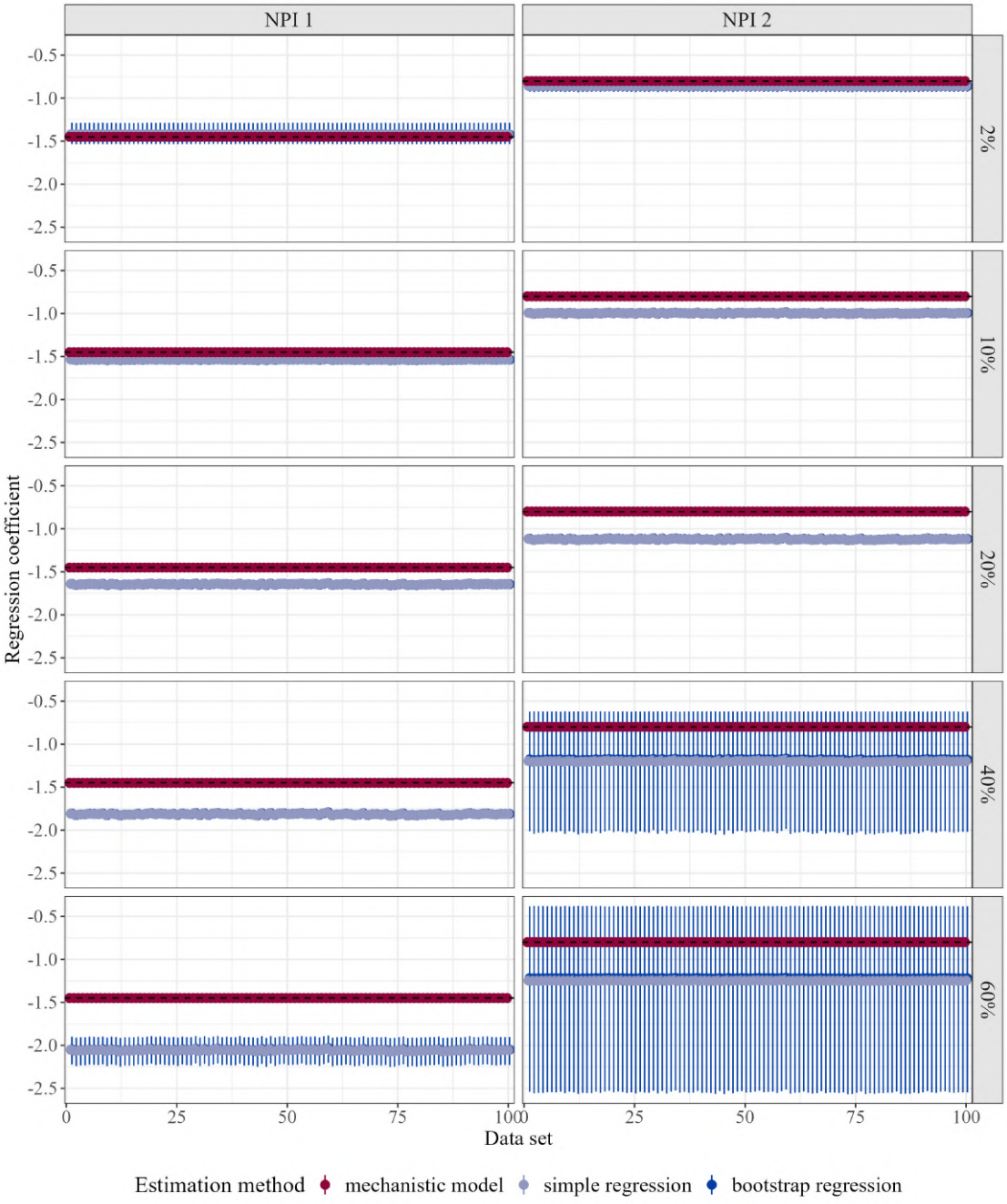

Figure S5.5: Estimation results from SIR-generated data under different scenarios of depletion of susceptibles. For each NPI separately, the point estimate and 95% CIs are shown for each estimation method. The dashed black lines indicate the value used in simulation.

SEIRAHD-generated data

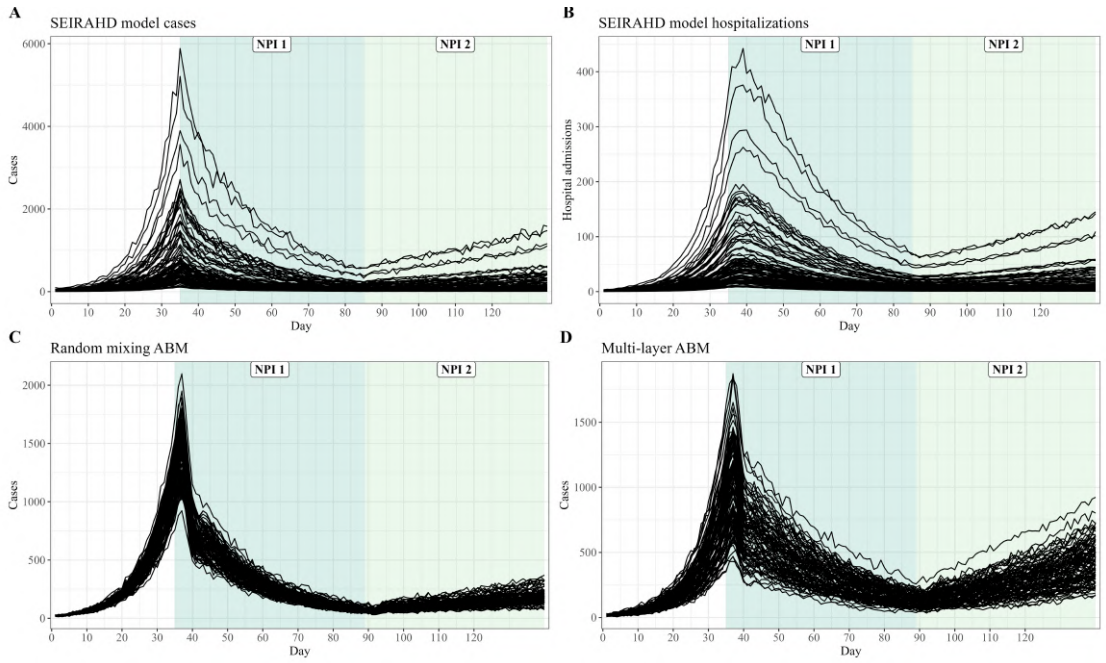

Figure S5.6: Illustration of created data with SEIRAHD model and ABMs. **A:** Simulated cases with SEIRAHD model, **B:** simulated hospitalizations with SEIRAHD model, **C:** simulated cases with random mixing agent-based model, **D:** simulated cases with layered agent-based model.

Analysis with true $\mathcal{R}_t$

When the regression model was applied to ABM-created datasets, the bias in NPI effect estimation was larger, likely due to higher fluctuations in $\mathcal{R}_t$ (Figure S5.7).

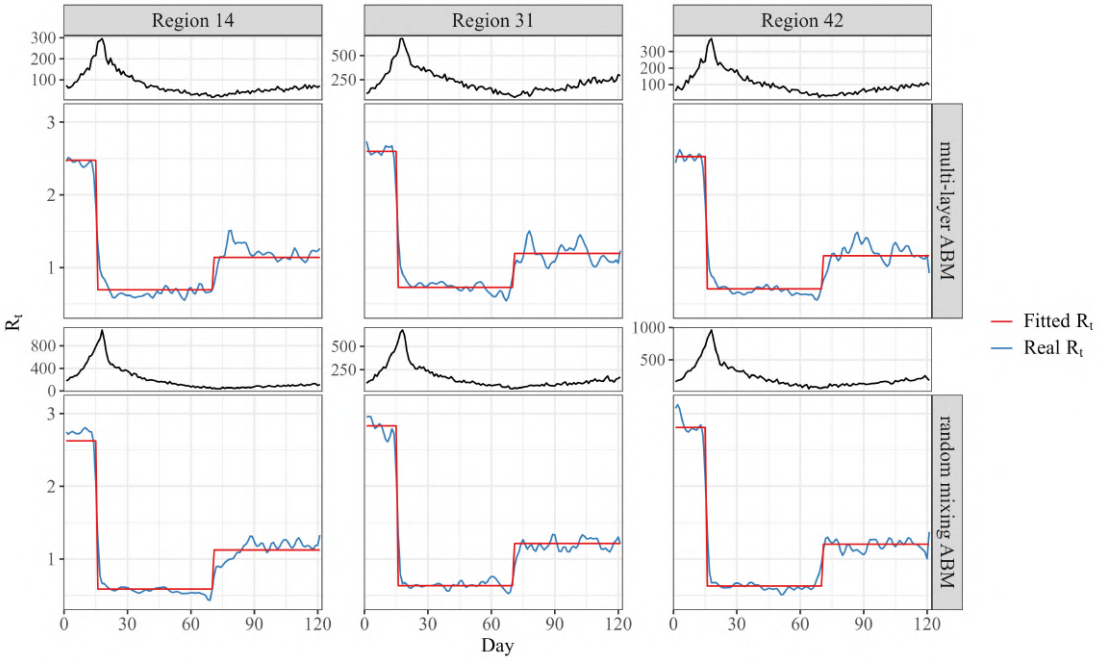

Figure S5.7: Regression fits of true $\mathcal{R}_t$ in three randomly selected regions. Each panel represents one geographic region with data generated by either a random mixing ABM or a multi-layer ABM. The true $\mathcal{R}_t$ is depicted in blue and the corresponding regression fit in red. The panels on top show the respective case time series.

Metric	SEIRAHD model	Random mixing ABM	Multi-layer ABM
NPI 1			
Absolute bias	0.04	0.05	-0.18
Relative bias (%)	2.9	3.6	12.3
95% CI (%)	0	0	0
NPI 2			
Absolute bias	0.05	0.06	-0.02
Relative bias (%)	6.7	6.9	2.9
95% CI (%)	0	0	0

Table S5.6: Evaluation metrics for regressions with known $\mathcal{R}_t$ (average of 100 datasets). Note that the main part of the manuscript only describes results from SEIRAHD-created data, but ABM-generated data results were added for completeness. ABM agent-based model, CI confidence interval, NPI non-pharmaceutical intervention

NPI implementation scenarios

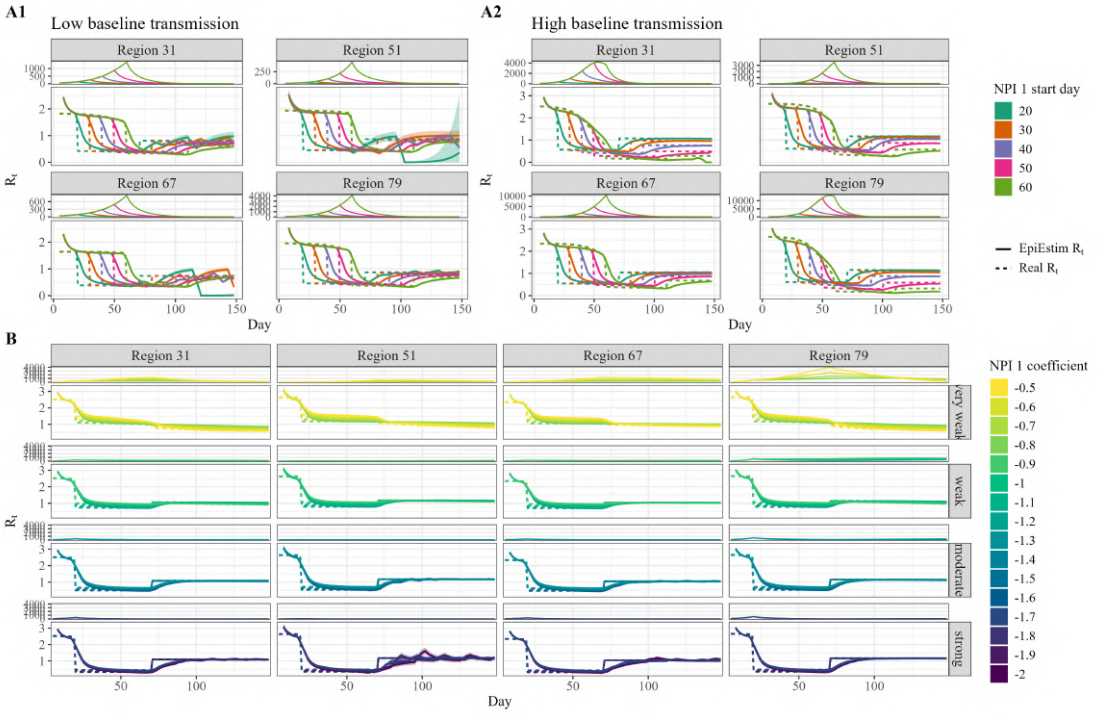

Figure S5.8: $\mathcal{R}_t$ fits by EpiEstim for varying NPI 1 scenarios. Scenarios are shown for four selected geographical regions, indicated by the numbers above the panels. The panels on top depict the case time series. **A1:** Scenarios are shown for varying NPI 1 start days where the basic transmission rate was adjusted to prevent a reduction in $\mathcal{R}_t$ due to high population immunity. **A2:** Scenarios for varying NPI 1 start days, with the basic transmission rate remaining consistent with the main analysis. Especially in the later NPI implementation scenarios, a notable decrease in $\mathcal{R}_t$ by population herd immunity becomes evident. **B:** $\mathcal{R}_t$ estimates for three selected regions in scenarios with varying NPI 1 strength. Considering the presentation of numerous scenarios, we organized the trajectories into four rows based on NPI strength.
NPI non-pharmaceutical intervention

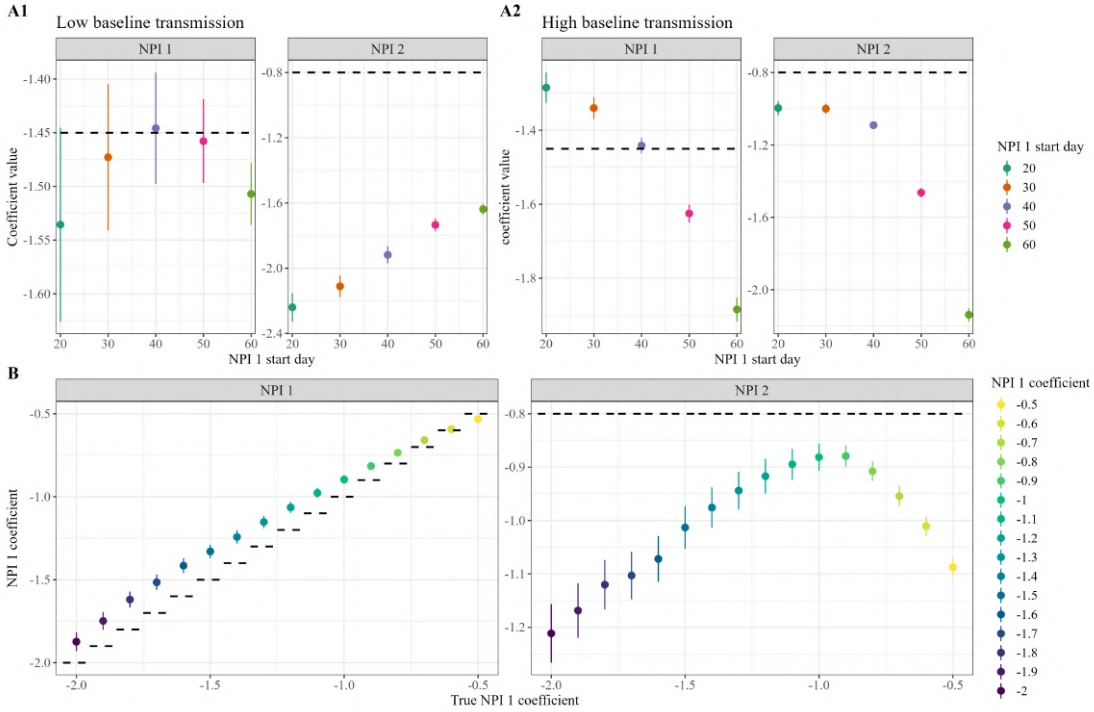

Figure S5.9: Regression coefficients from the two-step regression for varying NPI 1 scenarios. Results are shown separately by NPI. The dashed lines indicate the true NPI values. **A1:** Coefficients with corresponding 95% CIs are shown for varying NPI 1 start days where the basic transmission rate was adjusted to prevent a reduction in $\mathcal{R}_t$ due to high population immunity. **A2:** Coefficients with corresponding 95% CIs for varying NPI 1 start days, with the basic transmission rate remaining consistent with the main analysis. **B:** Coefficients with corresponding 95% CIs for scenarios with varying NPI 1 strength. Considering the presentation of numerous scenarios, we organized the trajectories into four rows based on NPI strength.
NPI non-pharmaceutical intervention

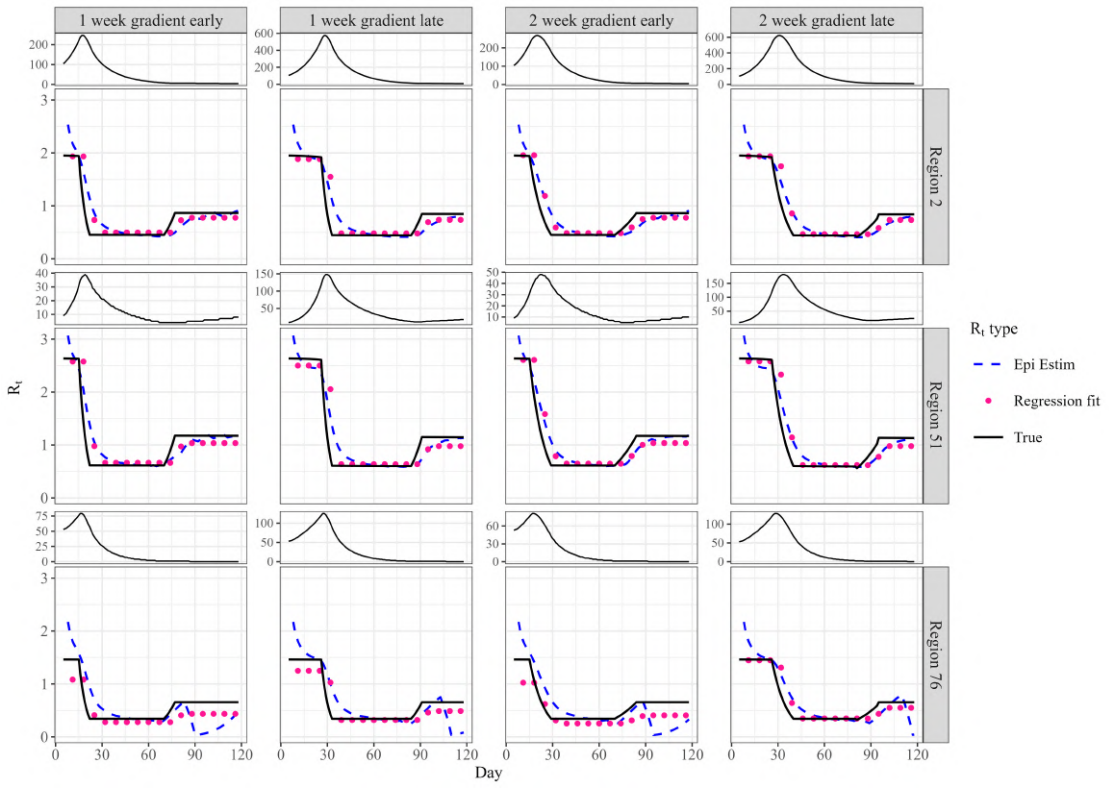

Figure S5.10: $\mathcal{R}_t$ and regression fits from the two-step model with gradual NPI implementation. NPIs were either implemented "early" (i.e. as in the main analysis after on day 16) or "late" (i.e. on day 27) and with a linear gradient either over 1 or 2 weeks.

	1 week		2 weeks	
Metric	**Gradient early**	**Gradient late**	**Gradient early**	**Gradient late**
NPI 1				
Absolute bias	-0.08	-0.06	-0.04	-0.01
Relative bias (%)	5.6	4.4	3.0	0.6
95% CI (%)	0	0	0	88
NPI 2				
Absolute bias	0.03	0.10	0.06	0.15
Relative bias (%)	4.2	12.1	7.1	19.0
95% CI (%)	26	0	0	0

Table S5.7: Results from the two-step model with gradual NPI implementation (average of 100 datasets). NPIs were either implemented "early" (i.e. as in the main analysis after on day 16) or "late" (i.e. on day 27) and with a linear gradient either over 1 or 2 weeks.

Incident infections vs. incident cases

Metric	Estimation with incident cases	Estimation with incident infections
NPI 1		
Absolute bias	-0.26	0.07
Relative bias (%)	18.3	4.5
NPI 2		
Absolute bias	-0.11	0.18
Relative bias (%)	13.7	22.9

Table S5.8: Comparison of bias in regression parameters, using incident cases (= entry into the I compartment) and incident infections (= entry into the E compartment)

ABM-generated data

Due to the unexpected underperformance of the mechanistic model approach in the data generated with the random mixing ABM, we conducted a sensitivity analysis of the bootstrap procedure. In our original bootstrap procedure, we resample "individuals" (i.e. geographical regions) and vary the starting parameters of the SAEM algorithm in Monolix. We observe that simulated data from the random mixing models exhibit less heterogeneity compared to the multi-layer models (Figure S5.6C-D). While this is expected, as the clustering in the multi-layer models can lead to more heterogeneous epidemics, there is less variability to be sampled from when conducting the bootstrap procedure on the random mixing data compared to the multi-layer data. It is also important to note that our confidence intervals were derived from only 100 bootstrap runs due to high computational demands. We hypothesize that 100 bootstrap runs may be insufficient to adequately capture the "tails" of the variability, particularly when the underlying data exhibit low heterogeneity. This limitation likely explains why the empirical 95% CIs do not cover the true value in all simulated datasets. However, when we account for variability by calculating the bootstrap standard error (SE) and then making a normal approximation of the distribution, the 95% CIs cover the true value in all but one dataset (Figure S5.11 and Table S5.9).

Metric	SEIR ABM random mixing	SEIR ABM multi-layer
NPI 1		
Absolute bias	0.04	-0.02
Relative bias (%)	2.60	1.28
Empirical dist. bootstrap CI coverage (%)	100	100
Bootstrap SE CI coverage (%)	100	100
NPI 2		
Absolute bias	-0.04	0.02
Relative bias (%)	4.72	3.23
Empirical dist. bootstrap CI coverage (%)	71	100
Bootstrap SE CI coverage (%)	99	100

Table S5.9: Comparison of confidence interval coverage with two different confidence interval calculation methods in ABM-generated data. Bias and CI coverage were calculated across 100 datasets created with the agent-based model. The empirical distribution bootstrap CI is taken from the main analysis and was calculated using the empirical distribution of the bootstrap estimates, i.e., taking the 2.5th and 97.5th percentiles of the bootstrap results as the lower and upper limits of the CI, respectively. In contrast, in the bootstrap SE approach, the standard errors for each NPI are estimated from the distribution of bootstrap estimates and the CIs are derived as $point\ estimate \pm 1.96 \times SE$. This method produces symmetric CIs around the point estimate.
ABM agent-based model, CI confidence interval, dist. distribution, NPI non-pharmaceutical intervention, SE standard error

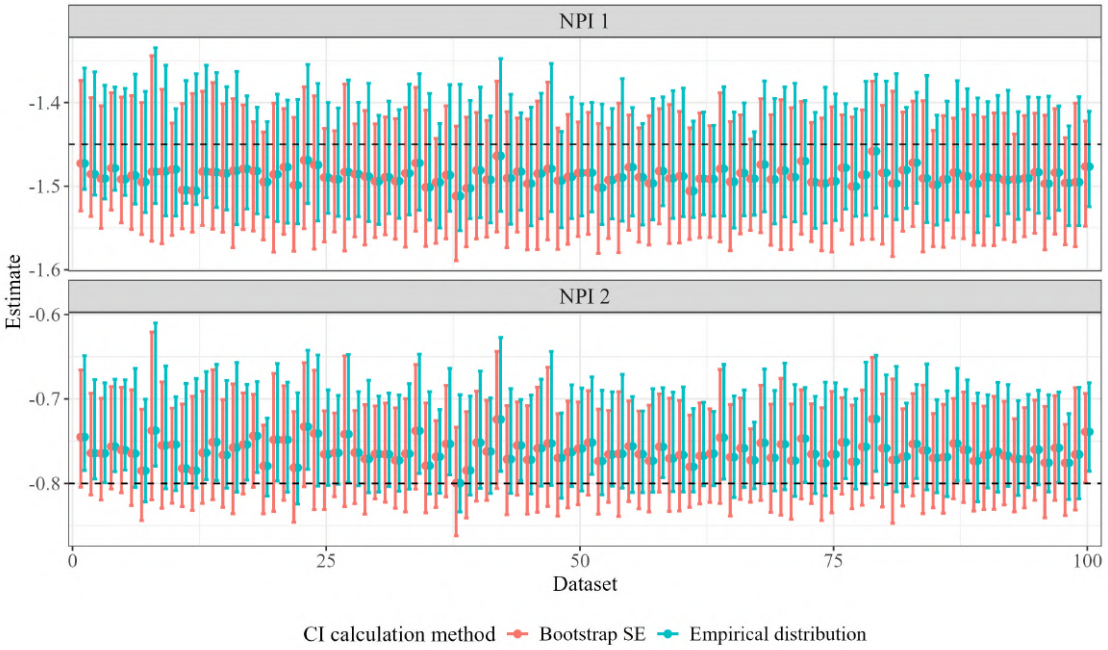

Figure S5.11: Comparison of confidence interval coverage in the random mixing ABM-generated data with two different confidence interval calculation methods. The empirical distribution bootstrap CI is taken from the main analysis and was calculated using the empirical distribution of the bootstrap estimates, i.e., taking the 2.5th and 97.5th percentiles of the bootstrap results as the lower and upper limits of the CI, respectively. In contrast, in the bootstrap SE approach, the standard errors for each NPI are estimated from the distribution of bootstrap estimates and the CIs are derived as $point\ estimate \pm 1.96 \times SE$. This method produces symmetric CIs around the point estimate and covers the true value in all datasets but one.

5.6 Manuscript 2: Supplementary References

150. Collin A, Hejblum BP, Vignals C, et al. Using a population-based Kalman estimator to model the COVID-19 epidemic in France: estimating associations between disease transmission and non-pharmaceutical interventions. *International Journal of Biostatistics*. 2023; 20(1):13–41.

353. Heffernan JM, Smith RJ, Wahl LM. Perspectives on the basic reproductive ratio. *Journal of The Royal Society Interface*. 2005; 2():281–293. URL: https://dx.doi.org/10.1098/rsif.2005.0042.

367. Li R, Pei S, Chen B, et al. Substantial undocumented infection facilitates the rapid dissemination of novel coronavirus (SARS-CoV-2). *Science*. 2020; 368():489–493. URL: https://dx.doi.org/10.1126/science.abb3221.

368. Cevik M, Tate M, Lloyd O, Maraolo AE, Schafers J, Ho A. SARS-CoV-2, SARS-CoV, and MERS-CoV viral load dynamics, duration of viral shedding, and infectiousness: a systematic review and meta-analysis. *The Lancet Microbe*. 2021; 2():e13–e22. URL: https://dx.doi.org/10.1016/s2666-5247(20)30172-5.

378. Perasso A. An Introduction to The Basic Reproduction Number in Mathematical Epidemiology. *ESAIM: Proceedings and Surveys*. 2018; 62():123–138. URL: https://dx.doi.org/10.1051/proc/201862123.

383. Ganser I, Buckeridge DL, Heffernan J, Prague M, Thiébaut R. Estimating the population effectiveness of interventions against COVID-19 in France: A modelling study. *Epidemics*. 2024; 46():100744. URL: https://www.sciencedirect.com/science/article/pii/S1755436524000057.

386. Wallinga J, Lipsitch M. How generation intervals shape the relationship between growth rates and reproductive numbers. *Proceedings of the Royal Society B: Biological Sciences*. 2007; 274(1609):599–604. URL: https://dx.doi.org/10.1098/rspb.2006.3754.

387. Kerr CC, Stuart RM, Mistry D, et al. Covasim: An agent-based model of COVID-19 dynamics and interventions. *PLOS Computational Biology*. 2021; 17(7):e1009149. URL: https://dx.doi.org/10.1371/journal.pcbi.1009149.

396. Faes C, Abrams S, Van Beckhoven D, Meyfroidt G, Vlieghe E, Hens N. Time between Symptom Onset, Hospitalisation and Recovery or Death: Statistical Analysis of Belgian COVID-19 Patients. *International Journal of Environmental Research and Public Health*. 2020; 17(20):7560. URL: https://dx.doi.org/10.3390/ijerph17207560.

6

Manuscript 3

6.1 Preface to Manuscript 3

An essential step in enhancing studies on NPI effectiveness and other mathematical models used during the COVID-19 pandemic is the continuous refinement of fixed input parameters, such as the duration of immunity. The study period in Manuscript 1 ended just as the Omicron variant began to spread globally, which marked a substantial change in the characteristics of SARS-CoV-2 due to its many mutations. Many previously established parameters, such as the length of the incubation period, basic transmissibility, and the protection offered by prior infection and vaccination, became uncertain. As large parts of the population became infected with Omicron, many individuals soon possessed hybrid immunity, that is, immunity from both vaccination and natural infection.

To adapt and improve models to the newly emerging Omicron variant and its sub-variants, new parameters were necessary. One of the critical knowledge gaps was the level and duration of protection conferred by prior vaccination and infection. Waning immunity had been observed with other viral strains both as decreasing protection from infection and decreasing antibody levels over time. Estimating these parameters is crucial for public health decision-makers, particularly regarding the timing and frequency of booster shots. Moreover, these estimates can also inform modelers for updating key parameters for serosurveillance studies and forecasting models.

In Manuscript 3, we used a large dataset of anti-SARS-CoV-2 nucleocapsid and spike antibodies from Canadian blood donors. While these data were originally collected for serosurveillance, they presented an promising opportunity to address these critical questions about immune protection conferred by antibodies and the duration of this protection.

This manuscript is in preparation and intended for submission to Nature Communications.

6.2 Manuscript 3: Waning immunity against SARS-CoV-2 and the risk of re-infection

Iris Ganser[1,2], Tanya J Murphy[3], Mélanie Prague[2,4,5], Sheila F O'Brien[6,7], Rodolphe Thiébaut[2,4,5], David L Buckeridge[1,3*]

[1] McGill Health Informatics, School of Population and Global Health, McGill University, Montreal, Quebec, Canada
[2] Univ. Bordeaux, Inserm, BPH Research Center, SISTM Team, UMR 1219, Bordeaux, France
[3] COVID-19 Immunity Task Force, School of Population and Global Health, McGill University, Montreal, Quebec, Canada
[4] Inria Bordeaux - Sud-Ouest, SISTM Team, Talence, France
[5]Vaccine Research Institute, Creteil, France
[6]Epidemiology and Surveillance, Canadian Blood Services, Ottawa, Ontario, Canada
[7]School of Epidemiology and Public Health, University of Ottawa, Ottawa, Ontario, Canada

Abstract

A large proportion of the global population now possesses hybrid immunity, derived from both infection and vaccination, against SARS-CoV-2. However, there is uncertainty about the extent and duration of protection conferred by antibodies produced from hybrid immunity. Using longitudinal antibody measurements from over 448,270 Canadian blood donors, we evaluated the association between total anti-spike (anti-S) and anti-nucleocapsid (anti-N) antibody levels and the risk of SARS-CoV-2 infection in Cox proportional hazards models, and we used mechanistic models to analyze the waning dynamics of these antibodies over time. Both anti-S and anti-N antibodies significantly reduced the hazard of infection, with higher titers providing greater protection. The mechanistic models showed that antibodies waned in a bi-phasic way, with a rapid initial decline followed by a slower decay. While multiple immunizing events resulted in more durable protection, anti-S levels fell below thresholds providing 50% protection within months post-immunization, and anti-N levels fell below this threshold within two years. Our results suggest that maintaining high antibody levels is crucial for sustained protection and underscore the need for regular booster vaccinations. The strong correlation of anti-N antibodies with protection makes them a valuable marker for assessing natural immunity.
Keywords: SARS-CoV-2, vaccination, antibodies, infection-derived immunity, hybrid immunity, waning dynamics, durability

Introduction

COVID-19 continues to pose a significant public health challenge, even though the world has transitioned from the pandemic to an endemic phase [31]. A large part of the global population is anticipated to possess hybrid immunity, which is derived from both infection and vaccination, to SARS-CoV-2 [397]. This combined immunity offers superior protection compared to immunity from infection or vaccination alone [232, 398], but neither immunity from infection or vaccination alone, nor hybrid immunity guarantee protection against SARS-CoV-2 infection. While vaccines, especially booster doses, have been effective in preventing severe disease, their ability to prevent infection is limited and diminishes over time [77, 218, 229, 399]. This limitation can be attributed to two related, yet distinct factors: the emergence of new viral variants (variants of concern, VoCs), which can evade immunity established by previous infection and vaccinations [79, 400, 401], and the waning of immunity over time [219, 232]. The combination of these factors results in reduced overall immunity in the population and an increased risk of (re-)infection.

Infections with different SARS-CoV-2 variants and vaccination with different vaccine products, together with diverse individual immune factors, shape the population's immunity landscape. The adaptive immune response to SARS-CoV-2 is complex and multifaceted, involving both cellular and humoral components [402]. Most vaccines used in North America and Europe are based on messenger RNA (mRNA) technology and target the viral spike (S) protein only. Neutralizing antibodies towards the S protein have been identified as a correlate of protection against the original strain of the virus as well as VoCs [211, 403], and total antibody levels, which are easier to measure, correlate well with neutralizing antibody levels [222, 404]. While a negative correlation between total antibody level and risk of infection has been demonstrated [405], the exact levels of antibodies required to confer protection are unclear. Many studies have examined the effectiveness of vaccination or infection in preventing COVID-19 [101], but few have correlated these outcomes with antibody titers [251–253, 405, 406]. In particular, antibodies against the viral nucleocapsid protein (anti-N antibodies), which are not elicited by most vaccines and thus indicative of natural immunity, have rarely been taken into consideration [407, 408].

Another area of uncertainty is the duration of protection conferred by individual vaccine doses and infection. Recently, a large cohort study with extended follow-up periods provided more detailed insights into anti-S antibody dynamics, mainly after vaccinations [225]. However, there is limited research on the waning of immunity from infection, as represented by anti-N antibodies: Most studies on immunity following infection were conducted early in the pandemic, with small participant numbers, highly selected cohorts, short follow-up periods, and some-

times before vaccinations were widely available [95, 102, 222–224, 355]. This gap in knowledge is significant as a clear understanding of natural and hybrid immunity is necessary for evidence-based implementation of public health interventions. Understanding the duration of this immunity and its effectiveness in preventing reinfection, particularly with heterologous viral strains, is therefore important for guiding public health policies and vaccination strategies.

More precisely, it is important to 1) quantify the association between hybrid immunity, as measured by anti-S and anti-N antibodies, and the risk of (re)infection, and 2) assess the relationship between hybrid immunity and the duration of protection. As anti-N antibodies are produced exclusively following infection, while anti-S antibodies are generated both after infection and vaccination, tracking the trajectories of these antibodies allows for differentiation between immunity derived from infection and immunity derived from vaccination. In this context, anti-N antibodies can be used as a proxy for immunity derived from infection.

We take advantage of a unique dataset of antibody measurements from blood donors across Canada, including data from over one million donations with extensive follow-up over more than three years. Insights into the waning of immunity not only inform the timing of booster doses and vaccination campaigns, but are also important for epidemiological and seroprevalence modeling, aiding in the accurate assessment of population immunity through serosurveys [409, 410]. Additionally, this study seeks to contribute to the existing knowledge by identifying potential protective thresholds for anti-N and anti-S antibodies, thereby enhancing our understanding of the correlation of readily available serum antibody levels with SARS-CoV-2 infection and reinfection.

Results

Cohort characteristics

Canadian Blood Services (CBS) manages blood and plasma donations across Canada, with the exception of the province of Quebec. Following blood and plasma donations, a portion of the residual blood was randomly selected by CBS for SARS-CoV-2 antibody testing. Anti-N antibodies were measured in blood samples from April 2020 to December 2023, and anti-S antibodies were measured from January 2021 to December 2023. Samples were chosen randomly until June 2021, after which sampling was stratified by age group. Results of the tests, along with donor demographic information was shared with the Canadian COVID-19 Immunity Task Force. The initial cohort comprised 448,270 blood donors and 1,039,298 antibody measurements, from which three cohorts with analytical samples were derived for different study objectives: The risk of infection (ROI) cohort, the anti-N waning cohort, and the anti-S waning cohort (Table 6.1, and for participant selection flowcharts, see Figures S6.2, S6.3 and S6.4). We inferred dates of infection and

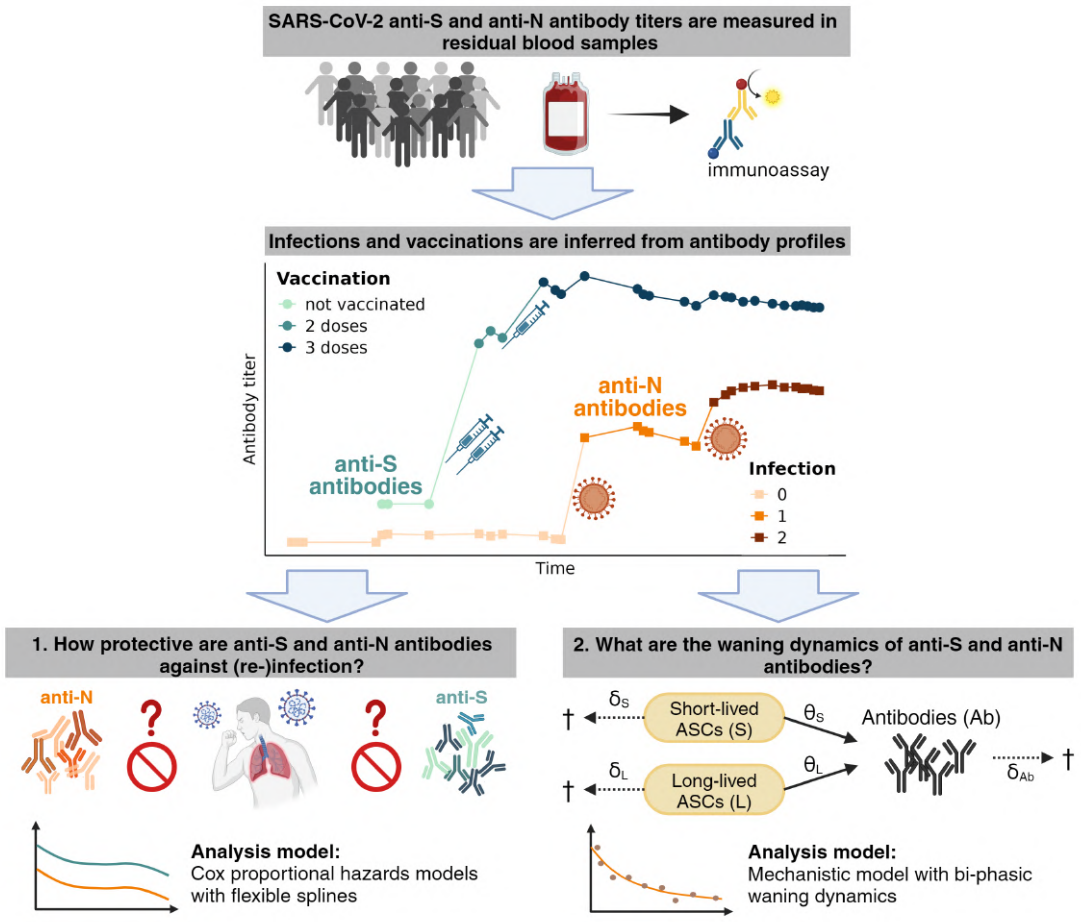

Figure 6.1: Overview of study procedures and goals. Figure created with BioRender (biorender.com)

vaccination from longitudinal antibody profiles, with increases in anti-N antibodies indicating infections and increases in anti-S antibodies without corresponding increases in anti-N antibodies indicating vaccinations (Figures 6.1 and S6.1).

We included participants in the ROI cohort regardless of their infection or vaccination status. However, since antibody levels decrease after each immunization and because we could only detect infections once an antibody measurement was performed, we implemented restrictions on gaps between antibody measurements in this cohort to limit measurement error and interval censoring. For each participant, we calculated the intervals between antibody measurements and selected the longest consecutive sequence of measurements with a maximum inter-measurement interval of 180 days for inclusion into the analysis (for a detailed explanation see

Methods Section *Samples and donors*). In sensitivity analyses, we explored shorter interval lengths, which is assumed to reduce interval censoring and measurement error, but could introduce selection bias. Trends in infection rates remained consistent across filtering intervals, but more participants, observations, and infections were included at longer intervals (see Figure S6.5). Moreover, as the length of filtering intervals decreased, the percentage of men, the percentage of participants identifying as white, and the mean age in the cohorts increased (Table S6.1). The 180 day cohort, which we used in the main analysis, consisted of 134,652 individuals (Table 6.1). The median number of observations per participant was 4 (IQR: 2-7), with nearly 40,000 infections detected. The cohort was predominantly of white ethnicity (approximately 82%), with a mean age of 50.9 years (SD: 15.5 years). Most participants had received at least two vaccine doses.
The anti-N and anti-S waning cohorts were selected on the infection/vaccination episode level, with an infection/vaccination episode comprising all data points from a detected increase in antibody levels to the next increase. In the anti-N waning cohort, we included infection episodes with at least one measurement within 90 days prior to the newly detected infection (to ensure accurate peak level antibody measurements) and a minimum of four antibody measurements per episode. The analysis sample could thus include multiple infections of the same donor, but not necessarily all of them. In the anti-S waning cohort, we included infection/vaccination episodes that met the same inclusion criteria. The final cohort for the anti-N waning analysis included 3176 infection episodes from a total of 2965 donors, while the final cohort for the anti-S waning analysis included 2911 infection episodes and 2752 vaccination episodes from 4479 donors. With the more stringent inclusion criteria for the waning analysis cohorts, the percentage of male donors and the donor age increased, as well as the percentage of donors with white ethnicity. This is because plasma donors (who are primarily male, older, and white) with more frequent donations than whole blood donors are selected at a higher proportion.

Risk of infection and re-infection in relation to antibody levels

We observed non-linear associations between anti-N and anti-S antibody titers and the hazard of infection (Figure 6.2). The associations between both types of antibodies and the hazard of infection was estimated in the same model, thus yielding the effects of each type of antibody independent of the other type. For anti-S antibodies (measured in U/ml), the adjusted hazard ratio (HR, adjusted for anti-N levels, donor age, sex, and race, weekly difference in seroprevalence, and circulation of VoCs) decreased significantly as titers increased from detectable levels to approximately 10 U/ml, plateaued at intermediate titers (10 to 1,000 U/ml), and further decreased at very high titers (>1,000 U/ml), reaching a HR of 0.3 (95% CI 0.28-0.33) at 100,000 U/ml (the assay's limit of quantification). In

	All donors	Risk of infection cohort (180 day interval)	Anti-S waning cohort	Anti-N waning cohort
Number of participants	448,720	134,652	4,479	2,965
Number of observations	1,039,298	431,833	40,226	24,243
Median number of observations per participant (IQR)	3 (2, 6)	4 (2, 7)	13 (5, 25)	10 (5, 19)
Total number of detected infections	194,033	39,044	2,911	3,176
Total number of detected vaccinations	411,151	246,347	12,097	7,483
Median number of vaccinations per participant (IQR)	0 (0, 2)	2 (2, 2)	3 (2, 3)	2 (2, 3)
Male participants (%)	49.5	60.6	83.6	83.8
Mean age (SD)	46.82 (15.87)	50.9 (15.49)	56.34 (14.41)	54.47 (14.45)
Participants of white ethnicity (%)	74.8	81.6	87.3	86.8
Participants of Asian ethnicity (%)	9.5	7.7	5.8	6.1
Participants of Aboriginal ethnicity (%)	1.4	1.2	1.2	1.2
Participants of other ethnicity (%)	9.7	6.0	3.1	3.4
Participants with missing ethnicity (%)	4.7	3.4	2.6	2.5

Table 6.1: Demographic characteristics of blood donors, separated by analysis cohort.
IQR: Interquartile range, SD: standard deviation

contrast, anti-N antibodies (measured as a cutoff index [COI] on a signal-to-cutoff scale) showed a more linear relationship with the hazard of infection above the seropositivity threshold of 1 COI, reaching an adjusted HR of 0.5 at 14.6 COI and further decreasing to 0.08 at the highest titers (>100 COI). Although we did not observe any distinct protection thresholds for anti-N, we identified the points where the HRs corresponded to 25%, 50%, and 75% reductions in hazard of infection, which occurred at 4.3, 14.6, and 61.7 COI, respectively. For anti-S, we defined protection thresholds at three levels: 13% protection, corresponding to the middle of the plateau (100 U/ml); 25% protection at 10,000 U/ml; and 50% protection at 41,783 U/ml.

Week-to-week differences in seroprevalence, as an overall measure of infectiousness, increased the hazard of infection (Figure S6.6 panel C). We also observed a strong association between infection risk and VoCs, parameterized as periods of calendar time with predominant circulation of the respective VoC (HRs: Alpha 1.08, 95% CI [0.77-1.50]; Delta 14.14, 95% CI [10.71-18.67]; Omicron 37.3, 95% CI [28.33-49.09], all compared to the ancestral strain). The Omicron VoC had the strongest effect, reflecting its increased transmissibility and immune-evasive properties. Increasing age was associated with a lower hazard of infection (HR per 10-year increase 0.88, 95% CI [0.87-0.89]), while sex and self-reported race did not significantly affect the hazard of infection (HRs 0.98, 95% CI [0.96-1.00] and 0.97, 95% CI [0.95-1.00], respectively).
Upon visual inspection, we found no substantial differences between models using different filter intervals in terms of effect estimates, apart from slightly attenuated effects with longer intervals, possibly due to interval censoring (Figure S6.6 panels A and B). Similarly, results were robust across different imputation strategies for the infection date (start or end point of the interval; Figures S6.10 and S6.9) and time scales (calendar day vs. day since cohort entry; Figures S6.7-S6.8, Table S6.2).

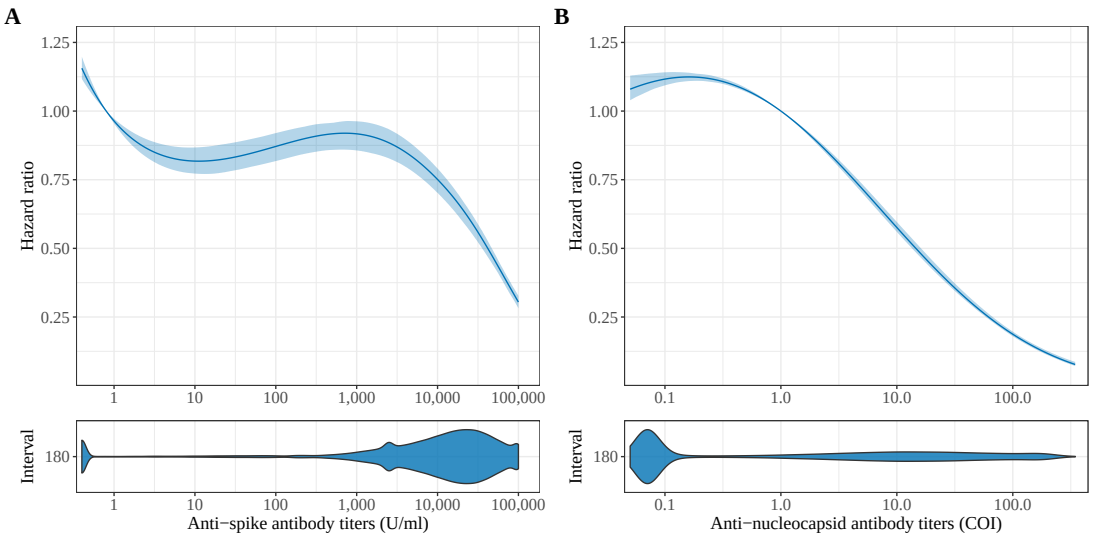

Figure 6.2: Adjusted hazard ratios for the association of antibody levels with hazard of infection. Hazard ratios with corresponding 95% CIs are shown over the range of anti-S (panel A) and anti-N antibodies (panel B). Anti-S antibodies hazard ratios were referenced to the assay's positivity cutoff point of 0.8, and anti-N to the assay's positivity cutoff point of 1. Hazard ratios were adjusted for donor age, sex, and race, weekly difference in seroprevalence, and circulation of VoCs. The violin plots below indicate the distribution of the respective antibody levels.

Antibody waning dynamics and duration of protection

Anti-N antibody dynamics To characterize anti-N antibody waning, we applied a mechanistic model to analyze waning patterns, separately for each infection episode. A bi-phasic decay model with an initial rapid decline followed by a slower waning phase was fit to the data. We found significant differences between first and subsequent infection episodes, with higher initial antibody production and slower waning rates in subsequent infections. Estimated model parameters, their interpretations, and fit assessments are provided in the Supplementary Results Section *Anti-N antibody waning results*.

To illustrate the duration of protection, we simulated individual waning trajectories over a three-year period using the parameter estimates from the mechanistic model and protection thresholds defined from the previously estimated risk-of-infection models. After three years, 47.7% (95% CI: 33.1-58.1) of individuals with a first infection remained above the seropositivity threshold (1 COI), compared to 78.9% (95% CI: 53.8-86.0) and 83.8 % (95% CI: 48.9-92.2) of individuals with two and three infections, respectively (Figure 6.3, Table 6.2). Notably, after a single infection, few individuals reached antibody levels associated with 50% or 75% protection, and only 12.2% (95% CI: 11.2–13.7) and 1.1% (95% CI: 0.7–1.6) remained above these thresholds at one year post-infection, respectively. Protection was more durable after subsequent infections, but still declined substantially, with only 49.5% (95% CI 46.4–52.6) and 20.5% (95% CI 18.0–23.6) remaining above the 50% and 75% protection thresholds one year after a second infection.

Anti-S antibody dynamics As anti-S antibodies are elicited both by infection and vaccination, we analyzed waning dynamics separately by immunizing event. The parameters estimated by the mechanistic model are detailed in the Supplementary Results Section *Anti-S antibody waning results*. Waning was slower following infection than vaccination, with a 28% reduction (95% CI 20.5-30%) in the rate of decline and a higher initial antibody production after infection. Simulations showed that individuals remained above the anti-S seropositivity threshold of 0.8 U/ml for the simulation period of three years, due to initially high antibody levels (Figure 6.4). Since anti-S antibodies showed a plateau the risk of infection analysis, we adjusted the protection thresholds to 13% (HR plateau), 25%, and 50% protection. Over 90% of individuals reached the 25% protection threshold after at least two immunizing events, but most fell below this level within a year (Table 6.3). The 50% protection threshold was attained by less than half of the individuals after multiple immunizing events, and dropped to approximately 5% one year post-immunization.

infection	% above threshold t=0	% above threshold t=1Y	% above threshold t=2Y	% above threshold t=3Y	mean waning time (days)
positivity cutoff (1 COI)					
1	98.9 (98.5-99.4)	81.7 (80.6-83.1)	60.7 (53.0-66.7)	47.7 (33.1-58.1)	534 (474-577)
2	99.7 (99.3-100)	89.9 (87.5-92.2)	83.6 (74.8-88.3)	78.9 (53.8-86.0)	438 (332-662)
3	99.0 (97.1-100)	92.4 (88.6-97.4)	88.6 (76.4-94.2)	83.8 (48.9-92.2)	455 (138-782)
25% hazard reduction (4.3 COI)					
1	91.5 (90.4-92.6)	44.5 (42.2-46.5)	18.6 (13.4-24)	13.4 (7.1-19.2)	352 (338-371)
2	92.9 (91.3-94.6)	70.0 (66.8-73.9)	44.6 (39.7-49.5)	30.8 (25.6-40.4)	488 (442-515)
3	91.4 (87.2-95.7)	78.1 (70.6-84.7)	41.9 (35-52.8)	25.7 (16.9-42)	572 (482-621)
50% hazard reduction (14.6 COI)					
1	71.2 (69.7-72.9)	12.2 (11.2-13.7)	4.5 (2.7-6.6)	3.3 (1.3-5.3)	218 (210-232)
2	81.0 (78.9-83.7)	49.5 (46.4-52.6)	24.2 (21.5-30.8)	17.3 (13.3-27.8)	402 (337-440)
3	84.8 (78.6-89.8)	54.3 (43.8-61.8)	20.0 (13.5-34.8)	13.3 (6.5-33.8)	429 (316-483)
75% hazard reduction (61.7 COI)					
1	22.6 (21-24.2)	1.1 (0.7-1.6)	0.4 (0-1.0)	0.2 (0-0.7)	136 (123-144)
2	71.3 (68.7-74.9)	20.5 (18.0-23.6)	11.4 (6.8-19.7)	10.3 (3.1-19)	237 (199-299)
3	74.3 (67.3-81.2)	16.2 (10.5-27.4)	9.5 (3.4-24.3)	9.5 (1.4-20.8)	228 (194-299)

Table 6.2: Simulated anti-N antibody waning results over three years. The percentage of donors above each threshold is depicted at the time of infection detection, one year, two years, and three years after infection. Individual waning trajectories were simulated and Kaplan-Meier analyses of time to falling below antibody thresholds were conducted, separately by infection episodes and waning thresholds. We simulated trajectories for each individual included in the initial model estimation and using the estimated parameters, separate by infection number. The protection thresholds were determined with the previous risk of infection model.
Y = year

immuniz-ing episode	% **above threshold t=0**	**% above threshold t=1Y**	**% above threshold t=2Y**	**% above threshold t=3Y**	**mean waning time (days)**
13% hazard reduction (100 U/ml)					
1	92.9 (90.5-95.4)	86.6 (82.6-90.1)	84 (79.4-86.9)	82.4 (76.1-85.0)	368 (325-526)
2	99.7 (99.5-100)	99 (98.7-99.4)	98.7 (98.2-99.1)	98.4 (97.9-98.9)	397 (287-501)
3	99.9 (99.8-100)	99.9 (99.8-100)	99.8 (99.6-100)	99.8 (99.6-99.9)	499 (16-1004)
4	100 (100-100)	100 (100-100)	100 (100-100)	100 (100-100)	-
5	100 (100-100)	100 (100-100)	100 (100-100)	100 (100-100)	-
25% hazard reduction (10,000 U/ml)					
1	9.7 (7-13.1)	1.8 (0.5-3)	0.3 (0-0.8)	0 (0-0)	186 (126-245)
2	90.6 (89.8-91.7)	37.1 (35.7-39.1)	18.9 (15.8-21.4)	9.5 (6.6-12.1)	319 (305-331)
3	93.9 (93-95)	40.3 (37.7-42.5)	19.6 (15.6-21.3)	11.5 (7.5-13.1)	320 (307-335)
4	95 (93.3-96.7)	41.6 (36.6-44.7)	18.7 (14.1-23.6)	10.9 (7.2-13.7)	335 (314-356)
5	95.3 (92.7-97.5)	35.8 (28.8-42.0)	16 (11.3-22.5)	8 (4.9-11.7)	323 (281-356)
50% hazard reduction (41,783 U/ml)					
1	2.1 (0.8-3.3)	0 (0-0)	0 (0-0)	0 (0-0)	42 (30-51)
2	44.8 (43.0-46.6)	4.6 (3.7-5.2)	0.8 (0.5-1.2)	0.3 (0.2-0.7)	157 (147-164)
3	46.8 (44.7-48.6)	5.3 (4.2-6.1)	1.6 (0.8-2.1)	0.3 (0.1-0.7)	162 (147-169)
4	49.8 (44.9-53)	5 (3.8-6.7)	1 (0.3-1.8)	0.3 (0-0.7)	139 (121-159)
5	46.7 (39.3-60.9)	2.8 (0.5-5.2)	1.4 (0-3.2)	0.9 (0-2.4)	109 (82-137)

Table 6.3: Simulated anti-S waning results over three years. The percentage of donors above each threshold is depicted at the time of anti-S increase detection (i.e., vaccination or infection), and one year, two years, and three years after an anti-S increase detection. The protection thresholds were determined with the previous risk of infection model. Waning below the seropositivity threshold (0.8 U/ml) was not included in the analysis, as >99% of individuals did not wane below this threshold.
Y = year

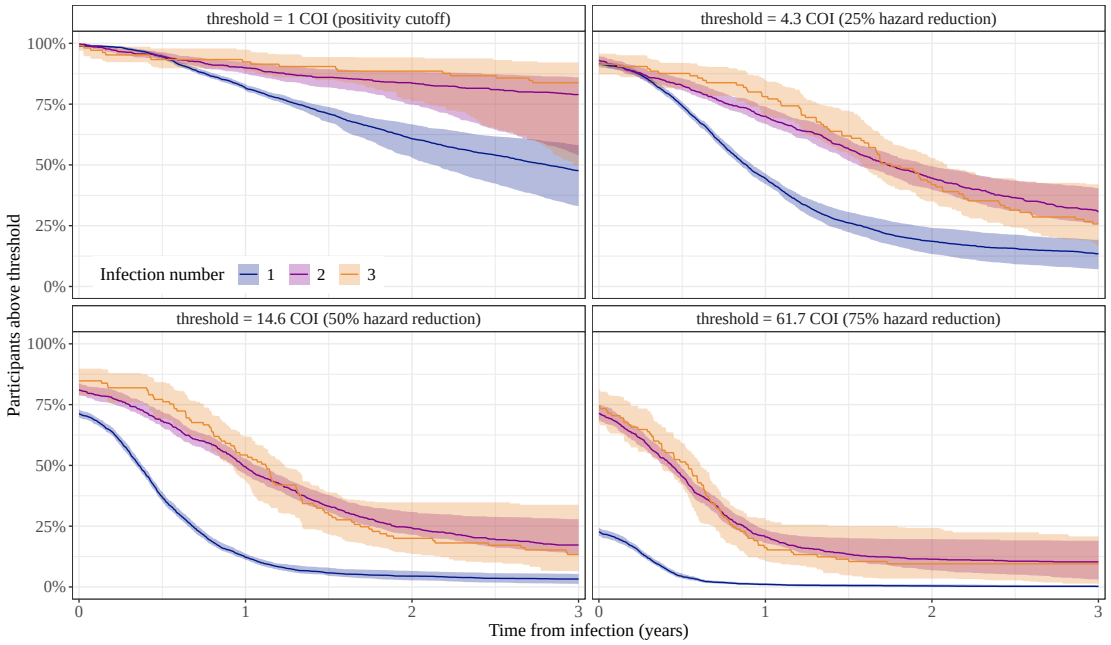

Figure 6.3: Simulated anti-N antibody waning results over three years. Individual waning trajectories were simulated and Kaplan-Meier analyses of time to falling below antibody thresholds were conducted, separately by infection episodes and waning thresholds. We simulated trajectories for each individual included in the initial model estimation and using the estimated parameters, separate by infection number. Waning was determined as falling under a pre-determined threshold, using four values as cut-offs: The seropositivity cutoff (1 COI), 25% hazard reduction (4.3 COI), 50% hazard reduction (14.6 COI), and 75% hazard reduction (61.7 COI). The latter three thresholds were determined with the previous risk of infection model. As individuals often did not attain the waning threshold throughout their course of infection, the survival curves do not start at 100%. 95% confidence intervals were derived from the bootstrap runs, by taking the 2.5th and 97.5th percentile of the trajectories for each day, separately for each infection number and waning threshold.

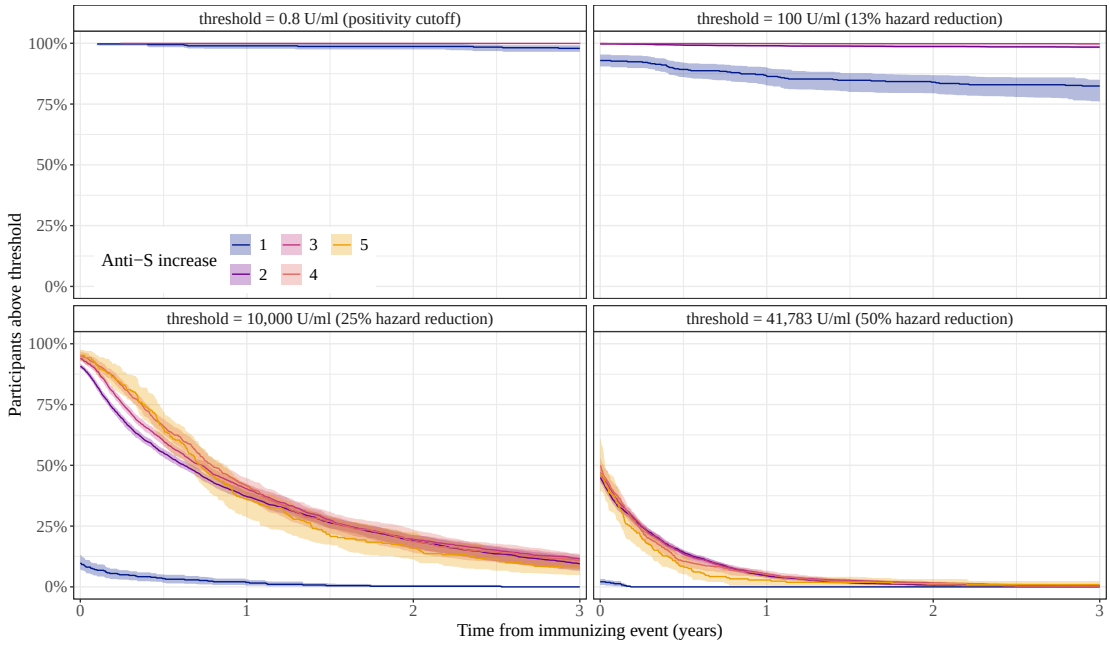

Figure 6.4: Simulated anti-S antibody waning results over three years. Individual waning trajectories were simulated and Kaplan-Meier analyses of time to falling below antibody thresholds were conducted, separately by immunizing episodes and waning thresholds. An immunizing episode can either be a vaccination or an infection. We simulated trajectories for each individual included in the initial model estimation and using the estimated parameters, separate by immunizing episode. Waning was determined as falling under a pre-determined threshold, using three values as cutoffs: 13% hazard reduction (100 U/ml), 25% hazard reduction (10,000 U/ml), and 50% hazard reduction (41,783 U/ml), determined with the previous risk of infection model. Contrary to the anti-N model, waning below the seropositivity threshold (0.8 U/ml) was not included in the analysis, as >99% of individuals did not wane below this threshold. 95% confidence intervals were derived from the bootstrap runs, by taking the 2.5th and 97.5th percentile of the trajectories for each day, separately for each infection number and waning threshold.

Discussion

To our knowledge, this study is the largest investigation to date of the effect of SARS-CoV-2 antibodies on the risk of subsequent infection, with a cohort of over 130,000 blood and plasma donors and over 39,000 infections. Unlike other studies, which focused solely on anti-S antibodies [225, 251–253], our analyses take into account the effects of both anti-N and anti-S antibodies. By examining the waning dynamics of antibodies, our study offers a comprehensive view of how SARS-CoV-2 immunity evolves over time, allowing us to simultaneously assess the implications on infection risk while accounting for the decline in antibody levels over time. Most infections were observed during the Omicron period, reflecting the higher probability of transmission and immune escape properties of the Omicron variant and the increased sampling during this period [411]. Our findings demonstrate that both anti-S and anti-N antibodies significantly reduce the risk of SARS-CoV-2 infection, even during the Omicron period. Consistent with studies conducted before and during the Omicron period [180, 251–253, 405], we found that higher anti-S antibody levels were associated with increased protection. Anti-S antibodies are the only SARS-CoV-2 antibodies with neutralizing activity, and spike-targeting neutralizing antibodies have been discussed as a correlate of protection against SARS-CoV-2 infection [211]. Nonetheless, recent evidence indicates that neutralizing antibodies account only for a small portion of the protection against infection with Omicron variants [412]. Interestingly, we found that anti-N antibodies confer a comparable level of protection to anti-S antibodies. Although they do not have neutralizing capacity, anti-N antibodies can mediate Fc-dependent functions, including complement activation, phagocytosis, and cellular cytotoxicity [413]. Moreover, as anti-N antibodies are produced only following infections, they likely reflect induction of antibodies with increased potency and breadth and other immune responses elicited by infection, such as local immune responses in lung tissues [89, 202, 414, 415]. Previous studies have reported stronger protection following infection compared to vaccination, but none of these studies related risk of infection directly to antibody levels [220, 221]. Moreover, our findings show that previous infection (in the form of anti-N antibodies), provides substantial protection, while anti-S antibodies have an independent protective effect. This can be interpreted as support of previous evidence indicating that hybrid immunity—immunity derived from both vaccination and infection—is more effective than either type of immunity alone [234, 246].

Our detailed analysis of antibody waning revealed that SARS-CoV-2 specific antibodies persist longer than initially assumed. Early studies reported half-lives ranging from 60-140 days for anti-S [102, 222] and 60-85 days for anti-N [95, 102, 222]. However, these studies did not have a follow-up time that was sufficiently

long to observe a second phase of antibody decay, where the rate of waning slows. Another study estimated with a bi-phasic model that only 7% (1%–31%) of initial anti-nucleocapsid IgG remains one year post symptom onset [416], but their follow-up period did not extend beyond one year and they had few longitudinal follow-up samples. The extended follow-up period of our study enabled us to observe bi-phasic waning dynamics with a persistence of long-lived antibody-secreting cells over multiple years. However, we found the duration of antibody levels providing high levels of protection to be much more short-lived. Single immunizing events (i.e., one infection or vaccination) failed to elicit high antibody titers and durable protection, while multiple immunizing events resulted in more durable protection. However, even after multiple immunizing events, anti-S titers fell below levels providing 50% within less than one year and anti-N titers waned below the 50% protection threshold in under two years.

Our study is not without limitations. First, the anti-N assay was only officially validated by the manufacturer to give qualitative results around the positivity cutoff value and is thus not numerically validated across its whole range. We addressed this limitation by modeling anti-N values with flexible splines in the risk of reinfection analysis, thus not relying on any linearity assumptions. Although measurements are highly internally consistent, they can not be compared to anti-N levels from other assays. Additionally, the anti-N assay was changed in January 2021; however, only three participants in the anti-N waning analyses were affected by this anti-N change. In all analyses where anti-S antibodies were used (i.e., risk of infection models and anti-S waning), we excluded observations before January 2021 since anti-S measurements only started in that month.
Second, the anti-S assay had an upper limit of quantification (LOQ) at 2,500 U/ml before September 2021. After a change in dilution protocol, the LOQ increased to 100,000 U/ml, but some participants still exceeded that limit. We took this factor into account in the waning analyses by right-censoring these observations, meaning that these observations were assumed to have a numerical value above 100,000 U/ml. No upper LOQ was observed in the anti-N measurements. Moreover, as with all antibody binding assays, the measured antibody levels are not only influenced by the antibody concentration but also their avidity—the overall strength with which an antibody binds to its antigen. Avidity tends to increase over time following an immunizing event as the immune response matures [417, 418]. In our study, the assays were unable to differentiate between the effects of antibody concentration and avidity.
Third, our study cohort consisted of blood donors, which are healthier than the general population, and may thus not be representative. Blood donors self-select into donating, and the cohort lacks individuals under 17 years of age and is un-

derrepresented in rural areas. Additionally, we require data after an infection to model the antibody waning dynamics, which means only individuals who survived their infection and were healthy enough to donate blood or plasma afterward were included in these analyses. Antibody responses tend to be lower and waning might be faster in less healthy and older individuals [77, 419–421]. Thus, limiting our study population to only healthy individuals might have biased the waning analysis towards longer antibody persistence and a higher percentage of blood donors being above the defined protection thresholds compared to the general population. Moreover, our stringent selection criteria, particularly for the waning cohorts, led to higher donor ages (mean age approx. 55 years vs. 47 years in the overall donor cohort), a higher proportion of males (83% vs. 50%), and a higher percentage of white individuals (97% vs. 75%). However, we observed no differences in waning parameters according to sex, age, or race, nor did our risk of (re-)infection results change as selection criteria became more stringent. Furthermore, in terms of cohort selection, our study complements existing research conducted on hospitalized patients [93, 422] and healthcare workers, who are predominantly younger and female [95, 224, 225, 416]. Our results therefore allow insights into infection and immunity in a broader demographic context [423].
Additionally, we lacked confirmed data on vaccine products, vaccination dates, infection dates and infection severity. Instead, we inferred infection and vaccination status from changes in antibody titers. This way, we did not rely on potentially incomplete reporting, but we might have missed infections or vaccinations if they did not result in an increase antibody titers.

Despite these limitations, our study provides valuable insights into the immune response to COVID-19. Although we were unable to identify a clear protective threshold for anti-N or anti-S antibodies, our findings suggest that maintaining high antibody levels is crucial for sustained protection. Due to bi-phasic decay dynamics, these antibody levels decline rapidly following an immunizing event, but persist at lower levels for longer than initially assumed. The quickly diminishing protective effects of antibodies underscores the need for regular booster vaccinations. Additionally, while anti-N antibodies may not play a direct biological role in preventing infections, their strong correlation with protection suggests that assessing serum anti-N levels may be valuable in informing personalized vaccination decisions. As serum antibody measurements are quicker and more cost-effective to obtain than measurements of cellular or mucosal immunity, they may be a feasible option for some public health studies.

Methods

Samples and donors

Early in the COVID-19 pandemic, Canadian Blood Services (CBS), in partnership with the Canadian COVID-19 Immunity Task Force, began testing residual samples from blood, plasma and platelet donors for SARS-CoV-2 antibodies, in all Canadian regions except Quebec and the Northern Territories. From May to December 2020, residual samples were tested only for anti-N antibodies, while after December 2020 testing was added for anti-S antibodies. Initially sampling was performed for two weeks every month, starting January 2022. Before donation, donors answer screening questions to ensure that they are in good health, and their temperature is checked. Additionally, donations were deferred if the donor had a SARS-CoV-2 infection in the previous two weeks, had been hospitalized for COVID-19 in the previous three weeks, or had been in contact with a SARS-CoV-2 infected individual. For more details on donor eligibility, sample collection, and residual blood sampling strategies, see reference [411]. Available demographic data were linked from the CBS donor database and included year of birth, sex, self-reported ethnicity, and Forward Sortation Area (FSA) of the residential postal code. Given the predominantly white donor population, we categorized ethnicity as white versus non-white. Donors reporting conflicting ethnicity information were coded as non-white if they ever reported non-white status.

The donors can be conceptualized as an open cohort with multiple measurements on many donors, who could enter and leave the cohort at any time. We compiled different cohorts for different analyses: For the risk of infection cohort, all donors with at least two antibody measurements were eligible, regardless of infection status. To ensure accurate measurement of Ab levels and to limit interval censoring, we imposed a restriction on the gap between antibody measurements, requiring the gap to be 180 days or less. For each donor, we selected the longest consecutive sequence of measurements where the gaps between data points remained within the 180-day interval (Figure 6.5). In sensitivity analyses, we explored shorter intervals (90, 100, 120, and 150 days) to further enhance the precision of antibody measurements. However, these more restrictive criteria increased the risk of selection bias. Exploring different intervals represents a trade-off between measurement error and selection bias.

For the anti-N waning analyses, we limited the cohort to donors who had experienced between one and three infections. For the anti-S waning analysis, we included measurements up to the sixth increase in anti-S antibodies (either due to vaccination or infection). For both analyses, we applied inclusion criteria at the level of infection/vaccination episodes. We required 1) an antibody measurement within 90 days before the detection of a new infection (anti-N analysis) or new infection/vaccination (anti-S analysis) to ensure accurate antibody peak height

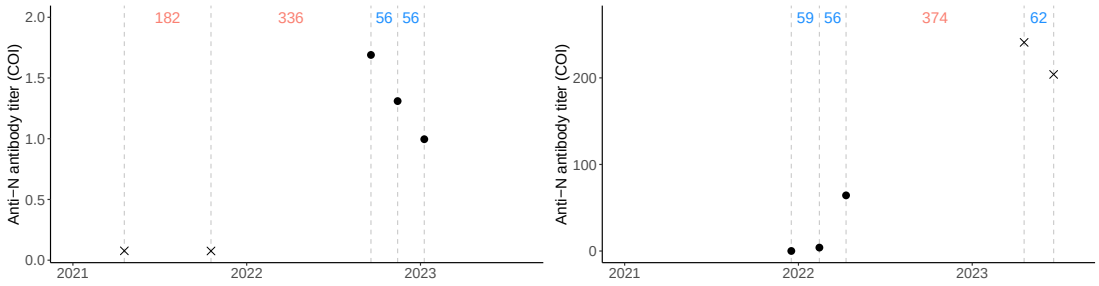

Figure 6.5: Illustration of the interval selection criterion for the risk of infection analysis. The anti-N antibody profiles of two donors are shown, with the respective intervals between measurements. Data points included into the main analysis (180 day filtering interval) are shown as black points. Data points not included because they did not satisfy the condition of one measurement within 180 days before or do not belong to the longest eligible measurement sequence are shown as X's.

estimation and 2) at least four measurements per infection/vaccination episode to estimate waning dynamics accurately.

This study was approved by the Canadian Blood Services Research Ethics Board and the Instutional Review Board of the McGill Faculty of Medicine and Health Sciences.

Serological assays

Two assays were used to measure antibodies. Total anti-SARS-CoV-2 spike antibody (including IgA, IgG, and IgM) was measured with the semi-quantitative Roche Elecsys® spike immunoassay. Total anti-SARS-CoV-2 nucleocapsid antibody was measured with the Abbott Architect SARS-Cov-2 IgG assay until December 2020, and with the qualitative Roche Elecsys® nucleocapsid immunoassay afterwards. The Anti-S assay uses a standard curve, allowing results to be expressed in U/ml, with a validated positivity cutoff value of 0.8 U/ml (sensitivity of 98.8% and specificity of 99.6%). In September 2021, the dilution factor was increased because many samples were exceeding the maximum detection level, which increased the upper limit of quantification from 2,500 to 100,000 U/ml. The Anti-N assay was only validated as a qualitative test, i.e., designed only to determine whether a sample is SARS-CoV-2 negative or positive. The positivity threshold for this assay was validated with a sensitivity of 99.5% and specificity of 99.8%. All numerical values of the assay are referenced to the cutoff value, resulting in a cutoff index (COI) scale. While the anti-N values are internally comparable and reproducible, they cannot be standardized to a U/ml scale.

Infection and vaccination detection algorithm

SARS-CoV-2 infection dates were not reported and vaccination details were self-reported by donors, leading to unreliable vaccination information. Therefore, we developed an algorithm to infer infections and vaccinations from antibody data. The algorithm used heuristics that were visually confirmed. Anti-N antibodies are produced exclusively after infections, whereas anti-S antibodies are formed following both infection and vaccination. This distinction allows us to differentiate between immunity derived from infection and immunity derived from vaccination (illustrated in Figure S6.1). We identified infections by a 0.4 increase on the log10 scale in anti-N antibodies (corresponding to a 2.5-fold increase on the natural scale) or a transition from anti-N seronegative to seropositive. For subsequent infections, we applied a lower threshold (0.2 on log10 scale, approx. 50% on the natural scale). If anti-N levels continued to rise after an infection, we only counted the first significant change within 60 days to avoid double-counting infections. Visual inspection of individual time-series confirmed the algorithm's accuracy in detecting infection-related increases in anti-N levels. When donors had detectable anti-N levels at their first measurement, we assigned them the status of having been infected once. For vaccinations, we applied the same procedure using anti-S antibodies, adjusting the threshold for very high anti-S levels to 0.2 on the log10 scale. Moreover, we ignored anti-S increases that coincided with anti-N increases to exclude infection-induced changes. Given the difficulty in distinguishing closely timed first and second doses due to temporal resolution limits, we did not detect the first vaccination but focused on the primary vaccination series (i.e., first and second dose). If donors entered the cohort with existing anti-S antibody levels, we assigned them the vaccination status of a completed primary series, although we acknowledge the probability of them having received booster doses.

Risk of infection and re-infection

We fit Cox proportional hazards models with time to infection as the outcome and both antibody levels (anti-S and anti-N) as exposure. Participants were censored if the antibody measurements were not included in the filtering intervals or at the end of the study period (December 2023). Antibody levels were treated as time-varying variables and fitted using cubic splines with three knots. As both antibody types were included in the same model, the effects of each antibody type can be interpreted as independent of the other effect. We did not explore interactions between the two antibody types. Covariates included donor age, sex, and ethnicity (white vs. not white). Age was included as a linear term since no significant non-linearity was found. Additionally, we included information on the circulation of variants of concern (VoCs), reported by the Public Health Agency of Canada [424] and archived by the COVID-19 Canada Open Data Working Group

[425]. We parameterized the VoC variable as predominant VoC (among Alpha, Delta, and Omicron) at the time of measurement, with a two-week lag to account for the time from infection to antibody response. We also included a marker of overall infectiousness in the population, derived from weekly seroprevalence differences, modeled at the province scale [409, 426]. We added a frailty effect for individual donors to account for multiple infections and addressed interval censoring by imputing infection dates to the midpoint of the interval. The full equation for the Cox model is as follows:

$$\lambda(t|X_i, z_i) = \lambda_0(t) \times exp(b_1(anti\text{-}S(t)) + b_2(anti\text{-}N(t)) + b_3(seroprev\text{-}diff(t)) + \beta_4 age + \beta_5 sex + \beta_6 race + \beta_7 Alpha(t) + \beta_8 Delta(t) + \beta_8 Omicron(t) + z_i) \quad (6.1)$$

where $b(X)$ stands for the spline terms of the respective variables and z_i is the frailty term, with assumed distribution $z_i \sim \mathcal{N}(0, \sigma_z)$.
Sensitivity analyses were conducted by varying the imputation of infection dates and using calendar day instead of the cohort entry date as the time scale. In these cases, VoC predictors were excluded, as they were equal across all individuals for a given calendar day. All model assumptions were checked visually and with statistical tests, and no violation of the proportional hazards assumption was detected. Coefficients were exponentiated to yield hazard ratios. Hazard ratios for the spline terms were referenced to the respective positivity cutoff values for antibodies (1 for anti-N and 0.8 for anti-S) and 0 for the seroprevalence difference. We derived 95% confidence intervals (CIs) for the spline terms using 100 bootstrap samples, taking the 2.5th and 97.5th quantiles of the bootstrapped distribution.

Model of antibody waning

Mechanistic model description To analyze the waning of antibody response, we used a mechanistic model divided into three layers: a mathematical model, a statistical model, and an observation model. The mathematical model is governed by ordinary differential equations (ODEs), which describe the antibody production and waning dynamics. The statistical model is a mixed effect model which accounts for inter-individual and inter-infection variability of parameters, while the observation model addresses measurement errors. The mathematical model of waning describes a biphasic decay [91, 222, 225], parameterized according to the work of [427, 428]. In brief, this model assumes antibody secretion from two types of antibody-secreting cells (ASCs, also called plasma cells), which are short-lived (S) and long-lived (L) ASCs. These cells decrease over time with decay parameters δ_S and δ_L, respectively. The ASCs secrete antibody into the bloodstream at production rates θ_S and θ_L. In the blood, the antibodies decay with rate δ_{Ab}. These dynamics are detailed in equation 6.2.

$$\begin{aligned}\frac{dS}{dt} &= -\delta_S S \\ \frac{dL}{dt} &= -\delta_L L \\ \frac{dAb}{dt} &= \theta_S S + \theta_L L - \delta_{Ab} Ab\end{aligned} \tag{6.2}$$

As neither short-lived nor long-lived ASC populations are observed in this study, we had to modify the system to allow for parameter identification. Specifically, the initial conditions of the S and L compartments, S_0 and L_0, could not be identified separately from the production rates θ_S and θ_L. Following the approach by Pasin et al. [428], we re-wrote the dynamic system with the antibody compartment as the only observation as:

$$\frac{dAb}{dt} = \phi_S e^{-\delta_S t} + \phi_L e^{-\delta_L t} - \delta_{Ab} Ab \tag{6.3}$$

with $\phi_S = \theta_S S_0$ and $\phi_L = \theta_L L_0$. This leaves five parameters to estimate, three decay parameters and two antibody secretion parameters: $\xi = \{\delta_S, \delta_L, \delta_{Ab}, \phi_S, \phi_L\}$.

In the statistical model, we accounted for two sources of variability, inter-individual variability and inter-infection/vaccination episode variability. We incorporated these with two types of random effects, at the individual level and at the infection/vaccination episode level, respectively. To ensure positivity, we took the natural logarithm of the parameter for estimation. The value of parameter ξ for each subject i and infection/vaccination episode n is therefore written as:

$$\begin{aligned}log(\xi_{in}) &= log(\xi_0) + u_i + u_n \\ u_i &\sim \mathcal{N}(0, \omega^2) \\ u_n &\sim \mathcal{N}(0, \gamma^2)\end{aligned} \tag{6.4}$$

where ξ_0 represents the population mean parameter across all infection/vaccination episodes, u_i is the individual random effect and u_n is the infection/vaccination episode random effect. The two random effects are assumed to be independent of each other.

For the observation model, we used antibody titers on the log10 scale, assuming an additive, normally distributed error on the observations Y for participant i at time t:

$$\begin{aligned}Y_{it} &= log_{10}(Ab_{it}) + \epsilon_{it} \\ \epsilon_{ij} &\sim \mathcal{N}(0, \sigma^2_{Ab})\end{aligned} \tag{6.5}$$

Parameter estimation and model selection Parameters were estimated via maximum likelihood estimation using a stochastic approximation expectation maximization (SAEM) algorithm implemented in the software Monolix, version 2023R2 (www.lixoft.com). We conducted extensive convergence assessments and model selection procedures. The theoretical and practical identifiability of the model has been confirmed in previous work [428]. However, as not all parameters could be identified with only antibody titer data available, we fixed δ_{Ab} to 0.033, which corresponds to a half-life of 21 days [429, 430]. Additionally, we determined the decay parameter for long-lived cells, δ_L, using profile likelihood estimation [431]. This process involves sequentially fixing δ_L at various values, running model estimation, and selecting the value that maximizes the likelihood. As expected, given the extended lifespan of L cells and the relatively short three-year observation period, the likelihood profile remained flat at slower decay rates, indicating that multiple rates were equally supported by the data. Consequently, we fixed δ_L to the largest decay rate where further increases in likelihood were minimal. In a backwards selection process, we found that applying random effects to the remaining three parameters (δ_S, ϕ_S, ϕ_L) at the infection/vaccination episode level and applying additional random effects to δ_S and ϕ_S at the individual level yielded the lowest Akaike information criterion (AIC) while demonstrating good convergence. Conversely, models that included regression coefficients (e.g., number of infections instead of random effects) failed to converge, indicating practical identifiability issues. CIs were computed using a bootstrapping approach, which involved resampling participants with replacement and randomly varying the initial values of the SAEM algorithm.

To nevertheless assess possible differences of waning parameters across different infection episodes, we ran post-hoc linear mixed effects models separately for each estimated parameter as follows:

$$log(\delta_S) = log(\delta_{S1}) + \beta_2 inf_2 + \beta_3 inf_3 \tag{6.6}$$

To accurately include uncertainty from the mechanistic models into the regression models, we ran the regression models also on the bootstrap runs and took the 2.5th and 97.5th percentile as the 95% confidence intervals. Since we used a log link, the the beta parameters can be interpreted as having a multiplicative effect on the baseline value of the parameter. Associations of demographic variables with estimated parameters were examined the same way, while controlling for the effect of the number of infections. Regression models were fit using R Statistical Software version 4.4.1 [432], using the package lme4 version 1.1.35.3 [393].

Simulation of time to seroreversion To estimate when individuals were likely to fall below different thresholds we simulated trajectories for all participants using their individual estimated parameters. For anti-N, we used the assay detection

threshold of 1 COI (i.e. seroreversion) and antibody levels determined by the Cox model to reduce the hazard of infection by 25% (4.3 COI), 50% (14.6 COI), and 75% (61.7 COI). For anti-S, the thresholds were 0.8 U/ml (seroreversion), 100 U/ml (13% hazard reduction), 10,000 U/ml (25% hazard reduction), and 41,783 U/ml (50% hazard reduction). We simulated waning trajectories separately for each infection episode, with each simulation starting at time 0. The simulations covered a period of 3 years, as extrapolating beyond this time is less meaningful due to the likelihood of reinfection, the high uncertainty in parameters after this time, and reduced public health relevance. After obtaining individual trajectories, we conducted Kaplan-Meier analyses of the time to seroreversion. To account for uncertainty in previous parameter estimation, we also conducted the waning analysis using the previous bootstrap runs and calculated the 95% CIs as the 2.5th and 97.5th percentiles of the bootstrap distribution. The simulations were implemented in R version 4.4.1 [432] using the package deSolve version 1.40 [433], and the Kaplan-Meier analysis was performed with the package survival version 3.7.0 [434].

Contributors

Iris Ganser: Formal Analysis, Data Curation, Conceptualization, Methodology, Writing – Original Draft Preparation. **Tanya J Murphy:** Data Curation, Methodology, Writing – Review & Editing. **Mélanie Prague:** Methodology, Writing – Review & Editing. **Sheila F O'Brien:** Resources, Writing – Review & Editing. **Rodolphe Thiébaut:** Methodology, Supervision, Writing – Review & Editing. **David L Buckeridge:** Conceptualization, Methodology, Resources, Supervision, Writing – Review & Editing.

Declaration of interests

The authors have no competing interests to declare.

Data sharing

Data may be made available upon request from Canadian Blood Services (contact person: Sheila F O'Brien), subject to internal review, privacy legislation, data sharing agreements and research ethics approval.

Acknowledgements

IG is supported by the Digital Public Health Graduate Program within the framework of the PIA3 (Investment for the Future), project reference: 17-EURE-0019, and by a doctoral award from the Fonds de recherche du Québec-Santé.
We thank Simulations Plus, Lixoft division for the free academic use of the MonolixSuite.
This work has been pursued in the EMERGEN project framework of the French Agency for Research on AIDS and Emerging Infectious Diseases (ANRS0151) and supported by INSERM and the Investissements d'Avenir program, Vaccine Research Institute (VRI), managed by the ANR under reference ANR-10-LABX-77–01. The funding source was not involved in the design, execution, analysis, interpretation of the research findings, or manuscript writing.

6.3 Manuscript 3: References

31. *WHO Director-General's opening remarks at the media briefing – 5 May 2023*. [Online; accessed 27. Apr. 2024]. 2023. URL: https://www.who.int/news-room/speeches/item/who-director-general-s-opening-remarks-at-the-media-briefing---5-may-2023.

77. Andrews N, Stowe J, Kirsebom F, et al. Covid-19 Vaccine Effectiveness against the Omicron (B.1.1.529) Variant. *N. Engl. J. Med.* 2022().

79. Cao Y, Wang J, Jian F, et al. Omicron escapes the majority of existing SARS-CoV-2 neutralizing antibodies. *Nature*. 2022; 602():657–663.

89. Sette A, Crotty S. Adaptive immunity to SARS-CoV-2 and COVID-19. *Cell*. 2021; 184(4):861–880.

91. Lapuente D, Winkler TH, Tenbusch M. B-cell and antibody responses to SARS-CoV-2: infection, vaccination, and hybrid immunity. *Cell. Mol. Immunol.* 2024; 21():144–158.

95. Lumley SF, Wei J, O'Donnell D, et al. The Duration, Dynamics, and Determinants of Severe Acute Respiratory Syndrome Coronavirus 2 (SARS-CoV-2) Antibody Responses in Individual Healthcare Workers. *Clin. Infect. Dis.* 2021; 73(3):e699–e709.

101. Pooley N, Abdool Karim SS, Combadière B, et al. Durability of Vaccine-Induced and Natural Immunity Against COVID-19: A Narrative Review. *Infect. Dis. Ther.* 2023; 12(2):367–387.

102. Dan JM, Mateus J, Kato Y, et al. Immunological memory to SARS-CoV-2 assessed for up to 8 months after infection. *Science*. 2021; 371(6529).

180. Humphries RM. Immunity to SARS-CoV-2: What Do We Know and Should We Be Testing for It? *J. Clin. Microbiol.* 2022(). URL: https://journals.asm.org/doi/full/10.1128/jcm.00482-21.

202. Tang J, Zeng C, Cox TM, et al. Respiratory mucosal immunity against SARS-CoV-2 after mRNA vaccination. *Sci. Immunol.* 2022; 7(76).

211. Khoury DS, Cromer D, Reynaldi A, et al. Neutralizing antibody levels are highly predictive of immune protection from symptomatic SARS-CoV-2 infection. *Nat. Med.* 2021; 27():1205–1211.

218. Ssentongo P, Ssentongo AE, Voleti N, et al. SARS-CoV-2 vaccine effectiveness against infection, symptomatic and severe COVID-19: a systematic review and meta-analysis. *BMC Infect. Dis.* 2022; 22(1):1–12.

219. Feikin DR, Higdon MM, Abu-Raddad LJ, et al. Duration of effectiveness of vaccines against SARS-CoV-2 infection and COVID-19 disease: results of a systematic review and meta-regression. *Lancet*. 2022; 399(10328):924–944.

220. Gazit S, Shlezinger R, Perez G, et al. Severe Acute Respiratory Syndrome Coronavirus 2 (SARS-CoV-2) Naturally Acquired Immunity versus Vaccine-induced Immunity, Reinfections versus Breakthrough Infections: A Retrospective Cohort Study. *Clin. Infect. Dis.* 2022; 75(1):e545–e551.

221. Shenai MB, Rahme R, Noorchashm H. Equivalency of Protection From Natural Immunity in COVID-19 Recovered Versus Fully Vaccinated Persons: A Systematic Review and Pooled Analysis. *Cureus*. 2021; 13(10).

222. Steenhuis M, Mierlo G van, Derksen NIL, et al. Dynamics of antibodies to SARS-CoV-2 in convalescent plasma donors. *Clin. Transl. Immunol.* 2021; 10(5):e1285.

223. Ripperger TJ, Uhrlaub JL, Watanabe M, et al. Orthogonal SARS-CoV-2 Serological Assays Enable Surveillance of Low-Prevalence Communities and Reveal Durable Humoral Immunity. *Immunity*. 2020; 53(5):925–933.e4.

224. Gallais F, Gantner P, Bruel T, et al. Evolution of antibody responses up to 13 months after SARS-CoV-2 infection and risk of reinfection. *eBioMedicine*. 2021; 71():103561.

225. Srivastava K, Carreño JM, Gleason C, et al. SARS-CoV-2-infection- and vaccine-induced antibody responses are long lasting with an initial waning phase followed by a stabilization phase. *Immunity*. 2024; 57(3):587–599.e4.

229. Menegale F, Manica M, Zardini A, et al. Evaluation of Waning of SARS-CoV-2 Vaccine–Induced Immunity: A Systematic Review and Meta-analysis. *JAMA Netw. Open*. 2023; 6(5):e2310650.

232. Bobrovitz N, Ware H, Ma X, et al. Protective effectiveness of previous SARS-CoV-2 infection and hybrid immunity against the omicron variant and severe disease: a systematic review and meta-regression. *Lancet Infect. Dis.* 2023; 23(5):556–567.

246. Lasrado N, Barouch DH. SARS-CoV-2 Hybrid Immunity: The Best of Both Worlds. *J. Infect. Dis.* 2023; 228(10):1311–1313.

251. Yamamoto S, Mizoue T, Ohmagari N. Analysis of Previous Infection, Vaccinations, and Anti–SARS-CoV-2 Antibody Titers and Protection Against Infection With the SARS-CoV-2 Omicron BA.5 Variant. *JAMA Netw. Open*. 2023; 6(3):e233370.

252. Tai CG, Haviland MJ, Kissler SM, et al. Low antibody levels associated with significantly increased rate of SARS-CoV-2 infection in a highly vaccinated population from the US National Basketball Association. *J. Med. Virol.* 2024; 96(3):e29505.

253. Kadowaki T, Sasaki A, Matsumoto N, et al. Antibody Titers and the Risk of Infection During the SARS-CoV-2 Omicron Phase in Bizen City, Japan. *J. Infect. Dis.* 2024():jiae207.

355. Clairon Q, Prague M, Planas D, et al. Modeling the kinetics of the neutralizing antibody response against SARS-CoV-2 variants after several administrations of Bnt162b2. *PLoS Comput. Biol.* 2023; 19(8):e1011282.

393. Bates D, Mächler M, Bolker B, Walker S. Fitting Linear Mixed-Effects Models Using lme4. *Journal of Statistical Software*. 2015; 67(1):1–48.

397. Crotty S. Hybrid immunity. *Science*. 2021; 372(6549):1392–1393.

398. Carazo S, Skowronski DM, Brisson M, et al. Protection against omicron (B.1.1.529) BA.2 reinfection conferred by primary omicron BA.1 or pre-omicron SARS-CoV-2 infection among health-care workers with and without mRNA vaccination: a test-negative case-control study. *Lancet Infect. Dis.* 2023; 23(1):45–55.

399. Gram MA, Emborg HD, Schelde AB, et al. Vaccine effectiveness against SARS-CoV-2 infection or COVID-19 hospitalization with the Alpha, Delta, or Omicron SARS-CoV-2 variant: A nationwide Danish cohort study. *PLoS Med.* 2022; 19(9):e1003992.

400. Wang L, Møhlenberg M, Wang P, Zhou H. Immune evasion of neutralizing antibodies by SARS-CoV-2 Omicron. *Cytokine Growth Factor Rev.* 2023; 70():13–25.

401. Xia S, Wang L, Zhu Y, Lu L, Jiang S. Origin, virological features, immune evasion and intervention of SARS-CoV-2 Omicron sublineages. *Sig. Transduct. Target. Ther.* 2022; 7(241):1–7.

402. Silva Antunes R da, Grifoni A, Frazier A, Weiskopf D, Sette A. An update on studies characterizing adaptive immune responses in SARS-CoV-2 infection and COVID-19 vaccination. *Int. Immunol.* 2023; 35(8):353–359.

403. Alexandre M, Marlin R, Prague M, et al. Modelling the response to vaccine in non-human primates to define SARS-CoV-2 mechanistic correlates of protection. *elife*. 2022; 11():e75427.

404. Woudenberg T, Pinaud L, Garcia L, et al. Estimated protection against COVID-19 based on predicted neutralisation titres from multiple antibody measurements in a longitudinal cohort, France, April 2020 to November 2021. *Eurosurveillance*. 2023; 28(25):2200681.

405. Perry J, Osman S, Wright J, et al. Does a humoral correlate of protection exist for SARS-CoV-2? A systematic review. *PLoS One*. 2022; 17(4):e0266852.

406. Cheetham NJ, Kibble M, Wong A, et al. Antibody levels following vaccination against SARS-CoV-2: associations with post-vaccination infection and risk factors in two UK longitudinal studies. *eLife*. 2023().

407. Martín Pérez C, Aguilar R, Jiménez A, et al. Correlates of protection and determinants of SARS-CoV-2 breakthrough infections 1 year after third dose vaccination. *BMC Med.* 2024; 22(1):1–16.

408. Terpos E, Stellas D, Rosati M, et al. SARS-CoV-2 antibody kinetics eight months from COVID-19 onset: Persistence of spike antibodies but loss of neutralizing antibodies in 24% of convalescent plasma donors. *European Journal of Internal Medicine*. 2021; 89():87–96.

409. Murphy TJ, Swail H, Jain J, et al. The evolution of SARS-CoV-2 seroprevalence in Canada: a time-series study, 2020–2023. *CMAJ*. 2023; 195(31):E1030–E1037.

410. Arora RK, Joseph A, Van Wyk J, et al. SeroTracker: a global SARS-CoV-2 seroprevalence dashboard. *Lancet Infect. Dis.* 2021; 21(4):e75–e76.

411. Canadian Blood Services. *COVID-19 Seroprevalence Report #41: December 2023 Survey*. Feb. 2024. URL: `https://www.covid19immunitytaskforce.ca/wp-content/uploads/2024/02/cbs-sero-report-full-december-2023.pdf`.

412. Sun K, Bhiman JN, Tempia S, et al. SARS-CoV-2 correlates of protection from infection against variants of concern. *Nat. Med.* 2024; 30():2805–2812.

413. Reinig S, Shih SR. Non-neutralizing functions in anti-SARS-CoV-2 IgG antibodies. *Biomedical Journal*. 2024; 47(1):100666.

414. Poon MML, Rybkina K, Kato Y, et al. SARS-CoV-2 infection generates tissue-localized immunological memory in humans. *Sci. Immunol.* 2021; 6(65).

415. Kaplonek P, Deng Y, Shih-Lu Lee J, et al. Hybrid immunity expands the functional humoral footprint of both mRNA and vector-based SARS-CoV-2 vaccines. *Cell Reports Medicine*. 2023; 4(5):101048.

416. Pelleau S, Woudenberg T, Rosado J, et al. Kinetics of the Severe Acute Respiratory Syndrome Coronavirus 2 Antibody Response and Serological Estimation of Time Since Infection. *J. Infect. Dis.* 2021; 224(9):1489–1499.

417. Tauzin A, Gendron-Lepage G, Nayrac M, et al. Evolution of Anti-RBD IgG Avidity following SARS-CoV-2 Infection. *Viruses*. 2022; 14(3):532.

418. Garcia L, Woudenberg T, Rosado J, et al. Kinetics of the SARS-CoV-2 Antibody Avidity Response Following Infection and Vaccination. *Viruses*. 2022; 14(7):1491.

419. Shrotri M, Fragaszy E, Nguyen V, et al. Spike-antibody responses to COVID-19 vaccination by demographic and clinical factors in a prospective community cohort study. *Nat. Commun.* 2022; 13(5780):1–10.

420. Mrak D, Kartnig F, Sieghart D, et al. Accelerated waning of immune responses to a third COVID-19 vaccination in patients with immune-mediated inflammatory diseases. *J. Autoimmun.* 2023; 135():102981.

421. Levin EG, Lustig Y, Cohen C, et al. Waning Immune Humoral Response to BNT162b2 Covid-19 Vaccine over 6 Months. *N. Engl. J. Med.* 2021().

422. Xiang T, Liang B, Fang Y, et al. Declining Levels of Neutralizing Antibodies Against SARS-CoV-2 in Convalescent COVID-19 Patients One Year Post Symptom Onset. *Front. Immunol.* 2021; 12():708523.

423. Jones JM, Stone M, Sulaeman H, et al. Estimated US Infection- and Vaccine-Induced SARS-CoV-2 Seroprevalence Based on Blood Donations, July 2020-May 2021. *JAMA*. 2021; 326(14):1400–1409. eprint: 34473201.

424. Public Health Agency Of Canada. *COVID-19 epidemiology update: Testing and variants — Canada.ca*. Apr. 2024. URL: https://health-infobase.canada.ca/covid-19/testing-variants.html.

425. COVID-19 Canada Open Data Working Group. *Canadian COVID-19 Data Archive*. June 2024. URL: https://github.com/ccodwg/Covid19CanadaArchive.

426. Swail H, Murphy T, Buckeridge D. *SARS-CoV-2 Seroprevalence in Canada*. 2023. URL: https://doi.org/10.5683/SP3/LAEQ5L.

427. Alexandre M, Prague M, Mclean C, et al. Prediction of long-term humoral response induced by the two-dose heterologous Ad26.ZEBOV, MVA-BN-Filo vaccine against Ebola. *npj Vaccines*. 2023; 8(1).

428. Pasin C, Balelli I, Van Effelterre T, et al. Dynamics of the Humoral Immune Response to a Prime-Boost Ebola Vaccine: Quantification and Sources of Variation. *Journal of Virology*. 2019; 93(18).

429. Morell A, Terry WD, Waldmann TA. Metabolic properties of IgG subclasses in man. *Journal of Clinical Investigation*. 1970; 49(4):673–680.

430. Saxena A, Wu D. Advances in Therapeutic Fc Engineering – Modulation of IgG-Associated Effector Functions and Serum Half-life. *Frontiers in Immunology*. 2016; 7(). URL: https://dx.doi.org/10.3389/fimmu.2016.00580.

431. Cole SR, Chu H, Greenland S. Maximum Likelihood, Profile Likelihood, and Penalized Likelihood: A Primer. *Am. J. Epidemiol.* 2014; 179(2):252–260.

432. R Core Team. *R: A Language and Environment for Statistical Computing*. R Foundation for Statistical Computing. Vienna, Austria, 2024. URL: https://www.R-project.org/.

433. Soetaert K, Petzoldt T, Setzer RW. Solving Differential Equations in R: Package deSolve. *J. Stat. Soft.* 2010; 33():1–25.

434. Therneau TM. *A Package for Survival Analysis in R*. 2024. URL: https://CRAN.R-project.org/package=survival.

6.4 Manuscript 3: Supplementary Methods

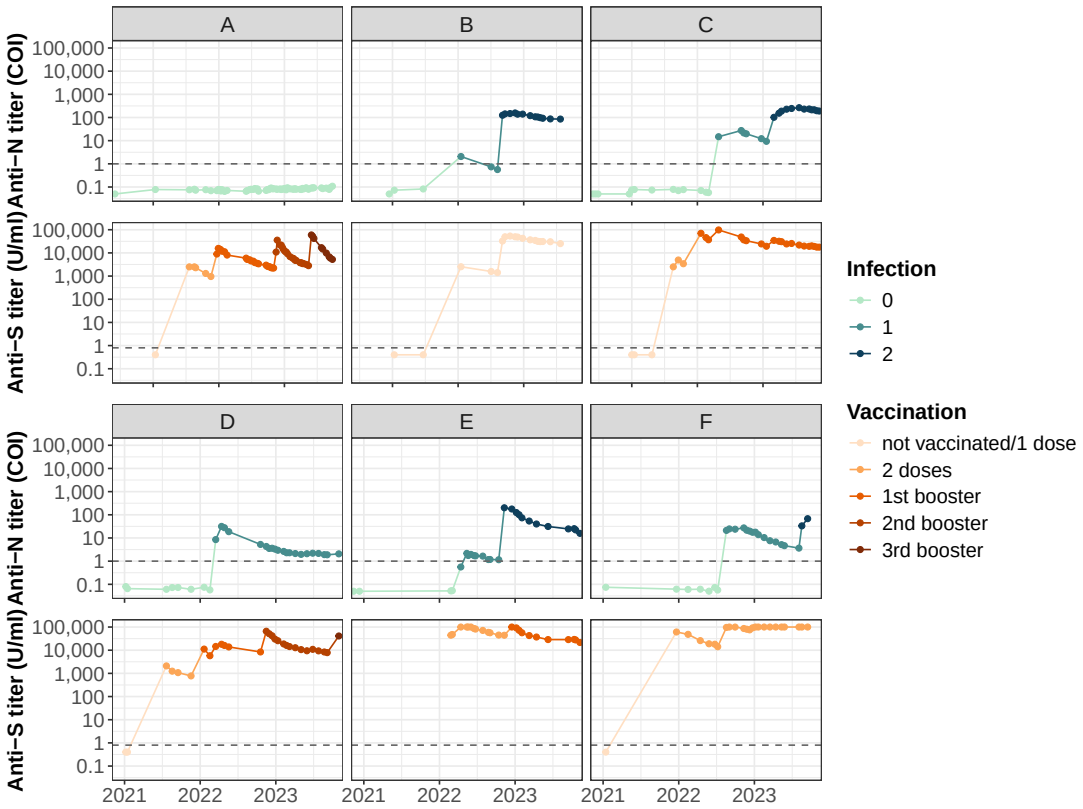

Figure S6.1: Exemplary antibody profiles of six repeat blood donors (A-F), illustrating how we inferred infection and vaccination dates. Antibody assay cutoff values are shown as dashed lines.
A: This donor has not been infected over the course of the study period, as can be seen from the anti-N levels below the threshold of detection. In contrast, we could detect four vaccinations through four increases in exclusively anti-S antibodies. It can also be seen that the anti-S antibodies decrease quickly after an immunizing event.
B: In contrast, this donor has had two detected infections. As anti-S antibody levels increased exclusively simultaneously with anti-N antibodies, we derived that this donor has never received a vaccine dose.
C: In donor C, we were able to detect two vaccinations (by anti-S increases without anti-N increases only), followed by two infections (simultaneous increases of anti-N and anti-S antibodies).
D: Similarly, donor D first got vaccinated at least twice before they became infected. After infection, we could detect two more anti-S increases, corresponding to two more doses of vaccine.
E: Donor E presented already high anti-S antibodies at the first anti-S measurements. Thus, we assigned them a vaccination status of completed primary series. However, they could have received more vaccine doses before they entered the study cohort.
F: Similarly, donor F entered the study with already high anti-S levels. After an infection the anti-S levels increased to the upper limit of quantification of the anti-S assay, thus we were not able to detect any additional vaccine doses this donor might have received.
N nucleocapsid, S spike

6.5 Manuscript 3: Supplementary Results

Cohort selection

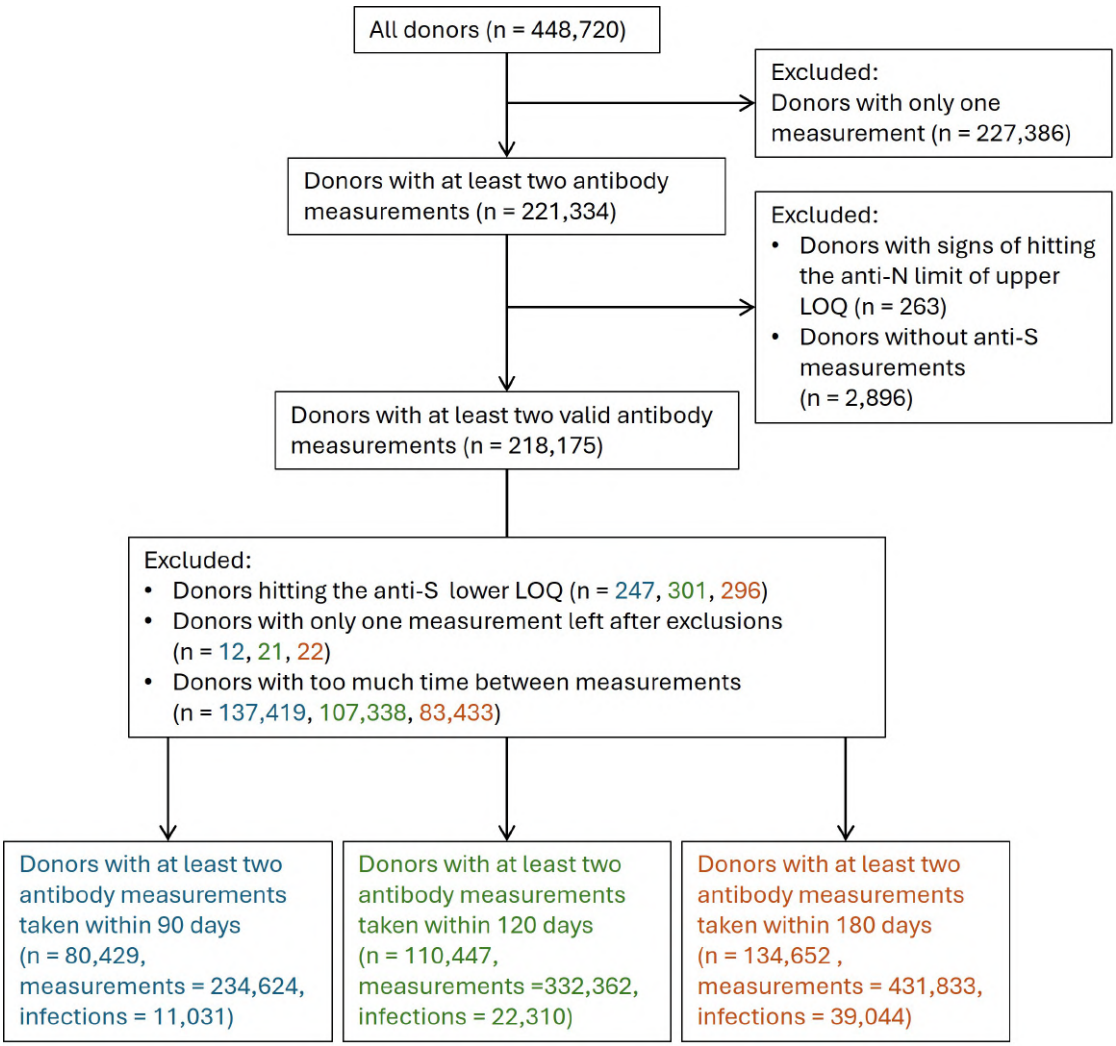

Figure S6.2: Flowchart of participant selection for the risk of infection analysis.

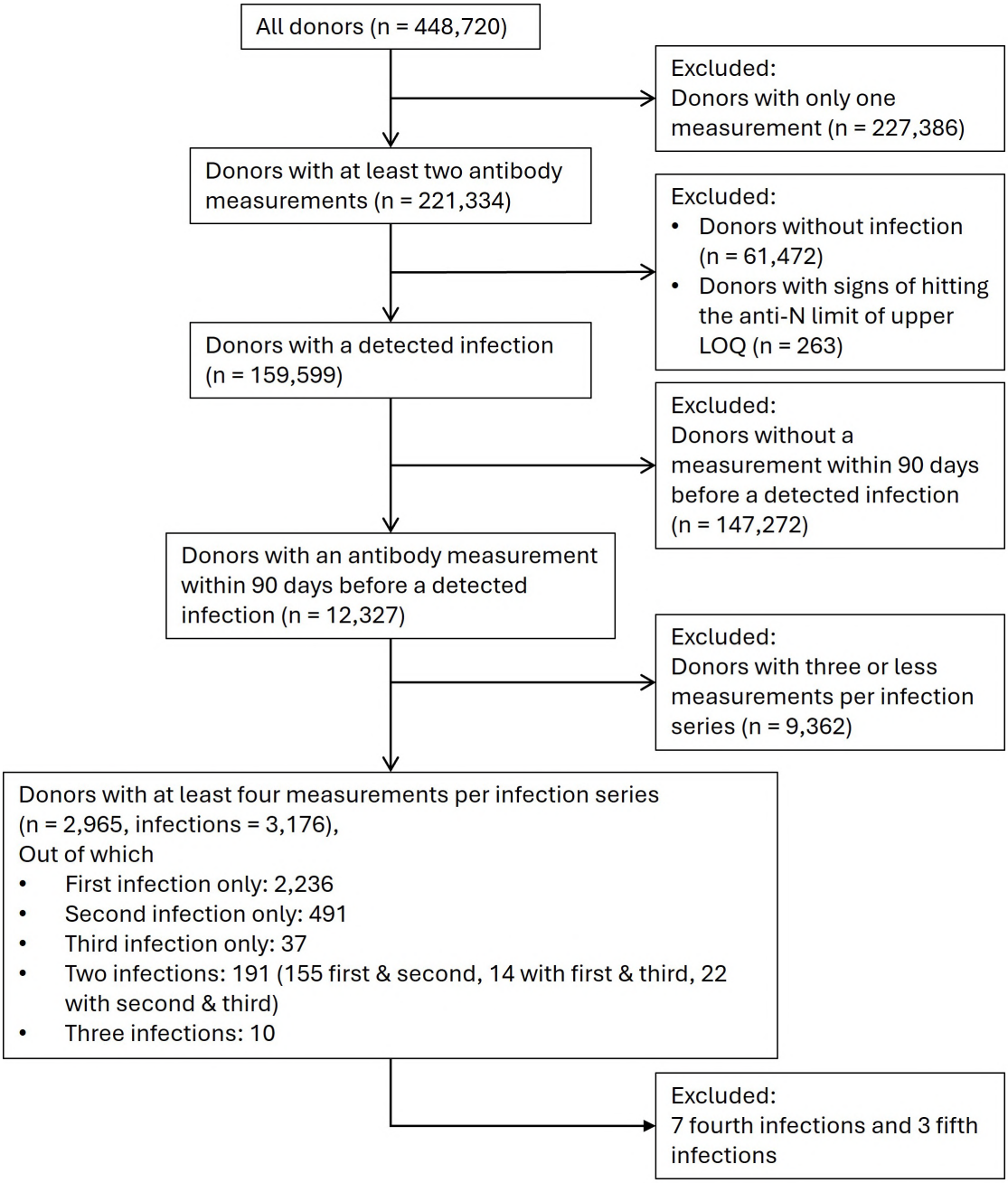

Figure S6.3: Flowchart of participant selection for the anti-N waning analysis.

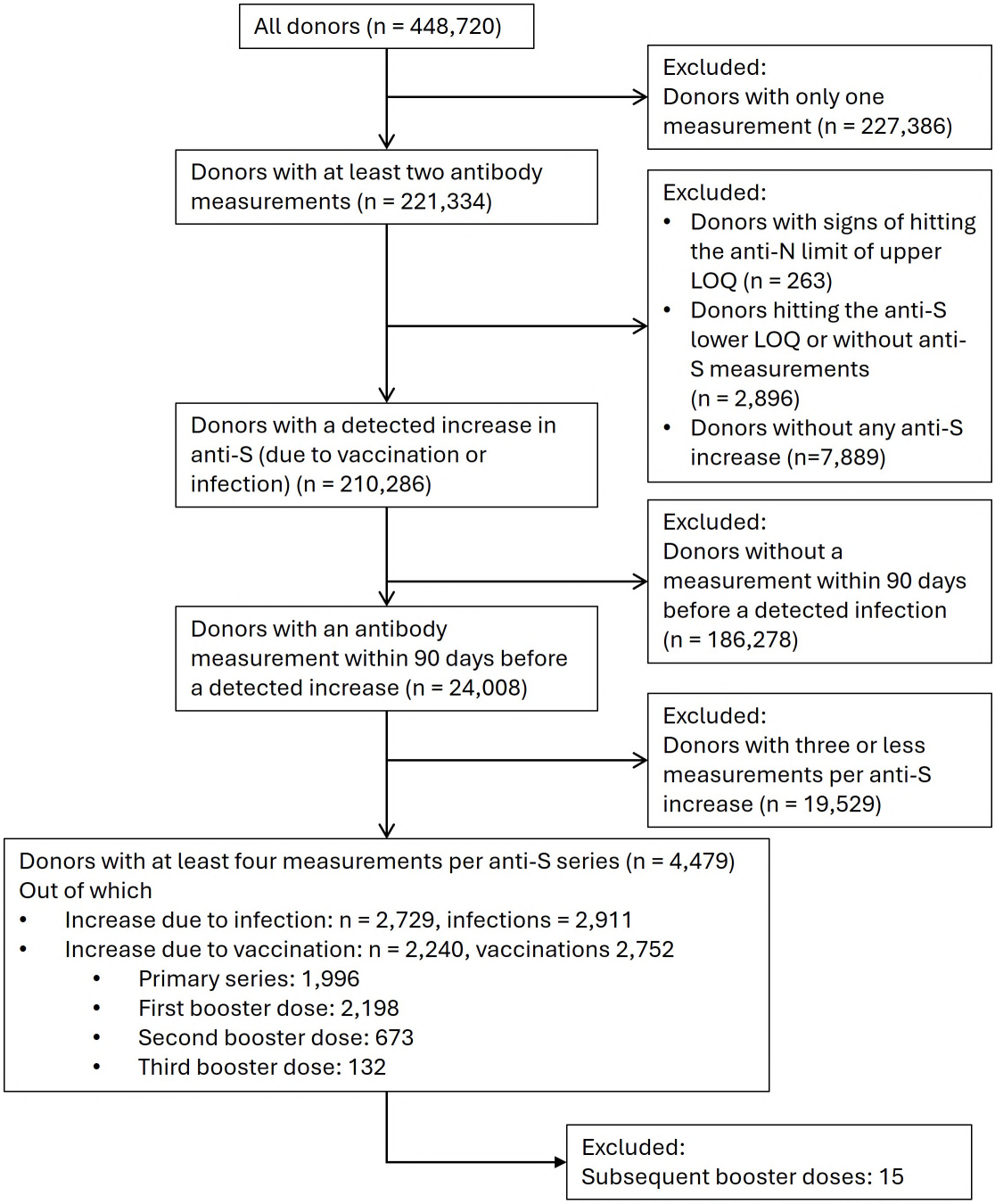

Figure S6.4: Flowchart of participant selection for the anti-S waning analysis.

Additional descriptives for all Cox model cohorts

	90 day interval	100 day interval	120 day interval	150 day interval	180 day interval
Number of participants	80,429	96,052	110,447	122,791	134,652
Number of observations	234,624	278,735	332,362	381,173	431,833
Median number of observations per participant (IQR)	3 (2, 7)	3 (2, 7)	3 (2, 7)	4 (2, 7)	4 (2, 7)
Total number of infections	11,031	15,017	22,310	29,835	39,044
Total number of vaccinations	147,045	173,162	200,474	223,622	246,347
Median number of vaccinations per participant (IQR)	2 (2, 2)	2 (2, 2)	2 (2, 2)	2 (2, 2)	2 (2, 2)
Male participants (%)	70.3	64.4	62.8	62.0	60.6
Mean age (SD)	51.65 (15.42)	51.49 (15.42)	51.26 (15.45)	51.02 (15.47)	50.9 (15.49)
Participants of white ethnicity (%)	82.1	82.4	82.1	81.8	81.6
Participants of Asian ethnicity (%)	7.6	7.4	7.5	7.7	7.7
Participants of Aboriginal ethnicity (%)	1.2	1.2	1.2	1.2	1.2
Participants of other ethnicity (%)	5.7	5.6	5.8	5.9	6
Participants with missing ethnicity (%)	3.3	3.4	3.3	3.4	3.4

Table S6.1: Demographic characteristics of the risk of infection cohorts, all filtering intervals. As filtering intervals get less stringent with increasing time between measurements, the proportion of male participants decreases. This trend is likely due to two factors: male donors are permitted to donate blood more frequently (every 56 days, compared to 84 days for female donors), and the majority of plasma donors, who can donate every week, are male.
IQR: Interquartile range, SD: standard deviation

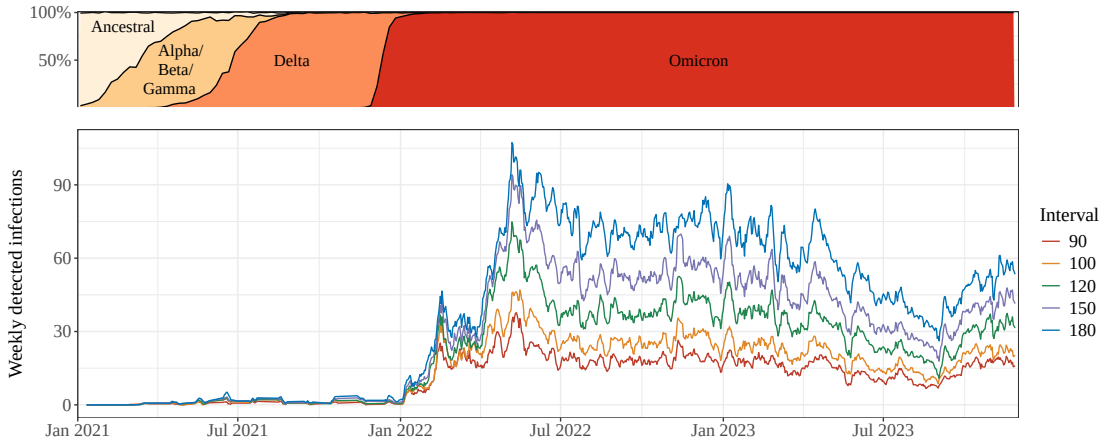

Figure S6.5: Weekly number of infections detected with different filtering intervals.

Results from additional Cox models

Sensitivity analysis of filtering intervals

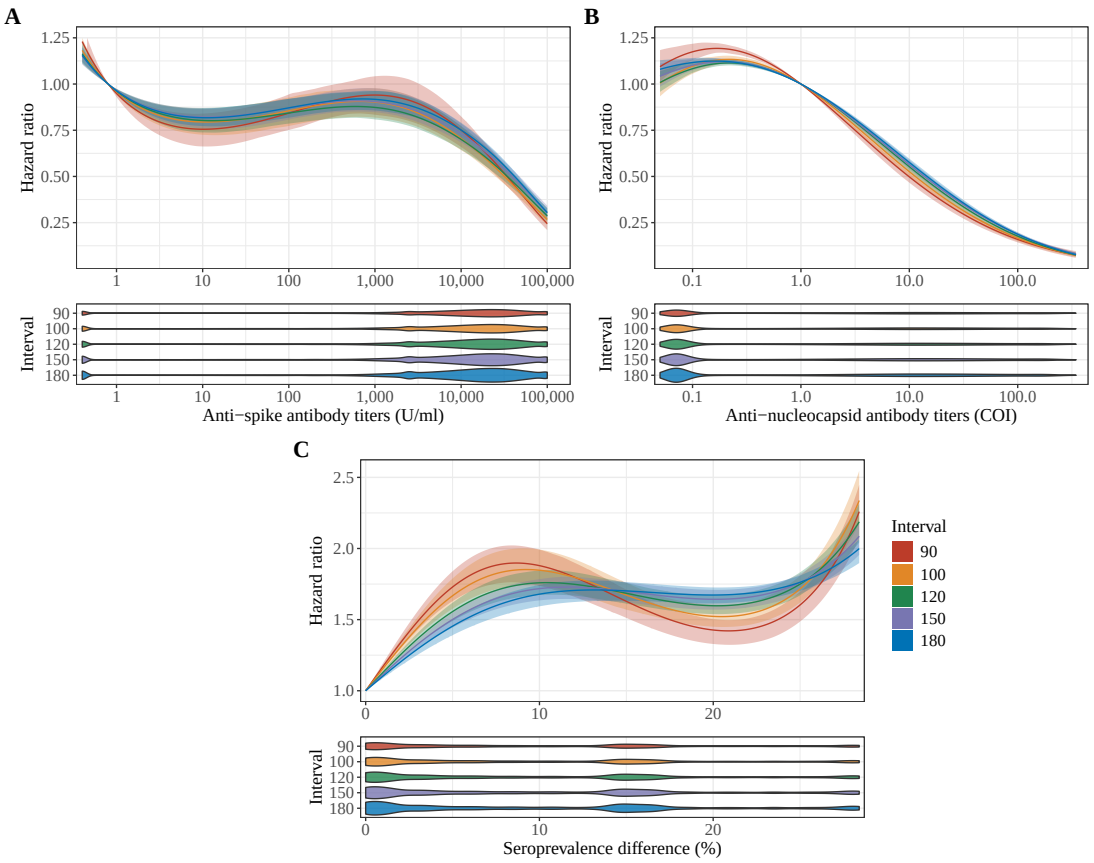

Figure S6.6: Adjusted hazard ratios for the association of spline-modeled variables with the hazard of infection. Hazard ratios with corresponding 95% CIs are shown over the range of assessed variables, and all assessed intervals are depicted. The violin plots below indicate the distribution of the respective variables, with violin area proportional to the amount of data in the respective datasets. **A:** Adjusted hazard ratios for the association of anti-S antibody levels with hazard of infection. Hazard ratios were referenced to the assay's positivity cutoff point of 0.8 U/ml. **B:** Adjusted hazard ratios for the association of anti-N antibody levels with hazard of infection. Hazard ratios were referenced to the assay's positivity cutoff point of 1 COI. **C:** Adjusted hazard ratios for the association of weekly seroprevalence difference (a marker of overall infectiousness in the population) with hazard of infection. The seroprevalence difference variable, can range in theory from 0 (=no difference in seroprevalence to previous week) to 100% (the whole population was infected within the last week). The seroprevalence difference hazard ratios were referenced to 0.

Sensitivity analysis on choice of time scale

Parameter	90 day interval		120 day interval		180 day interval	
	Calendar day	Cohort entry	Calendar day	Cohort entry	Calendar day	Cohort entry
sex (male)	1.05 (1.01-1.10)	0.99 (0.95-1.03)	0.97 (0.94-1)	0.93 (0.9-0.95)	0.98 (0.96-1.00)	0.98 (0.96-1.00)
age (10 years)	0.88 (0.87-0.9)	0.88 (0.87-0.89)	0.88 (0.87-0.89)	0.88 (0.87-0.88)	0.88 (0.88-0.89)	0.88 (0.87-0.89)
race (white)	0.99 (0.94-1.04)	0.99 (0.94-1.04)	0.99 (0.95-1.03)	0.99 (0.95-1.02)	0.98 (0.95-1.00)	0.97 (0.95-1.00)
Alpha	-	2.08 (1.03-4.21)	-	1.63 (1.02-2.63)	-	1.08 (0.77-1.50)
Delta	-	12.69 (6.65-24.22)	-	14.21 (9.36-21.59)	-	14.14 (10.71-18.67)
Omicron	-	62.02 (32.85-117.07)	-	54 (35.78-81.52)	-	37.3 (28.33-49.09)

Table S6.2: Comparison of hazard ratios when model was fitted using different time scales (Calendar day vs. cohort entry).

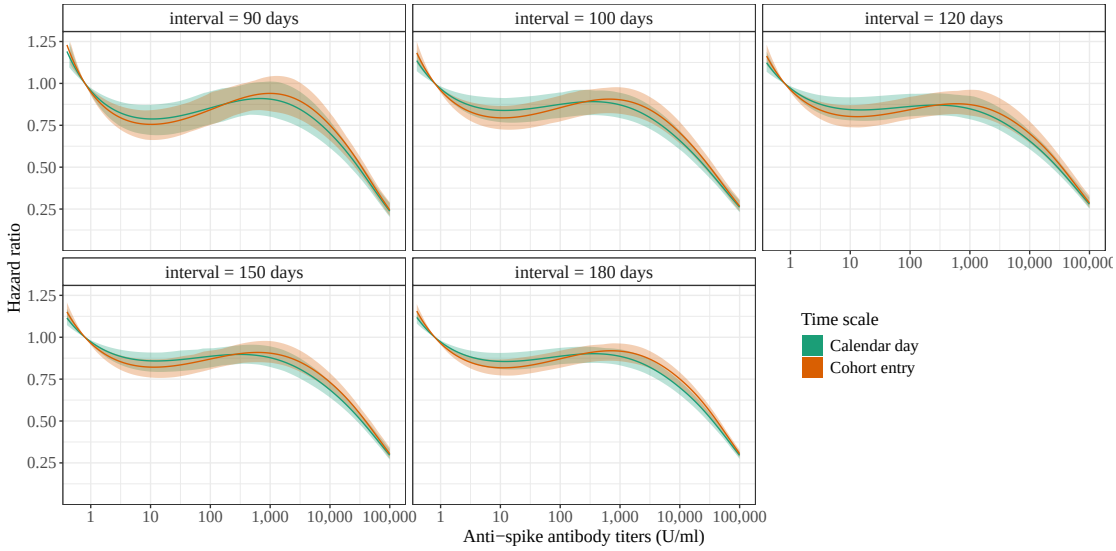

Figure S6.7: Comparison of anti-S splines when models were fitted using different time scales (Calendar day vs. cohort entry).

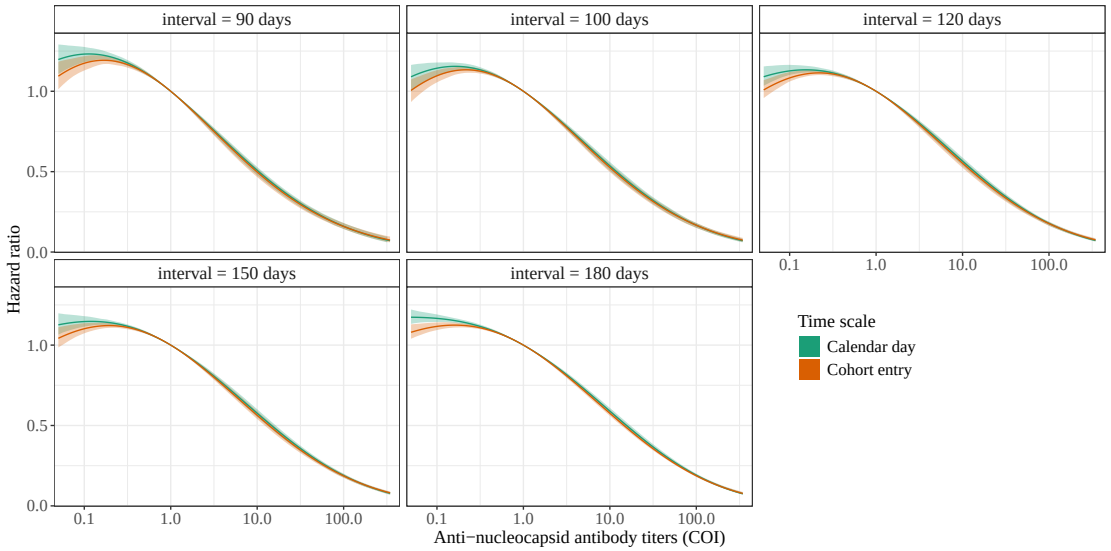

Figure S6.8: Comparison of anti-N splines when models were fitted using different time scales (Calendar day vs. cohort entry).

Sensitivity analysis on imputation of infection date

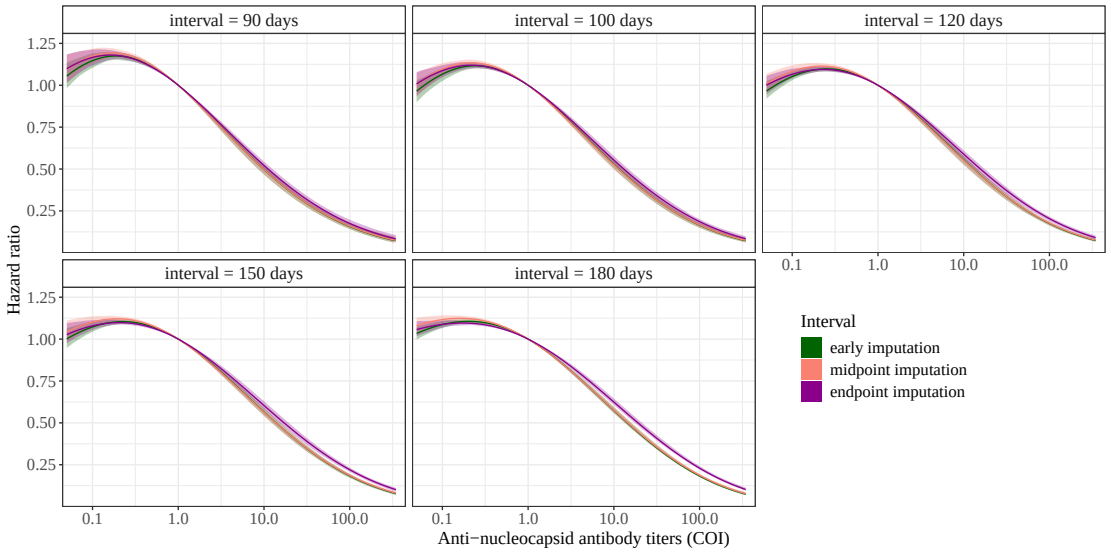

Figure S6.9: Comparison of anti-N splines across all time intervals and event imputation methods (directly after interval starts, interval mid point or interval end point).

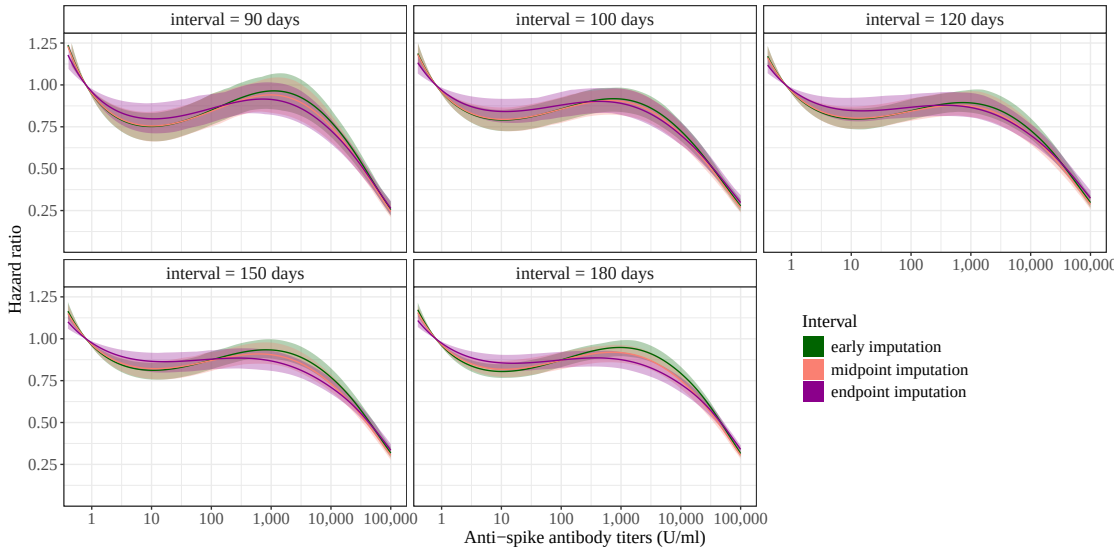

Figure S6.10: Comparison of anti-S splines across all time intervals and event imputation methods (directly after interval starts, interval mid point or interval end point).

Antibody waning models

Anti-N antibody waning results

We determined the values for the decay rate of long-lived antibody-secreting cells (ASCs) by profile likelihood, separately for first and subsequent infections, as we hypothesized the value might differ according to infection number. Because the maximum follow-up duration was only slightly over three years, the likelihood was flat toward lower δ_L values, indicating a half-life of long-lived ASCs of over three years. Therefore, we fixed δ_L to the value where the likelihood plateaued, which was 0.000543 for the first infection and 0.000345 for subsequent infections. These correspond to half-lives of 3.5 and 5.5 years, respectively. For the other parameters, we estimated population-level values with our mechanistic model and afterwards applied linear mixed models to assess parameter differences between infections. The population estimate for the decay rate of short-lived ASCs (δ_S) was 0.008 (95% CI: 0.007-0.009), corresponding to a half-life of 84 days (95% CI: c days, see Table S6.3). The ϕ-parameters are more complex to interpret because they are the product of the initial concentration of the respective cells and their production rate. We observed a higher value of ϕ_S than ϕ_L, indicating higher production or higher starting values of short-lived than long-lived ASCs.
We found significant differences in estimates between infection numbers. Specifically, the waning parameters (δ_S and δ_L) were reduced in second and third infections compared to the first, indicating a higher ASC half-life. Likewise, the

production parameters (ϕ_S and ϕ_L) were increased, suggesting higher initial ASC concentration or higher ASC generation rates. Moreover, antibody titers at the beginning of the first infection were substantially lower than after subsequent infections (population values estimated as 12.9 (95% CI: 12.1-13.7) after first infection, 52.4 (95% CI: 48.5-58.3) after second infection and 77.5 (95% CI: 44.9-84.5) after third infection). The uncertainty increases with increasing number of infections as less data was available for second and third infections than for first infections. Note that we report these values without units, as the anti-N assay used, despite being highly internally consistent, is not numerically comparable across laboratories. We tested the associations between demographic variables (sex, age, and race) with the model parameters in linear mixed effects models, but no significant associations were found.

Parameter	Population estimate (95% CI)	% difference 2nd to 1st infection (95% CI)	% difference 3rd to 1st infection (95% CI)
δ_S	0.008 (0.007-0.009)	-17.5 (-32.0 - -7.0)	-22.8 (-38.5 - -9.0)
ϕ_S	0.91 (0.81-1.06)	78.8 (3.5 - 202.8)	62.1 (-9.5 - 263.1)
δ_L[a]	0.000543[b]	-36.5[c]	-36.5[c]
ϕ_L	0.05 (0.04-0.07)	95.3 (60 - 154.7)	144.7 (48.8 - 250.6)

Table S6.3: Anti-N waning parameters estimated with the mechanistic model. δ_{Ab} is not mentioned in the parameter table, as it was fixed to 0.033. Mechanistic model parameters were estimated on a log10-scale.
[a] No CIs for estimates determined by profile likelihood
[b] Estimate for the first infection only
[c] Estimated by profile likelihood

Anti-S antibody waning results

Anti-S waning dynamics were modelled both for anti-S increases after vaccination and infection. The decay rate δ_S was found to be comparable in magnitude to that of anti-N antibodies, but ϕ_S and ϕ_L were estimated much higher (Table S6.4). This is expected given that anti-S levels are significantly greater than anti-N levels by several orders of magnitude. There was considerable uncertainty in the dynamics of ϕ_L, as reflected by the wide confidence intervals. For long-lived cells, we identified an inflection point in the profile likelihood curves at 0.00076, corresponding to a half-life of 2.5 years. This value was determined as a consensus across all vaccination/infection episodes.

Parameter	Population estimate (95% CI)	% difference between infection and vaccination (95% CI)
δ_S	0.007 (0.005-0.008)	-25.3 (-26 - -17)
ϕ_S	449.8 (418.9 - 498.7)	108.6 (101.5 - 139.6)
δ_L[a]	0.00076[b]	-
ϕ_L	106.8 (61.4 - 127.1)	86.6 (46.9 - 87.5)

Table S6.4: Anti-S waning parameters estimated with the mechanistic model. δ_{Ab} is not mentioned in the parameter table, as it was fixed to 0.033.
[a] No CIs for estimates determined by profile likelihood
[b] Estimated across all anti-S increases

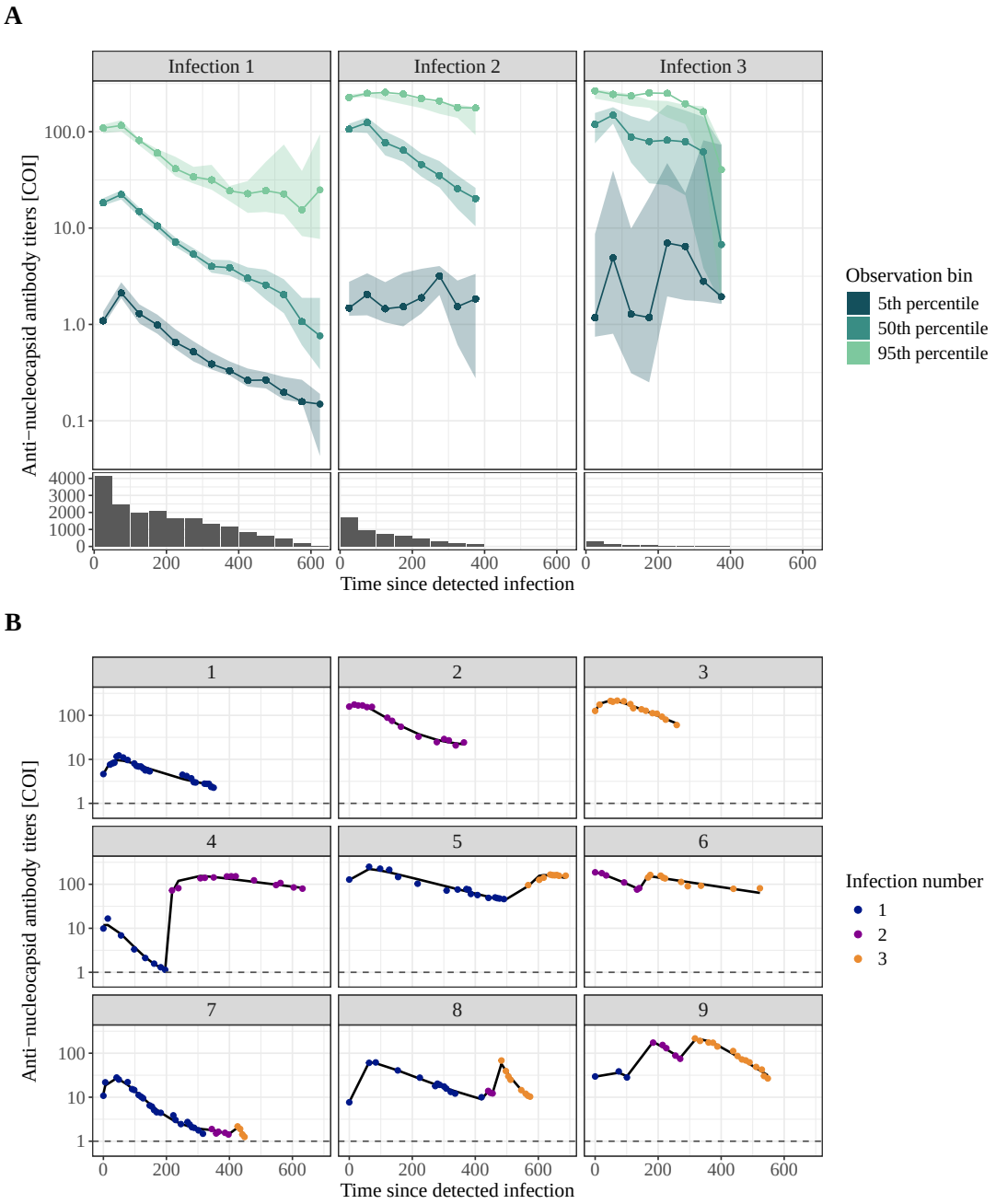

Figure S6.11: Fits of anti-N waning model.
A: Visual predictive check of the anti-N waning dynamics, separated by infection number. The dots and lines depict the 5th, 50th, and 90th percentile of individual observed data, binned into 50-day intervals. The shaded areas are calculated as the 95% prediction interval from the bootstraps for the same percentiles, by taking the individual predictions per bootstrap run, extracting the 5th, 50th, and 95th percentile, respectively, and then calculating the 2.5th and 97.5th percentile of these values as prediction intervals. The bar plots below indicate the number of observations that were used for every bin. Since the observations per bin become scarce in the later time points of infections 2 and 3, the observations curves can sometimes unexpectedly increase.
B: Individual fits for nine randomly selected donors with only one infection (panels 1-3), two infections (panels 4-6) and all three infections (panels 7-9). The dots indicate observed data and the black lines the fits.

7

Discussion

7.1 Summary of the results

My thesis focused on applying mathematical models to data collected during the COVID-19 pandemic to improve our understanding of how viral spread can be controlled. We developed sophisticated models to exploit data that were not originally intended for the purposes of my research. These included publicly available epidemiological data provided by Santé Publique France, primarily collected for surveillance and public information, and a large antibody dataset from Canadian Blood Services, gathered for serosurveillance. Both data sources came with unique advantages and limitations. The modeling approaches we used spanned various techniques, such as linear mixed effects models, Cox proportional hazards models, and mechanistic models, each of which required addressing different challenges. The mechanistic models were applied on two different scales: between-host transmission dynamics (Manuscripts 1 and 2) and within-host immunity waning (Manuscript 3). While my research began after the initial stages of the pandemic, it provides a retrospective analysis of pandemic events, contributes to ongoing debates, and informs future policies. When I started my research, many topics addressed in my thesis were the focus of considerable research and public discourse: the effectiveness of vaccines in reducing hospitalizations and deaths, the validity of lockdowns and other strong NPIs, and the duration of immunity from vaccination and infection.

In Manuscript 1, we developed a mechanistic model to estimate the effectiveness of NPIs and vaccines in France from the start of the pandemic until the emergence of Omicron. One strength of the model was that it estimated all parameters in a single step. Our findings showed that all major NPIs enforced by the French government were effective in curbing SARS-CoV-2 spread, with the first lockdown reducing transmission the most. Simulations demonstrated that enforcing lockdowns one or two weeks earlier could have saved 20,000 or 33,000 lives, respectively. In counterfactual vaccine scenarios, we showed that vaccines in France alone prevented over 158,000 deaths during the study period. If vaccines had been available just 100 days after the SARS-CoV-2 genome was sequenced, more than 70,000 additional lives could have been saved.

In Manuscript 2, we comparatively evaluated the optimal way to conduct NPI effectiveness studies in terms of methodology. We simulated data using various models, from simple SIR models to agent-based models with complex contact networks. We then assessed the performance of two widely-used approaches for estimating NPI effectiveness: a two-step $\mathcal{R}_t$ regression model and the mechanistic model from Manuscript 1. Our analysis revealed that the confidence intervals for NPI parameters estimated by the two-step regression procedure were consistently too narrow, as these methods fail to account for uncertainty of the first step. We mitigated this bias by implementing a bootstrap procedure, where the estimated $\mathcal{R}_t$ distribution from the first step was used in the second step. Additionally, we showed that depletion of susceptibles and challenges in the R_t estimation step could strongly bias NPI estimates and that the regression approach should only be applied in low-transmission scenarios to avoid misattributing herd immunity effects to NPIs. Mechanistic models, on the other hand, produced more reliable NPI estimates and accurate confidence intervals, even under minor model misspecification and random measurement errors applied to observations.

Manuscript 3 focused on SARS-CoV-2 antibody data from a large cohort of Canadian blood donors. We inferred infection and vaccination dates from antibody trajectories and used these data to examine the impact of antibodies on reinfection risk. The analysis revealed that both anti-nucleocapsid and anti-spike antibodies provided protection against reinfection. This finding may not be due to antibody activity itself—since only anti-spike antibodies exhibit neutralizing capacity—but rather due to the correlation between anti-nucleocapsid antibodies and other immune responses triggered by natural infection. We also modeled antibody waning dynamics in a longitudinal sub-cohort using a biphasic mechanistic model, finding that antibodies exhibited longer durability than expected, with a steep initial decline followed by a slow waning phase. While few donors seroreverted over several years, many fell below the threshold for sufficient protection, confirming that immunity providing high levels of protection wanes relatively quickly.

7.2 Strengths and limitations

The three chapters of my thesis altogether bring up more general questions and raise several common issues that I will discuss in what follows.

7.2.1 Data challenges

Throughout my thesis, we used data that were not collected explicitly for the purpose of my research. Re-using data in two different contexts came with unique challenges, but the data also provided some strengths. By exploiting biological knowledge and using mechanistic approaches, we could circumvent some of the limitations.

Many challenges pertaining to NPI effectiveness studies have already been discussed in Section 2.4.2. NPI studies conducted early during the COVID-19 pandemic often faced issues related to data availability and quality. Surveillance data, like COVID-19 cases, hospitalizations, and mortality, are the most direct indicators of an epidemic, but greatly depend on the reporting systems in place, with limitations such as under-reporting, reporting errors and lags, and missing geographical information. This is especially true in low- and middle-income countries (LMIC), where the quality of data collection might be inconsistent within a country or not exist at all [435, 436]. In Manuscript 1, we retrospectively analyzed data provided by Santé Publique France, with exceptionally high quality and geographical resolution. Still, to account for remaining reporting errors, we did not rely on one type of observation, but used four types of observations (cases adjusted for under-reporting, hospital admissions, hospital occupancy, and deaths) and modeled measurement errors on the reported data. In Manuscript 2, we only simulated observations with a random measurement error, and we did not explore the influence on other data problems. In Manuscript 3, we analyzed blood donor data provided by Canadian blood services, which contained highly accurate and reliable SARS-CoV-2 antibody measurements, but no information on vaccination or infection dates. Moreover, since the cohort was based on blood donors only, the findings might not be generalizable.

Beyond the surveillance data used for calibration, mechanistic models must be parameterized with biological information of disease transmission. While this parameterization increases the biological and causal relevance of the models, the models can be highly sensitive to some assumptions and input parameters, many of which are uncertain [257]. In Manuscript 1, results are sensitive to parameters like the assumed proportion of asymptomatics and the duration of incubation and infectious periods. Moreover, the uncertainty in fixed parameters is usually not accounted for in the modeling process and thus not reflected in the confidence

intervals of estimated NPI parameters. However, we conducted sensitivity analyses to assess the influence of some fixed parameters. Furthermore, the study presented in Manuscript 1 benefited from data collected over almost two years of the COVID-19 pandemic, so the input parameters were more reliable than at the start of the pandemic. One example of how we could improve parameters thanks to a better knowledge of the disease is my Manuscript 3, in which we estimated the duration of immunity derived from infection. This estimate-or a distribution of this estimate-can then be used to better inform models that include waning immunity.

Another issue relates to the lag of epidemiological surveillance reports relative to the actual transmission process, due to incubation periods and the period from infection or symptom onset to testing or care-seeking. Understanding these lags is crucial for assessing the effectiveness of interventions, as one needs to account for the time passed from NPI implementation until the effects are visible in surveillance data. In Manuscript 1, the mechanistic model accounted for the incubation period and the time from symptom onset to hospitalization. Moreover, observational data reported by Santé Publique France were corrected for reporting delays. In Manuscript 2, we did not explore in depth the issue of data delays, neither by simulating them explicitly, nor when assessing NPI effectiveness with the two-step regression model. Instead, we lagged NPIs in regression models to account for the incubation period, similar to many other studies [1, 135, 151, 155]. In an exploratory analysis, we found that by using the-in reality unobserved-new infections to estimate $\mathcal{R}_t$, we alleviated some of the bias in parameter estimates, but did not remove it completely.
Several software packages are available to decompose the delay distributions resulting from incubation period, time from symptom onset to testing, and time from symptom onset to hospitalization [394, 395]. This decomposition allows for estimation of the actual infection process, and therefore more accurate estimations of $\mathcal{R}_t$. Beyond improved $\mathcal{R}_t$ estimates, the deconvolution of time lags would also have increased the uncertainty in $\mathcal{R}_t$ estimates, which is not taken into account in the second step, unless a bootstrap approach is used.

Another data issue pertains to the quality of NPI data. For Manuscript 1, we manually coded NPIs by gathering information from administrative websites, a highly labor-intensive process, which is hardly feasible on an international scale. Many studies thus relied on data gathered by NPI trackers, which come with their own challenges (as discussed in Section 2.4.2). We used the Oxford COVID-19 Government Response Tracker (OxGCRT) [126] as a guide for coding NPIs, but we adapted the categories to our needs. A comparison between our NPIs and the

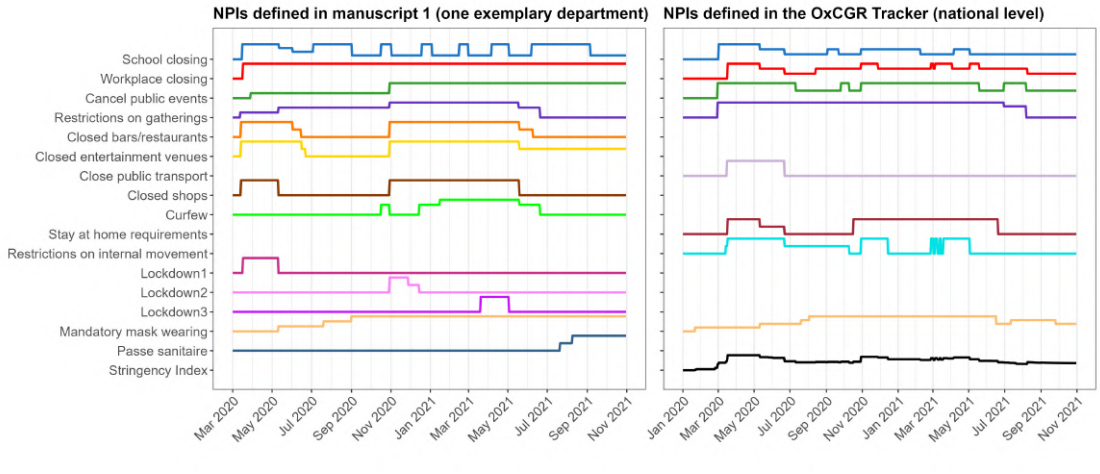

Figure 7.1: Comparison between all NPIs coded in the NPI dataset for Manuscript 1 and the NPIs coded in the OxCGRT dataset. The OxCGRT dataset provided NPI data for France only at the national level, whereas we gathered data for 94 administrative units (departments), capturing variations across departments. For illustration, we present NPI data for a single department (91, Essonne). Some NPIs are coded with multiple levels, reflecting variations in the strictness of implementation. For example, curfews in France were enforced at different times of the day (ranging from 6-9pm). Additionally, the OxCGRT includes a "stringency index", which is supposed to summarize the overall strictness of NPIs in one measure.

OxGCRT is shown in Figure 7.1. The largest difference between the two datasets is that we gathered data on 94 departments, whereas the OxCGRT only made NPI data available for France on the national level. Discrepancies in the Figure 7.1 might stem from these different levels of NPI enforcement. Additionally, despite orienting ourselves to the OxCGRT NPI categories, we formed our own categories of NPIs to include in our analysis. For example, the OxCGRT category "Stay at home requirements" was divided into three lockdowns in our dataset. Due to identifiability issues, we could not include all of the gathered NPIs into our analysis model. For example, we were not able to include "closed bars and restaurants" or "closed shops"; however, one could argue that these measures are parts of a lockdown.

Similar to Manuscript 1, we had access to data about a very large population in Manuscript 3, although the data was lacking detail at the individual level. The greatest advantage of the blood donor dataset is its extremely large sample size and thus high statistical power: Overall, it contained over 1 million antibody measurements collected from over 400,000 donors. Since its primary envisaged use was surveillance of SARS-CoV-2 immunity in the Canadian population, it also has limitations regarding the re-purposing for our study. Some of these have not been

discussed in depth in the manuscript and will be presented here: First, the dataset contains exclusively individuals healthy enough to donate blood and is predominantly composed of men. Moreover, as the filtering criteria become more stringent to increase the number of data points per participant, both the proportion of men and their average age increase. Thus, the analysis conducted in Manuscript 3 can complement other analyses which obtained their data from healthcare workers, who are mainly younger and female. In post-hoc analyses, we found no differences in waning according to demographic variables (age, sex, race), but this may be due to limited variation in the cohort. The data collected by Canadian Blood Services did not contain information on comorbidities (e.g. obesity, hypertension, immune system impairment) or health-related behaviors (e.g. tobacco and alcohol consumption). Furthermore, dates of infections and vaccinations were not included in the data, which also means we lacked information on the severity or symptoms of infection and the vaccine types. This type of information could easily be collected via questionnaires, and there is potential for these questions to be included during blood or plasma donation appointments in the future. Second, due to the lack of information on vaccinations and infections, we developed an algorithm to detect these immunizing events based on antibody data only. An important limitation to emphasize is that infections and vaccinations risk being missed if antibody levels do not increase enough after an immunizing event. This could happen in immunocompromised individuals—who are probably not blood donors anyways—or if the upper LOQ of antibody assays is reached. Indeed, in some cases, we observed increases in anti-nucleocapsid antibodies indicating an infection, while anti-spike antibodies remained unchanged, mainly in individuals with anti-spike antibodies close to or at the upper LOQ. Another reason for this phenomenon could also be an asymptomatic infection, which has been shown to result in lower antibody increases [437].

7.2.2 Modeling challenges

Modeling inherently requires a series of decisions, such as selecting the type of model, determining how to parameterize it, choosing the appropriate level of complexity, deciding which covariates to include and in what functional form, considering whether to incorporate random effects, and identifying which variables to fix. Some of these choices are dictated by the research question, the availability of data, or the data structure. Others require more arbitrary judgments by the modeler.

Age is one of the most important characteristics in the modeling of infectious diseases in populations [259]. In Manuscript 1, we were limited by the nonavailability of daily age-stratified hospitalization data on the lowest geographical level in France (department). Thus, a choice needed to be made to either 1) fit an

age-stratified model but with aggregated weekly data from 12 larger regions instead of daily data from 94 small administrative units or 2) use daily data with high geographical resolution but do not fit an age-stratified model. In the end, we opted for the latter. Thus, we do not to estimate age-specific effectiveness of NPIs or vaccines, nor do our simulations take into account the age-dependent effects of vaccines or stratify by age when calculating the counterfactual number of deaths and hospitalizations. For instance, we do not model age-specific risks of hospitalization or differential contact rates between age strata [438].
Incorporation of age stratification would make our model more realistic, as the disease dynamics in reality are not homogeneous and contacts are not random. Age stratification is particularly relevant for estimating effects of age-targeted vaccination programs, which only affect certain segments of the population or have larger benefits for certain groups. During the COVID-19 pandemic in France, high risk-groups like healthcare workers, the elderly, and the immunocompromised were prioritized for vaccination due to their high risk of exposure (healthcare workers) or high risk of severe disease (elderly and immunocompromised). However, younger people had a more important role in transmission [439, 440]. By ignoring age structure, our model might have underestimated vaccine effectiveness against transmission, but potentially overestimated vaccine effectiveness against hospitalization, as the most susceptible individuals were vaccinated first. Nevertheless, our effectiveness estimates against hospitalization were within the range of other estimates [179]. Moreover, incorporating age structure requires additional model parameters that need to be estimated or assumed, which adds complexity [441]. Age-structured models also require accurate and up-to-date contact matrices, which can be challenging to obtain, especially during a pandemic where contact patterns can change in unpredictable ways.

Another modeling choice we made in Manuscript 1 was to account for regional variation across 94 administrative units with a mixed effects model. However, our model did not take into account population flows between individual administrative units, treating each as a closed population. This might have affected the results, for example during school holiday periods, where population movements are more frequent [442]. These movements have the possibility to increase viral transmission in some places while decreasing it in others, or carrying the virus to places where the epidemic had already died out, for example during the summer of 2020, where viral transmission was very low or nonexistent in some places. Overall, this might have led to a misspecification of the random effects of the model, where we assume a normal distribution of parameters across departments. However, the fixed effects of NPI effectiveness should be robust to this misspecification. Other studies have incorporated the population movement by using metapopulation net-

work models, which are parameterized according to the movement of individuals between geographical units [443, 444].

Another choice we faced in Manuscript 1 was how to incorporate vaccinations into our mechanistic model. The data provided by Santé Publique France provided information on the number of vaccinated individuals in each geographical region, but lacked details on what proportion of these individuals had been previously infected. Adding explicit "vaccinated" compartments to the model would thus have required assumptions about the distribution of vaccinated individuals across compartments and about vaccine failure at the individual level [445]. For instance, if vaccine effectiveness is assumed to be 70%, do vaccines protect 70% of individuals completely or do they provide equal protection to all individuals, but only 70% of the time? To avoid introducing these assumptions, we opted to represent vaccines as the population vaccine effect, a parameter that modulates transmission and the risk of hospitalization. This effect was parameterized as the product of population vaccine coverage (available in Santé Publique France data) and vaccine effectiveness (estimated). While this approach removed the need to assume additional fixed parameters, it did not account for different modes of vaccine failure, which could have introduced bias into the results. Lee et al. find that infection levels are generally lower with all-or-nothing vaccines compared to leaky vaccines [445]. This discrepancy increases with intermediate vaccine efficacy, high $\mathcal{R}_0$ and a higher proportion of vaccinated individuals. This is because if the epidemic is not controlled early and continues to spread, vaccinated individuals will be repeatedly exposed and thus face a higher probability of infection when the vaccine is leaky. When simulating a scenario similar to the one in France during the Delta wave, Lee et al. find that the choice of vaccine failure mode has only a small (but significant) effect on final estimates [445].

In Manuscript 2, we evaluated the choice of methodology for NPI effectiveness studies more generally. Our criteria for model choice were focused on the accuracy of models to estimate parameters with little bias and high confidence interval coverage. However, one criterion that we did not take into account is the ease of implementation of the approaches used in modeling, neither did we evaluate approaches in terms of speed of parameter estimation and model development. There is a trade-off between timeliness and accuracy when assessing NPI effectiveness, especially at the start of an epidemic, when quicker but simpler models may be necessary for decision-making. Mechanistic models, while more accurate, are computationally intensive, requiring specialist software, high-performing computing infrastructure, and expert knowledge. For instance, the model built in Manuscript 1 and re-used as the comparison model in Manuscript 2 required several months of

model development and many hours of run time on a high-performance computing cluster. Another fact that is rarely considered is the growing impact of computing on resource use and carbon footprint, which should be included as a criterion of model selection in the future [446].

In Manuscript 3, one modeling choice we took was to use a model that does not focus on the increase in antibody-secreting cells (ASCs) after an infection or vaccination. The models by Pasin et al. [428] and Alexandre et al. [427], on which our model was based, assumed that ASCs reached equilibrium seven days after an immunizing event, and started modeling antibodies at this point. This also means that the initial values of ASC compartments (S_0 and L_0) are set to their respective values of day 7 post-immunization. After that, the number of ASCs only decreases, but they are nonetheless assumed to continue producing antibodies at rates θ_S and θ_L, which allows for initial increases in antibodies.
We cannot be certain that the 7-day assumption was met or that seven days really correspond to the time to reach equilibrium of ASCs triggered by a SARS-CoV-2 infection. However, the inclusion criteria into the analysis cohorts allow for 90 days to have passed between measurements, and eligibility criteria for blood donations do not allow donations during the symptomatic phase of a SARS-CoV-2 infection. Together, these two criteria ensure that for most donations, seven days have passed between the immunizing event and the antibody measurement.

Instead of modeling the establishment of an immune response after an immunizing event, we reset the ODE system for each detected infection or vaccination. However, this choice resulted in the estimation of model parameters that might have been more difficult to interpret (ϕ_S and ϕ_L), as they represent the product of two unidentifiable variables (θ parameters and initial values). More complex models have been proposed to account for the establishment, reactivation, and persistence of humoral immune responses following several vaccinations [355, 447]. The absence of antibodies does not imply absence of immunity, which could also be mediated by memory cells. Our model did not consider the presence of memory cells like other, more complex models did [447], but recent findings suggest that long-lived ASCs in bone marrow can secret antibodies continuously over long periods of time without replenishment from memory B cells [448].

Due to the lack of observations on ASCs, all parameters needed to be estimated from antibody data only. This forced us to fix one parameter (δ_{Ab}), replace others by combined parameters (θ_S and S_0 by ϕ_S, θ_L and L_0 by ϕ_L) and estimate one parameter by profile likelihood (δ_L). With the profile likelihood estimation, we could only determine a lower bound of the durability of long-lived ASCs, which

means that immunity is likely to last longer than estimated in the study. It also impeded us to estimate more complex models, such as those including memory compartments. Moreover, the uncertainties associated with the fixed parameter and the parameter determined by profile likelihood are not included in the confidence intervals of the waning simulations.

7.2.3 Causal interpretation of estimated parameters

Manuscript 1 estimated the effectiveness of NPIs in curbing viral spread, and used causal language to describe NPI effects. Mechanistic models have been proposed as an alternative to the potential outcomes framework when estimating causal effects of interventions [361, 385, 449]. In mechanistic models, causality is rooted in concepts of physical systems and expressed by mathematical equations, with time being explicitly incorporated into the model structure. A major advantage of mechanistic models is that they can directly integrate biological knowledge and thus allow the modeler to restrict the system to only biologically plausible mechanisms. Moreover, mechanistic models also offer the advantage of simulating trajectories. ABMs have also been suggested for exploration of causal mechanisms, as they allow for multiple interacting causes and thus can be used to test several competing theories about causal mechanisms [260]. Both mechanistic models and ABMs can account for phenomena that traditional regression models struggle with—such as the depletion of susceptibles in a population or the indirect protective effects of herd immunity, which regression models would erroneously attribute to implemented NPIs, as shown in Manuscript 2. Moreover, phenomena like herd immunity violate the i.i.d. (independent and identically distributed) assumption of regression models. In the comparative discussion of models for NPI effectiveness (Manuscript 2), this fact constitutes another advantage for mechanistic models.
However, it is important to note that in our mechanistic model, the effect of NPIs was included into the model structure as a regression term that acted directly on the transmission rate. While this assumes NPIs influence transmission, the exact causal pathways remain unexplored. The causal interpretations of NPI effectiveness rely on assumptions that may not hold. Specifically, as NPIs rely on population behavior, compliance with implemented NPIs plays a crucial role in determining NPI effectiveness. Moreover, studies across different populations or subgroups of populations can be confounded due to variations in compliance, but also in demographics, economic conditions, and previously implemented or co-implemented NPIs. Estimates could for example be biased by proactive population behavior [450] or spillover effects. Moreover, NPI effectiveness may change as the epidemic progresses, with virus evolution, public behavior shifts, and new protective measures influencing outcomes [175].
For example, in their study on NPI effectiveness, Bendavid et al. compared countries with "more restrictive NPIs"—like England, France, and Germany—to those

with "less restrictive NPIs" (South Korea and Sweden) [173]. However, they disregarded voluntary anti-contagion behaviors such as mask wearing and mobility reductions. For instance, Sweden saw voluntary changes in mobility, where the population avoided dense urban areas, traveled less distances in general, and opted for more individual modes of transportation [451–453]. In South Korea, mask wearing was common even before the pandemic, and compliance with implemented NPIs, such as quarantine, was extremely high [454–456]. Additionally, the analysis by Bendavid et al. overlooks the timing of NPI implementation. As Brauner et al. [134] and Banholzer et al. [135] (among others) observed, if stricter NPIs are implemented after less restrictive ones, their effectiveness is reduced. The study also fails to account for the lag between NPI implementation and its effects on case numbers, which is particularly important if highly restrictive NPIs are implemented in response to high viral transmission.

Manuscript 1 and 2 use government-enforced NPIs as modifying factors of the transmission rate or R_t, but do not account for how actual population behavior may differ from mandated behavior. Non-adherence to NPIs, especially as the pandemic progressed, could be a reason for the diminishing effectiveness of lockdowns over time found in Manuscript 1 and more generally in the literature [151, 340, 457–459]. Our analysis also lacks individual-level insights and only provides results on a population-wide scale. Understanding how individual behaviors and exposure patterns influence the transmission dynamics under NPIs is crucial. For example, mask mandates could encourage more public interaction, or school closures might lead parents to work from home more frequently [175]. Moreover, evaluating NPI effectiveness in a causal manner is challenging because public awareness of disease transmission, or even the mere discussion of potential NPIs, can influence people's contact behaviors [460]. Researching these behavioral mechanisms could shed light on why and when specific NPIs work and how they interact with each other. Individual-level studies on risk factors and behaviors can further inform policy decisions [461, 462], but these data might be challenging to obtain [435, 463]. Furthermore, keeping the balance between privacy and accurate individual information can be difficult.

In Manuscript 3, we used a Cox proportional hazards model to assess the protective effect of antibody levels on the risk of SARS-CoV-2 infection. For anti-spike antibodies, the findings could be interpreted in a causal way, i.e. higher levels of anti-spike antibodies provide protection from infection directly. This is possible because neutralizing anti-spike antibodies have been discussed as a mechanistic correlate of protection [211]. Anti-nucleocapsid antibodies, however, are not recognized as a mechanistic correlate of protection. It is more likely that they are

correlated with a range of immune mechanisms induced by natural infection, such as mucosal and cellular immunity. The highly protective effect of anti-nucleocapsid antibodies should thus be interpreted as an association, not as a direct causal effect—although it could of course be causal.

7.2.4 Missing embedding into the broader societal context

In Manuscript 1, we retrospectively confirmed the effectiveness of lockdowns, curfews, and school closures in France using a sophisticated mechanistic model. However, we did not address the broader societal impacts of NPIs beyond reducing transmission, although this is a critical issue. Stringent NPIs had profound impacts on various aspects of society, including disruptions in essential services, worsening mental health, and exacerbating social inequalities [464, 465]. These measures disproportionately affected more vulnerable groups like children, low-income families, ethnic minorities, and women [113]. NPIs have been linked to increased risks for several non-communicable diseases, as they for instance decreased levels of physical activity and increased obesity rates [466–468]. Moreover, during lockdowns, studies reported spikes in depression and anxiety [469–471]. Furthermore, essential health services were severely disrupted during the pandemic. Public fears, social distancing, reduced public transportation, and the restructuring of healthcare institutions to handle surges in COVID-19 cases all made it more difficult for individuals to obtain the services they needed [472]. A survey from the WHO noted that virtually all health services were affected, both for communicable and non-communicable diseases [473]. Another WHO report stated that mental health services were notably impacted, with over 40% of countries reporting full or partial closures of inpatient and 60–70% of countries reporting full or partial closures of home care and day care services [474].

Due to their implementation directly and the broader economic disruptions they caused [475, 476], NPIs also came with significant economic costs. Understanding which NPIs are most effective in different contexts is therefore crucial for avoiding overly severe and unnecessarily prolonged restrictions [477]. Optimization approaches using machine learning have been developed to simultaneously reduce overall mortality and minimize economic losses [478–481]. Our simulations in Manuscript 1 indicate that earlier implementation of lockdowns could have resulted in fewer deaths and hospitalizations, even with the same duration. Many studies report that early intervention interrupts viral transmission more effectively and allows societies to return to normal more quickly [115, 116]. However, early implementation of restrictive NPIs requires strong political leadership. Beyond lockdowns, strategies like high vaccination rates, efficient contact tracing and testing systems, and widespread mask usage can replace more restrictive NPIs. For instance, we estimated curfews to be nearly as effective as lockdowns. Some ex-

perts have suggested protecting only vulnerable populations rather than imposing universal lockdowns, advocating for interventions that balance social and economic needs while safeguarding high-risk individuals [119, 482].
In Manuscript 3, we observed that natural immunity appears to offer more robust protection than vaccine-induced immunity. However, this does not necessarily imply that countries should pursue a "herd immunity" strategy, as some politicians advocated by at the onset of the COVID-19 pandemic [483]. This approach overlooks the significant health risks associated with widespread infection, particularly for vulnerable populations, and the unpredictable consequences of emerging variants.

8

Conclusions and Future Work

8.1 Implications

The research conducted in this thesis during and after the COVID-19 pandemic has yielded several important findings: First, it contributed to the identification of effective NPIs and emphasized the importance of timely NPI implementation. For future pandemics or waves of COVID-19, I showed that lockdowns could be a good policy instrument to rapidly and drastically curb spread. However, their social and economic costs may limit their long-term feasibility. Alternative, less disruptive interventions, such as early curfews paired with bar and restaurant closures and hygiene protocols can achieve similar results. Overall, the sooner NPIs are implemented, the more successful they are at controlling viral spread.
Second, I showed that an early and rapid rollout of vaccines is essential in curbing both viral transmission and severe disease outcomes. Moreover, I demonstrated that high antibody titers provided effective protection against infection. These high antibody titers can be reached both through infection and vaccination, but quickly wane below thresholds needed to maintain high protection. Compared to vaccine-induced immunity, infection-induced immunity may offer more durable and effective protection than vaccine-induced immunity.
The third contribution of my thesis is to the methodology used in NPI effectiveness studies. I showed that careful consideration is needed when applying two-step regression models for estimating effectiveness of interventions, although they can

yield results a lot faster. Robust methods such as bootstrapping are required to accurately capture the uncertainty in two-step models.

8.2 Outlook

Looking ahead, although the COVID-19 pandemic has been officially declared over, SARS-CoV-2 continues to circulate and infect people globally. The virus has become endemic in most countries, but it has not yet settled into a predictable seasonal pattern like influenza. Ongoing challenges include the continued evolution of the virus, which may still become more pathogenic or immune-evasive, reducing the effectiveness of existing vaccines and natural immunity [484, 485]. Current vaccine development lags behind viral mutations, though efforts are underway to create a pan-coronavirus vaccine that can offer broader protection [486]. The timing and necessity of vaccine booster doses are also debated. As long follow-ups are rarely available, the long-term dynamics of immunity are still uncertain.
Another challenge lying ahead is the co-circulation of SARS-CoV-2 with other respiratory viruses, such as influenza and RSV, which could lead to severe health impacts in co-infected individuals [487]. Beyond the direct health effects, the pandemic has significantly reversed progress toward global goals like the Sustainable Development Goals and disproportionally affected vulnerable and disadvantaged populations. These groups have borne the brunt of the crisis and will likely continue to face its long-term consequences [488].

Thus, preparing for the threat of an (inevitable) next pandemic is critical, and addressing it will require applying the lessons learned from COVID-19. Many of these lessons involve the use of mathematical models, which played an essential role during the pandemic. Modeling has been shown to be a powerful tool for exploring alternative policy scenarios, estimating health and economic impacts, forecasting epidemiological trends, and assessing interventions both prospectively and retrospectively. Models enable policymakers to understand the burden of illness and the effects of mitigation measures, helping to inform health economic assessments of population-level interventions.
Despite the success of modeling during the COVID-19 pandemic, there are still many ways it can be improved to better inform public health decisions in the future [64, 435, 436, 460, 489]. One key area is data standards and sharing protocols. Establishing consistent data collection procedures at the start of an outbreak—which means that protocols need to be in place before the outbreak—can improve the reliability of observational data [435, 436]. Furthermore, databases should include meta-data on the epidemiological context at the time the interventions were implemented, such as changes in reporting practices [175]. Linking surveillance data with administrative health data could improve data analyses tremendously. For

instance, data linkage of the antibody data provided by Canadian Blood Services with provincial health records—as already done for residents of Ontario—enables analyses beyond those conducted in Manuscript 3. These analyses could provide insights into optimal vaccine combinations and timings, and enable validation of algorithms used to detect infections and vaccinations.

While mathematical modeling has provided significant public health benefits during the COVID-19 pandemic, there remain numerous opportunities to improve models. Future models could for example be more complex and realistic, incorporating factors such as individual behaviors [463], household and workplace dynamics, and spatial variability in transmission patterns. Moreover, results from within-host models could be integrated with between-host models, for example with a changing infectivity profile over the course of an infection or adjusted effects of vaccines according to viral variants [460]. Similarly, the immunity waning parameters estimated in Manuscript 3 could be integrated into the model from Manuscript 1, allowing for a more accurate representation of waning immunity and its impact on viral spread. Moreover, model averaging, which has proven useful for instance in forecasting pandemic trajectories [310, 311, 490], should be explored further to enhance the reliability of model predictions.

Another ongoing challenge is how best to communicate model results. Effective communication, particularly about the limitations of the models and uncertainties in their predictions, is essential for ensuring that decision-makers are fully informed. Modelers should distinguish in their communication between worst-case scenarios and more likely outcomes, helping policymakers make informed decisions under uncertainty [460, 489]. By addressing these challenges, modeling can better inform health interventions, enhance pandemic preparedness, and contribute to more effective management of future global health crises.

Bibliography

1. Paireau J, Charpignon ML, Larrieu S, et al. Impact of non-pharmaceutical interventions, weather, vaccination, and variants on COVID-19 transmission across departments in France. *BMC Infect. Dis.* 2023; 23(1):1–12.
2. Zhou P, Yang XL, Wang XG, et al. A pneumonia outbreak associated with a new coronavirus of probable bat origin. *Nature*. 2020; 579():270–273. URL: https://dx.doi.org/10.1038/s41586-020-2012-7.
3. Zhu N, Zhang D, Wang W, et al. A Novel Coronavirus from Patients with Pneumonia in China, 2019. *New England Journal of Medicine*. 2020; 382():727–733. URL: https://dx.doi.org/10.1056/nejmoa2001017.
4. Gorbalenya AE, Baker SC, Baric RS, et al. The species Severe acute respiratory syndrome-related coronavirus: classifying 2019-nCoV and naming it SARS-CoV-2. *Nature Microbiology*. 2020; 5():536–544. URL: https://dx.doi.org/10.1038/s41564-020-0695-z.
5. *WHO Director-General's opening remarks at the media briefing on COVID-19 - 11 March 2020*. [Online; accessed 27. Apr. 2024]. 2020. URL: https://www.who.int/director-general/speeches/detail/who-director-general-s-opening-remarks-at-the-media-briefing-on-covid-19---11-march-2020.
6. Pullano G, Di Domenico L, Sabbatini CE, et al. Underdetection of cases of COVID-19 in France threatens epidemic control. *Nature*. 2021; 590():134–139.
7. Biggs AT, Littlejohn LF. How Asymptomatic Transmission Influences Mitigation and Suppression Strategies during a Pandemic. *Risk Anal.* 2023; 43(4):649–659.
8. O'Driscoll M, Santos GRD, Wang L, et al. Age-specific mortality and immunity patterns of SARS-CoV-2. *Nature*. 2021; 590():140–145. URL: https://dx.doi.org/10.1038/s41586-020-2918-0.

9. Ssentongo P, Ssentongo AE, Heilbrunn ES, Ba DM, Chinchilli VM. Association of cardiovascular disease and 10 other pre-existing comorbidities with COVID-19 mortality: A systematic review and meta-analysis. *PloS one*. 2020; 15(). URL: https://pubmed.ncbi.nlm.nih.gov/32845926/.

10. Gao Y dong, Ding M, Dong X, et al. Risk factors for severe and critically ill COVID-19 patients: A review. *Allergy*. 2021; 76():428–455. URL: https://pubmed.ncbi.nlm.nih.gov/33185910/.

11. Demeulemeester F, Punder K de, Heijningen M van, Doesburg F van. Obesity as a Risk Factor for Severe COVID-19 and Complications: A Review. *Cells 2021, Vol. 10, Page 933*. 2021; 10():933. URL: https://www.mdpi.com/2073-4409/10/4/933/htm%20https://www.mdpi.com/2073-4409/10/4/933.

12. Yek C, Warner S, Wiltz JL, et al. Risk Factors for Severe COVID-19 Outcomes Among Persons Aged ≥18 Years Who Completed a Primary COVID-19 Vaccination Series — 465 Health Care Facilities, United States, December 2020–October 2021. *Morbidity and Mortality Weekly Report*. 2022; 71(1):19.

13. *WHO COVID-19 dashboard*. [Online; accessed 27. Apr. 2024]. 2024. URL: https://data.who.int/dashboards/covid19.

14. *COVID-19 Dashboard by the Center for Systems Science and Engineering (CSSE) at Johns Hopkins University (JHU)*. [Online; accessed 27. Apr. 2024]. 2020. URL: https://coronavirus.jhu.edu/map.html.

15. Msemburi W, Karlinsky A, Knutson V, Aleshin-Guendel S, Chatterji S, Wakefield J. The WHO estimates of excess mortality associated with the COVID-19 pandemic. *Nature 2022 613:7942*. 2022; 613():130–137. URL: https://www.nature.com/articles/s41586-022-05522-2.

16. Wang H, Paulson KR, Pease SA, et al. Estimating excess mortality due to the COVID-19 pandemic: a systematic analysis of COVID-19-related mortality, 2020–21. *The Lancet*. 2022; 399():1513–1536. URL: https://dx.doi.org/10.1016/s0140-6736(21)02796-3.

17. Schöley J, Karlinsky A, Kobak D, Tallack C. Conflicting COVID-19 excess mortality estimates. *The Lancet*. 2023; 401():431–432. URL: https://linkinghub.elsevier.com/retrieve/pii/S0140673623001162.

18. Donzelli A. Conflicting COVID-19 excess mortality estimates. *The Lancet*. 2023; 401():432. URL: https://linkinghub.elsevier.com/retrieve/pii/S0140673623001174.

19. Moeti M, Makubalo L, Gueye AS, et al. Conflicting COVID-19 excess mortality estimates. *The Lancet*. 2023; 401():431.

20. Bager P, Nielsen J, Bhatt S, Nielsen LB, Krause TG, Vestergaard LS. Conflicting COVID-19 excess mortality estimates. *The Lancet*. 2023; 401():432–433. URL: https://linkinghub.elsevier.com/retrieve/pii/S0140673623001150.

21. Teglia F, Angelini M, Astolfi L, Casolari G, Boffetta P. Global Association of COVID-19 Pandemic Measures With Cancer Screening. *JAMA Oncology*. 2022; 8(9):1287.

22. Hsieh E, Dey D, Grainger R, et al. Global Perspective on the Impact of the COVID-19 Pandemic on Rheumatology and Health Equity. *Arthritis Care Res.* 2024; 76(1):22–31.

23. Seyedalinaghi S, Mirzapour P, Pashaei Z, et al. The impacts of COVID-19 pandemic on service delivery and treatment outcomes in people living with HIV: a systematic review. *AIDS Research and Therapy*. 2023; 20(1).

24. Chang AY, Cullen MR, Harrington RA, Barry M. The impact of novel coronavirus COVID-19 on noncommunicable disease patients and health systems: a review. *Journal of Internal Medicine*. 2021; 289(4):450–462.

25. Moynihan R, Sanders S, Michaleff ZA, et al. Impact of COVID-19 pandemic on utilisation of healthcare services: a systematic review. *BMJ Open*. 2021; 11(3):e045343.

26. Shet A, Carr K, Danovaro-Holliday MC, et al. Impact of the SARS-CoV-2 pandemic on routine immunisation services: evidence of disruption and recovery from 170 countries and territories. *The Lancet Global Health*. 2022; 10(2):e186–e194.

27. Mcgowan VJ, Bambra C. COVID-19 mortality and deprivation: pandemic, syndemic, and endemic health inequalities. *The Lancet Public Health*. 2022; 7(11):e966–e975.

28. Xia Y, Ma H, Moloney G, et al. Geographic concentration of SARS-CoV-2 cases by social determinants of health in metropolitan areas in Canada: a cross-sectional study. *Canadian Medical Association Journal*. 2022; 194(6):E195–E204.

29. Khanijahani A, Iezadi S, Gholipour K, Azami-Aghdash S, Naghibi D. A systematic review of racial/ethnic and socioeconomic disparities in COVID-19. *Int. J. Equity Health*. 2021; 20(1):248. eprint: 34819081.

30. McIntyre PB, Aggarwal R, Jani I, et al. COVID-19 vaccine strategies must focus on severe disease and global equity. *Lancet*. 2022; 399(10322):406–410.

31. *WHO Director-General's opening remarks at the media briefing – 5 May 2023*. [Online; accessed 27. Apr. 2024]. 2023. URL: https://www.who.int/news-room/speeches/item/who-director-general-s-opening-remarks-at-the-media-briefing---5-may-2023.

32. Lu R, Zhao X, Li J, et al. Genomic characterisation and epidemiology of 2019 novel coronavirus: implications for virus origins and receptor binding. *Lancet*. 2020; 395(10224):565–574.

33. Origins of Novel Pathogens (SAGO) SAG for the. *Preliminary Report of the SAGO*. Report. World Health Organization, June 2022. URL: https://www.who.int/publications/m/item/scientific-advisory-group-on-the-origins-of-novel-pathogens-report.

34. Alwine James C, Casadevall A, Enquist Lynn W, Goodrum Felicia D, Imperiale Michael J. A Critical Analysis of the Evidence for the SARS-CoV-2 Origin Hypotheses. *Journal of Virology*. 2023; 97(4):e00365–23. URL: https://doi.org/10.1128/jvi.00365-23.

35. Holmes EC, Goldstein SA, Rasmussen AL, et al. The origins of SARS-CoV-2: A critical review. *Cell*. 2021; 184(19):4848–4856.

36. Crits-Christoph A, Levy JI, Pekar JE, et al. Genetic tracing of market wildlife and viruses at the epicenter of the COVID-19 pandemic. *Cell*. 2024; 187(19):5468–5482.e11.

37. Doremalen N van, Bushmaker T, Morris DH, et al. Aerosol and Surface Stability of SARS-CoV-2 as Compared with SARS-CoV-1. *New England Journal of Medicine*. 2020; 382():1564–1567. URL: https://www.nejm.org/doi/full/10.1056/nejmc2004973.

38. Moschovis PP, Yonker LM, Shah J, Singh D, Demokritou P, Kinane TB. Aerosol transmission of SARS-CoV-2 by children and adults during the COVID-19 pandemic. *Pediatric Pulmonology*. 2021; 56():1389–1394. URL: https://onlinelibrary.wiley.com/doi/full/10.1002/ppul.25330%20https://onlinelibrary.wiley.com/doi/abs/10.1002/ppul.25330%20https://onlinelibrary.wiley.com/doi/10.1002/ppul.25330.

39. Zhou L, Ayeh SK, Chidambaram V, Karakousis PC. Modes of transmission of SARS-CoV-2 and evidence for preventive behavioral interventions. *BMC Infectious Diseases*. 2021; 21():1–9. URL: https://bmcinfectdis.biomedcentral.com/articles/10.1186/s12879-021-06222-4.

40. Billah MA, Miah MM, Khan MN. Reproductive number of coronavirus: A systematic review and meta-analysis based on global level evidence. *PLOS ONE*. 2020; 15():e0242128. URL: https://journals.plos.org/plosone/article?id=10.1371/journal.pone.0242128.

41. Endo A, Abbott S, Kucharski AJ, Funk S. Estimating the overdispersion in COVID-19 transmission using outbreak sizes outside China. *Wellcome Open Research*. 2020; 5():1–18. URL: /pmc/articles/PMC7338915/%20/pmc/articles/PMC7338915/?report=abstract%20https://www.ncbi.nlm.nih.gov/pmc/articles/PMC7338915/.

42. Harrison AG, Lin T, Wang P. Mechanisms of SARS-CoV-2 Transmission and Pathogenesis. *Trends Immunol.* 2020; 41(12):1100–1115.

43. Beyerstedt S, Casaro EB, Rangel ÉB. COVID-19: angiotensin-converting enzyme 2 (ACE2) expression and tissue susceptibility to SARS-CoV-2 infection. *Eur. J. Clin. Microbiol. Infect. Dis.* 2021; 40(5):905–919.

44. Jackson CB, Farzan M, Chen B, Choe H. Mechanisms of SARS-CoV-2 entry into cells. *Nat. Rev. Mol. Cell Biol.* 2022; 23():3–20.

45. V'kovski P, Kratzel A, Steiner S, Stalder H, Thiel V. Coronavirus biology and replication: implications for SARS-CoV-2. *Nat. Rev. Microbiol.* 2021; 19():155–170.

46. Lauer SA, Grantz KH, Bi Q, et al. The Incubation Period of Coronavirus Disease 2019 (COVID-19) From Publicly Reported Confirmed Cases: Estimation and Application. *Ann. Intern. Med.* 2020().

47. He J, Guo Y, Mao R, Zhang J. Proportion of asymptomatic coronavirus disease 2019: A systematic review and meta-analysis. *Journal of Medical Virology*. 2021; 93():820–830. URL: https://onlinelibrary.wiley.com/doi/abs/10.1002/jmv.26326.

48. Ma Q, Liu J, Liu Q. Global Percentage of Asymptomatic SARS-CoV-2 Infections Among the Tested Population and Individuals With Confirmed COVID-19 Diagnosis: A Systematic Review and Meta-analysis. *JAMA Netw. Open*. 2021; 4(12):e2137257.

49. Johansson MA, Quandelacy TM, Kada S, et al. SARS-CoV-2 Transmission From People Without COVID-19 Symptoms. *JAMA Network Open*. 2021; 4(1):e2035057.

50. Jeong YD, Ejima K, Kim KS, et al. Revisiting the guidelines for ending isolation for COVID-19 patients. *eLife*. 2021().

51. Hernandez-Vargas EA, Velasco-Hernandez JX. In-host Mathematical Modelling of COVID-19 in Humans. *Annual Reviews in Control*. 2020; 50():448–456. URL: https://www.sciencedirect.com/science/article/pii/S1367578820300638.

52. Walsh KA, Jordan K, Clyne B, et al. SARS-CoV-2 detection, viral load and infectivity over the course of an infection. *J. Infect.* 2020; 81(3):357–371.

53. Kissler SM, Fauver JR, Mack C, et al. Viral dynamics of acute SARS-CoV-2 infection and applications to diagnostic and public health strategies. *PLoS Biol.* 2021; 19(7):e3001333.

54. Ke R, Zitzmann C, Ho DD, Ribeiro RM, Perelson AS. In vivo kinetics of SARS-CoV-2 infection and its relationship with a person's infectiousness. *Proc. Natl. Acad. Sci. U.S.A.* 2021; 118(49):e2111477118.

55. Marc A, Kerioui M, Blanquart F, et al. Quantifying the relationship between SARS-CoV-2 viral load and infectiousness. *eLife.* 2021().

56. Wölfel R, Corman VM, Guggemos W, et al. Virological assessment of hospitalized patients with COVID-2019. *Nature.* 2020; 581(7809):465–469.

57. Markov PV, Ghafari M, Beer M, et al. The evolution of SARS-CoV-2. *Nat. Rev. Microbiol.* 2023; 21():361–379.

58. Mistry P, Barmania F, Mellet J, et al. SARS-CoV-2 Variants, Vaccines, and Host Immunity. *Front. Immunol.* 2022; 12():809244.

59. O'Toole Á, Pybus OG, Abram ME, Kelly EJ, Rambaut A. Pango lineage designation and assignment using SARS-CoV-2 spike gene nucleotide sequences. *BMC Genomics.* 2022; 23(1):1–13.

60. Rambaut A, Holmes EC, O'Toole Á, et al. A dynamic nomenclature proposal for SARS-CoV-2 lineages to assist genomic epidemiology. *Nat. Microbiol.* 2020; 5():1403–1407.

61. Konings F, Perkins MD, Kuhn JH, et al. SARS-CoV-2 Variants of Interest and Concern naming scheme conducive for global discourse. *Nat. Microbiol.* 2021; 6():821–823.

62. World Health Organization. *Historical working definitions and primary actions for SARS-CoV-2 variants.* Tech. rep. [Online; accessed 1. Aug. 2024]. World Health Organization, Mar. 2023. URL: `https://www.who.int/publications/m/item/historical-working-definitions-and-primary-actions-for-sars-cov-2-variants`.

63. Harvey WT, Carabelli AM, Jackson B, et al. SARS-CoV-2 variants, spike mutations and immune escape. *Nat. Rev. Microbiol.* 2021; 19():409–424.

64. Funk T, Pharris A, Spiteri G, et al. Characteristics of SARS-CoV-2 variants of concern B.1.1.7, B.1.351 or P.1: data from seven EU/EEA countries, weeks 38/2020 to 10/2021. *Eurosurveillance.* 2021; 26(16):2100348.

65. Karim SSA, Oliveira T de. New SARS-CoV-2 Variants — Clinical, Public Health, and Vaccine Implications. *N. Engl. J. Med.* 2021().

66. Davies NG, Abbott S, Barnard RC, et al. Estimated transmissibility and impact of SARS-CoV-2 lineage B.1.1.7 in England. *Science.* 2021; 372(6538).

67. Korber B, Fischer WM, Gnanakaran S, et al. Tracking Changes in SARS-CoV-2 Spike: Evidence that D614G Increases Infectivity of the COVID-19 Virus. *Cell*. 2020; 182(4):812–827.e19.

68. Meng B, Kemp SA, Papa G, et al. Recurrent emergence of SARS-CoV-2 spike deletion H69/V70 and its role in the Alpha variant B.1.1.7. *Cell Rep.* 2021; 35(13):109292.

69. Garcia-Beltran WF, Lam EC, St. Denis K, et al. Multiple SARS-CoV-2 variants escape neutralization by vaccine-induced humoral immunity. *Cell*. 2021; 184(9):2372–2383.e9.

70. Cele S, Gazy I, Jackson L, et al. Escape of SARS-CoV-2 501Y.V2 from neutralization by convalescent plasma. *Nature*. 2021; 593():142–146.

71. Planas D, Veyer D, Baidaliuk A, et al. Reduced sensitivity of SARS-CoV-2 variant Delta to antibody neutralization. *Nature*. 2021; 596():276–280.

72. Eyre DW, Taylor D, Purver M, et al. Effect of Covid-19 Vaccination on Transmission of Alpha and Delta Variants. *N. Engl. J. Med.* 2022().

73. Campbell F, Archer B, Laurenson-Schafer H, et al. Increased transmissibility and global spread of SARS-CoV-2 variants of concern as at June 2021. *Eurosurveillance*. 2021; 26(24):2100509.

74. Tegally H, Wilkinson E, Giovanetti M, et al. Detection of a SARS-CoV-2 variant of concern in South Africa. *Nature*. 2021; 592():438–443.

75. Pulliam JRC, Schalkwyk C van, Govender N, et al. Increased risk of SARS-CoV-2 reinfection associated with emergence of Omicron in South Africa. *Science*. 2022; 376(6593).

76. Dejnirattisai W, Huo J, Zhou D, et al. SARS-CoV-2 Omicron-B.1.1.529 leads to widespread escape from neutralizing antibody responses. *Cell*. 2022; 185(3):467–484.e15.

77. Andrews N, Stowe J, Kirsebom F, et al. Covid-19 Vaccine Effectiveness against the Omicron (B.1.1.529) Variant. *N. Engl. J. Med.* 2022().

78. Cele S, Jackson L, Khoury DS, et al. Omicron extensively but incompletely escapes Pfizer BNT162b2 neutralization. *Nature*. 2022; 602():654–656.

79. Cao Y, Wang J, Jian F, et al. Omicron escapes the majority of existing SARS-CoV-2 neutralizing antibodies. *Nature*. 2022; 602():657–663.

80. Relan P, Motaze NV, Kothari K, et al. Severity and outcomes of Omicron variant of SARS-CoV-2 compared to Delta variant and severity of Omicron sublineages: a systematic review and metanalysis. *BMJ Global Health*. 2023; 8(7):e012328.

81. Arabi M, Al-Najjar Y, Mhaimeed N, et al. Severity of the Omicron SARS-CoV-2 variant compared with the previous lineages: A systematic review. *J. Cell. Mol. Med.* 2023; 27(11):1443–1464.

82. Mathieu E, Ritchie H, Rodés-Guirao L, et al. Coronavirus Pandemic (COVID-19). *Our World in Data*. 2020(). URL: `https://ourworldindata.org/coronavirus`.

83. Diamond MS, Kanneganti TD. Innate immunity: the first line of defense against SARS-CoV-2. *Nat. Immunol.* 2022; 23():165–176.

84. Blanco-Melo D, Nilsson-Payant BE, Liu WC, et al. Imbalanced Host Response to SARS-CoV-2 Drives Development of COVID-19. *Cell*. 2020; 181(5):1036–1045.e9.

85. Arunachalam PS, Wimmers F, Mok CKP, et al. Systems biological assessment of immunity to mild versus severe COVID-19 infection in humans. *Science*. 2020; 369(6508):1210–1220.

86. Steiner S, Kratzel A, Barut GT, et al. SARS-CoV-2 biology and host interactions. *Nat. Rev. Microbiol.* 2024; 22():206–225.

87. Zhang A, Stacey HD, D'Agostino MR, Tugg Y, Marzok A, Miller MS. Beyond neutralization: Fc-dependent antibody effector functions in SARS-CoV-2 infection. *Nat. Rev. Immunol.* 2023; 23():381–396.

88. Lu LL, Suscovich TJ, Fortune SM, Alter G. Beyond binding: antibody effector functions in infectious diseases. *Nat. Rev. Immunol.* 2018; 18():46–61.

89. Sette A, Crotty S. Adaptive immunity to SARS-CoV-2 and COVID-19. *Cell*. 2021; 184(4):861–880.

90. Post N, Eddy D, Huntley C, et al. Antibody response to SARS-CoV-2 infection in humans: A systematic review. *PLoS One*. 2020; 15(12):e0244126.

91. Lapuente D, Winkler TH, Tenbusch M. B-cell and antibody responses to SARS-CoV-2: infection, vaccination, and hybrid immunity. *Cell. Mol. Immunol.* 2024; 21():144–158.

92. Wu J, Liang B, Chen C, et al. SARS-CoV-2 infection induces sustained humoral immune responses in convalescent patients following symptomatic COVID-19. *Nat. Commun.* 2021; 12(1813):1–9.

94. Arkhipova-Jenkins I, Helfand M, Armstrong C, et al. Antibody Response After SARS-CoV-2 Infection and Implications for Immunity. *Ann. Intern. Med.* 2021().

95. Lumley SF, Wei J, O'Donnell D, et al. The Duration, Dynamics, and Determinants of Severe Acute Respiratory Syndrome Coronavirus 2 (SARS-CoV-2) Antibody Responses in Individual Healthcare Workers. *Clin. Infect. Dis.* 2021; 73(3):e699–e709.

96. Isho B, Abe KT, Zuo M, et al. Persistence of serum and saliva antibody responses to SARS-CoV-2 spike antigens in COVID-19 patients. *Sci. Immunol.* 2020; 5(52).

97. Knies A, Ladage D, Braun RJ, Kimpel J, Schneider M. Persistence of humoral response upon SARS-CoV-2 infection. *Rev. Med. Virol.* 2022; 32(2):e2272.

98. Hansen CB, Jarlhelt I, Pérez-Alós L, et al. SARS-CoV-2 Antibody Responses Are Correlated to Disease Severity in COVID-19 Convalescent Individuals. *J. Immunol.* 2021; 206(1):109–117.

99. Park JH, Cha MJ, Choi H, et al. Relationship between SARS-CoV-2 antibody titer and the severity of COVID-19. *J. Microbiol. Immunol. Infect.* 2022; 55(6, Part 1):1094–1100.

100. Trinité B, Tarrés-Freixas F, Rodon J, et al. SARS-CoV-2 infection elicits a rapid neutralizing antibody response that correlates with disease severity. *Sci. Rep.* 2021; 11(2608):1–10.

101. Pooley N, Abdool Karim SS, Combadière B, et al. Durability of Vaccine-Induced and Natural Immunity Against COVID-19: A Narrative Review. *Infect. Dis. Ther.* 2023; 12(2):367–387.

102. Dan JM, Mateus J, Kato Y, et al. Immunological memory to SARS-CoV-2 assessed for up to 8 months after infection. *Science.* 2021; 371(6529).

103. Cox RJ, Brokstad KA. Not just antibodies: B cells and T cells mediate immunity to COVID-19. *Nat. Rev. Immunol.* 2020; 20():581–582.

104. Havervall S, Marking U, Svensson J, et al. Anti-Spike Mucosal IgA Protection against SARS-CoV-2 Omicron Infection. *N. Engl. J. Med.* 2022().

105. Tan AT, Linster M, Tan CW, et al. Early induction of functional SARS-CoV-2-specific T cells associates with rapid viral clearance and mild disease in COVID-19 patients. *Cell Rep.* 2021; 34(6).

106. Moderbacher CR, Ramirez SI, Dan JM, et al. Antigen-Specific Adaptive Immunity to SARS-CoV-2 in Acute COVID-19 and Associations with Age and Disease Severity. *Cell.* 2020; 183(4):996–1012.e19.

107. World Health Organization. *WHO Public Health and Social Measures Initiative.* [Online; accessed 14. Aug. 2024]. Aug. 2024. URL: `https://www.who.int/initiatives/who-public-health-and-social-measures-initiative`.

108. Desvars-Larrive A, Dervic E, Haug N, et al. A structured open dataset of government interventions in response to COVID-19. *Sci. Data.* 2020; 7(285):1–9.

109. Yang Chan EY, Shahzada TS, Sham TST, et al. Narrative review of non-pharmaceutical behavioural measures for the prevention of COVID-19 (SARS-CoV-2) based on the Health-EDRM framework. *Br. Med. Bull.* 2020; 136(1):46–87.

110. Aledort JE, Lurie N, Wasserman J, Bozzette SA. Non-pharmaceutical public health interventions for pandemic influenza: an evaluation of the evidence base. *BMC Public Health.* 2007; 7(1):208. URL: https://dx.doi.org/10.1186/1471-2458-7-208.

111. Biggerstaff M, Slayton RB, Johansson MA, Butler JC. Improving Pandemic Response: Employing Mathematical Modeling to Confront Coronavirus Disease 2019. *Clin. Infect. Dis.* 2022; 74(5):913–917.

112. James LP, Salomon JA, Buckee CO, Menzies NA. The Use and Misuse of Mathematical Modeling for Infectious Disease Policymaking: Lessons for the COVID-19 Pandemic. *Med. Decis. Making.* 2021; 41(4):379–385.

113. OhAiseadha C, Quinn GA, Connolly R, et al. Unintended Consequences of COVID-19 Non-Pharmaceutical Interventions (NPIs) for Population Health and Health Inequalities. *International Journal of Environmental Research and Public Health.* 2023; 20(7). URL: https://www.mdpi.com/1660-4601/20/7/5223.

114. Banholzer N, Lison A, Özcelik D, Stadler T, Feuerriegel S, Vach W. The methodologies to assess the effectiveness of non-pharmaceutical interventions during COVID-19: a systematic review. *Eur. J. Epidemiol.* 2022; 37(10):1003–1024.

115. Iezadi S, Gholipour K, Azami-Aghdash S, et al. Effectiveness of non-pharmaceutical public health interventions against COVID-19: A systematic review and meta-analysis. *PLoS One.* 2021; 16(11):e0260371.

116. Mendez-Brito A, El Bcheraoui C, Pozo-Martin F. Systematic review of empirical studies comparing the effectiveness of non-pharmaceutical interventions against COVID-19. *J. Infect.* 2021; 83(3):281–293.

117. Herby J
bibinitperiodJ. A Literature Review and Meta-Analysis of the Effects of Lockdowns on COVID-19 Mortality. *Studies in Applied Economics.* 2022(). URL: https://ideas.repec.org/p/ris/jhisae/0200.html.

118. Rizvi RF, Craig KJT, Hekmat R, et al. Effectiveness of non-pharmaceutical interventions related to social distancing on respiratory viral infectious disease outcomes: A rapid evidence-based review and meta-analysis. *SAGE Open Medicine*. 2021; 9().

119. Talic S, Shah S, Wild H, et al. Effectiveness of public health measures in reducing the incidence of covid-19, SARS-CoV-2 transmission, and covid-19 mortality: systematic review and meta-analysis. *BMJ*. 2021; 375():e068302.

120. Ayouni I, Maatoug J, Dhouib W, et al. Effective public health measures to mitigate the spread of COVID-19: a systematic review. *BMC Public Health*. 2021; 21(1):1–14.

121. Girum T, Lentiro K, Geremew M, Migora B, Shewamare S, Shimbre MS. Optimal strategies for COVID-19 prevention from global evidence achieved through social distancing, stay at home, travel restriction and lockdown: a systematic review. *Arch. Public Health*. 2021; 79(1):1–18.

122. Viner RM, Russell SJ, Croker H, et al. School closure and management practices during coronavirus outbreaks including COVID-19: a rapid systematic review. *Lancet Child & Adolescent Health*. 2020; 4(5):397–404.

123. Walsh S, Chowdhury A, Braithwaite V, et al. Do school closures and school reopenings affect community transmission of COVID-19? A systematic review of observational studies. *BMJ Open*. 2021; 11(8):e053371.

124. Li Y, Liang M, Gao L, et al. Face masks to prevent transmission of COVID-19: A systematic review and meta-analysis. *Am. J. Infect. Control*. 2021; 49(7):900–906.

125. Islam N, Sharp SJ, Chowell G, et al. Physical distancing interventions and incidence of coronavirus disease 2019: natural experiment in 149 countries. *BMJ*. 2020; 370():m2743.

126. Hale T, Angrist N, Goldszmidt R, et al. A global panel database of pandemic policies (Oxford COVID-19 Government Response Tracker). *Nat. Hum. Behav.* 2021; 5():529–538.

127. Hale T, Angrist N, Hale AJ, et al. Government responses and COVID-19 deaths: Global evidence across multiple pandemic waves. *PLoS One*. 2021; 16(7):e0253116.

128. Koh WC, Naing L, Wong J. Estimating the impact of physical distancing measures in containing COVID-19: an empirical analysis. *Int. J. Infect. Dis.* 2020; 100():42–49.

129. Leffler CT, Ing E, Lykins JD, Hogan MC, McKeown CA, Grzybowski A. Association of Country-wide Coronavirus Mortality with Demographics, Testing, Lockdowns, and Public Wearing of Masks. *Am. J. Trop. Med. Hyg.* 2020; 103(6):2400–2411.

130. Liu X, Xu X, Li G, et al. Differential impact of non-pharmaceutical public health interventions on COVID-19 epidemics in the United States. *BMC Public Health*. 2021; 21(1):1–7.

131. Flaxman S, Mishra S, Gandy A, et al. Estimating the effects of non-pharmaceutical interventions on COVID-19 in Europe. *Nature*. 2020; 584():257–261.

132. Olney AM, Smith J, Sen S, Thomas F, Unwin HJT. Estimating the Effect of Social Distancing Interventions on COVID-19 in the United States. *Am. J. Epidemiol.* 2021; 190(8):1504–1509.

133. Haug N, Geyrhofer L, Londei A, et al. Ranking the effectiveness of worldwide COVID-19 government interventions. *Nat. Hum. Behav.* 2020; 4():1303–1312.

134. Brauner JM, Mindermann S, Sharma M, et al. Inferring the effectiveness of government interventions against COVID-19. *Science*. 2020; 371(6531).

135. Banholzer N, Weenen E van, Lison A, et al. Estimating the effects of non-pharmaceutical interventions on the number of new infections with COVID-19 during the first epidemic wave. *PLoS One*. 2021; 16(6):e0252827.

136. Courtemanche C, Garuccio J, Le A, Pinkston J, Yelowitz A. Strong Social Distancing Measures In The United States Reduced The COVID-19 Growth Rate. *Health Aff.* 2020(). URL: https://www.healthaffairs.org/doi/10.1377/hlthaff.2020.00608.

137. Auger KA, Shah SS, Richardson T, et al. Association Between Statewide School Closure and COVID-19 Incidence and Mortality in the US. *JAMA*. 2020; 324(9):859–870.

138. Hsiang S, Allen D, Annan-Phan S, et al. The effect of large-scale anti-contagion policies on the COVID-19 pandemic. *Nature*. 2020; 584():262–267.

139. Malheiro R, Figueiredo AL, Magalhães JP, et al. Effectiveness of contact tracing and quarantine on reducing COVID-19 transmission: a retrospective cohort study. *Public Health*. 2020; 189():54–59.

140. Kraemer MUG, Yang CH, Gutierrez B, et al. The effect of human mobility and control measures on the COVID-19 epidemic in China. *Science*. 2020; 368(6490):493–497.

141. Wells CR, Sah P, Moghadas SM, et al. Impact of international travel and border control measures on the global spread of the novel 2019 coronavirus outbreak. *Proc. Natl. Acad. Sci. U.S.A.* 2020; 117(13):7504–7509.

142. Grépin KA, Aston J, Burns J. Effectiveness of international border control measures during the COVID-19 pandemic: a narrative synthesis of published systematic reviews. *Philosophical transactions. Series A, Mathematical, physical, and engineering sciences*. 2023; 381(2257).

143. Li Z, Yang B, Wang J, et al. Global border restrictions in 2020–2021: Adherence and the effectiveness in long-term COVID-19 epidemic control. *Travel Med. Infect. Dis.* 2023; 52():102556.

144. Chu DK, Akl EA, Duda S, et al. Physical distancing, face masks, and eye protection to prevent person-to-person transmission of SARS-CoV-2 and COVID-19: a systematic review and meta-analysis. *Lancet*. 2020; 395(10242):1973–1987.

145. Xu J, Hussain S, Lu G, et al. Associations of Stay-at-Home Order and Face-Masking Recommendation with Trends in Daily New Cases and Deaths of Laboratory-Confirmed COVID-19 in the United States. *Exploratory Research and Hypothesis in Medicine*. 2020; 5(3):77–86.

146. Chernozhukov V, Kasahara H, Schrimpf P. Causal impact of masks, policies, behavior on early covid-19 pandemic in the U.S. *J. Econometrics*. 2021; 220(1):23–62.

147. Sharma M, Mindermann S, Rogers-Smith C, et al. Understanding the effectiveness of government interventions against the resurgence of COVID-19 in Europe. *Nat. Commun.* 2021; 12(5820):1–13.

148. Li Y, Campbell H, Kulkarni D, et al. The temporal association of introducing and lifting non-pharmaceutical interventions with the time-varying reproduction number (R) of SARS-CoV-2: a modelling study across 131 countries. *Lancet Infect. Dis.* 2021; 21(2):193–202.

149. Ge Y, Zhang WB, Liu H, et al. Impacts of worldwide individual non-pharmaceutical interventions on COVID-19 transmission across waves and space. *Int. J. Appl. Earth Obs. Geoinf.* 2022; 106():102649.

150. Collin A, Hejblum BP, Vignals C, et al. Using a population-based Kalman estimator to model the COVID-19 epidemic in France: estimating associations between disease transmission and non-pharmaceutical interventions. *International Journal of Biostatistics*. 2023; 20(1):13–41.

151. Torres AR, Rodrigues AP, Sousa-Uva M, et al. Impact of stringent non-pharmaceutical interventions applied during the second and third COVID-19 epidemic waves in Portugal, 9 November 2020 to 10 February 2021: an ecological study. *Eurosurveillance*. 2022; 27(23):2100497.

152. Lau H, Khosrawipour T, Kocbach P, Ichii H, Bania J, Khosrawipour V. Evaluating the massive underreporting and undertesting of COVID-19 cases in multiple global epicenters. *Pulmonology*. 2021; 27(2):110–115.

153. Mader S, Rüttenauer T. The Effects of Non-pharmaceutical Interventions on COVID-19 Mortality: A Generalized Synthetic Control Approach Across 169 Countries. *Front. Public Health*. 2022; 10():820642.

154. Siedner MJ, Harling G, Reynolds Z, et al. Social distancing to slow the US COVID-19 epidemic: Longitudinal pretest–posttest comparison group study. *PLoS Med.* 2020; 17(8):e1003244.

155. Liu Y, Morgenstern C, Kelly J, Lowe R, Jit M. The impact of non-pharmaceutical interventions on SARS-CoV-2 transmission across 130 countries and territories. *BMC Med.* 2021; 19(1):1–12.

156. Google. *COVID-19 Community Mobility Report*. [Online; accessed 15. Aug. 2024]. Mar. 2024. URL: `https://www.google.com/covid19/mobility`.

157. Spatial Data Lab. *Baidu Mobility Data*. Version V21. 2020. URL: `https://doi.org/10.7910/DVN/FAEZIO`.

158. *COVID-19 Datasets*. [Online; accessed 15. Aug. 2024]. July 2020. URL: `https://www.ecdc.europa.eu/en/covid-19/data`.

159. Worldometer. *Coronavirus Statistics*. [Online; accessed 15. Aug. 2024]. Apr. 2020. URL: `https://www.worldometers.info/coronavirus`.

160. *ACAPS*. [Online; accessed 14. Aug. 2024]. Aug. 2024. URL: `https://www.acaps.org`.

161. Shen Y, Powell G, Ganser I, et al. Monitoring non-pharmaceutical public health interventions during the COVID-19 pandemic. *Sci. Data*. 2021; 8(225):1–6.

162. Bundgaard H, Bundgaard JS, Raaschou-Pedersen DET, et al. Effectiveness of Adding a Mask Recommendation to Other Public Health Measures to Prevent SARS-CoV-2 Infection in Danish Mask Wearers. *Ann. Intern. Med.* 2020().

163. Varela AR, Gurruchaga AP, Restrepo SR, et al. Effectiveness and adherence to closed face shields in the prevention of COVID-19 transmission: a non-inferiority randomized controlled trial in a middle-income setting (COV-PROSHIELD). *Trials*. 2022; 23(1):1–13.

164. Abaluck J, Kwong LH, Styczynski A, et al. Impact of community masking on COVID-19: A cluster-randomized trial in Bangladesh. *Science*. 2021; 375(6577).

165. Lyu W, Wehby GL. Comparison of Estimated Rates of Coronavirus Disease 2019 (COVID-19) in Border Counties in Iowa Without a Stay-at-Home Order and Border Counties in Illinois With a Stay-at-Home Order. *JAMA Network Open*. 2020; 3(5):e2011102.

166. Dandekar R, Rackauckas C, Barbastathis G. A Machine Learning-Aided Global Diagnostic and Comparative Tool to Assess Effect of Quarantine Control in COVID-19 Spread. *Patterns*. 2020; 1(9):100145.

167. Li BZ, Cao NW, Zhou HY, Chu XJ, Ye DQ. Strong policies control the spread of COVID-19 in China. *J. Med. Virol.* 2020; 92(10):1980–1987.

168. Li Y, Li M, Rice M, et al. The Impact of Policy Measures on Human Mobility, COVID-19 Cases, and Mortality in the US: A Spatiotemporal Perspective. *Int. J. Environ. Res. Public Health*. 2021; 18(3):996.

169. Di Domenico L, Pullano G, Sabbatini CE, Boëlle PY, Colizza V. Impact of lockdown on COVID-19 epidemic in Île-de-France and possible exit strategies. *BMC Med.* 2020; 18(1):1–13.

170. Xia Y, Flores Anato JL, Colijn C, et al. Canada's provincial COVID-19 pandemic modelling efforts: A review of mathematical models and their impacts on the responses. *Can. J. Public Health*. 2024; 115(4):541–557.

171. Voor in 't holt AF, Haanappel CP, Rahamat-Langendoen J, et al. Admissions to a large tertiary care hospital and Omicron BA.1 and BA.2 SARS-CoV-2 polymerase chain reaction positivity: primary, contributing, or incidental COVID-19. *Int. J. Infect. Dis.* 2022; 122():665–668.

172. Kelly JD, Leonard S, Boscardin WJ, et al. Re-thinking all-cause COVID-19 hospitalizations as a surrogate measure for severe illness in observational surveillance studies. *Sci. Rep.* 2024; 14(14555):1–7.

173. Bendavid E, Oh C, Bhattacharya J, Ioannidis JPA. Assessing mandatory stay-at-home and business closure effects on the spread of COVID-19. *Eur. J. Clin. Invest.* 2021; 51(4):e13484.

174. Thomson S, Ip EC, Lee SF. International comparisons of COVID-19 case and mortality data and the effectiveness of non-pharmaceutical interventions: a plea for reconsideration. *J. Biosocial Sci.* 2022; 54(5):735–741.

175. Lison A, Banholzer N, Sharma M, et al. Effectiveness assessment of non-pharmaceutical interventions: lessons learned from the COVID-19 pandemic. *Lancet Public Health*. 2023; 8(4):e311–e317.

176. Sompayrac L. *How the immune system works*. Chichester, West Sussex ; Ames, Iowa : John Wiley & Sons, Ltd., 2016., 2016.

177. Abbas AK, Lichtman AH, Pillai S. *Basic immunology : functions and disorders of the immune system*. Philadelphia, PA : Elsevier Inc., [2023], 2023.

178. Krammer F. SARS-CoV-2 vaccines in development. *Nature*. 2020; 586():516–527.

179. Tregoning JS, Flight KE, Higham SL, Wang Z, Pierce BF. Progress of the COVID-19 vaccine effort: viruses, vaccines and variants versus efficacy, effectiveness and escape. *Nat. Rev. Immunol.* 2021; 21():626–636.

180. Humphries RM. Immunity to SARS-CoV-2: What Do We Know and Should We Be Testing for It? *J. Clin. Microbiol.* 2022(). URL: `https://journals.asm.org/doi/full/10.1128/jcm.00482-21`.

181. Mulligan MJ, Lyke KE, Kitchin N, et al. Phase I/II study of COVID-19 RNA vaccine BNT162b1 in adults. *Nature*. 2020; 586():589–593.

182. Pardi N, Hogan MJ, Porter FW, Weissman D. mRNA vaccines — a new era in vaccinology. *Nat. Rev. Drug Discovery*. 2018; 17():261–279.

183. McCann N, O'Connor D, Lambe T, Pollard AJ. Viral vector vaccines. *Curr. Opin. Immunol.* 2022; 77():102210.

184. Heath PT, Galiza EP, Baxter DN, et al. Safety and Efficacy of NVX-CoV2373 Covid-19 Vaccine. *N. Engl. J. Med.* 2021().

185. Wu Z, Hu Y, Xu M, et al. Safety, tolerability, and immunogenicity of an inactivated SARS-CoV-2 vaccine (CoronaVac) in healthy adults aged 60 years and older: a randomised, double-blind, placebo-controlled, phase 1/2 clinical trial. *Lancet Infect. Dis.* 2021; 21(6):803.

186. Baden LR, Sahly HME, Essink B, et al. Efficacy and Safety of the mRNA-1273 SARS-CoV-2 Vaccine. *N. Engl. J. Med.* 2021().

187. Polack FP, Thomas SJ, Kitchin N, et al. Safety and Efficacy of the BNT162b2 mRNA Covid-19 Vaccine. *N. Engl. J. Med.* 2020().

188. Higdon MM, Wahl B, Jones CB, et al. A Systematic Review of Coronavirus Disease 2019 Vaccine Efficacy and Effectiveness Against Severe Acute Respiratory Syndrome Coronavirus 2 Infection and Disease. *Open Forum Infect. Dis.* 2022; 9(6):ofac138.

189. Israel A, Shenhar Y, Green I, et al. Large-Scale Study of Antibody Titer Decay following BNT162b2 mRNA Vaccine or SARS-CoV-2 Infection. *Vaccines*. 2021; 10(1):64.

190. Wang Z, Schmidt F, Weisblum Y, et al. mRNA vaccine-elicited antibodies to SARS-CoV-2 and circulating variants. *Nature*. 2021; 592():616–622.

191. Widge AT, Rouphael NG, Jackson LA, et al. Durability of Responses after SARS-CoV-2 mRNA-1273 Vaccination. *N. Engl. J. Med.* 2021().

192. Schultz NH, Sørvoll IH, Michelsen AE, et al. Thrombosis and Thrombocytopenia after ChAdOx1 nCoV-19 Vaccination. *N. Engl. J. Med.* 2021().

193. Greinacher A, Thiele T, Warkentin TE, Weisser K, Kyrle PA, Eichinger S. Thrombotic Thrombocytopenia after ChAdOx1 nCov-19 Vaccination. *N. Engl. J. Med.* 2021().

194. Mathieu E, Ritchie H, Ortiz-Ospina E, et al. A global database of COVID-19 vaccinations. *Nat. Hum. Behav.* 2021; 5():947–953.

195. Watson OJ, Barnsley G, Toor J, Hogan AB, Winskill P, Ghani AC. Global impact of the first year of COVID-19 vaccination: a mathematical modelling study. *Lancet Infect. Dis.* 2022; 22(9):1293–1302.

196. Yasmin F, Najeeb H, Moeed A, et al. COVID-19 Vaccine Hesitancy in the United States: A Systematic Review. *Front. Public Health*. 2021; 9():770985.

197. Mutombo PN, Fallah MP, Munodawafa D, et al. COVID-19 vaccine hesitancy in Africa: a call to action. *Lancet Global Health*. 2022; 10(3):e320–e321.

198. Bergeri I, Whelan MG, Ware H, et al. Global SARS-CoV-2 seroprevalence from January 2020 to April 2022: A systematic review and meta-analysis of standardized population-based studies. *PLoS Med.* 2022; 19(11):e1004107.

199. Wagner CE, Saad-Roy CM, Morris SE, et al. Vaccine nationalism and the dynamics and control of SARS-CoV-2. *Science*. 2021; 373(6562).

200. Wells CR, Galvani AP. The global impact of disproportionate vaccination coverage on COVID-19 mortality. *Lancet Infect. Dis.* 2022; 22(9):1254–1255.

201. McDonald I, Murray SM, Reynolds CJ, Altmann DM, Boyton RJ. Comparative systematic review and meta-analysis of reactogenicity, immunogenicity and efficacy of vaccines against SARS-CoV-2. *npj Vaccines*. 2021; 6(74):1–14.

202. Tang J, Zeng C, Cox TM, et al. Respiratory mucosal immunity against SARS-CoV-2 after mRNA vaccination. *Sci. Immunol.* 2022; 7(76).

203. Azzi L, Dalla Gasperina D, Veronesi G, et al. Mucosal immune response in BNT162b2 COVID-19 vaccine recipients. *eBioMedicine*. 2022; 75():103788.

204. Keeton R, Tincho MB, Ngomti A, et al. T cell responses to SARS-CoV-2 spike cross-recognize Omicron. *Nature*. 2022; 603():488–492.

205. Liu J, Chandrashekar A, Sellers D, et al. Vaccines elicit highly conserved cellular immunity to SARS-CoV-2 Omicron. *Nature*. 2022; 603():493–496.

206. Gilbert PB, Montefiori DC, McDermott AB, et al. Immune correlates analysis of the mRNA-1273 COVID-19 vaccine efficacy clinical trial. *Science*. 2021; 375(6576):43–50.

207. Benkeser D, Montefiori DC, McDermott AB, et al. Comparing antibody assays as correlates of protection against COVID-19 in the COVE mRNA-1273 vaccine efficacy trial. *Sci. Transl. Med.* 2023; 15(692).

208. Piccoli L, Park YJ, Tortorici MA, et al. Mapping Neutralizing and Immunodominant Sites on the SARS-CoV-2 Spike Receptor-Binding Domain by Structure-Guided High-Resolution Serology. *Cell*. 2020; 183(4):1024–1042.e21.

209. Dai L, Gao GF. Viral targets for vaccines against COVID-19. *Nat. Rev. Immunol.* 2021; 21():73–82.

210. Altmann DM, Boyton RJ. COVID-19 vaccination: The road ahead. *Science*. 2022; 375(6585):1127–1132.

211. Khoury DS, Cromer D, Reynaldi A, et al. Neutralizing antibody levels are highly predictive of immune protection from symptomatic SARS-CoV-2 infection. *Nat. Med.* 2021; 27():1205–1211.

212. Plotkin SA, Gilbert PB. Nomenclature for Immune Correlates of Protection After Vaccination. *Clin. Infect. Dis.* 2012; 54(11):1615–1617.

213. Barouch DH. Covid-19 Vaccines — Immunity, Variants, Boosters. *N. Engl. J. Med.* 2022().

214. Pilz S, Theiler-Schwetz V, Trummer C, Krause R, Ioannidis JPA. SARS-CoV-2 reinfections: Overview of efficacy and duration of natural and hybrid immunity. *Environ. Res.* 2022; 209():112911.

215. Goldberg Y, Mandel M, Bar-On YM, et al. Protection and Waning of Natural and Hybrid Immunity to SARS-CoV-2. *N. Engl. J. Med.* 2022().

216. Israel A, Merzon E, Schäffer AA, et al. Elapsed time since BNT162b2 vaccine and risk of SARS-CoV-2 infection: test negative design study. *BMJ*. 2021; 375():e067873.

217. Rosenberg ES, Dorabawila V, Easton D, et al. Covid-19 Vaccine Effectiveness in New York State. *N. Engl. J. Med.* 2022().

218. Ssentongo P, Ssentongo AE, Voleti N, et al. SARS-CoV-2 vaccine effectiveness against infection, symptomatic and severe COVID-19: a systematic review and meta-analysis. *BMC Infect. Dis.* 2022; 22(1):1–12.

219. Feikin DR, Higdon MM, Abu-Raddad LJ, et al. Duration of effectiveness of vaccines against SARS-CoV-2 infection and COVID-19 disease: results of a systematic review and meta-regression. *Lancet*. 2022; 399(10328):924–944.

220. Gazit S, Shlezinger R, Perez G, et al. Severe Acute Respiratory Syndrome Coronavirus 2 (SARS-CoV-2) Naturally Acquired Immunity versus Vaccine-induced Immunity, Reinfections versus Breakthrough Infections: A Retrospective Cohort Study. *Clin. Infect. Dis.* 2022; 75(1):e545–e551.

221. Shenai MB, Rahme R, Noorchashm H. Equivalency of Protection From Natural Immunity in COVID-19 Recovered Versus Fully Vaccinated Persons: A Systematic Review and Pooled Analysis. *Cureus*. 2021; 13(10).

222. Steenhuis M, Mierlo G van, Derksen NIL, et al. Dynamics of antibodies to SARS-CoV-2 in convalescent plasma donors. *Clin. Transl. Immunol.* 2021; 10(5):e1285.

223. Ripperger TJ, Uhrlaub JL, Watanabe M, et al. Orthogonal SARS-CoV-2 Serological Assays Enable Surveillance of Low-Prevalence Communities and Reveal Durable Humoral Immunity. *Immunity*. 2020; 53(5):925–933.e4.

224. Gallais F, Gantner P, Bruel T, et al. Evolution of antibody responses up to 13 months after SARS-CoV-2 infection and risk of reinfection. *eBioMedicine*. 2021; 71():103561.

225. Srivastava K, Carreño JM, Gleason C, et al. SARS-CoV-2-infection- and vaccine-induced antibody responses are long lasting with an initial waning phase followed by a stabilization phase. *Immunity*. 2024; 57(3):587–599.e4.

226. Chivese T, Matizanadzo JT, Musa OAH, et al. The prevalence of adaptive immunity to COVID-19 and reinfection after recovery – a comprehensive systematic review and meta-analysis. *Pathogens and Global Health*. 2022().

227. Mateus J, Dan JM, Zhang Z, et al. Low-dose mRNA-1273 COVID-19 vaccine generates durable memory enhanced by cross-reactive T cells. *Science*. 2021; 374(6566).

228. Goel RR, Painter MM, Apostolidis SA, et al. mRNA vaccines induce durable immune memory to SARS-CoV-2 and variants of concern. *Science*. 2021; 374(6572).

229. Menegale F, Manica M, Zardini A, et al. Evaluation of Waning of SARS-CoV-2 Vaccine–Induced Immunity: A Systematic Review and Meta-analysis. *JAMA Netw. Open*. 2023; 6(5):e2310650.

230. Edara VV, Manning KE, Ellis M, et al. mRNA-1273 and BNT162b2 mRNA vaccines have reduced neutralizing activity against the SARS-CoV-2 omicron variant. *Cell Reports Medicine*. 2022; 3(2):100529.

231. Lyke KE, Atmar RL, Islas CD, et al. Rapid decline in vaccine-boosted neutralizing antibodies against SARS-CoV-2 Omicron variant. *Cell Reports Medicine*. 2022; 3(7):100679.

232. Bobrovitz N, Ware H, Ma X, et al. Protective effectiveness of previous SARS-CoV-2 infection and hybrid immunity against the omicron variant and severe disease: a systematic review and meta-regression. *Lancet Infect. Dis.* 2023; 23(5):556–567.

233. VanBlargan LA, Errico JM, Halfmann PJ, et al. An infectious SARS-CoV-2 B.1.1.529 Omicron virus escapes neutralization by therapeutic monoclonal antibodies. *Nat. Med.* 2022; 28():490–495.

234. Altarawneh HN, Chemaitelly H, Ayoub HH, et al. Effects of Previous Infection and Vaccination on Symptomatic Omicron Infections. *N. Engl. J. Med.* 2022().

235. Winokur P, Gayed J, Fitz-Patrick D, et al. Bivalent Omicron BA.1–Adapted BNT162b2 Booster in Adults Older than 55 Years. *N. Engl. J. Med.* 2023().

236. Davis-Gardner ME, Lai L, Wali B, et al. Neutralization against BA.2.75.2, BQ.1.1, and XBB from mRNA Bivalent Booster. *N. Engl. J. Med.* 2023().

237. Mateo-Urdiales A, Sacco C, Fotakis EA, et al. Relative effectiveness of monovalent and bivalent mRNA boosters in preventing severe COVID-19 due to omicron BA.5 infection up to 4 months post-administration in people aged 60 years or older in Italy: a retrospective matched cohort study. *Lancet Infect. Dis.* 2023; 23(12):1349–1359.

238. Lin DY, Xu Y, Gu Y, et al. Effectiveness of Bivalent Boosters against Severe Omicron Infection. *N. Engl. J. Med.* 2023().

239. Hachmann NP, Miller J, Collier ArY, et al. Neutralization Escape by SARS-CoV-2 Omicron Subvariants BA.2.12.1, BA.4, and BA.5. *N. Engl. J. Med.* 2022().

240. Moghadas SM, Vilches TN, Zhang K, et al. Evaluation of COVID-19 vaccination strategies with a delayed second dose. *PLoS Biol.* 2021; 19(4):e3001211.

241. Imai N, Rawson T, Knock ES, et al. Quantifying the effect of delaying the second COVID-19 vaccine dose in England: a mathematical modelling study. *Lancet Public Health.* 2023; 8(3):e174–e183.

242. Shioda K, Breskin A, Harati P, et al. Comparative effectiveness of alternative intervals between first and second doses of the mRNA COVID-19 vaccines. *Nat. Commun.* 2024; 15(1214):1–9.

243. Klemis V, Schmidt T, Schub D, et al. Comparative immunogenicity and reactogenicity of heterologous ChAdOx1-nCoV-19-priming and BNT162b2 or mRNA-1273-boosting with homologous COVID-19 vaccine regimens. *Nat. Commun.* 2022; 13(4710):1–11.

244. Lv J, Wu H, Xu J, Liu J. Immunogenicity and safety of heterologous versus homologous prime-boost schedules with an adenoviral vectored and mRNA COVID-19 vaccine: a systematic review. *Infect. Dis. Poverty.* 2022; 11(1):1–17.

245. Le TP, Abell I, Conway E, et al. Modelling the impact of hybrid immunity on future COVID-19 epidemic waves. *BMC Infect. Dis.* 2024; 24(1):1–14.

246. Lasrado N, Barouch DH. SARS-CoV-2 Hybrid Immunity: The Best of Both Worlds. *J. Infect. Dis.* 2023; 228(10):1311–1313.

247. Hall V, Foulkes S, Insalata F, et al. Protection against SARS-CoV-2 after Covid-19 Vaccination and Previous Infection. *N. Engl. J. Med.* 2022().

248. Cohen KW, Linderman SL, Moodie Z, et al. Longitudinal analysis shows durable and broad immune memory after SARS-CoV-2 infection with persisting antibody responses and memory B and T cells. *Cell Reports Medicine.* 2021; 2(7):100354.

249. Chen Y, Tong P, Whiteman N, et al. Immune recall improves antibody durability and breadth to SARS-CoV-2 variants. *Sci. Immunol.* 2022; 7(78).

250. Rodda LB, Morawski PA, Pruner KB, et al. Imprinted SARS-CoV-2-specific memory lymphocytes define hybrid immunity. *Cell.* 2022; 185(9):1588–1601.e14.

251. Yamamoto S, Mizoue T, Ohmagari N. Analysis of Previous Infection, Vaccinations, and Anti–SARS-CoV-2 Antibody Titers and Protection Against Infection With the SARS-CoV-2 Omicron BA.5 Variant. *JAMA Netw. Open.* 2023; 6(3):e233370.

252. Tai CG, Haviland MJ, Kissler SM, et al. Low antibody levels associated with significantly increased rate of SARS-CoV-2 infection in a highly vaccinated population from the US National Basketball Association. *J. Med. Virol.* 2024; 96(3):e29505.

253. Kadowaki T, Sasaki A, Matsumoto N, et al. Antibody Titers and the Risk of Infection During the SARS-CoV-2 Omicron Phase in Bizen City, Japan. *J. Infect. Dis.* 2024():jiae207.

254. Box GEP. Robustness in the Strategy of Scientific Model Building. *Robustness in Statistics.* Cambridge, MA, USA: Academic Press, Jan. 1979:201–236.

255. Adiga A, Dubhashi D, Lewis B, Marathe M, Venkatramanan S, Vullikanti A. Mathematical Models for COVID-19 Pandemic: A Comparative Analysis. *J. Indian Inst. Sci.* 2020; 100(4):793–807.

256. Handel A, La Gruta NL, Thomas PG. Simulation modelling for immunologists. *Nat. Rev. Immunol.* 2020; 20():186–195.

257. Jit M, Cook AR. Informing Public Health Policies with Models for Disease Burden, Impact Evaluation, and Economic Evaluation. *Annual Reviews*. 2023().

258. Vynnycky E, White R. *An Introduction to Infectious Disease Modelling*. Oxford, England, UK: Oxford University Press, July 2010. URL: https://global.oup.com/academic/product/an-introduction-to-infectious-disease-modelling-9780198565765.

259. Brauer F, Driessche P van den, Wu J. *Mathematical Epidemiology*. Berlin, Germany: Springer, 2008. URL: https://link.springer.com/book/10.1007/978-3-540-78911-6.

260. Tracy M, Cerdá M, Keyes KM. Agent-Based Modeling in Public Health: Current Applications and Future Directions. *Annu. Rev. Public Health*. 2018(; Volume 39, 2018):77–94.

261. Ross R. *The Prevention of malaria*. J. Murray, 1910.

262. Ross R. Some a priori pathometric equations. *Br. Med. J.* 1915; 1(2830):546.

263. Ross R. An application of the theory of probabilities to the study of a priori pathometry.—Part I. *Proc. R. Soc. London A*. 1916; 92(638):204–230.

264. Ross R, Hudson HP. An application of the theory of probabilities to the study of a priori pathometry.—Part III. *Proc. R. Soc. London A*. 1917; 93(650):225–240.

265. Kermack WO, Mckendrick AG. A contribution to the mathematical theory of epidemics. *Proceedings of the Royal Society of London. Series A, Containing Papers of a Mathematical and Physical Character*. 1927; 115(772):700–721.

266. Fine P, Eames K, Heymann DL. "Herd Immunity": A Rough Guide. *Clin. Infect. Dis.* 2011; 52(7):911–916.

267. Heesterbeek JAP, Dietz K. The concept of R in epidemic theory. *Stat. Neerl.* 1996; 50(1):89–110.

268. Lessler J, Cummings DAT. Mechanistic Models of Infectious Disease and Their Impact on Public Health. *American Journal of Epidemiology*. 2016; 183(5):415–422. URL: https://dx.doi.org/10.1093/aje/kww021.

269. Salje H, Kiem CT, Lefrancq N, et al. Estimating the burden of SARS-CoV-2 in France. *Science*. 2020; 369():208–211. URL: https://dx.doi.org/10.1126/science.abc3517.

270. Roux J, Massonnaud CR, Colizza V, Cauchemez S, Crépey P. Modeling the impact of national and regional lockdowns on the 2020 spring wave of COVID-19 in France. *Sci. Rep.* 2023; 13(1834):1–9.

271. Sofonea MT, Reyné B, Elie B, et al. Memory is key in capturing COVID-19 epidemiological dynamics. *Epidemics*. 2021; 35():100459.

272. Arino J, Portet S. A simple model for COVID-19. *Infectious Disease Modelling*. 2020; 5():309–315.

273. Britton T, Pardoux E. Chapter 1 Stochastic Epidemic Models. *Stochastic Epidemic Models with Inference*. Cham, Switzerland: Springer, Dec. 2019:5–19.

274. Beneteau T, Elie B, Sofonea MT, Alizon S. Estimating dates of origin and end of COVID-19 epidemics. *Peer Community Journal*. 2021; 1().

275. Friji H, Hamadi R, Ghazzai H, Besbes H, Massoud Y. A Generalized Mechanistic Model for Assessing and Forecasting the Spread of the COVID-19 Pandemic. *IEEE Access*. 2021; 9():13266.

276. Aronna MS, Guglielmi R, Moschen LM. A model for COVID-19 with isolation, quarantine and testing as control measures. *Epidemics*. 2021; 34():100437.

277. Giordano G, Colaneri M, Di Filippo A, et al. Modeling vaccination rollouts, SARS-CoV-2 variants and the requirement for non-pharmaceutical interventions in Italy. *Nat. Med.* 2021; 27():993–998.

278. Childs L, Dick DW, Feng Z, Heffernan JM, Li J, Röst G. Modeling waning and boosting of COVID-19 in Canada with vaccination. *Epidemics*. 2022; 39():100583.

279. Chung HW, Apio C, Goo T, et al. Effects of government policies on the spread of COVID-19 worldwide. *Sci. Rep.* 2021; 11(20495):1–10.

280. Yang B, Huang AT, Garcia-Carreras B, et al. Effect of specific non-pharmaceutical intervention policies on SARS-CoV-2 transmission in the counties of the United States. *Nat. Commun.* 2021; 12(3560):1–10.

281. Jo Y, Shrestha S, Radnaabaatar M, Park H, Jung J. Optimal Social Distancing Policy for COVID-19 Control in Korea: A Model-Based Analysis. *J. Korean Med. Sci.* 2022; 37(23).

282. Moore S, Hill EM, Tildesley MJ, Dyson L, Keeling MJ. Vaccination and non-pharmaceutical interventions for COVID-19: a mathematical modelling study. *Lancet Infect. Dis.* 2021; 21(6):793–802.

283. Massey A, Boennec C, Restrepo-Ortiz CX, Blanchet C, Alizon S, Sofonea MT. Real-time forecasting of COVID-19-related hospital strain in France using a non-Markovian mechanistic model. *PLoS Comput. Biol.* 2024; 20(5):e1012124.

284. Baguelin M, Flasche S, Camacho A, Demiris N, Miller E, Edmunds WJ. Assessing Optimal Target Populations for Influenza Vaccination Programmes: An Evidence Synthesis and Modelling Study. *PLoS Med.* 2013; 10(10):e1001527.

285. White LF, Wallinga J, Finelli L, et al. Estimation of the reproductive number and the serial interval in early phase of the 2009 influenza A/H1N1 pandemic in the USA. *Influenza and Other Respiratory Viruses*. 2009; 3(6):267.

286. Ferguson NM, Cummings DAT, Fraser C, Cajka JC, Cooley PC, Burke DS. Strategies for mitigating an influenza pandemic. *Nature*. 2006; 442():448–452.

287. Meltzer MI, Santibanez S, Fischer LS, et al. Modeling in Real Time During the Ebola Response. *MMWR Suppl.* 2016; 65().

288. Legrand J, Grais RF, Boelle PY, Valleron AJ, Flahault A. Understanding the dynamics of Ebola epidemics. *Epidemiol. Infect.* 2007; 135(4):610–621.

289. Lewnard JA, Mbah MLN, Alfaro-Murillo JA, et al. Dynamics and control of Ebola virus transmission in Montserrado, Liberia: a mathematical modelling analysis. *Lancet Infect. Dis.* 2014; 14(12):1189–1195.

290. Li Q, Guan X, Wu P, et al. Early Transmission Dynamics in Wuhan, China, of Novel Coronavirus-Infected Pneumonia. *N. Engl. J. Med.* 2020; 382(13):1199–1207. eprint: `31995857`.

291. Read JM, Bridgen JRE, Cummings DAT, Ho A, Jewell CP. Novel coronavirus 2019-nCoV (COVID-19): early estimation of epidemiological parameters and epidemic size estimates. *Philosophical Transactions of the Royal Society B: Biological Sciences*. 2021; 376(1829):20200265.

292. Zhou T, Liu Q, Yang Z, et al. Preliminary prediction of the basic reproduction number of the Wuhan novel coronavirus 2019-nCoV. *Journal of Evidence-Based Medicine*. 2020; 13(1):3–7.

293. Imai N, Dorigatti I, Cori A, Donnelly C, Riley S, Ferguson N. *Report 2: Estimating the potential total number of novel Coronavirus cases in Wuhan City, China*. [Online; accessed 29. Aug. 2024]. Jan. 2020. URL: `https://spiral.imperial.ac.uk/handle/10044/1/77150`.

294. Wu JT, Leung K, Bushman M, et al. Estimating clinical severity of COVID-19 from the transmission dynamics in Wuhan, China. *Nat. Med.* 2020; 26(4):506–510. eprint: `32284616`.

295. Wu JT, Leung K, Leung GM. Nowcasting and forecasting the potential domestic and international spread of the 2019-nCoV outbreak originating in Wuhan, China: a modelling study. *Lancet*. 2020; 395(10225):689–697.

296. Faria NR, Mellan TA, Whittaker C, et al. Genomics and epidemiology of the P.1 SARS-CoV-2 lineage in Manaus, Brazil. *Science*. 2021; 372(6544):815–821.

297. Néant N, Lingas G, Le Hingrat Q, et al. Modeling SARS-CoV-2 viral kinetics and association with mortality in hospitalized patients from the French COVID cohort. *Proc. Natl. Acad. Sci. U.S.A.* 2021; 118(8):e2017962118.

298. Kissler SM, Fauver JR, Mack C, et al. Viral Dynamics of SARS-CoV-2 Variants in Vaccinated and Unvaccinated Persons. *N. Engl. J. Med.* 2021().

299. Kim KS, Ejima K, Iwanami S, et al. A quantitative model used to compare within-host SARS-CoV-2, MERS-CoV, and SARS-CoV dynamics provides insights into the pathogenesis and treatment of SARS-CoV-2. *PLoS Biol.* 2021; 19(3):e3001128.

300. Cao Y, Gao W, Caro L, Stone JA. Immune-viral dynamics modeling for SARS-CoV-2 drug development. *Clin. Transl. Sci.* 2021; 14(6):2348–2359.

301. Ferguson N, Laydon D, Nedjati Gilani G, et al. *Report 9: Impact of non-pharmaceutical interventions (NPIs) to reduce COVID19 mortality and healthcare demand*. [Online; accessed 29. Aug. 2024]. Mar. 2020. URL: `https://spiral.imperial.ac.uk/handle/10044/1/77482`.

302. Marchant R, Samia NI, Rosen O, Tanner MA, Cripps S. Learning as We Go: An Examination of the Statistical Accuracy of COVID19 Daily Death Count Predictions. *medRxiv*. 2020():2020.04.11.20062257. eprint: `2020.04.11.20062257`. URL: `https://doi.org/10.1101/2020.04.11.20062257`.

303. Jewell NP, Lewnard JA, Jewell BL. Caution Warranted: Using the Institute for Health Metrics and Evaluation Model for Predicting the Course of the COVID-19 Pandemic. *Ann. Intern. Med.* 2020().

304. Kociurzynski R, D'Ambrosio A, Papathanassopoulos A, et al. Forecasting local hospital bed demand for COVID-19 using on-request simulations. *Sci. Rep.* 2023; 13().

305. Zhang J, Pathak HS, Snowdon A, Greiner R. Learning models for forecasting hospital resource utilization for COVID-19 patients in Canada. *Sci. Rep.* 2022; 12(8751):1–14.

306. Moghadas SM, Shoukat A, Fitzpatrick MC, et al. Projecting hospital utilization during the COVID-19 outbreaks in the United States. *Proceedings of the National Academy of Sciences*. 2020; 117(16):9122–9126.

307. Ferté T, Jouhet V, Griffier R, Hejblum BP, Thiébaut R, Force BUHC1CT. The benefit of augmenting open data with clinical data-warehouse EHR for forecasting SARS-CoV-2 hospitalizations in Bordeaux area, France. *Jamia Open*. 2022; 5(4):ooac086.

308. Ray EL, Wattanachit N, Niemi J, et al. Ensemble Forecasts of Coronavirus Disease 2019 (COVID-19) in the U.S. *medRxiv*. 2020():2020.08.19.20177493. eprint: 2020.08.19.20177493. URL: https://doi.org/10.1101/2020.08.19.20177493.

309. Coroneo L, Iacone F, Paccagnini A, Santos Monteiro P. Testing the predictive accuracy of COVID-19 forecasts. *International Journal of Forecasting*. 2023; 39(2):606–622.

310. Cramer EY, Ray EL, Lopez VK, et al. Evaluation of individual and ensemble probabilistic forecasts of COVID-19 mortality in the United States. *Proc. Natl. Acad. Sci. U.S.A.* 2022; 119(15):e2113561119.

311. Howerton E, Contamin L, Mullany LC, et al. Evaluation of the US COVID-19 Scenario Modeling Hub for informing pandemic response under uncertainty. *Nat. Commun.* 2023; 14(7260):1–15.

312. Giordano G, Blanchini F, Bruno R, et al. Modelling the COVID-19 epidemic and implementation of population-wide interventions in Italy. *Nature Medicine*. 2020; 26(6):855–860.

313. Ogden NH, Fazil A, Arino J, et al. Modelling scenarios of the epidemic of COVID-19 in Canada. *Canada Communicable Disease Report*. 2020; 46(6). URL: https://doi.org/10.14745/ccdr.v46i06a08.

314. López L, Rodó X. The end of social confinement and COVID-19 re-emergence risk. *Nature Human Behaviour*. 2020; 4(7):746–755.

315. Hou C, Chen J, Zhou Y, et al. The effectiveness of quarantine of Wuhan city against the Corona Virus Disease 2019 (COVID-19): A well-mixed SEIR model analysis. *J. Med. Virol.* 2020; 92(7):841–848.

316. Kucharski AJ, Klepac P, Conlan AJK, et al. Effectiveness of isolation, testing, contact tracing, and physical distancing on reducing transmission of SARS-CoV-2 in different settings: a mathematical modelling study. *Lancet Infect. Dis.* 2020; 20(10):1151–1160.

317. Davies NG, Kucharski AJ, Eggo RM, et al. Effects of non-pharmaceutical interventions on COVID-19 cases, deaths, and demand for hospital services in the UK: a modelling study. *Lancet Public Health*. 2020; 5(7):e375–e385.

318. Ferretti L, Wymant C, Kendall M, et al. Quantifying SARS-CoV-2 transmission suggests epidemic control with digital contact tracing. *Science (New York, N.y.)* 2020; 368(6491).

319. Hogan AB, Winskill P, Watson OJ, et al. Within-country age-based prioritisation, global allocation, and public health impact of a vaccine against SARS-CoV-2: A mathematical modelling analysis. *Vaccine*. 2021; 39(22):2995–3006.

320. Bubar KM, Reinholt K, Kissler SM, et al. Model-informed COVID-19 vaccine prioritization strategies by age and serostatus. *Science*. 2021; 371(6532):916–921.

321. Saad-Roy CM, Morris SE, Metcalf CJE, et al. Epidemiological and evolutionary considerations of SARS-CoV-2 vaccine dosing regimes. *Science*. 2021; 372(6540):363–370.

322. Jung Sm, Loo SL, Howerton E, et al. Potential impact of annual vaccination with reformulated COVID-19 vaccines: Lessons from the US COVID-19 scenario modeling hub. *PLoS Med.* 2024; 21(4):e1004387.

323. Li J, Giabbanelli P. Returning to a Normal Life via COVID-19 Vaccines in the United States: A Large-scale Agent-Based Simulation Study. *JMIR Medical Informatics*. 2021; 9(4):e27419.

324. Patel MD, Rosenstrom E, Ivy JS, et al. Association of Simulated COVID-19 Vaccination and Nonpharmaceutical Interventions With Infections, Hospitalizations, and Mortality. *JAMA Netw. Open*. 2021; 4(6):e2110782. eprint: 34061203.

325. Massonnaud CR, Roux J, Colizza V, Crépey P. Evaluating COVID-19 Booster Vaccination Strategies in a Partially Vaccinated Population: A Modeling Study. *Vaccines*. 2022; 10(3):479.

326. Borchering RK, Viboud C, Howerton E, et al. Modeling of Future COVID-19 Cases, Hospitalizations, and Deaths, by Vaccination Rates and Nonpharmaceutical Intervention Scenarios - United States, April-September 2021. *MMWR Morb. Mortal. Wkly. Rep.* 2021; 70(19):719–724. eprint: 33988185.

327. Beukenhorst AL, Koch CM, Hadjichrysanthou C, et al. SARS-CoV-2 elicits non-sterilizing immunity and evades vaccine-induced immunity: implications for future vaccination strategies. *Eur. J. Epidemiol.* 2023; 38(3):237–242.

328. Massonis G, Banga JR, Villaverde AF. Structural identifiability and observability of compartmental models of the COVID-19 pandemic. *Annual Reviews in Control*. 2021; 51():441–459.

329. Kao YH, Eisenberg MC. Practical unidentifiability of a simple vector-borne disease model: Implications for parameter estimation and intervention assessment. *Epidemics*. 2018; 25():89–100.

330. Chowell G. Fitting dynamic models to epidemic outbreaks with quantified uncertainty: A primer for parameter uncertainty, identifiability, and forecasts. *Infectious Disease Modelling*. 2017; 2(3):379–398.

331. Cunniffe N, Hamelin F, Iggidr A, Rapaport A, Sallet G. *Identifiability and Observability in Epidemiological Models - a survey -*. [Online; accessed 21. Sep. 2024]. May 2023. URL: https://hal.science/hal-02995562v3.

332. Bellu G, Saccomani MP, Audoly S, D'Angio L. DAISY: A new software tool to test global identifiability of biological and physiological systems. *Computer Methods and Programs in Biomedicine*. 2007; 88(1):52–61. URL: https://dx.doi.org/10.1016/j.cmpb.2007.07.002.

333. Fisher R. A. On the mathematical foundations of theoretical statistics. *Philosophical Transactions of the Royal Society of London. Series A, Containing Papers of a Mathematical or Physical Character*. 1922; 222(594-604):309–368.

334. Lindstrom MJ, Bates DM. Newton-Raphson and EM Algorithms for Linear Mixed-Effects Models for Repeated-Measures Data. *J. Am. Stat. Assoc.* 1988; 83(404):1014–1022. URL: https://www.jstor.org/stable/2290128.

335. Dempster AP, Laird NM, Rubin DB. *Maximum Likelihood from Incomplete Data via the EM Algorithm*. 1977. URL: https://www.jstor.org/stable/2984875.

336. Kuhn E, Lavielle M. Maximum likelihood estimation in nonlinear mixed effects models. *Comput. Statist. Data Anal.* 2005; 49(4):1020–1038.

337. Chan PLS, Jacqmin P, Lavielle M, McFadyen L, Weatherley B. The use of the SAEM algorithm in MONOLIX software for estimation of population pharmacokinetic-pharmacodynamic-viral dynamics parameters of maraviroc in asymptomatic HIV subjects. *J. Pharmacokinet. Pharmacodyn.* 2011; 38(1):41–61.

338. Lixoft. *Simulx 2021R2*. 2021. URL: https://simulx.lixoft.com/.

340. Crane MA, Shermock KM, Omer SB, Romley JA. Change in Reported Adherence to Nonpharmaceutical Interventions During the COVID-19 Pandemic, April-November 2020. *JAMA*. 2021; 325():883. URL: https://dx.doi.org/10.1001/jama.2021.0286.

355. Clairon Q, Prague M, Planas D, et al. Modeling the kinetics of the neutralizing antibody response against SARS-CoV-2 variants after several administrations of Bnt162b2. *PLoS Comput. Biol.* 2023; 19(8):e1011282.

361. Aalen OO, Røysland K, Gran JM, Ledergerber B. Causality, Mediation and Time: A Dynamic Viewpoint. *J. R. Stat. Soc. Ser. A Stat. Soc.* 2012; 175(4):831–861.

369. Dol J, Boulos L, Somerville M, et al. Health system impacts of SARS-CoV-2 variants of concern: a rapid review. *BMC Health Services Research*. 2022; 22(). URL: https://dx.doi.org/10.1186/s12913-022-07847-0.

379. He Y, Chen Y, Yang L, Zhou Y, Ye R, Wang X. The impact of multi-level interventions on the second-wave SARS-CoV-2 transmission in China. *PLOS ONE*. 2022; 17(9):1–12. URL: https://doi.org/10.1371/journal.pone.0274590.

385. Prague M, Commenges D, Gran JM, et al. Dynamic models for estimating the effect of HAART on CD4 in observational studies: Application to the Aquitaine Cohort and the Swiss HIV Cohort Study. *Biometrics*. 2017; 73():294–304. URL: https://dx.doi.org/10.1111/biom.12564.

387. Kerr CC, Stuart RM, Mistry D, et al. Covasim: An agent-based model of COVID-19 dynamics and interventions. *PLOS Computational Biology*. 2021; 17(7):e1009149. URL: https://dx.doi.org/10.1371/journal.pcbi.1009149.

394. Sam Abbott, Joel Hellewell, Katharine Sherratt, et al. *EpiNow2: Estimate Real-Time Case Counts and Time-Varying Epidemiological Parameters*. 2020.

395. Scire J, Huismman JS, Grosu A, et al. estimateR: an R package to estimate and monitor the effective reproductive number. *BMC Bioinformatics*. 2023; 24(1). URL: https://dx.doi.org/10.1186/s12859-023-05428-4.

427. Alexandre M, Prague M, Mclean C, et al. Prediction of long-term humoral response induced by the two-dose heterologous Ad26.ZEBOV, MVA-BN-Filo vaccine against Ebola. *npj Vaccines*. 2023; 8(1).

428. Pasin C, Balelli I, Van Effelterre T, et al. Dynamics of the Humoral Immune Response to a Prime-Boost Ebola Vaccine: Quantification and Sources of Variation. *Journal of Virology*. 2019; 93(18).

435. Kretzschmar ME, Ashby B, Fearon E, et al. Challenges for modelling interventions for future pandemics. *Epidemics*. 2022; 38():100546.

436. Shadbolt N, Brett A, Chen M, et al. The challenges of data in future pandemics. *Epidemics*. 2022; 40():100612.

437. Le Bert N, Samandari T. Silent battles: immune responses in asymptomatic SARS-CoV-2 infection. *Cell. Mol. Immunol.* 2024; 21():159–170.

438. Mossong J, Hens N, Jit M, et al. Social Contacts and Mixing Patterns Relevant to the Spread of Infectious Diseases. *PLoS Med.* 2008; 5(3):e74.

439. Tran Kiem C, Bosetti P, Paireau J, et al. SARS-CoV-2 transmission across age groups in France and implications for control. *Nat. Commun.* 2021; 12(6895):1–12.

440. Rodiah I, Vanella P, Kuhlmann A, et al. Age-specific contribution of contacts to transmission of SARS-CoV-2 in Germany. *Eur. J. Epidemiol.* 2023; 38(1):39–58.

441. Jaouimaa FZ, Dempsey D, Van Osch S, et al. An age-structured SEIR model for COVID-19 incidence in Dublin, Ireland with framework for evaluating health intervention cost. *PLoS One*. 2021; 16(12).

442. Deville P, Linard C, Martin S, et al. Dynamic population mapping using mobile phone data. *Proc. Natl. Acad. Sci. U.S.A.* 2014; 111(45):15888–15893.

443. Calvetti D, Hoover AP, Rose J, Somersalo E. Metapopulation Network Models for Understanding, Predicting, and Managing the Coronavirus Disease COVID-19. *Front. Phys.* 2020; 8():560678.

444. Costa GS, Cota W, Ferreira SC. Outbreak diversity in epidemic waves propagating through distinct geographical scales. *Phys. Rev. Res.* 2020; 2(4):043306.

445. Lee DI, Nande A, Anderson TL, Levy MZ, Hill AL. Vaccine failure mode determines population-level impact of vaccination campaigns during epidemics. *medRxiv*. 2024():2024.09.30.24314493. eprint: 2024.09.30.24314493.

446. Henderson P, Hu J, Romoff J, Brunskill E, Jurafsky D, Pineau J. Towards the Systematic Reporting of the Energy and Carbon Footprints of Machine Learning. *Journal of Machine Learning Research*. 2020; 21(248):1–43. URL: https://www.jmlr.org/papers/v21/20-312.html.

447. Balelli I, Pasin C, Prague M, et al. A model for establishment, maintenance and reactivation of the immune response after vaccination against Ebola virus. *J. Theor. Biol.* 2020; 495():110254.

448. Langley WA, Wieland A, Ahmed H, et al. Persistence of Virus-Specific Antibody after Depletion of Memory B Cells. *J. Virol.* 2022; 96(9):e0002622. eprint: 35404084.

449. Commenges D, Gégout-Petit A. A general dynamical statistical model with causal interpretation. *Journal of the Royal Statistical Society: Series B (Statistical Methodology)*. 2009; 71(3):719–736.

450. Deforche K, Vercauteren J, Müller V, Vandamme AM. Behavioral changes before lockdown and decreased retail and recreation mobility during lockdown contributed most to controlling COVID-19 in Western countries. *BMC Public Health*. 2021; 21().

451. Shuttleworth I, Toger M, Türk U, Östh J. Did Liberal Lockdown Policies Change Spatial Behaviour in Sweden? Mapping Daily Mobilities in Stockholm Using Mobile Phone Data During COVID-19. *Appl. Spatial Analysis*. 2024; 17(1):345–369.

452. Toger M, Kourtit K, Nijkamp P, Östh J. Mobility during the COVID-19 Pandemic: A Data-Driven Time-Geographic Analysis of Health-Induced Mobility Changes. *Sustainability*. 2021; 13(7):4027.

453. Östh J, Toger M, Türk U, Kourtit K, Nijkamp P. Leisure mobility changes during the COVID-19 pandemic – An analysis of survey and mobile phone data in Sweden. *Research in Transportation Business & Management*. 2023; 48():100952.

454. Chung JB, Kim BJ, Kim ES. Mask-wearing behavior during the COVID-19 pandemic in Korea: The role of individualism in a collectivistic country. *Int. J. Disaster Risk Reduct.* 2022; 82():103355.

455. Lim B, Kyoungseo Hong E, Mou J, Cheong I. COVID-19 in Korea: Success Based on Past Failure. *Asian Economic Papers*. 2021; 20(2):41–62.

456. Kang S, Guak S, Bataa A, et al. Mask-wearing Characteristics an COVID-19 in Indoor and Outdoor Environments in Seoul in 2020. *Journal of Environmental Health Sciences*. 2020; 46(6):750–756.

457. Gelfand MJ, Jackson JC, Pan X, et al. The relationship between cultural tightness–looseness and COVID-19 cases and deaths: a global analysis. *Lancet Planetary Health*. 2021; 5(3):e135–e144.

458. N'konzi JPN, Chukwu CW, Nyabadza F. Effect of time-varying adherence to non-pharmaceutical interventions on the occurrence of multiple epidemic waves: A modeling study. *Front. Public Health*. 2022; 10():1087683.

459. Joshi YV, Musalem A. Lockdowns lose one third of their impact on mobility in a month. *Sci. Rep.* 2021; 11(22658):1–10.

460. Marion G, Hadley L, Isham V, et al. Modelling: Understanding pandemics and how to control them. *Epidemics*. 2022; 39():100588.

461. Chang S, Pierson E, Koh PW, et al. Mobility network models of COVID-19 explain inequities and inform reopening. *Nature*. 2021; 589():82–87.

462. Galmiche S, Charmet T, Schaeffer L, et al. Exposures associated with SARS-CoV-2 infection in France: A nationwide online case-control study. *Lancet Regional Health – Europe*. 2021; 7().

463. Funk S, Bansal S, Bauch CT, et al. Nine challenges in incorporating the dynamics of behaviour in infectious diseases models. *Epidemics*. 2015; 10():21–25.

464. Aspachs O, Durante R, Graziano A, Mestres J, Reynal-Querol M, Montalvo JG. Tracking the impact of COVID-19 on economic inequality at high frequency. *PLoS One*. 2021; 16(3):e0249121.

465. Binns C, Low WY. The Rich Get Richer and the Poor Get Poorer: The Inequality of COVID-19. *Asia Pac. J. Public Health*. 2021; 33(2-3):185–187.

466. Stockwell S, Trott M, Tully M, et al. Changes in physical activity and sedentary behaviours from before to during the COVID-19 pandemic lockdown: a systematic review. *BMJ OPEN SP EX MED*. 2021; 7(1):e000960.

467. Neira C, Godinho R, Rincón F, Mardones R, Pedroso J. Consequences of the COVID-19 Syndemic for Nutritional Health: A Systematic Review. *Nutrients*. 2021; 13(4):1168.

468. Chang TH, Chen YC, Chen WY, et al. Weight Gain Associated with COVID-19 Lockdown in Children and Adolescents: A Systematic Review and Meta-Analysis. *Nutrients*. 2021; 13(10):3668.

469. Salari N, Hosseinian-Far A, Jalali R, et al. Prevalence of stress, anxiety, depression among the general population during the COVID-19 pandemic: a systematic review and meta-analysis. *Global. Health*. 2020; 16(1):1–11.

470. Wang Y, Shi L, Que J, et al. The impact of quarantine on mental health status among general population in China during the COVID-19 pandemic. *Mol. Psychiatry*. 2021; 26():4813–4822.

471. Santomauro DF, Herrera AMM, Shadid J, et al. Global prevalence and burden of depressive and anxiety disorders in 204 countries and territories in 2020 due to the COVID-19 pandemic. *Lancet*. 2021; 398(10312):1700–1712.

472. Pujolar G, Oliver-Anglès A, Vargas I, Vázquez ML. Changes in Access to Health Services during the COVID-19 Pandemic: A Scoping Review. *Int. J. Environ. Res. Public Health*. 2022; 19(3):1749.

473. World Health Organization, Health Services Performance Assessment. *Fourth round of the global pulse survey on continuity of essential health services during the COVID-19 pandemic: November 2022–January 2023*. May 2023. URL: https://www.who.int/publications/i/item/WHO-2019-nCoV-EHS_continuity-survey-2023.1.

474. World Health Organization. *The impact of COVID-19 on mental, neurological and substance use services*. Oct. 2020. URL: https://www.who.int/publications/i/item/978924012455.

475. Skarp JE, Downey LE, Ohrnberger JWE, et al. A Systematic Review of the Costs Relating to Non-pharmaceutical Interventions Against Infectious Disease Outbreaks. *Appl. Health Econ. Health Policy*. 2021; 19(5):673–697.

476. Mandel A, Veetil V. The Economic Cost of COVID Lockdowns: An Out-of-Equilibrium Analysis. *EconDisCliCha*. 2020; 4(3):431–451.

477. Ludolph R, Takahashi R, Shroff ZC, et al. A global research agenda on public health and social measures during emergencies. *Bull. World Health Organ.* 2023; 101(11):717.

478. Colas C, Hejblum B, Rouillon S, et al. EpidemiOptim: A Toolbox for the Optimization of Control Policies in Epidemiological Models. *Journal of Artificial Intelligence Research*. 2021; 71():479–519. URL: https://dx.doi.org/10.1613/jair.1.12588.

479. Janko V, Reščič N, Vodopija A, et al. Optimizing non-pharmaceutical intervention strategies against COVID-19 using artificial intelligence. *Front. Public Health*. 2023; 11().

480. Djidjou-Demasse R, Michalakis Y, Choisy M, Sofonea MT, Alizon S. Optimal COVID-19 epidemic control until vaccine deployment. *medRxiv*. 2020(). URL: https://doi.org/10.1101/2020.04.02.20049189.

481. Biswas D, Alfandari L. Designing an optimal sequence of non-pharmaceutical interventions for controlling COVID-19. *Eur. J. Oper. Res.* 2022; 303(3):1372–1391.

482. Han E, Tan MMJ, Turk E, et al. Lessons learnt from easing COVID-19 restrictions: an analysis of countries and regions in Asia Pacific and Europe. *Lancet*. 2020; 396(10261):1525–1534.

483. Brett TS, Rohani P. COVID-19 herd immunity strategies: walking an elusive and dangerous tightrope. *medRxiv*. 2024().

484. Shanmugaraj B. Ever-evolving SARS-CoV-2: Latest variant KP.2 is on the rise. *Asian Pacific Journal of Tropical Medicine*. 2024; 17(6):241.

485. Jacobs JL, Haidar G, Mellors JW. COVID-19: Challenges of Viral Variants. *Annu. Rev. Med.* 2023(; Volume 74, 2023):31–53.

486. Cankat S, Demael MU, Swadling L. In search of a pan-coronavirus vaccine: next-generation vaccine design and immune mechanisms. *Cell. Mol. Immunol.* 2024; 21():103–118.

487. Patel TA, Jain B, Raifman J. Revamping Public Health Systems: Lessons Learned From the Tripledemic. *Am. J. Prev. Med.* 2024; 66(1):185–188.

488. United Nations. *The Sustainable Development Goals Report*. [Online; accessed 5. Sep. 2024]. July 2021. URL: `https://unstats.un.org/sdgs/report/2021/The-Sustainable-Development-Goals-Report-2021.pdf`.

489. Hadley L, Challenor P, Dent C, et al. Challenges on the interaction of models and policy for pandemic control. *Epidemics*. 2021; 37():100499.

490. Gonçalves A, Mentré F, Lemenuel-Diot A, Guedj J. Model Averaging in Viral Dynamic Models. *AAPS J.* 2020; 22(2):1–11.

Scientific Production

Articles

- Ganser I, Murphy T, Prague M, O'Brien S, Thiébaut R, Buckeridge DL (2024). **Investigating waning of natural immunity against SARS-CoV-2: implications for infection risk**. *[In preparation]*

- Ganser I, Paireau J, Buckeridge DL, Cauchemez S, Thiébaut R, Prague M (2024). **Comparative evaluation of methodologies for estimating the effectiveness of non-pharmaceutical interventions in the context of COVID-19: a simulation study**. *[Submitted for publication to American Journal of Epidemiology]*

- Ganser I, Buckeridge DL, Heffernan JM, Prague M, Thiébaut R (2024). **Estimating the Population Effectiveness of Interventions Against COVID-19 in France: A Modelling Study**. *Epidemics*, Volume 46, Pages 100744, https://doi.org/10.1016/j.epidem.2024.100744.

- Teichmann PNN*, Ganser I*, Shimizu-Jozi A*, Luo A, Yu R, Arora RK, Duarte N, Wagner CE (2024). **Pathosim: A multi-pathogen agent-based model for infectious disease transmission**. *[In preparation]*

- Meng Z, Okhmatovskaia A, Polleri M, Shen Y, Powell G, Fu Z, Ganser I, Zhang M, King NB, Buckeridge DL, Collier N (2022). **BioCaster in 2021: automatic disease outbreaks detection from global news media**. *Bioinformatics*, Volume 38, Issue 18, Pages 4446–4448, `www.doi.org/10.1093/bioinformatics/btac497`

- Xia Y, Ma H, Buckeridge DL, Brisson M, Sander B, Chan A, Verma A, Ganser I, Kronfli N, Mishra S, Maheu-Giroux M (2022). **Mortality trends and length of stays among hospitalized patients with COVID-19 in Ontario and Québec (Canada): a population-based cohort study of the first three epidemic waves**. *International Journal of Infectious Diseases*, Volume 121:1-10, www.doi.org/10.1016/j.ijid.2022.04.048

- Shen Y, Powell G, Ganser I, Zheng Q, Grundy C, Okhmatovskaia A, Buckeridge DL (2021). **Monitoring non-pharmaceutical public health interventions during the COVID-19 pandemic**. *Scientific Data*, Volume 8, Number 225, Pages 1-6, www.doi.org/10.1038/s41597-021-01001-x

Communications

Communications at international conferences

- Ganser I, Buckeridge DL, Heffernan JM, Prague M, Thiébaut R. **Estimating the population effectiveness of interventions against COVID-19 in France: a modelling study**. *Epidemics*, Bologna, Italy. November 2023, Poster presentation

- Ganser I, Buckeridge DL, Prague M, Thiébaut R. **Effects of public health interventions against COVID-19 in France**. *CROI*, Seattle, USA. February 2023, Poster presentation

- Ganser I, Buckeridge DL, Prague M, Thiébaut R. **Estimation of the effects of non-pharmaceutical interventions and vaccination against COVID-19 in France using dynamical models**. *ASPHER Young Researcher's Forum*, Berlin, Germany. November 2022, Oral presentation

Communications at national conferences

- Ganser I, O'Brien SF, Murphy T, Swail H, Buckeridge DL. **Observing longitudinal trends of immunity from repeat blood donors**. *Hema-Net Serosurveillance Meeting*, Montréal, Canada, February 2024, Oral presentation

- Ganser I, Buckeridge DL, Heffernan JM, Prague M, Thiébaut R. **Estimating the population effectiveness of interventions against COVID-19 in France: a modelling study**. *Journée des jeunes chercheurs, Bordeaux Population Health Research Centre*, Bordeaux, France. September 2023, Oral presentation

- Ganser I, Buckeridge DL, Prague M, Thiébaut R. **Estimating the population effectiveness of interventions against COVID-19 in France: a modelling study**. *Les journées de l'AC modélisation ANRS MIE (Emerging infectious diseases)*, Bordeaux, France. November 2022, Oral presentation

News articles

Manuscript 1 has been cited in the news, amongst others:

- **Covid-19 : sans la vaccination, le nombre de morts aurait été le double en France**, *Le Monde*, Feburary 2024 (www.lemonde.fr/planete/article/2024/02/08/covid-19-sans-la-vaccination-le-nombre-de-morts-aurait-ete-le-double-en-france_6215444_3244.html)

- **Covid-19: des milliers de vies ont été sauvées par le premier confinement, selon une étude**, *Le Figaro*, Feburary 2024 (www.sante.lefigaro.fr/social/sante-publique/covid-19-des-milliers-de-vies-ont-ete-sauvees-par-le-premier-confinement-selon-une-etude-20240207)

- **Les vaccins anti-Covid sont-ils responsables de myocardites ? Les conclusions d'une nouvelle étude**, *L'Express*, Feburary 2024 (www.lexpress.fr/sciences-sante/sciences/les-vaccins-anti-covid-sont-ils-responsables-de-myocardites-les-conclusions-dune-nouvelle-etude-UPGQSLXWYRGXDOHLU4ZDHMK52Y)

Manuscript 1 has also been cited in a French policy report on the effect of COVID-19 vaccines in France:
M. Philippe Berta, M. Gérard Leseul et Mme Florence Lassarade (2024). **Rapport n2707 de l'office parlementaire d'évaluation des choix scientifiques et technologiques établi au nom de l'office, sur les effets indésirables des vaccins et les dernières évolutions des connaissances scientifiques sur la covid-19**, www.assemblee-nationale.fr/dyn/16/rapports/ots/l16b2707_rapport-information.pdf